

Chemical Ozone Loss in the Arctic Polar Stratosphere Derived from Satellite Observations



Dissertation
zur Erlangung des Doktorgrades
der Naturwissenschaften

vorgelegt beim
Fachbereich Geowissenschaften / Geographie
der Johann Wolfgang Goethe-Universität
in Frankfurt am Main

von
Dipl. Geophys. Simone Tilmes
aus Borken, Westf.

Frankfurt 2003

(D F 1)

Vom Fachbereich **Geowissenschaften / Geographie** der
Johann Wolfgang Goethe-Universität als Dissertation angenommen.

Dekan: Prof. Dr. Ulrich Schmidt, Universität Frankfurt
Gutachter: Prof. Dr. Ulrich Schmidt, Universität Frankfurt
Prof. Dr. Martin Riese, Forschungszentrum Jülich
Datum der Disputation: 10. 12. 2003

Abstract

In this thesis, the chemical ozone loss in the Arctic stratosphere was investigated for eleven years between 1991 and 2002. The accumulated local ozone loss and the column ozone loss in a certain altitude range were derived using the ozone-tracer correlation technique. This technique considers the relation between ozone and a long-lived tracer during the lifetime of the polar vortex.

Results are presented on the basis of observations obtained from two solar occultation satellite instruments: ILAS (Improved Limb Atmospheric Spectrometer) aboard the ADEOS satellite (Advanced Earth Observing Satellite) and HALOE (Halogen Occultation Experiment) aboard the UARS satellite (Upper Atmosphere Research Satellite). The HALOE observations used in the present work have been available since October 1991. The instrument made measurements during a period of a few days every two or three months in high northern latitudes during the entire period between 1991 and 2002. The ILAS instrument performed measurements continuously from November 1996 to June 1997 in the high latitude region of both hemispheres.

In the present work, the ozone-tracer correlation method was confirmed against criticism raised in the past. The improved and extended method permits both a reduction and a better quantification of uncertainties. New procedures implemented in the method allow the ozone loss for the winter to be calculated, in case where no results could have been derived in the past. Therefore, a consistent analysis is possible for the eleven winters between 1991–92 and 2001–02.

An intensive analysis of chemical ozone loss is performed considering as an example the winter 1996–97, for which measurements from both HALOE and ILAS are available. The ILAS observations allow a detailed analysis of the temporal evolution of the ozone-tracer correlation inside the polar vortex for the first time and in particular of the development of the early vortex. Especially the influence of mixing between vortex air and air from outside the vortex is discussed. The evolution of significant PSC-related chemical ozone loss can be followed over the entire lifetime of the vortex, from mid-February to May 1997 from ILAS observations. HALOE measurements are available between March and May 1997. Calculated ozone loss is partly larger than calculated from ILAS observations. Especially, at the end of March substantial differences arose between the results of the two instruments. These discrepancies may be partly due to discrepancies in mixing ratio of the very low ozone minimum measured at the 475 K potential temperature level at the end of March 1997 from ILAS and HALOE observations.

Both data sets consistently show a distinct inhomogeneity in the derived ozone loss inside the vortex in spring 1997, which is a specific feature in comparison to the other observed winters between 1991–92 and 2001–02.

During these eleven winters the ozone loss was consistently derived mainly on the basis of HALOE observations. With the use of the ozone-tracer correlation technique, this study demonstrates the interaction between meteorology and ozone loss. As expected, strong accumulated ozone loss is found to occur in conjunction with a strong cold vortex containing a large potential area of PSCs, whereas moderate ozone loss is found if the vortex is less strong and moderately warm. A confirmation of the technique is that hardly any ozone loss could be calculated in very warm winters with small amounts of possible PSC areas during the entire winter.

The effect of meteorological conditions on the chlorine activation becomes obvious in the HCl signal, as well as the dependence between chlorine activation and ozone loss. Additionally, the degree of homogeneity of ozone loss is shown to depend on the meteorological conditions, as there is a possible influence of horizontal mixing on the air inside a weak polar vortex. Further, the evolution of the CH₄/HF relation over the eleven-year period is investigated and the growth rate of HF as a function of different stratospheric altitudes.

The analysis of the relationship between the area of possible PSC existence (derived using the PSC threshold temperature) and the accumulated ozone loss indicates that this relationship is not a linear relation. An influence of other factors could be identified such as the increased burden of aerosols in the atmosphere, for example after the Pinatubo volcanic eruption in 1991. Furthermore, the different exposure of solar radiation caused by different equatorward excursions in different years may impact the extent of chemical ozone loss. These new insights on the issue of polar ozone depletion improve the understanding of the processes responsible for chemical ozone loss in the lower stratosphere.

Contents

Abstract	iii
1 Introduction	1
1.1 Stratospheric Ozone – Overview	1
1.2 Polar Ozone Depletion	5
2 Stratospheric Chemistry	9
2.1 The Chemistry of Stratospheric Ozone	9
2.1.1 Loss Cycles of Ozone	9
2.1.2 Chlorine-Containing Trace Species	11
2.2 The Chemistry of Stratospheric Polar Ozone	12
2.2.1 Polar Stratospheric Clouds (PSCs) and Sulphate Aerosols	12
2.2.2 Heterogeneous Chemistry	13
2.2.3 Deactivation of Chlorine	14
2.2.4 Denitrification	15
3 The Arctic Polar Vortex	17
3.1 Dynamics of the Stratospheric Polar Vortex	17
3.1.1 The Polar Vortex Edge Region	22
3.2 Dynamical Tracers	23
3.3 Total Ozone in High Northern Latitudes Based on TOMS Observations	24
4 The Quantification of Chemical Ozone Loss in the Polar Region	29
4.1 The Principles of the Tracer-Tracer Correlation (TRAC) Technique	30
4.2 Presentation of Several Methods of Calculating Ozone Loss	34
4.3 Criticism of the TRAC Technique	36
4.4 Specific Improvements and Extensions in the TRAC Methodology	38
4.4.1 New Methodology for the Meteorological Analysis	39
4.4.2 Improved Determination of the Early Winter Reference Function	41
4.4.3 Specific Improvements to the HALOE Analysis	44

5	Verification of the (TRAC) Technique Using ILAS Data in 1996–	97
	97	47
5.1	Meteorology of the Polar Vortex 1996–97	47
5.2	Evolution of Ozone-Tracer Relations in the Early Vortex	48
5.3	Evolution of Ozone Loss over the Entire Lifetime of the Vortex	50
5.4	Influence of Mixing on the Ozone-Tracer Relationship	54
6	Re-analysis of HALOE and ILAS Observations in Winter 1996–	97
	97	57
6.1	Comparison of ILAS and HALOE Ozone Observations	57
6.2	Ozone Loss in the Winter 1996–97, ILAS and HALOE in Comparison	60
6.2.1	Ozone Loss Derived From HALOE Measurements	60
6.2.2	Ozone Loss Derived From ILAS Measurements	70
6.2.3	Comparison of HALOE and ILAS Results	70
7	Development of the Tracer-Tracer Relation from 1991 to 2002	75
7.1	The CH ₄ /HF Relation for all Winters	75
7.2	The Early Winter Ozone-Tracer Reference Relation	79
7.3	Meteorological Conditions and the HCl-Tracer and O ₃ -Tracer Relation in Arctic Winters 1991–2002	84
8	Column Ozone Loss and Ozone Loss Profiles	95
8.1	Vertical Ozone Loss Profiles in Arctic Winters 1991–2002	95
8.2	Column Ozone Loss in Arctic Winters 1991–2002	100
8.3	Discussion of the TRAC Technique	108
9	Comparison of Results With Earlier Studies	111
9.1	HALOE Results in Comparison With Earlier Studies Based on HALOE	111
9.2	Comparison of Ozone Loss Derived Using Different Methods	114
9.3	The Relationship Between Ozone Loss and the Area of PSCs	118
10	Summary and Outlook	121
A	Zusammenfassung	123
B	Satellite Measurements	129
B.1	ILAS	129
B.2	HALOE	130
C	Tracer-Tracer Reference Relations	133
	List of Figures	139
	List of Tables	143
	Abbreviations and Symbols	145

Bibliography	149
Acknowledgements	163

Chapter 1

Introduction

Human impact can be observed in a great variety of different ecosystems, especially under complex conditions as they appear in the earth's atmosphere. One of the most obvious examples of changes in the environment due to anthropogenic activities is the appearance of strong ozone depletion in the stratosphere. This is found in high and mid-latitudes both in the upper stratosphere and in the lower stratosphere (see Figure 1.1). Recent assessments indicate that the global mean total ozone for 1997–2001 was about 3 % below the pre-1980 value for high and mid-latitudes [WMO, 2003]. The corresponding increase of 6–14 % in UV irradiance since the early 1980s [WMO, 2003] may have a serious impact on life on earth.

The ozone depletion in the polar stratosphere has been a major focus of stratospheric research since the discovery of the so-called “ozone hole” in the Antarctic [Farman *et al.*, 1985]. The interest in Arctic ozone depletion has increased over the past decade, but the key processes are still not satisfactorily understood today. In particular, our ability to produce reliable forecasts is limited. In this thesis a contribution is presented for enhancing the understanding of stratospheric ozone reduction, with the focus on the Arctic polar regions.

In Section 1.1 the main characteristics of stratospheric ozone distribution are presented as well as past changes due to anthropogenic activities. An overview of polar ozone is given in Section 1.2 and the major priorities of this work are outlined.

1.1 Stratospheric Ozone – Overview

The major part of the earth's atmosphere (more than 99.9 % of the volume) consists of molecular nitrogen (N_2), molecular oxygen (O_2) and the noble gas argon (Ar). However, the most important chemical processes in the atmosphere are controlled by gases with concentrations many orders of magnitudes smaller than that of nitrogen, oxygen and argon. Ozone (O_3) is the most important of these gases. Most of the ozone resides at greater altitudes in our atmosphere, in the stratosphere, about 10–50 km above the earth's surface. The ozone layer at

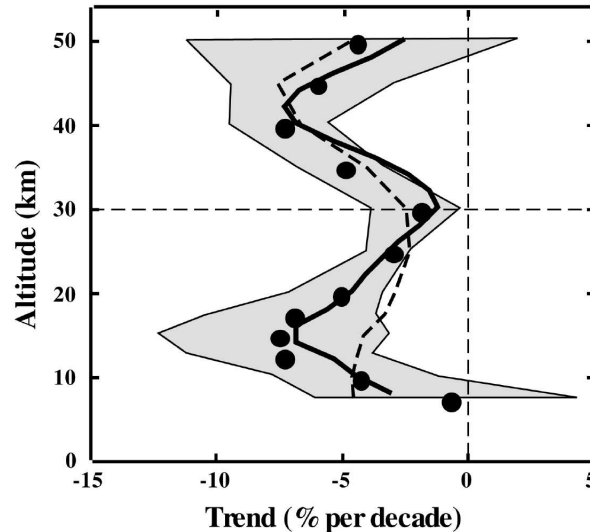


Figure 1.1: The vertical distribution of stratospheric ozone decline in northern and mid-latitudes (solid circles) and its uncertainties (grey area) derived from the 1980 to 1996 trend. In comparison a 2-D model calculation of the ozone trend due to catalytic destruction by halogen radicals: solid line from *Solomon et al.* [1998], and a calculation using the model of *Jackman et al.* [1996]: dashed line, after *WMO* [1999].

altitudes between between 15 and 40 km contains about 90 % of the atmospheric ozone. It has two major effects on the earth's climate. Due to the absorption of the solar UV-B radiation by ozone (at wavelengths between 190 and 310 nm), only a small amount of the harmful ultraviolet light (UV-B) reaches the earth's surface. On the other hand, ozone absorbs in the infrared, near $9,6 \mu\text{m}$, and it acts as a source of heat. Therefore, the temperature rises with altitudes up to a height of 50 km in the stratosphere. Thus, a decrease of the stratospheric ozone increases the UV-B radiation reaching the biosphere. This results in harmful effects on plants, animals and human beings [*WMO*, 2003] and may also have an impact on climate, due to the changing heat balance in the stratosphere.

The distribution of the ozone mixing ratio along altitude and equivalent latitude¹ is shown in Figure 1.2. This ten-year (1992–2001) climatology of satellite observations for September indicates a maximum of the ozone mixing ratio of about 10 ppmv at an altitude of roughly 30 km (10 hPa) in the tropics and smaller mixing ratios towards higher latitudes. In Figure 1.2, the “ozone hole” is noticeable as very low ozone mixing ratios between 100–50 hPa south of $\approx 60^\circ\text{S}$ (see further discussion below).

The main production of stratospheric ozone occurs in tropical latitudes [*Dessler*, 2000]. Ozone is mainly produced by the photolysis of molecular oxygen

¹The equivalent latitude is an approximate measure of geographic latitude that allows for a good separation of polar vortex and non-vortex air [e.g., *Nash et al.*, 1996; *Lary et al.*, 1995].

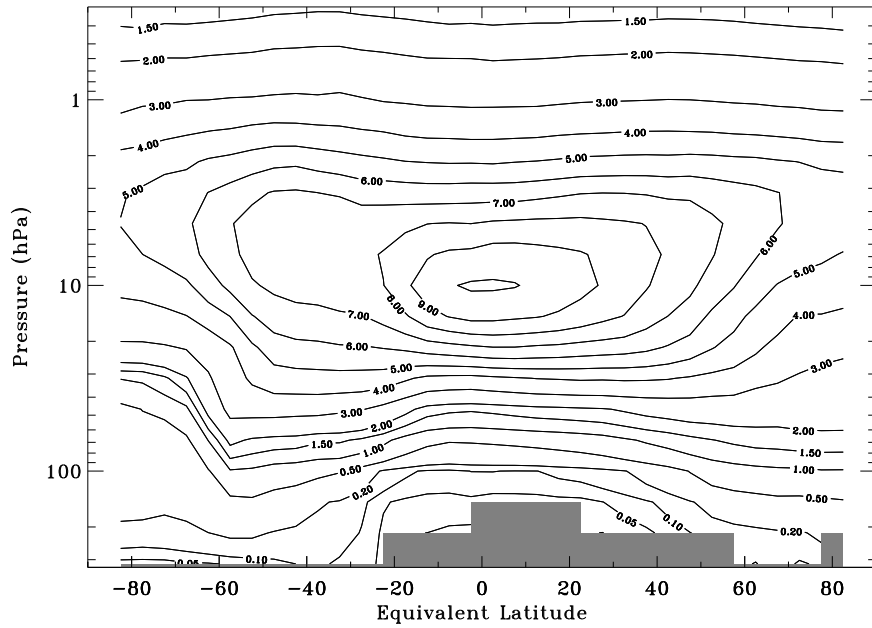
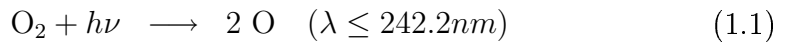


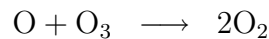
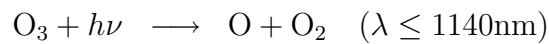
Figure 1.2: Zonally averaged distribution of ozone mixing ratios in ppmv in September. Shown is a ten-year (1992–2001) average of HALOE measurements. Missing data are indicated as a grey area (J.-U. Grooß, pers. comm., 2003).

(O₂) into two oxygen atoms, followed by the reaction of the photolysis product, the oxygen atoms (O), with O₂ to form ozone.

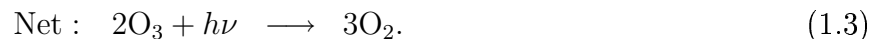


where $h\nu$ is the energy of a photon with the frequency ν , the wavelength λ , and M is a neutral molecule that removes excess energy without participating in the reaction, mostly molecular nitrogen (N₂) or O₂.

Stratospheric ozone is converted back into molecular oxygen by various reactions. Historically, the first ozone-destroying reaction that was discovered was the recombination of atomic oxygen with ozone:



— — —



Together with (1.1) and (1.2) it constitutes the so-called Chapman cycle [Chapman, 1930]. Furthermore, very effective ozone-destroying catalytic cycles are driven by certain radicals (e.g., NO, NO₂, OH, HO₂, Cl, ClO, BrO). The importance of the different catalytic cycles depends on altitude and meteorological conditions and are described in more detail in Chapter 2.

Due to the anthropogenic emissions of halogen-containing gases (e.g., chlorofluorocarbons (CFCs), halons and chlorocarbons), the ozone chemistry is strongly perturbed. During the last century, the mixing ratio of such gases that act as source gases for ozone-destroying chemicals in the atmosphere has increased rapidly. Large amounts of these chemicals (mainly CFCs) have been used, for example, as refrigerant in air conditioning systems, in spray bottles and in foam production.

Emissions of these species, which are extremely stable in the troposphere, resulted in a dramatic increase in the tropospheric mixing ratio [WMO, 1999; Engel *et al.*, 2002]. These anthropogenic compounds are uniformly distributed in the background troposphere and enter the stratosphere through upward transport in the tropical region. Therefore, with a delay of some years, the mixing ratio of these compounds also increase in the stratosphere. Due to the increasing intensity of UV radiation with increasing altitude in the stratosphere these compounds are destroyed by photochemical reactions to result (mainly) in HCl and ClONO₂.

Analyses of air trapped in the snow above glaciers or in firn air clearly demonstrated the extent of the anthropogenic influence [e.g., Butler *et al.*, 1999]. The mixing ratios of, e.g., CFCs, halons, carbon tetrachloride (CCl₄) measured in air samples from the late 19th century are generally less than 2 % of those found today in the background atmosphere. For example, at the beginning of the nineties the amount of chlorine-containing species from anthropogenic sources in the troposphere was 82 % of the total amount of chlorine [Keene *et al.*, 1999].

The connection between the accumulation of anthropogenic chlorofluorocarbons in the atmosphere and the increase in the chlorine-catalysed loss of O₃ was first described by Molina and Rowland [1974]. At that time, an enhanced ozone loss was predicted to appear mainly in the upper stratosphere. Early model studies [e.g., Crutzen, 1974] indicated that the largest loss of O₃ would occur at an altitude of about 40 km, a view that was subsequently confirmed by a variety of models [WMO, 1999]. Indeed, the observed vertical profile of ozone loss in the upper stratosphere (see Figure 1.1), with maximum losses at around 40 km, was predicted correctly by the first model studies. Nevertheless, there were still uncertainties in the quantitative understanding of the stratospheric ozone budget. Models predicted much smaller concentration of ozone in comparison to measurements in the upper stratosphere, which was called the “ozone deficit” problem [e.g., Crutzen and Schmailzl, 1983]. Today, this problem in the upper stratosphere has almost been resolved [Crutzen *et al.*, 1995; Grooß *et al.*, 1999].

Loss of ozone in the lower stratosphere first became apparent as a severe reduction of total ozone over the Antarctic, detected by Farman *et al.* [1985]. As a consequence, enormous scientific efforts were set in motion to find the reasons. Within about two years the “ozone hole” was shown to be caused by a perturbed chlorine chemistry. It was pointed out that the existence of polar stratospheric clouds (PSCs) was responsible for these perturbed conditions. PSCs are observed in the polar vortex, if temperatures are low enough (lower than ≈ 195 K). The exact nature of PSCs is still somewhat uncertain, as outlined in Section 2.2. Due

to heterogeneous reactions on the surface of PSCs in the polar region, the inactive chlorine reservoir species (e.g. HCl and ClONO₂) are converted into the reactive ozone-destroying species (Cl, ClO). The mixing ratio of these reservoir species is largest in the polar region, due to the stratospheric transport patterns (see Section 3.1). Thus, the potential for ozone-destroying chlorine radicals is likewise largest there. Moreover, it was discovered that bromine compounds, originating to a large extent from the anthropogenic release of halons, also contribute substantially to polar ozone loss cycles [McElroy *et al.*, 1986].

The discovery of the consequences of CFC emissions prompted activities leading to the Montreal Protocol in 1987 and the following amendments. The production of the most important CFCs responsible for the ozone loss (CFC-11, CFC-12) was totally stopped and their use was restricted. Later, the 1995 Vienna Protocol completely phased out the production and use of further CFCs by the year 1996.

Today, the consequence of the strong increase in the mixing ratio of ozone-destroying chlorine compounds, but also the dramatic breakup in CFC emissions, are obvious in atmospheric observations. The total amount of chlorine from long- and short-lived chlorocarbons in the troposphere peaked in 1992–94 at about 3.6 ppbv [WMO, 2003]. The major fraction of these 3.6 ppbv, about 3 ppbv of chlorine, was due to molecules resulting from human activities [Dessler, 2000]. Chlorine from most of the major chlorofluorocarbons (CFCs) is no longer increasing. In 2000 the value of total chlorine in the troposphere was about 5 % lower than at its maximum. On the other hand, total bromine from halons still continues to increase at about 3 % per year in the troposphere [WMO, 2003].

It should be mentioned that the first signs of the Antarctic ozone hole coincided with total chlorine levels of approximately 1.8 pptv at an altitude of 20 km [Engel *et al.*, 2002]. Only a slow recovery of the ozone layer can be expected in the next few years, because of the long lifetime of most of the CFCs in the atmosphere ranging from decades to one hundred years. Further, many additional factors have an influence on the ozone layer, such as the anthropogenic emissions of methane, nitrogen compounds and sulphate aerosols as well as climate change. Therefore, predictions of the future development of the stratospheric ozone are very uncertain. Nevertheless, with current regulations on further emissions of chlorine and bromine source gases and the assumption that the general transport characteristics of the stratosphere will not change, the ozone loss in the polar vortex can be anticipated to appear up to the year 2060 [Engel *et al.*, 2002].

1.2 Polar Ozone Depletion

The most severe losses of stratospheric ozone have been observed over Antarctica in austral spring since the late eighties of the last century [Farman *et al.*, 1985; Jones and Shanklin, 1995; WMO, 2003]. In recent years, in late spring ozone in the lower stratosphere has been almost completely removed within a layer lo-

cated at about 15–19 km [WMO, 1999]. A clear exception is the Antarctic winter in 2002. This winter was marked by an unusually large amount of atmospheric planetary wave activity and a major warming in late September [Allen and Nakamura, 2003; Sinnhuber et al., 2003]. The break-up of the typical cold Antarctic vortex appeared much earlier compared to previous winters. This resulted in about 20 % less chemical ozone loss than usual in past decades [Hoppel et al., 2003].

In the Arctic, climatological ozone levels in late winter and early spring are significantly larger than in the corresponding austral seasons [e.g., Dobson, 1966]. They exhibit a strong short-term variability due to perturbations in the atmospheric transport processes [e.g., Dobson et al., 1929; Weber et al., 2002].

Ozone depletion in the Arctic lower stratosphere has been inferred since 1989 from balloon and aircraft measurements [e.g., Hofmann et al., 1989; Proffitt et al., 1990, 1993; Hofmann and Deshler, 1991; Koike et al., 1991; Kyro et al., 1992; Browell et al., 1993; von der Gathen et al., 1995; Rex et al., 1998; Goutail et al., 1999] and more recently from satellite data [e.g., Manney et al., 1994; Manney et al., 1996b; Müller et al., 1996; Tilmes et al., 2003]. In 1999–2000 the most extensive measurement campaign so far, SOLVE-THESEO 2000, was carried out in the Arctic polar region [Newman et al., 2002]. It was followed by the VINTERSOL-SOLVE2 campaign in 2002–03. The motivation for these campaign activities was to obtain a better quantitative understanding of the key processes involved in polar ozone destruction. In particular, one intention was to quantify the ozone depletion due to chemical losses. To achieve this, different approaches were applied to the measurements in order to separate dynamic processes and chemical ozone loss, as described in Chapter 4. Substantial discrepancies between the results of different methods have arisen in the past. Moreover, very large discrepancies between measurements and model analysis of chemical ozone loss rates were found consistently in several studies [e.g., Becker et al., 1998, 2000; Woyke et al., 1999; Kilbane-Dawe et al., 2001]. Therefore, the processes leading to chemical polar ozone depletion cannot, at present, be considered completely and quantitatively understood. A main problem is the discrepancy between the results of the different techniques applied to derive the chemical ozone loss from observations. In this thesis a contribution is presented to address the latter issue.

The method for determining chemical ozone loss used in the present work is called the tracer-tracer correlation (TRAC) technique. If employed to calculate just the chemical ozone loss, it is called the ozone-tracer correlation (O_3 -TRAC) technique. The principle of this technique was developed by Proffitt et al. [1989, 1990] and is described in detail in Section 4.1. The methodology is based on the consideration of the relation of two long-lived tracers and the evolution of this relation during the lifetime of the polar vortex. It was used in the past to derive ozone depletion [Proffitt et al., 1990; Müller et al., 2001; Salawitch et al., 2002] and denitrification [Fahey et al., 1990; Fahey et al., 1990; Rex et al., 1999; Esler and Waugh, 2002]. For several years now since 1991–92, the technique has

also been applied to analyse satellite observations from the HALOE instrument (see Appendix B.2) [Müller *et al.*, 1996, 2002; Tilmes *et al.*, 2003]. Recently, the technique has been criticised by Michelsen *et al.* [1998] and [Plumb *et al.*, 2000]. It was suggested that owing to the neglect of the impact of mixing on the tracer-tracer correlation ozone loss may be overestimated by the TRAC technique. The criticism is described and discussed in Section 4.3.

In the present work, results from two different satellite instruments, namely ILAS on ADEOS and HALOE on UARS (see Appendix B) were used. The comprehensive set of measurements taken by ILAS in the Arctic polar region allowed for the first time a detailed investigation of the temporal evolution of the ozone-tracer correlation (O_3 -TRAC) inside the polar vortex for a particular winter period (1996–97). Additionally, a long-term study of stratospheric ozone loss in the Arctic is possible with the HALOE data set available for an eleven-year period between 1991–92 and 2001–02.

Important improvements and extensions to the TRAC methodology were made in this work and are presented in detail in Section 4.4. Extensions were made with regard to the meteorological analysis for identifying distinct vortex regions. This permits an exact decision on the location of profiles with respect to vortex regions and, thus, for a more profound interpretation of the impact of the dynamic evolution of the vortex on chemical ozone loss. Further improvements and extensions were introduced by the use of the long-lived tracers CH_4 and HF measured by HALOE as well as by the consistent application of the technique to HALOE observations over an eleven-year period. This led to more comparable, consistent results and established the method as a reliable tool for calculating ozone loss from measurements.

A verification of the improved method is presented in Chapter 5, as well as a detailed analysis of the impact of mixing. A comprehensive re-analysis and comparison of calculated ozone loss has been performed based on HALOE and ILAS measurements for the year 1996–97 in Chapter 6. Furthermore, the consistent application of the improved method to the new HALOE data-set Version 19 over a period of eleven years is shown in Chapters 7 and 8. The evolution of the CH_4 /HF relation over the eleven-year period is described in Section 7.1 as well as the growth rate of HF at different altitudes based on HALOE. Furthermore, the relation between chlorine activation and ozone loss can be shown by considering the development of the HCl-tracer relation of HALOE measurements in Section 7.3.

All in all, it is possible to clearly identify and quantify the limits and uncertainties of the technique and its impact on the results (see Section 8.3). The strongly varying meteorological influences on the polar vortex from year to year are consistent with the results derived using the TRAC method (see Chapter 8). A deeper understanding of the interaction between meteorological conditions, on the one hand, and ozone loss, on the other hand, allows the coupling between ozone loss and climate changes in the future to be assessed.

A comparison of the results derived in the present study with results from other techniques is described in Chapter 9. It is shown that the dependence

of ozone loss derived from HALOE and the accumulated area of PSCs over the entire winter for eleven years is not a simple relation. This is in contrast to the results derived from a method called “vortex average approach”. There, model analyses are included to estimate the impact of transport.

Chapter 2

Stratospheric Chemistry

In this chapter, the main aspects of stratospheric chemistry of relevance to ozone loss are summarised. The most important catalytic ozone loss cycles that impact stratospheric ozone mainly outside the polar regions, are described in Section 2.1. Further influence of the use of anthropogenic CFCs (chlorofluorocarbons) on chemical ozone loss is discussed. Owing to the presence of polar stratospheric clouds in the polar regions, strong ozone loss occurs in the polar lower stratosphere, as outlined in Section 2.2. There, the main heterogeneous reactions on polar stratospheric cloud particles and sulphate aerosol particles are described as well as the impact of deactivation reactions and denitrification on ozone loss.

2.1 The Chemistry of Stratospheric Ozone

Ozone (O_3) is an important atmospheric trace gas in the stratosphere due to its absorption of the biologically harmful ultraviolet solar radiation (UV-B). The absorption in the infrared is a source of heat and energy, which affects the temperature and winds in the stratosphere. The concentration of ozone in the stratosphere is determined by a balance of ozone production and loss. The ozone loss is caused by several catalytic cycles driven by a variety of chemical compounds depending on altitude and meteorological conditions. Nowadays, this balance is strongly perturbed by anthropogenic emissions of halogen-containing compounds into the atmosphere (see Chapter 1). The ultimate consequence of these emissions is a depletion of stratospheric ozone. The ozone depletion in northern and mid-latitudes (see Figure 1.1) has a distinct minimum around 30 km due to the different impacts of anthropogenic halogens in the upper and lower stratosphere see further discussion below.

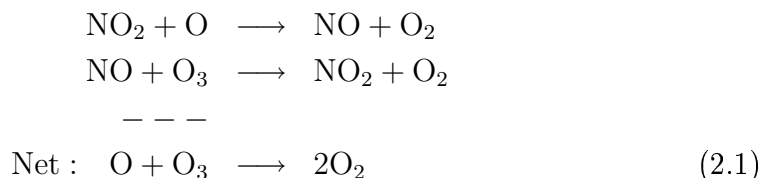
2.1.1 Loss Cycles of Ozone

Stratospheric and mesospheric ozone is produced by the photolysis of molecular oxygen with the subsequent reaction of the resulting oxygen atoms (O) with O_2 to form ozone (1.1). The sum ($O_3 + O$) is called odd oxygen or O_x . It is distinct from the much longer-lived O_2 (molecular oxygen) and varies slowly over a time

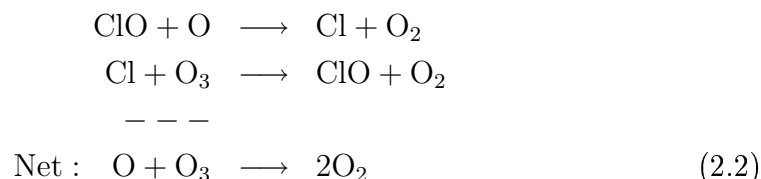
scale of one day. Ozone is converted back to molecular oxygen by reaction with atomic oxygen (Equation 1.3). This cycle, known as the Chapman cycle (and other catalytic cycles, described below) depends on the abundance of ground-state atomic oxygen in the stratosphere. Therefore, the importance of this cycle increases with altitude, owing to the strong increase of O with altitude in the stratosphere [WMO, 1999].

More important for the ozone destruction in the stratosphere are several catalytic cycles, which destroy O_x at a rate comparable to or faster than the rate of the Chapman reaction. A catalytic reaction is a reaction where a reactant increases the rate of a reaction without being consumed in the process. Thus, a small amount of the catalyst can have a large effect.

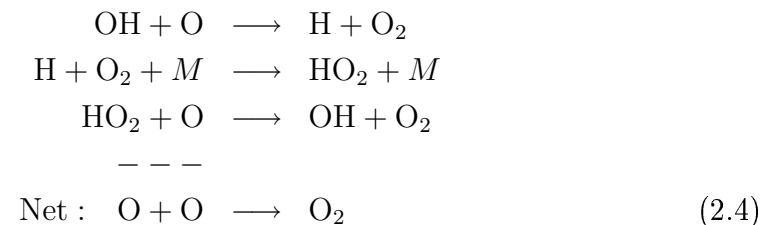
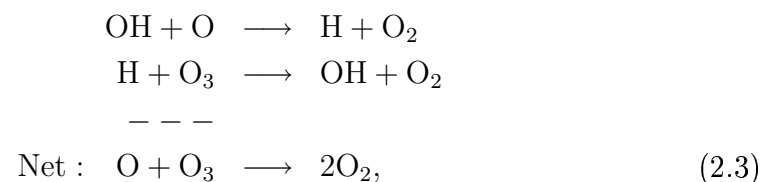
Different catalytic cycles are important at different altitudes, depending on the concentration of the radicals that regulate ozone [WMO, 1999]. Below 40 km, the most important loss cycle is one involving NO_x radicals [Crutzen, 1970]:



Cycles involving chlorine radicals [Molina and Rowland, 1974] are most effective around 40 km:

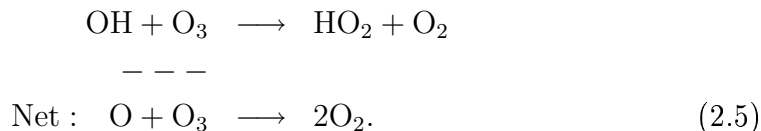


Cycles involving hydrogen radicals (important above 42-45 km) are



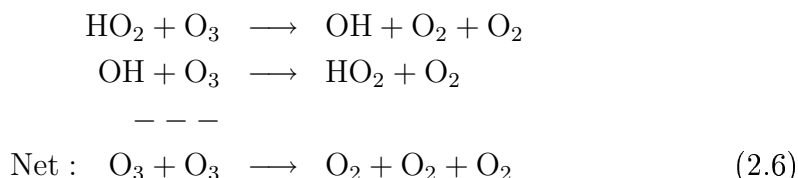
and





These cycles are important in mid-latitudes in the middle and upper stratosphere, because they are rate limited by reactions involving O atoms.

Other cycles are more important in regions where O atoms are rare (such as in the lower stratosphere). For example the cycle



is rate limited by the reaction between HO₂ and O₃. But the most important cycles, which are responsible for the strong decrease in ozone in high latitudes, where the main part of ozone loss occurs below 30 km, are described in Section 2.2.

2.1.2 Chlorine-Containing Trace Species

Trace species which control the stratospheric ozone chemistry are nitrogen compounds, chlorine compounds and hydrogen compounds, because of the catalytic cycles (2.2) to (2.6). The chlorine compounds play an important role for the ozone-destroying catalytic cycles, because their main sources are anthropogenic emissions of substances such as e.g. CFCs. The most important CFCs are CFC-11 (CFCl₃) and CFC-12 (CF₂Cl₂). In the troposphere, CFCs are chemically inert and stable against oxidation with radicals (especially against OH radicals). Therefore, they are not “washed out” in the troposphere and all of the CFCs are slowly transported into the stratosphere. In the stratosphere, beginning at altitudes above ≈ 20 km, CFCs are photolysed by energetic UV radiation with the ultimate products being mainly ClONO₂ and HCl. These chlorine compounds themselves are not ozone-destroying chemicals. However, they may be converted (“activated”) into ozone-destroying compounds (such as ClO).

In general, about 95 % of the total inorganic chlorine is tied up in the formation of the stable inorganic chlorine reservoirs (HCl and ClONO₂). Therefore, the ozone destruction due to the catalytic cycle (2.3) is not very strong [WMO, 1999]. However, with the presence of polar stratospheric clouds (PSC) in the lower stratosphere of the polar regions during winter and spring, the relation between activated and deactivated chlorine changes drastically, as outlined in the next section. The change from deactivated to activated chlorine due to chemical processes is called ‘chlorine activation’. The reversion to inactive chlorine reservoir species is called ‘chlorine deactivation’.

Chlorine activation can be detected by comparing HCl and HF mixing ratios. HF is photochemically stable and is also released by photolysis from CFCs, resulting in a similar altitude distribution as HCl. A reduction in the HCl/HF ratio is

therefore a good indicator of chlorine activation. On the other hand, an increase of the HCl/HF ratio is an indicator of deactivation of HCl (see Section 2.2.3).

2.2 The Chemistry of Stratospheric Polar Ozone

With the presence of polar stratospheric clouds (PSCs) (see Section 2.2.1) in chemically perturbed conditions the chlorine reservoirs are nearly completely activated by heterogeneous reactions in the Antarctic stratosphere and partly activated in the Arctic. Therefore, a substantial chlorine-catalysed ozone destruction is apparent in both polar regions.

2.2.1 Polar Stratospheric Clouds (PSCs) and Sulphate Aerosols

PSCs are observed during winter in the cold polar region with temperatures below 195 K from the tropopause up to about 26 km height. The exact temperature at which PSCs occur depends on pressure and trace gas abundance and on the precise nature of the particles that form. The composition and formation process of PSCs are still not satisfactorily understood. Following the present scientific understanding, PSCs can be divided into two classes, type I PSCs and type II PSCs. Type I PSCs form at temperatures several degrees above the frost point and are themselves divided into two types, type Ia and type Ib. Type Ia PSCs contain crystalline particles, probably nitric acid trihydrate ($\text{NAT} = \text{HNO}_3 \cdot 3\text{H}_2\text{O}$) or nitric acid dihydrate ($\text{NAD} = \text{HNO}_3 \cdot 2\text{H}_2\text{O}$). The fact that NAT particles actually occur in the stratosphere was recently demonstrated by balloon-borne mass spectrometer measurements in the Arctic polar region [Voigt *et al.*, 2000]. Type Ib contains so-called super-cooled ternary solutions (STS) such as liquid $\text{H}_2\text{O}/\text{HNO}_3/\text{H}_2\text{SO}_4$ aerosols. Type II PSCs are believed to be ice crystals and are much larger than type I PSCs [Peter, 1997]. Typically, they form several degrees Kelvin below the frost point. The characteristic radii of type I PSCs were conventionally assumed to be 0.5–0.1 μm and of type II PSCs 5–20 μm . However, from January to March 2000 large NAT particles with diameters of 10–20 μm (so-called “NAT rocks”) were detected by in situ measurements on high-flying aircraft [Fahey *et al.*, 2001]. Today, the connection between meteorological conditions and particle formation and growth rate is being investigated using various models [Carshaw *et al.*, 2002; Drdla *et al.*, 2002; Mann *et al.*, 2002; Fueglistaler *et al.*, 2002].

Like PSCs, background liquid sulphate aerosol particles are crucial to the ozone chemistry, because heterogeneous reactions can take place on their surfaces. The abundance of sulphate aerosols significantly increases in the lower stratosphere, in the case of strong volcanic eruptions [Wilson *et al.*, 1993; WMO, 1995]. This may have significant influence on ozone destruction. In June 1991, the eruption of Mount Pinatubo in the Philippines was the strongest eruption for several decades. A corresponding increase in the stratospheric aerosol surface

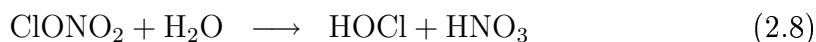
area density (SAD) was measured over the Antarctic in an altitude range of 11–14 km in 1991 [Deshler *et al.*, 1996]. Indeed, in 1991 unprecedented ozone loss was observed at an altitude of 10 to 14 km over the Antarctic, in correlation with the increase of the aerosols below 14 km. By 1994 strongly reduced sulphate aerosol levels were observed and the aerosol burden of the stratosphere is still decreasing today [WMO, 2003].

The influence of the Pinatubo eruption on the Arctic polar vortex was investigated with LIDAR measurements [Wirth *et al.*, 1994; Stein *et al.*, 1994; Girolamo *et al.*, 1994] and backscatter measurements [Larsen *et al.*, 1994]. LIDAR data taken on long-range flights with a Transall aircraft revealed that the core region of the stratospheric polar vortex was mainly free of volcanic aerosols above $\Theta = 485$ K. Below 420 K (≈ 16 km) there was a quicker exchange of air coming from different latitudes [Wirth *et al.*, 1994]. Similar results were found from multispectral LIDAR measurements at Sodankylä [Stein *et al.*, 1994] and from balloon-borne backscatter measurements at Thule, Greenland. There, a clear vortex edge can only be identified above 15 km with respect to the aerosol loading [Larsen *et al.*, 1994]. Evidence for enhanced ozone loss due to the increase of sulphate aerosols in the lower stratosphere is also found in the present work (see Chapter 7).

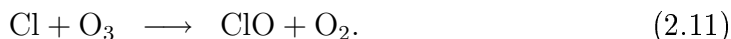
2.2.2 Heterogeneous Chemistry

Heterogeneous reactions take place on PSCs and liquid sulphate aerosols and convert chlorine reservoir species such as HCl and ClONO₂ to active chlorine.

Heterogeneous reactions on the surface of PSCs are

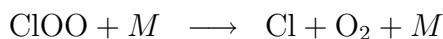
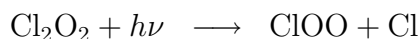


Further heterogeneous reactions on PSCs and sulphate aerosols are described in detail by Peter [1997]; Solomon [1999] and Dessler [2000]. The resulting photolabile forms of chlorine (Cl₂ and HOCl) are photolysed to Cl atoms upon exposure to sunlight even in spring at low sun. Follow-up reactions to ClO are, for example

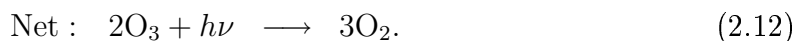


ClO drives the ozone-destroying catalytic cycles in the polar region. These cycles do not involve oxygen atoms and are, therefore, effective at lower altitudes.

The most important catalytic cycle is the ClO dimer cycle, where Cl₂O₂ is referred to as the dimer [Molina and Molina, 1987].

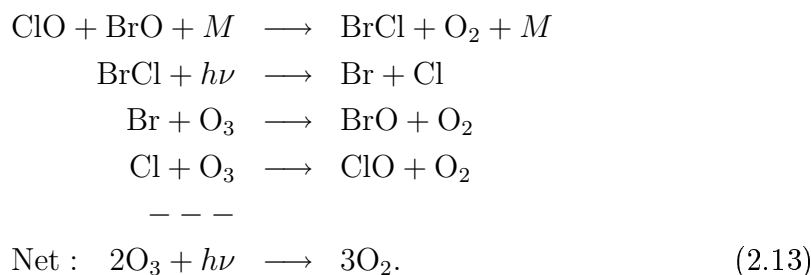


— — —



In darkness and at very low temperatures (below about 200 K) most of the activated chlorine appears in the form of the dimer. Under sunlight conditions and cold temperatures the photolysis rate is much larger than the concurring thermal decomposition of the dimer and the cycle is very effective. Therefore, this cycle is most important inside the lower stratosphere in the polar vortex towards the end of winter. At mid-latitudes the cycle is unimportant, because the ClO abundance is much smaller and the temperatures are much higher.

Moreover, cycles involving bromine and bromine oxide (BrO) are also important [McElroy *et al.*, 1986]:

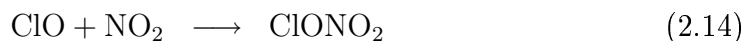


Although inorganic bromine compounds are about 200 times less abundant than chlorine species, catalytic cycles involving bromine are much faster than the ClO dimer cycle. These cycles also effective at higher temperatures, as they are more often apparent in the Arctic, because the dimer is not involved in the reactions. In the Antarctic, the dimer cycle makes up two-third of the ozone loss [Dessler, 2000]. The situation is different in the Arctic. There, the dimer cycle makes up about half of the total loss and the ClO-BrO accounts for most of the remainder. Therefore, the further increase of bromine may have a stronger relative influence on ozone destruction in the Arctic than in the Antarctic. Further catalytic cycles are of relevance such as e.g. the HOCl cycle [Solomon *et al.*, 1986].

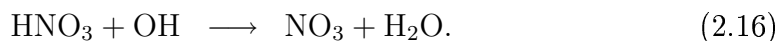
2.2.3 Deactivation of Chlorine

The process competing with chlorine activation is chlorine deactivation. The resulting interruption of catalytic cycles stops the ozone destruction.

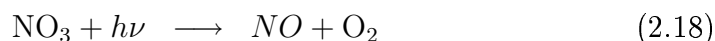
The deactivation of chlorine is mainly controlled by the abundance of HNO₃ in the atmosphere. The major channel for chlorine deactivation in the Arctic polar vortex after the disappearance of the PSCs [Müller *et al.*, 1994; Douglass *et al.*, 1995] is the formation of ClONO₂ via



and is thus limited by the rate of NO₂ released from the HNO₃ reservoir via



Due to the fast rate constant of the reaction of Equation (2.14), as long as high concentrations of ClO prevail, all the NO_x ($\text{NO}_x = \text{NO} + \text{NO}_2 + \text{NO}_3$)¹ produced is converted rapidly to ClONO₂, and thus NO₂ first remains at a very low level. When ClO concentrations have fallen to values low enough for the photolysis rate of ClONO₂ (which increases as the rising sun reaches smaller zenith angles) to exceed the production rate via (2.14), ClONO₂ decreases again. Then, the NO_x concentrations also rise via



From then on, HCl increases via



at the expense of ClONO₂. Therefore, in spring the HCl mixing ratios rise slowly, until the polar vortex breaks down.

2.2.4 Denitrification

Denitrification is the irreversible removal of NO_y ($\text{NO}_y = \text{NO} + \text{NO}_2 + \text{NO}_3 + 2 \cdot \text{N}_2\text{O}_5 + \text{ClONO}_2 + \text{BrONO}_2 + \text{HNO}_3 + \text{HO}_2\text{NO}_2$)² from the gaseous phase, due to the gravitational sedimentation of large ice or NAT PSC particles (see Section 2.2.1). In the Antarctic strong denitrification occurs due to very low temperatures. During the Antarctic winter, HNO₃ is practically completely removed from the lower stratosphere [Dessler, 2000]. Denitrification in the Arctic is less pronounced and much more variable. Nevertheless, in the Arctic winters of 1992–93, 1994–95, 1996–97 and 1999–2000 significant denitrification was observed by Waibel *et al.* [1999]; Kondo *et al.* [2000]; Fahey *et al.* [2001]; Esler and Waugh [2002]; Carslaw *et al.* [2002] and Mann *et al.* [2002].

The removal of NO_y causes a slowing down of the deactivation of chlorine (see Section 2.2.3). A reduced amount of NO_y will delay the recovery of chlorine reservoirs ClONO₂ and HCl and cause a longer period of ozone depletion. The lower denitrification in the Arctic leads to a faster deactivation of chlorine compared to the Antarctic. Nevertheless, several studies have demonstrated that denitrification has a significant impact on ozone depletion in the Arctic [e.g. Waibel *et al.*, 1999; Becker *et al.*, 2000; McKenna *et al.*, 2002]. Further, a model analysis by Grooß *et al.* [2002] showed that in March, 2000, denitrification was responsible for 0.3 ppmv (more than 10 %) of the simulated ozone depletion.

¹NO_x includes the members of the NO_y family which participate in catalytic cycles that destroy ozone, the “active” components of NO_y (described below).

²NO_y represents the abundance of N atoms that are not bound up in either N₂ or N₂O.

Chapter 3

The Arctic Polar Vortex

From about November to March the stratospheric circulation is dominated in high northern latitudes by a strong and persistent cyclonic flow that is commonly referred to as the Arctic polar vortex. The specific conditions inside the Arctic polar vortex, in particular, low temperatures favouring the existence of PSCs are responsible for strong chemical ozone loss (see Chapter 2). The ozone mixing ratio in the polar vortex is influenced by two phenomena, on the one hand, by the chemical ozone depletion, and on the other hand, by transport processes. Changes due to transport processes are often dominant. In the present work a methodology for quantifying the chemical ozone loss is developed and used which does not require a parameterisation of the dynamics of the vortex. The only prerequisite for this tracer-tracer correlation (TRAC) technique, as described in Section 4.1, is that the polar vortex is isolated from the surrounding air. This assumption is definitely valid if the vortex is strong. Usually, the Arctic vortex is less stable than its Antarctic counterpart. It is often more perturbed and temperatures are much more variable during the lifetime of the vortex (see Section 3.1). Therefore, a number of questions have to be addressed with regard to the dynamics of the Arctic vortex and chemical ozone depletion. When is the vortex isolated well enough so that the TRAC technique is valid? What are the characteristics of the vortex boundary and how can the boundary be most suitably defined? Has there been an evolution over past decades of the annual amount of ozone in the Arctic vortex at the time when the vortex forms; i.e. before chemical ozone depletion is expected. These questions are discussed in this and the following chapters.

3.1 Dynamics of the Stratospheric Polar Vortex

First, two dynamic quantities are introduced, the potential temperature and potential vorticity, which are useful for describing the dynamic features of e.g. the polar vortex. The potential temperature Θ of an air parcel is defined as the temperature which an air parcel would have if it were compressed adiabatically to a

standard pressure (p_0) of 1013 hPa

$$\Theta = T * \left(\frac{p_0}{p} \right)^\kappa . \quad (3.1)$$

Here, T and p are the temperature and pressure of the air parcel. $\kappa = R/c_p$ is about 2/7 for di-atomic gases, where R is the gas constant and c_p the specific heat for dry air. The potential temperature of an air parcel remains constant during adiabatic processes, that is in the absence of significant viscous forces or radiative cooling, air parcels stay on isentropic surfaces. For time scales up of to about two weeks (in most parts of the stratosphere) the approximation of adiabatic motion of an atmospheric air parcel is valid. This makes potential temperature a suitable altitude coordinate for many atmospheric applications [Hoskins, 1991; McIntyre, 1992].

Potential vorticity (PV) is a quantity that is widely used in the analysis of atmospheric dynamics [Ertel, 1942a; Hoskins, 1991; McIntyre, 1992]. A general formulation of the conservation principle of PV was formulated by Ertel [1942b,a].

$$\frac{d}{dt}P = 0 \quad \text{where} \quad P = \sigma_v (\nabla \times \mathbf{u} + 2\boldsymbol{\Omega}) \cdot \nabla \Theta \quad . \quad (3.2)$$

Here, \mathbf{u} is the wind velocity, $\boldsymbol{\Omega}$ is the angular velocity of the earth, t is time and $\sigma_v = 1/\rho$ the specific volume. The potential temperature Θ is used as the physical property of the flow that is conserved for individual fluid elements. For hydrostatic flow the vertical component of Equation 3.2 may be written as [e.g., Clough *et al.*, 1985]:

$$P = -g(\zeta_\theta + f) \frac{\partial \Theta}{\partial p} \quad \text{with} \quad \frac{dP}{dt} = 0 \quad . \quad (3.3)$$

ζ_θ is the relative vorticity perpendicular to an isentropic surface, $f = 2\Omega \sin \gamma$ is the Coriolis parameter, where γ is the latitude; g is the acceleration of gravity. A further approximation of potential vorticity (Equation 3.3) valid for the large-scale circulations typical of the stratosphere was given by e.g. Hartmann [1977]; Butchart and Remsberg [1986]:

$$P = -g \zeta_a \frac{\partial \theta}{\partial p} \quad . \quad (3.4)$$

Here, $\zeta_a = \zeta_p + f$ is the component of the absolute vorticity perpendicular to an isobaric surface. The calculation of relative vorticity ζ_p involves differentiation of the horizontal wind components on constant pressure levels. In the absence of diabatic and other non-conservative processes, the potential vorticity is a conserved quantity in an air parcel like the mixing ratio of a chemically inert trace gas. It may be used as a measure of the strength of the polar vortex and its maximum gradient on an isentropic surface as a measure of the location of the transport barrier at the edge of the vortex [e.g., Coy *et al.*, 1997; Nash *et al.*, 1996]. The potential vorticity thus permits a distinction between inside

and outside vortex air masses. On an isentropic surface the vortex edge is characterised as the largest isentropic gradient in PV, thus the vortex edge can be approximately defined by a specific PV value [Müller and Günther, 2003] (see further discussion in Section 3.1.1).

Now, the general large-scale atmospheric circulation will be described briefly. The stratosphere – in an altitude range of about 10–50 km – is statically stably stratified because the temperature increases with altitude. Nevertheless, the stratosphere is not a closed system. The interaction between troposphere,

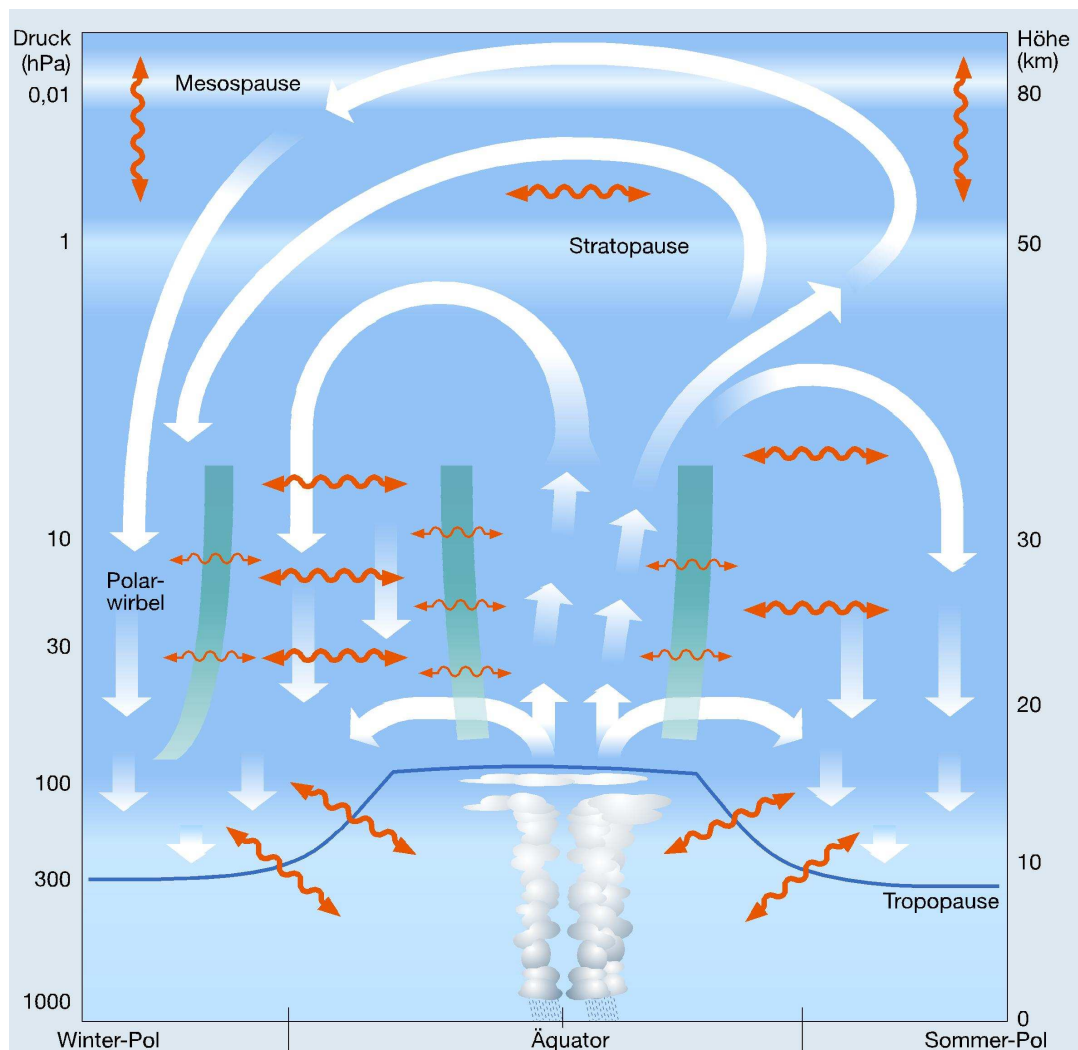


Figure 3.1: Schematic view of the meridional circulation in the stratosphere and interactions between troposphere and stratosphere. The main flow direction of the Brewer-Dobson circulation (see text) is shown in thick white arrows. Transport barriers are shown as thick green bars and orange arrows indicate mixing. Mixing processes in regions of the stratosphere and tropopause occur along isentropic surfaces (U. Schmidt, pers. comm., 2003)

stratosphere and mesosphere are shown schematically in Figure 3.1. The mean meridional circulation in the stratosphere is called the Brewer-Dobson circulation [Brewer, 1949; Dobson *et al.*, 1929].

In the tropics air rises through the tropopause and enters the stratosphere. Today, the idea of a well-defined tropical tropopause is increasingly seen as inappropriate, and instead the concept of a “tropical transition layer” TTL is being put forward. This TTL extends upwards from around 2 km below the top altitude of typical tropical deep convection and has a thickness of about 4 km [Folkins and Appenzeller, 1996]. Within the TTL, there is slow ascent as well as isentropic mixing with the extra-tropical stratosphere. Further, there is to some degree convective overshooting into this region with subsequent mixing. The relative importance of the different processes involved in the upward mass flux, such as slow ascent and energetic convection are still under discussion [Dessler, 2000, and references therein].

Above the TTL there is slow ascent, primarily driven due to extra-tropical waves in the stratosphere. Dissipation of planetary waves in the stratosphere and above lead to meridional flow in mid-latitudes (the so called “wave-driven pump”) and, ultimately, to the descent of air back towards the tropopause over high latitudes.

In addition to the mean meridional transport processes there is isentropic mixing across the subtropical tropopause that transports stratospheric air from the lowermost stratosphere into the tropical upper troposphere and thus across the stratospheric subtropical barrier (the so-called “tropical pipe”). This process is driven by the breaking of synoptic scale waves. Further, there is convective transport of air from the troposphere into the lowermost stratosphere in mid-latitudes.

In winter and spring, the boundary of the polar vortex constitutes a strong transport barrier [e.g., McIntyre and Palmer, 1983]. The isolated vortex is surrounded by a zone with strong isentropic mixing in mid-latitudes due to the breaking of Rossby waves [McIntyre and Palmer, 1983; McIntyre, 1992]. This region is called the “surf zone”. In Section 4.3, the amount of possible exchange though this transport barrier of the polar vortex is discussed in detail.

The Arctic polar vortex forms in autumn as the stratosphere cools radiatively as a result of the meridional temperature gradient. A westerly circulation in the winter hemisphere appears; as expressed as the thermal wind equation [Holton, 1992]. The beginning of the polar winter is defined as the change from easterly to westerly circulation. The time of this turning point of the circulation between September and November is strongly variable from year to year and can be detected in the evolution of total column ozone during the year (see Section 3.3, Figure 3.5).

The polar vortex essentially constitutes a cyclonic low pressure system (see Figure 3.2). It starts forming at altitudes above 40 km [e.g., Manney *et al.*, 2003b] and develops towards lower altitudes at about 380 K potential temperature. An increasingly strong westerly jet stream develops up to 60 m/s [e.g., Holton, 1992; Manney *et al.*, 2003a] and the polar vortex consequently establishes. Therefore,



Figure 3.2: Schematic view of the Arctic polar vortex. The polar jet is indicated in yellow with the strongest velocity of the jet, indicated in orange. Blue arrows indicate the descent of air inside the polar vortex.

the values of potential vorticity rise in the polar region. The boundary of the vortex acts as a kinematic barrier to transport of material into the vortex, as described above. Therefore, the vortex is largely isolated from mid-latitude air. During the Arctic winter, the vortex air continues to cool diabatically causing continuous descent of the air masses. Typical descent rates in the northern hemisphere observed by HALOE between early December and mid-April range from 120 K to 200 K potential temperature [Müller *et al.*, 1996]. The largest fraction of this descent takes place during the early winter months. The rate of descent ($d\Theta/dt$) increases with altitude [e.g., Rosenfield *et al.*, 1994; Müller *et al.*, 1996].

The average temperature inside the vortex is significantly lower than in the surrounding air. Additionally, due to the transport barrier, the chemical composition is substantially different from that of the mid-latitude [e.g., Schoeberl *et al.*, 1992; Nash *et al.*, 1996; Nakamura, 1996]. Any changes in the mixing ratio of chemically long-lived and practically inert compounds inside the vortex are an indication that isentropic horizontal transport between air from inside and outside the vortex has occurred. In Chapter 5 the influence of isentropic mixing across the vortex edge on tracer-tracer relations in an early vortex is outlined.

The winter 1996–97 is further investigated to observe the influence of horizontal transport processes through the vortex barrier during the lifetime of the vortex in 1996–97 (see Section 5.4).

Besides the influences of mixing in, for example, due to filaments, the mean zonal circulation of the polar vortex may be interrupted by a major stratospheric

warming. This event occurs every few years [e.g., *McIntyre and Palmer, 1983; Holton et al., 1995; Manney et al., 1999*]. Enhanced upward propagation of energy from the troposphere by planetary scale waves is essential for the development of such warming effects. The polar jet weakens and becomes distorted by the growing waves and the vortex may temporarily break down. A rapid easterly acceleration occurs in conjunction with a polar warming. Minor warmings occur nearly every winter and are generally followed by a quick recovery of the mean zonal circulation [e.g., *Schoeberl and Hartmann, 1991*]. In the Antarctic, the polar vortex is much stronger and in general no major warming occur. However, in September 2002, a major stratospheric warming was observed for the first time since observations began (see Section 1.2).

3.1.1 The Polar Vortex Edge Region

The polar night jet is the boundary between the polar vortex and the surf zone, and is commonly referred to as the vortex edge. The maximum wind velocity is located approximately at this boundary. The PV distribution in the winter polar region shows high values in the polar vortex core, a high PV gradient at the vortex edge, and a weak PV gradient in the broad region of the surf zone [*McIntyre, 1992; Nash et al., 1996*].

Based on these facts, *Nash et al.* [1996] developed objective criteria for characterising the location of different regions in the northern winter hemisphere vortices. The edge of the vortex is defined “to be the location of highest PV gradient, constrained by the proximity of a reasonably strong westerly jet” (see Figure 3.3, thick green line). The location of the local maximum convex and concave curvature in PV distribution (defined as the maximum of the second derivative of the PV distribution with respect to equivalent latitude) defines the poleward and equatorward edge of the vortex boundary region (see Figure 3.3, thin green lines).

In this work, the following vortex regions are defined. The area polewards of the poleward edge of the vortex boundary region is called vortex core (see Figure 3.3, dark orange area). The entire vortex is defined as the region polewards of the vortex edge, which also includes the vortex core. The boundary region itself is divided into two parts. The outer vortex is the region between the poleward edge of the boundary region and the vortex edge (see Figure 3.3). The outer part of the vortex boundary region is defined as the area between the vortex edge and the equatorward edge of the boundary region.

Using this definition it is possible to make a decision on the exact location with respect to the vortex centre on the basis of available measurements (see Section 4.4). Therefore, the impact of isentropic mixing processes on the chemical ozone loss in different vortex regions can be illustrated (see Chapters 5 and 8).

In earlier studies, where the TRAC method was applied to HALOE measurements [e.g., *Müller et al., 1997b*], the vortex edge definition was more simple. A certain PV threshold was empirically defined for three potential temperature levels for the entire lifetime of the vortex. This procedure resulted in a similar

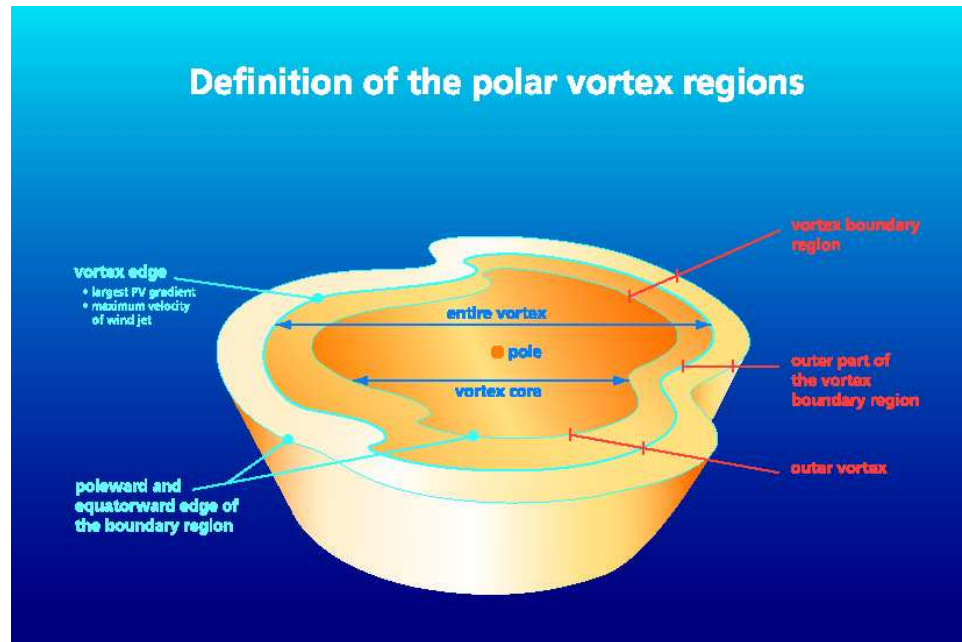


Figure 3.3: Schematic view of the polar vortex regions [Nash *et al.*, 1996].

decision pattern compared to the procedure used in this work. Nevertheless, the influence of profiles which were not sorted correctly in the previous procedure is very significant with respect to the derived ozone loss.

Another enhanced and more accurate method of defining the boundary of the vortex core (the poleward edge of the boundary region) based on high-resolution in situ measurements was introduced by *Greenblatt et al.* [2002]. The large gradient of N_2O across the vortex edge on the potential temperature surface permits a much more precise detection of filaments containing mid-latitude air entering the vortex. However, in terms of calculating ozone loss the Nash criteria are adequate for the identification of the vortex regions on a large scale.

3.2 Dynamical Tracers

Dynamical tracers are chemically long-lived gases. The vertical distribution of the mixing ratio of such gases in the atmosphere may have characteristic structures, resulting from their simple pattern of atmospheric sources and sinks. The dynamic processes, such as vertical advection and horizontal transport, are fast compared with the local chemical lifetime of the dynamical tracers. Ozone also can be considered as a long-lived tracer in winter at high latitudes where the lifetime of O_3 is larger than ≈ 100 days, as long as no halogen-catalysed chemical ozone loss process is active [e.g., *Proffitt et al.*, 1992; *WMO*, 1990].

Besides ozone, measurements of three dynamical tracers are considered in the present work, namely CH_4 , HF and N_2O . The stratospheric chemical life-

time of CH_4 and N_2O is 93 ± 18 years and 122 ± 24 years respectively [Volk *et al.*, 1997]. The only known sink of HF is transport to the troposphere [e.g., Chipperfield *et al.*, 1997]. CH_4 is emitted from the earth's surface and is decomposed by chemical reaction with OH, Cl and electronically excited oxygen atoms. The mixing ratio of CH_4 decreases with increasing altitude. The abundance of tropospheric CH_4 is approximately 1.7 ppmv and decreases to 0.2 ppmv up to the mesosphere. The increase of CH_4 in the troposphere between 1991–92 and 1999–2000 was calculated to be about 60 ppbv [Simpson *et al.*, 2002]. N_2O is also produced by ground emission. Like CH_4 the mixing ratio of N_2O decreases with altitude due to its reaction with excited oxygen atoms and decomposition by photolysis. The tropospheric mixing ratio of N_2O is about 310 ppbv with an approximated increase of 0.3 % per year. Unlike CH_4 and N_2O , HF increases with altitude. The source of HF is located in the stratosphere, where the molecule is produced owing to photolysis of CFCs.

Short-term vertical air motions can be detected by observing vertical profiles of a dynamical tracer, because there is a simple relationship between the mixing ratio of a dynamical tracer and the potential temperature as a measure of altitude. For example, increasing mixing ratios of the tracers CH_4 and N_2O with time at a certain theta level implies an ascent of air. In contrast, an increase of the HF mixing ratio implies a descent of air, due to generally higher mixing ratios of HF at higher altitudes.

3.3 Total Ozone in High Northern Latitudes Based on TOMS Observations

In this section, the evolution of the annual total vertical column ozone is investigated based on satellite observations made by TOMS (Total Ozone Mapping Spectrometer). The Nimbus 7 TOMS data were used for the years 1979 to 1993 and the Earth Probe TOMS (EP-TOMS) from 1996 to 1999, based on the TOMS Version 7 algorithm [Newman *et al.*, 1997].

In the present analysis, in particular the conditions of the turning point from summer to winter circulation of the polar vortex are investigated regarding the minimum of total ozone at that time in high northern latitudes.

In investigating chemical ozone loss it is worth considering the impact of the chemical stratospheric ozone destruction on the vertical column of total ozone. Observations of total ozone by various measurements in the Arctic indicate a downward trend of spatially or time-averaged spring column ozone [Newman *et al.*, 1997; Solomon, 1999; Weber *et al.*, 2002] in the 1990s. The annual ozone column density for twelve years between 1979 and 1999 clearly confirms a tendency to the occurrence of extremely low total ozone columns in spring (see Figure 3.4).

In the summer stratosphere, isentropic exchange between high and mid-latitudes is slow. Due to the NO_x chemistry enhanced by almost continuous sunlight (Equation 2.1) in the summer, the total column ozone decreases from

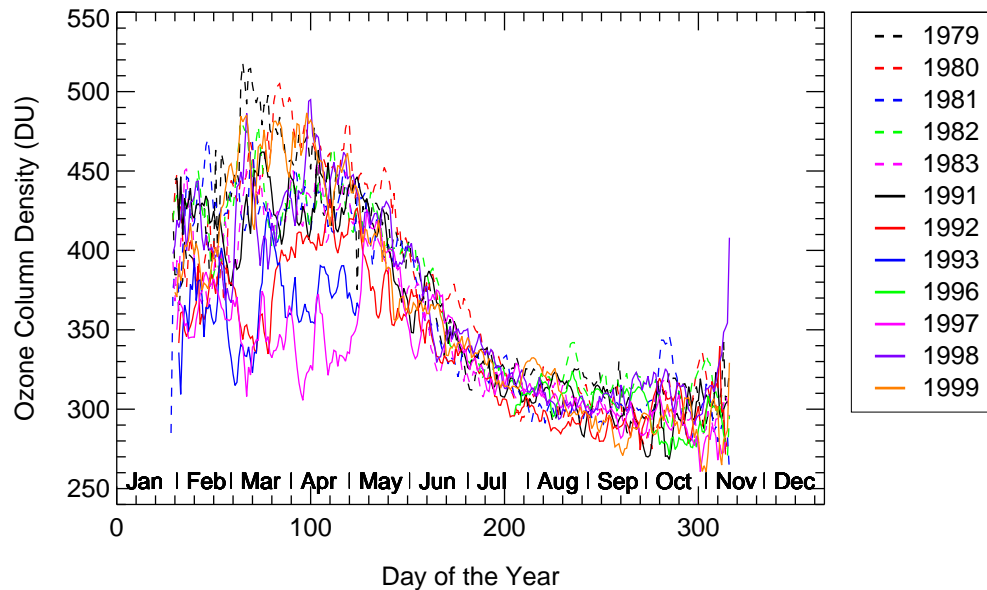


Figure 3.4: The annual ozone column density in DU for twelve years between 1979 and 1999. The area-weighted average of the column density over northern Europe (between 63–90 °N and 25–150 °E) was calculated from the measurements taken by the Nimbus 7 TOMS instrument from 1979 to 1993 and the Earth Probe TOMS (EP-TOMS) from 1996 to 1999.

about 420 DU in May down to below 300 DU in September/October (see Figure 3.4). With the change from summer to winter circulation, the total column ozone increases due to the descent of air and increasing horizontal mixing. In the eighties, the maximum of total ozone reached in March was above 450 DU (see Figure 3.4, dashed lines). In the nineties, the maximum was below 400 K at the beginning of February in some years, due to the strong ozone decrease in spring in the polar region. The total column ozone in March measured by TOMS (see Figure 3.4, solid lines) approached the ozone summer minimum in some years in the nineties. In recent years, three of the last four years, 1998, 1999 and 2001 (not included in Figure 3.4) show relatively high column O_3 , similar to the levels before 1990 [Newman *et al.*, 2002].

The turning point from summer to winter circulation between August and November coincides with the time of the annual total column ozone minimum. Changes in the time of this turning point may be an indication of changes in the global circulation and, therefore, of the earth's climate.

The minimum of the column ozone in September/Mid-November for different years between 1979 and 2000 based on TOMS observations is shown in Figure 3.5, bottom panel. The top panel illustrates the day of the year when the minimum of total ozone occurs, which is thus the turning point of the stratospheric circulation. The dashed line in Figure 3.5, bottom panel, indicates a possible evolution of the minimum of column ozone loss between 1979–99. A decrease in the minimum from 1979 to 2000 of about 10 DU (from 285 DU to 275 DU) can be derived from

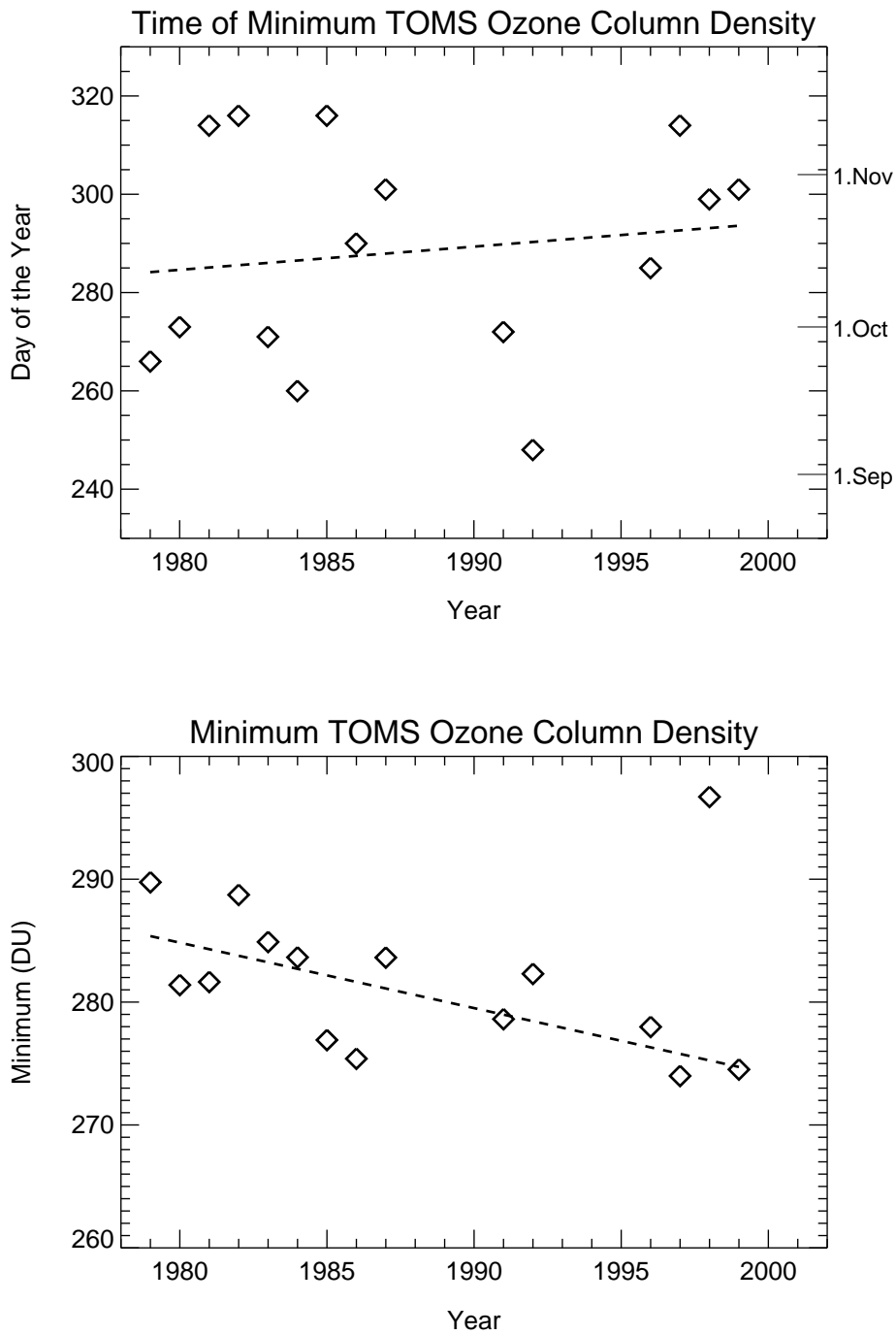


Figure 3.5: The time (in days of the year) of the minimum of TOMS ozone column density in one year averaged over northern Europe is shown in the top panel, for 16 years between 1979 and 2000. The corresponding minimum value in DU of the TOMS ozone column density average over northern Europe (as in Figure 3.4) is shown in the bottom panel. Values were taken from the annual ozone column density (see Figure 3.4) smoothed over four days to eliminate short time variations, such as short term weather phenomena. The dashed lines show the linear fits through the values (see text).

the observations. The minimum value from 1998 which is not included, seems to be an outlier. However, including this value still results in a decrease of about 4 DU. Such behaviour is consistent with a global decrease of total ozone from satellite measurements (SAGE I and II) [WMO, 2003].

On the other hand, over the considered twenty year period, the time of the circulation turning point is much more variable than the value of the corresponding total ozone minimum. Nevertheless, a trend can be identified. There is a delay of about ten days in the occurrence of the turning of the circulation in the late nineties compared to the beginning of this 20-year period (see Figure 3.5, top panel, dashed line). A possible cause for this observation could be a slow down of the global circulation, which would have a serious impact on the Earth's climate.

Chapter 4

The Quantification of Chemical Ozone Loss in the Polar Region

The mixing ratio of stratospheric ozone in the Arctic vortex is determined by two processes, on the one hand, by chemical reactions, and, on the other hand by transport. In particular, the most relevant transport process inside the polar vortex is the diabatic descent of air during winter, as described in Section 3.1. Air with large mixing ratios of ozone is transported downwards into the lower stratosphere where chemical ozone destruction occurs. Ozone variations due to transport are often greater than those due to chemical ozone destruction [e.g., *Manney et al.*, 1994; *von der Gathen et al.*, 1995; *Müller et al.*, 1996]. Therefore, it is necessary to separate these two processes in order to quantify the chemical ozone loss in the stratosphere.

Since the late eighties, a number of approaches have been independently developed to achieve this purpose. The method used here is based on the principle of tracer-tracer correlations, as described in Section 4.1, where transport processes do not have to be described explicitly. Other approaches were developed to separate transport and chemistry employing the explicit calculation of diabatic descent in contrast to the tracer-tracer correlation technique (see Section 4.2). However, the ozone loss deduced by the various methods shows significant discrepancies [*Harris et al.*, 2002]. Further, the validation of the tracer-tracer correlation technique was questioned, and it was suggested that the neglect of mixing across the vortex edge in this technique could lead to a substantial overestimate of the calculated ozone loss [*Michelsen et al.*, 1998; *Plumb et al.*, 2000] (see Section 4.3).

In response to the discussion in the literature, the tracer-tracer correlation technique was improved and extended within the framework of this thesis. New procedures were implemented, as outlined in Section 4.4, which led to significant improvements in the results.

4.1 The Principles of the Tracer-Tracer Correlation (TRAC) Technique

The tracer-tracer correlation (TRAC) technique was originally developed to quantify chemical ozone loss inside an isolated vortex [Proffitt *et al.*, 1989, 1990]. The relation of two long-lived tracers is considered, whereby the measurement location and time of the two tracers has to be (almost) identical. This is the case when using, for example, satellite measurements of the HALOE instrument (see Appendix B.2).

Compact relations are expected between tracers for which the time scale of quasi-horizontal mixing is fast compared to their local chemical lifetime [Plumb and Ko, 1992]. Further, over the course of the winter constant compact relationships are expected for tracers with sufficiently long lifetimes for the air mass inside the polar vortex that is largely isolated from the surrounding air masses [Plumb and Ko, 1992]. Therefore, considering relations between a chemically long-lived tracer (the passive tracer) and a potentially active tracer, which could be subject to chemical or physical change, such changes can be identified as changes in the relations.

Active tracers such as hydrochloric acid (HCl), total reactive nitrogen (NO_y) and ozone are tracers, that may be involved in chemical reactions and, therefore, change their concentrations during the course of the polar winter and spring in the polar stratosphere. NO_y is removed from the stratosphere because it is sequestered in polar stratospheric cloud (PSC) particles, as described in Section 2.2.4. HCl is destroyed by heterogeneous reactions (see Section 2.2.2) and increases due to the deactivation of chlorine. Chemical ozone loss occurs if large concentrations of chemically active halogen compounds are present. This is the case in late winter and spring inside the polar vortex in the presence of sunlight.

In summary, changes in the tracer-tracer relation during the lifetime of the vortex are expected to be possible only due to chemical or physical changes of the active tracer [Proffitt *et al.*, 1989, 1990, 1992; Strahan *et al.*, 1994; Fahey *et al.*, 1990; Borrmann *et al.*, 1993; Müller *et al.*, 1996, 2001; Rex *et al.*, 1999].

To derive chemical losses of the active tracer, first, the tracer-tracer relation has to be determined at a time before the active tracer has chemically changed, which is usually in the early winter when rather little sunlight is present. The mathematically formulated tracer-tracer relation is called “early winter reference function” and is a reference for chemically unperturbed conditions. Further discussion of the determination of the early winter reference function is outlined in Section 4.4.2.

The deviation of late winter and early spring measurements from the early winter reference function are obvious, for example, in the HALOE measurements in the Arctic vortex for the winter 1999–2000 (see Figure 4.1, top panel) where O_3 is the active tracer and HF is the passive tracer.

In this winter, HALOE profiles were measured in the Arctic vortex in February, March, and April. Deviations from the O_3/HF early winter reference function

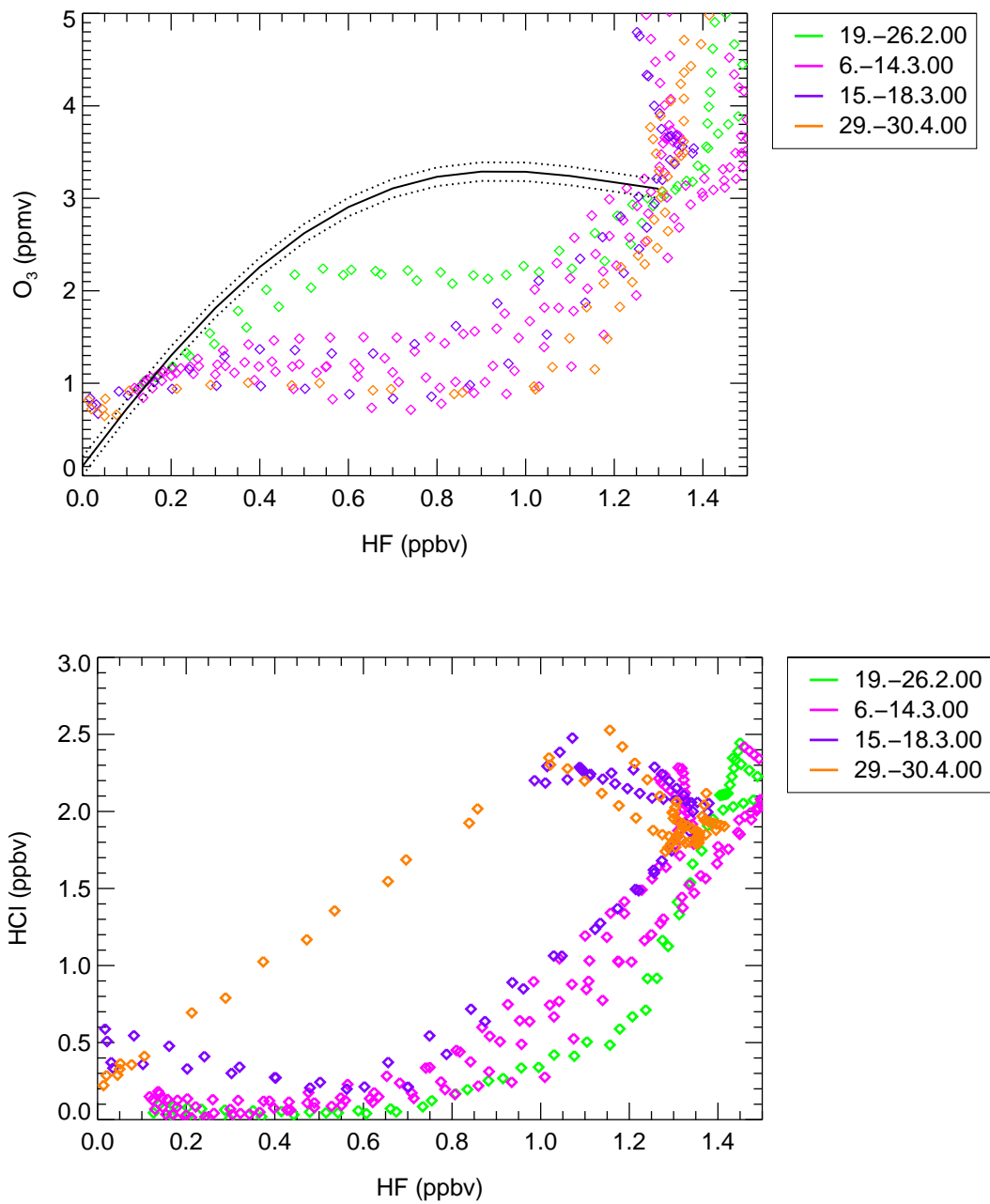


Figure 4.1: Tracer-tracer profiles inside the vortex of the year 1999–2000 from HALOE measurements with HF as the passive tracer. In the top panel, the active tracer is O₃ and bottom panel the active tracer is HCl. The early winter reference functions for the O₃/HF relation 1999–2000, top panel, derived from balloon observations (see Section 7.2), are indicated as a black solid line and the uncertainty of the reference function is represented by black dotted lines. Different colours of profiles indicate the different time intervals when profiles were observed: February (green), first part of March (magenta), second part of March (purple), first part of April (orange).

(black solid line) are already obvious in February and are enhanced in March and April. These deviations from the early winter reference function occur due to ozone destruction by halogen-catalysed reactions (see Section 2.2) [Proffitt *et al.*, 1993; Müller *et al.*, 1996, 2001; Salawitch *et al.*, 2002]. In the course of late winter and spring, ozone depletion increases due to increasing solar exposure of the polar vortex air (in the presence of sufficiently large mixing ratios of active chlorine) and is enhanced in some winters by significant denitrification [Fahey *et al.*, 1990; Fahey *et al.*, 1990; Rex *et al.*, 1999; Esler and Waugh, 2002].

In Figure 4.1, bottom panel, HCl is used as the active tracer. Changes in the HCl/HF relation during spring show very low HCl mixing ratios in February, indicating a strong chlorine activation. The increase of HCl relative to HF in the HCl/HF relation in March and especially in April indicates a recovery of the chlorine chemistry.

To quantify chemical ozone loss with the “ozone-TRAC technique”, the vertical distribution of the ozone mixing ratio of chemically unperturbed conditions¹ has to be compared with the vertical distribution of ozone mixing ratios in spring.

In Figure 4.2 this comparison of vertical ozone profiles is shown for March 2000. The red diamonds indicate the profiles of measured O₃ mixing ratios in March. The corresponding HF profiles, measured at the same time and location in March, are used to derive the ozone profiles expected for chemically unperturbed condition. This is done by converting the long-lived tracer profiles (for example HF) to ozone profiles by the use of the early winter reference function. This is possible because the early winter reference function should not be altered, but remains “frozen in” during the entire lifetime of the vortex as long as no chemical changes take place [Plumb and Ko, 1992]. These ozone proxy profiles (\hat{O}_3) derived in this way are shown as green diamonds (see Figure 4.2).

In this way, chemical ozone loss ΔO_3 can be quantified as the difference between the mixing ratio of the ozone proxy $\mu_{\hat{O}_3}$ the corresponding ozone mixing ratio μ_{O_3} actually measured (see Figure 4.2, black diamonds).

$$\Delta O_3 = \mu_{\hat{O}_3} - \mu_{O_3} \quad \text{where} \quad \hat{O}_3 = F(\text{tracer}) \quad (4.1)$$

The uncertainty of $\mu_{\hat{O}_3}$ is determined by the uncertainty of the early winter reference function F.

Another quantitative measure is the ozone loss in the column density in a certain layer of the stratosphere². Column ozone is usually given in DU; one Dobson unit is 2.69×10^{16} molecules/cm². To obtain the column ozone loss, the difference between the column of measured ozone (Col_{O_3}) and the column of the corresponding proxy ozone ($\text{Col}_{\hat{O}_3}$) has to be calculated.

$$\text{Col}_{O_3 \text{ loss}} = \text{Col}_{\hat{O}_3} - \text{Col}_{O_3} \quad (4.2)$$

¹The ozone mixing ratio of chemically unperturbed conditions is an estimate of the ozone mixing ratio expected if no chemical loss were to occur.

²The total amount of ozone molecules per area integrated over the altitude is called “column ozone” in the unit [molecules per cm²].

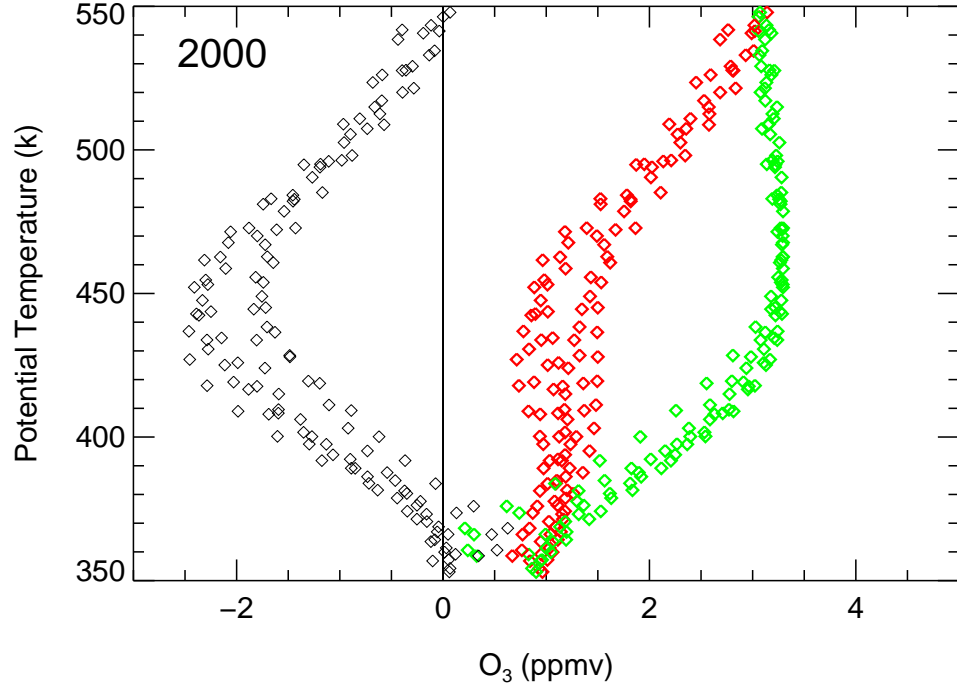


Figure 4.2: Vertical profiles (potential temperature as vertical coordinate) of measured O_3 mixing ratios (red diamonds) by HALOE. The ozone mixing ratios expected in the absence of chemical change, \hat{O}_3 (green diamonds), and the difference in mixing ratio between expected and observed O_3 (black diamonds) are shown for March in winter 1999–2000. \hat{O}_3 was deduced using HF as the long-lived tracer and the early winter reference functions (see Table C.4) from profiles inside the vortex core.

Lower stratospheric ozone loss occurs at altitudes between about 350 and 550 K potential temperature (see Figure 4.2). Thus, the calculated loss inside this altitude range is a good estimate of the ozone loss in the total column.

In detail, the number density of ozone $[O_3]$ (and $[\hat{O}_3]$) in molec/cm³ has to be vertically integrated over a certain altitude range dz (between the geometric heights z_1 and z_2) to obtain the column ozone in units molecules per cm².

$$\text{Col}_{O_3\text{loss}} = \int_{z_1}^{z_2} [\hat{O}_3] dz - \int_{z_1}^{z_2} [O_3] dz \quad (4.3)$$

$[O_3]$ (and $[\hat{O}_3]$) can be written as the ozone mixing ratio μ_{O_3} ($\mu_{\hat{O}_3}$) in ppmv (molecules per million molecules of air) multiplied by the number density of air M (in molec/cm³). Therefore, the column ozone can be calculated as follows:

$$\int_{z_1}^{z_2} [O_3] dz = \int_{z_1}^{z_2} \mu_{O_3} M dz. \quad (4.4)$$

The transformation to pressure coordinates is performed using $dp = -\rho g * dz$:

$$\int_{z_1}^{z_2} [O_3] dz = \int_{p_2}^{p_1} \frac{1}{g} * \frac{M}{\rho} \mu_{O_3} dp \quad (4.5)$$

where the acceleration of gravity $g = 9.81 \text{ m/sec}^{-2}$, ρ : mass density (in g/cm^3) and p = pressure (in hpa).

The ratio of the density of air M and mass density ρ

$$\frac{M(p, T)}{\rho(p, T)} = \frac{N_A}{m_L} = \text{const.} \quad (4.6)$$

is constant³, with Avogadro Number $N_A = 6.02205 * 10^{23} \text{ molec/mol}$ and the molecular mass of dry air $m_L = 29 \text{ g/Mol}$. Therefore,

$$\alpha = \frac{1}{g} * \frac{M}{\rho} = \frac{1}{g} * \frac{N_A}{m_L} \quad (4.7)$$

$$\alpha = \frac{1}{981} * \frac{6.0225 * 10^{23}}{29} \left[\frac{\text{molec} \cdot \text{sec}^2}{\text{cm} \cdot \text{g}} \right] \quad (4.8)$$

$$= 2.116 * 10^{19} \left[\frac{\text{molec} \cdot \text{sec}^2}{\text{cm} \cdot \text{g}} \right] \quad (4.9)$$

$$= 2.116 * 10^{22} \left[\frac{\text{molec}}{\text{hpa} \cdot \text{cm}^2} \right] \quad (4.10)$$

and Equation 4.5 becomes

$$\text{Col}_{\text{O}_3} = \alpha * \int_{p_2}^{p_1} \mu_{\text{O}_3} dp \quad (4.11)$$

The column ozone in a certain altitude range may be expressed in Dobson units (DU):

$$\int_{z_1}^{z_2} [\text{O}_3] dz = \frac{\alpha}{2.69 * 10^{16}} * \int_{p_2}^{p_1} \mu_{\text{O}_3} dp \quad (4.12)$$

$$\int_{z_1}^{z_2} [\hat{\text{O}}_3] dz = \frac{\alpha}{2.69 * 10^{16}} * \int_{p_2}^{p_1} \mu_{\hat{\text{O}}_3} dp \quad (4.13)$$

The main uncertainty in calculating the column ozone loss in Dobson units is introduced through the first term on the right hand side of Equation 4.2; the uncertainty of $\text{Col}_{\hat{\text{O}}_3}$ is largely a consequence of the uncertainty σ of the early winter reference function.

The column ozone loss quantifies the depletion of ozone throughout the lower stratosphere. The maximum of the chemical ozone loss profiles, ΔO_3 , at a certain altitude describes the strength of the local ozone loss. Thus, the description of ozone loss by both ozone loss profiles and column ozone loss covers all aspects of ozone loss.

4.2 Presentation of Several Methods of Calculating Ozone Loss

The TRAC technique was used in various studies in the past several years to calculate chemical ozone loss inside the polar vortex [Proffitt *et al.*, 1989; Müller

³Because of the ideal gas law, $M = (n * N_A)/V = (\rho * N_A) / (RT)$ and $\rho = (n * m_L) / V = (\rho * m_L) / (RT)$ with Volumen V and number of moles n .

et al., 1996, 1997a,b, 2001, 2002; *Salawitch et al.*, 2002; *Tilmes et al.*, 2003]. Further, it was employed to calculate the amount of denitrification (see Section 2.2.4) [*Fahey et al.*, 1990; *Fahey et al.*, 1990, 2001; *Rex et al.*, 1999; *Esler and Waugh*, 2002].

During the past decade a variety of other methods have been developed to calculate stratospheric ozone loss. The methods discussed in this section use meteorological analyses to calculate the effects of diabatic descent from long-wave radiation codes.

The Match technique compares ozone mixing ratios of air parcels that are measured twice within a ten-day period [e.g., *von der Gathen et al.*, 1995; *Rex et al.*, 2002; *Schulz et al.*, 2000]. The difference in ozone mixing ratio detected is interpreted as chemical ozone loss. Match is a pseudo-Lagrangian technique using meteorological data from ECMWF. Three-dimensional air mass trajectories are calculated to determine the location of the air parcel after a certain time period, thus the location of the second measurement location (that matches the air parcel measured before). This “match” can be measured by ozone sondes, with a maximum separation of 500 km displacement, the so-called “match radius”. To derive the vortex average ozone loss with a temporal resolution of about 2 weeks, a statistically significant number of such “matches” is required.

Manney et al. [1996b,a, 1997] and *Manney et al.* [2003a] used ozone measurements taken by the MLS (Microwave Sounder) instrument aboard the UARS satellite to calculate chemical ozone loss for the winters between 1991 and 2000. A Lagrangian transport (LT) model was used to calculate reverse trajectories for periods of a few weeks, based on the meteorological analysis from the UKMO. Measurement of ozone and long-lived tracers are interpolated in time and space to the starting and end points of these trajectories. These values are used to calculate the chemical ozone loss.

The method developed by *Knudsen et al.* [1998] uses the vortex average approach, which is conceptually similar to the one described above. In this approach, trajectory calculations – using meteorological data from ECMWF – were employed to calculate the temporal development of the average of ozone profiles in the vortex, measured by ozone sondes. The calculation of trajectories includes a correction for dynamic changes (the diabatic descent and mixing across the vortex edge from model calculations) to deduce chemical ozone change.

Goutail et al. [1999] used the 3D chemical transport model REPROBUS (Reactive Processes Ruling the Ozone Budget in the Stratosphere) [*Lefèvre et al.*, 1998] to estimate the loss of column ozone in the stratosphere for different winters. To calculate chemical ozone loss, ground-based ozone and balloon-borne measurements, SAOZ (Système d’analyse par observation zénithale) were used [*Goutail et al.*, 1999] as well as satellite measurements POAM (Polar Ozone and Aerosol Measurement) [*Deniel et al.*, 1998]. Proxy values of the ozone mixing ratios, in the absence of chemical changes (“passive ozone”) were calculated with the REPROBUS model. Differences between ozone measurements and passive ozone are assumed to be caused by the chemical ozone loss.

The O₃-TRAC method was previously applied to the satellite measurements

taken by HALOE (see Appendix B.2) to calculate the column ozone loss in the Arctic. For the six winters between 1991–92 and 1996–97 ozone loss was calculated using HALOE data Version 18 [Müller *et al.*, 1996, 1997a, 1999] and in 1999–2000 using Version 19 [Müller *et al.*, 2001].

A comparison of the results of the different methods is given in Table 4.1 and below in more detail, including the results of the present work (see Section 9.2). The results shown are not exactly comparable, because the column ozone loss from different methods was calculated for different altitude ranges (see Table 4.1). Nevertheless, large differences between the results are obvious.

Table 4.1: Calculated chemical loss in column ozone loss in the Arctic in winters 1992–93 to 1996–97. Comparison between HALOE results [Müller *et al.*, 1996, 1997a, 1999] and results from other methods described above.

date	SAOZ/ REPROBUS ^a in 380–600 K	Match ^a in 370–700 K	MLS ^b above 100 hPa	HALOE in 350–550 K
March 1993			55	133 ± 14
March 1994			35	102 ± 10
March 1995	140	127 ± 14	40	116 ± 20
March 1996	125		65	140 ± 20
March 1997	110		40	53 ± 23

^a taken from *Harris et al.* [2002], Table 4.

^b taken from *Manney et al.* [2003a], Figure 13.

4.3 Criticism of the TRAC Technique

A fundamental assumption of the TRAC technique is that transport due to mixing processes between air from inside and outside the vortex can be neglected in a largely isolated vortex.

Studies by *Michelsen et al.* [1998] and *Plumb et al.* [2000] discuss the impact of mixing between air masses from outside the vortex with air inside the vortex on ozone loss estimated on the basis of the TRAC technique. They argue that changes of the ozone-tracer relation during the polar winter could occur in the absence of chemical ozone loss. In particular, the descent of air inside the isolated polar vortex causes a gradient in the tracer mixing ratio at the vortex edge. *Plumb et al.* [2000] suggest that mixing across this transport barrier, for example due to the intrusion of filaments, would cause a so-called anomalous mixing which changes of the tracer-tracer relation.

The stronger the curvature of the tracer-tracer relation, the stronger the changes in the relation due to such mixing processes. The curvature of the tracer-tracer relation depends on the local lifetimes of the two species. Considering two

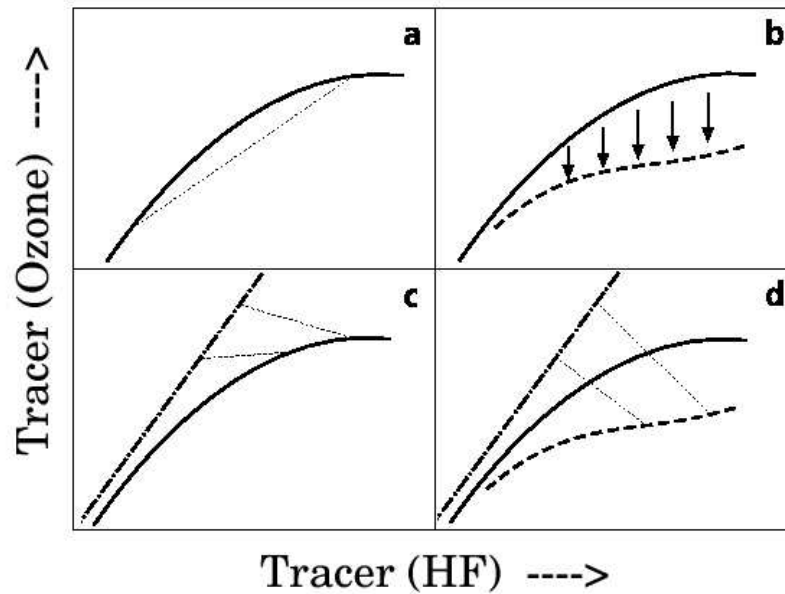


Figure 4.3: Schematic view of the impact of mixing and chemical ozone loss on the ozone-tracer (O_3/HF) relationship inside the vortex, similar to Figure 4.1, top panel. Thick lines indicate ozone-tracer relations, thin dotted lines “mixing lines” showing the results (in tracer-tracer space) of the mixing of two distinct air masses. The solid line (all panels) indicates the “early vortex” ozone-tracer relationship, the dashed line (panel b and d) an ozone-tracer relationship showing the impact of chemical ozone loss, and the dash-dot line (panel c and d) an “outside vortex” ozone-tracer relationship. Panel a shows the impact of the mixing of two air masses having the same initial tracer-tracer relation, panel b the impact of chemical ozone loss on a vortex ozone-tracer relation, panel c the impact of mixing on a chemically unperturbed vortex ozone-tracer relation, panel d the impact of both mixing and chemical ozone loss concurrently on the ozone-tracer relation in the vortex [adapted from, Müller *et al.*, 2001].

tracers with a similar chemical lifetime (for example CH_4 and HF) this relation is quasi-linear, whereas the relation of ozone (which has a much shorter lifetime than e.g. CH_4 or HF) and HF (or CH_4) displays a strong curvature (for example Figure 4.3, all panels, black solid line). The quasi-linear correlation between, for example, CH_4 and HF, cannot significantly change due to anomalous mixing since mixing lines are always linear. Considering a concave curve, as is the case for the ozone-tracer correlation, anomalous mixing would lead to a straight line in a correlation diagram (compare Figure 4.3, panel a, dotted line). Therefore, such changes in the tracer-tracer correlation would be due to mixing. Figure 4.3, panel b, dashed line indicates changes in an ozone-tracer relation caused by chemical ozone loss during spring. In both cases (see Figure 4.3, panel a and b) the deviation from the reference leads to lower O_3 mixing ratios for the same values

of the long lived-tracer. *Michelsen et al.* [1998] and *Plumb et al.* [2000] have put forward the idea that changes of the ozone-tracer relation due to mixing across the vortex edge could be incorrectly interpreted as chemical ozone loss. If this were true, the TRAC technique would overestimate chemical ozone loss.

The problems with this argumentation are discussed in detail in *Müller et al.* [2001]. The TRAC method uses the assumption that the same tracer-tracer correlation holds everywhere inside the vortex. In the critique it is assumed that the same tracer-tracer correlation also holds outside of the vortex during the lifetime of the vortex [*Michelsen et al.*, 1998; *Plumb et al.*, 2000]. However, this is not the case. The ozone-tracer relation outside the vortex clearly shows higher ozone mixing ratios [e.g., *Tilmes et al.*, 2003; *Proffitt et al.*, 2003] (see also schematic view in Figure 4.3, panel c, dashed dotted line). This is due to the poleward transport of tropical ozone-rich air to higher latitudes. Therefore, quasi-horizontal mixing across isentropic lines (see Figure 4.3, panel c, dotted lines) between the tracer-tracer relation inside the vortex and outside the vortex would result in an increase of the O₃-tracer relation to higher ozone mixing ratios.

On the other hand, the difference between the ozone mixing ratio inside the vortex and outside the vortex is even enhanced by chemical ozone destruction inside the vortex (see Figure 4.3, panel b). Therefore, if mixing of air from outside the vortex occurs, the ozone-tracer relation would rise (see Figure 4.3, panel d). This effect should lead to an underestimation of the chemical ozone loss.

In this thesis, this view is confirmed and corroborated through a detailed investigation of mixing across the vortex edge in February and March 1997 based on ILAS observations (see Section 5.4). However, possible mixing between polar air and mid-latitudes in the early winter, when the vortex is not yet formed, is outlined in Section 5.2. Very low ozone mixing ratios, existing at the pole until summer [*Fahey and Ravishankara*, 1999] are mixed in autumn or early winter with higher ozone mixing ratios from mid-latitudes. Therefore, the observed O₃-tracer relation in early winter may still change until the vortex is isolated.

At the end of the winter or in early spring, when the polar vortex breaks down, exchanges between polar air masses and mid-latitude air occurs. The high ozone mixing ratios in mid-latitudes are mixed with the low ozone mixing ratios in the polar region and a recovery of low ozone occurs [*Waugh et al.*, 1997].

All in all, the effect of anomalous mixing through the transport barrier at the vortex would result in an underestimation of ozone loss, but not an overestimation of ozone loss, as is argued by the critics. Furthermore, it is shown in Section 5.4 that these kinds of mixing processes are insignificant when calculating ozone loss.

4.4 Specific Improvements and Extensions in the TRAC Methodology

The TRAC technique, as introduced in Section 4.1, was applied to HALOE observations for several Arctic winters between 1991–92 and 1999–2000. Earlier results

derived using this technique show inconsistencies and deviations from other results. One reason for this was the rapid change of data versions of the HALOE data set used [Müller *et al.*, 1999]. Further, the technique was still under development and no consistent analysis was conducted for all winters. For example, early winter references were derived from profiles partly sorted “by hand”. Moreover, the definition of the vortex edge was less precise.

The ILAS instrument on the ADEOS – operated from November 1996 to May 1997 – provided measurements over high northern latitudes over the entire lifetime of the vortex (see Appendix B.1). This permitted for the first time a detailed study of the evolution of the ozone-tracer relation over the entire winter. Problems of the TRAC technique were identified and eliminated, e.g. the exact definition of the vortex edge. These important improvements of meteorological analysis are described in Section 4.4.1. The exact determination of the early winter reference function is very important to achieve a preferably small uncertainty of the result, as is discussed in Section 4.4.2. In addition, the availability of a consistent HALOE data set (Version 19) (see Appendix B.2) allowed further improvements and enhancements of the technique (see Section 4.4.3).

4.4.1 New Methodology for the Meteorological Analysis

The methodology of the ozone-tracer correlation technique employed in this study has been substantially improved and extended with respect to earlier studies, as described below. A major improvement of the methodology, a modified selection criteria to decide whether profiles are inside or outside the vortex, is described in this section. This improvement is very important for reliable and consistent results, because the characteristics of air masses outside the polar vortex are very different compared to air masses inside the vortex (see Section 3.1.1). The results are very sensitive to changes in the selection algorithm.

In the present work, an algorithm derived by Nash *et al.* [1996] was used to define particular regions of the vortex, the vortex core, the outer vortex and the outer part of the vortex boundary region (see Figure 3.3). The algorithm (described in Section 3.1.1) was applied to the UKMO meteorological analysis at 12 UTC each day and at three different altitudes (potential temperature Θ : 475, 550, 650 K). In this way, a certain threshold PV value on each of the three Θ levels was defined at 12 UTC for each vortex region on each day of the year under consideration. Figure 4.4 displays the temporal development of threshold PV values for different vortex regions, for example of the winter 1996–97. The use of the threshold, calculated in this way, leads to a much more precise definition of the vortex edge than using one definite PV threshold for each theta level during the entire spring, as it was done before.

The HALOE and ILAS instruments made measurements about 15 times per day along two latitude belts, and thus, the locations of the major part of the available measurements do not correspond to the time at which UKMO meteorological analysis is available, which is once a day at 12 UTC. To decide whether a profile measured by the HALOE or ILAS instrument is inside a particular region

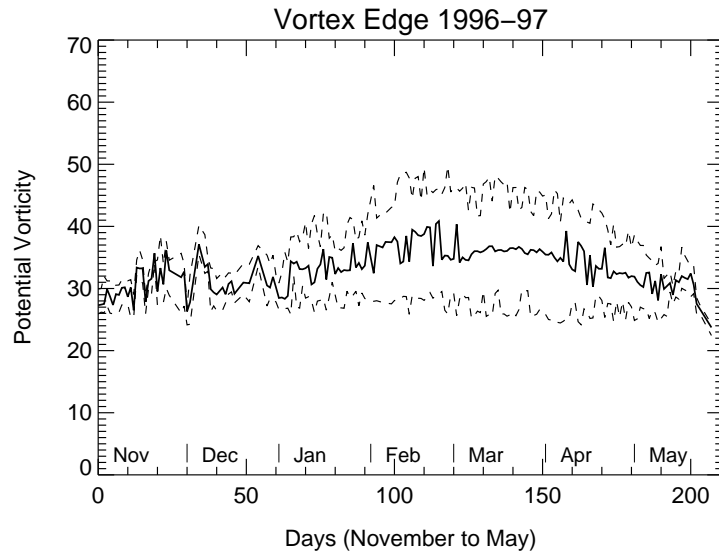


Figure 4.4: Threshold potential vorticity value in PV-units ($1\text{PVU} = 10^{-6} \text{ K m}^2/(\text{kg s})$) for the vortex edge (solid line) and the poleward and equatorward edge of the vortex boundary region (dashed lines) for the winter 1996–97, derived from UKMO data on the 475 K potential temperature level, using the algorithm derived by Nash *et al.* [1996].

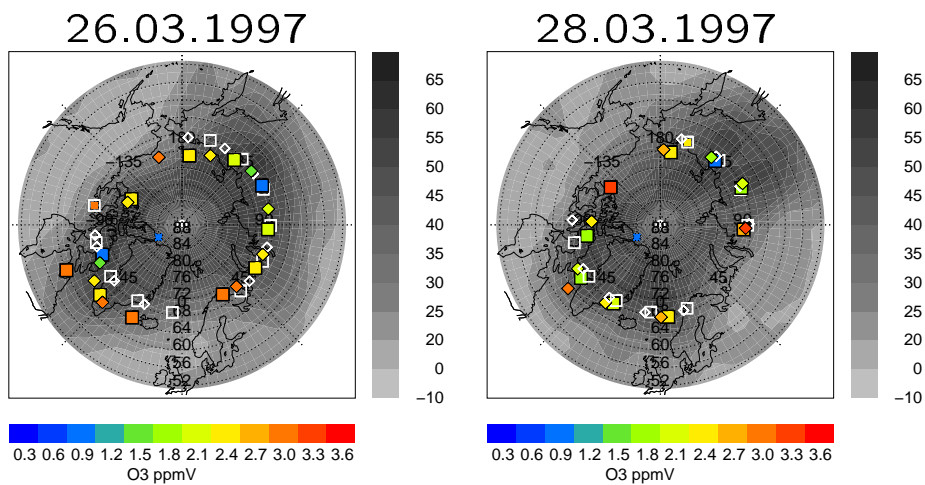


Figure 4.5: The potential vorticity derived from UKMO data on the 475 K potential temperature level valid for March 26 and 28, 1997 12 UTC, shown on a grey scale. For the same Θ level, ozone mixing ratios in ppmv as derived from the satellite profiles are represented as colour-coded diamonds (ILAS) and squares (HALOE), the location of profiles measured by ozone sondes is presented as a colour-coded asterisk. All satellite profiles were repositioned to 12 UTC by trajectory calculations. Also shown are the positions of satellite profiles at the time of measurement (different from 12 UTC) in white diamonds (ILAS) and squares (HALOE) (copyright by AGU).

of the vortex – using the PV threshold derived with the Nash algorithm – the location of each measured profile has therefore to be repositioned to noon. In the present work, trajectory calculations were used to reposition the location of HALOE and ILAS profiles to 12 UTC [Morris *et al.*, 1995] (see Figure 4.5).

This new methodology for the meteorological analysis permits a much more detailed and consistent analysis of the measurements of all considered winters.

4.4.2 Improved Determination of the Early Winter Reference Function

It is necessary to derive an early winter reference function to determine chemical ozone loss. As described above, the early winter reference function is a mathematically formulated tracer-tracer relation for chemically unperturbed conditions. To derive this reference function, the observation time of the underlying profiles considered has to be chosen carefully.

The turning point from summer to winter circulation describes the formation of the polar vortex (see Section 3.3). Thus, the time of the minimum of the ozone column density (see Figure 3.5) is the earliest time at which the early winter reference function can be determined. On the other hand, it may be not the most suited time if the early vortex is not yet strong enough, because horizontal mixing across the vortex edge may change the tracer-tracer relation without chemical changes. A case in point is the winter 1996–97, where the tracer-tracer relation changed until the beginning of January 1997, due to horizontal mixing processes (as described in detail in Section 5.2).

In summary, the early winter reference function has to be determined at a time when the vortex has already formed and, additionally, is sufficiently isolated from mid-latitude air, but early enough so that no ozone loss has already taken place. Therefore, if the vortex is isolated, the reference function has to be derived as early as possible, if observations are available, to be sure that no chemical changes have already occurred.

In practice, in most years considered, only a few observations are available inside the early vortex each winter, other than for the winter 1996–97 (see Chapter 5). For example, in winter 1995–96 the HALOE instrument measured only three profiles inside the outer early vortex; still inside the vortex edge in November 18–23, 1995. At this time, the vortex was already formed and isolated (as could be seen on the basis of meteorological analysis from UKMO). Considering Figure 3.5, top panel, black line, the vortex started forming at the beginning of November. Although there are no measurements between the beginning of November and November 18–23, no chemical ozone loss can be expected, because no chlorine activation was found in November 18–23, and is therefore not expected before. At the end of January (see Figure 4.6, bottom panel) strong chlorine activation can be identified due to the changes in the HCl/HF relation (see Figure 4.6, bottom panel), but still no changes in the O₃/HF relation are detected (see Figure 4.6, top panel). Therefore, this single January profile would still describe an undisturbed O₃/HF relation. Thus, the early winter reference

function in this winter was derived from both November and January profiles.

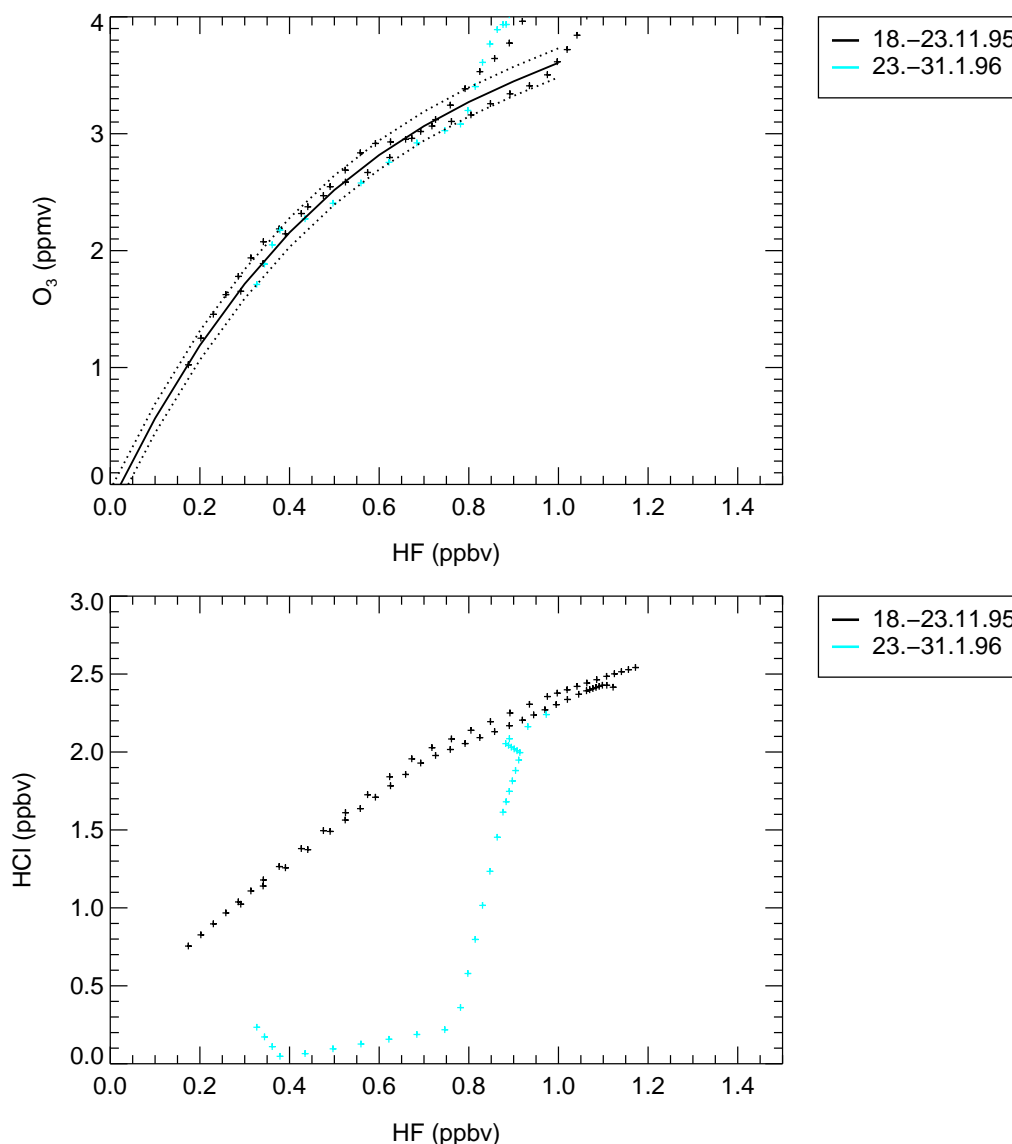


Figure 4.6: Tracer-tracer profiles inside the outer early vortex of the year 1995–96 from HALOE measurements with HF as the passive tracer. In the top panel, the chemical active tracer is O₃ and in the bottom panel the chemical active tracer is HCl. The early winter reference function for the O₃/HF relation 1995–96, top panel, is indicated as a black solid line and the uncertainty of the reference function is represented by black dotted lines.

The consideration of the value of “area of possible PSC existence” is useful to draw conclusions on possible chlorine activation and therefore possible ozone loss in a certain time period, for example, if no other measurements are available. In this way, it is furthermore shown that significant chlorine activation is not

possible without the existence of PSCs (see Section 7.3). The area of possible PSC existence describes the total area on a certain potential temperature level, where the temperature (determined from the UKMO analysis) does not exceed the PSC threshold temperature. This PSC threshold temperature was calculated [Hanson and Mauersberger, 1988] for a HNO_3 mixing ratio of 10 ppbv and a H_2O mixing ratio of 5 ppmv. The area of possible PSC existence is shown in Figure 4.7, for example, the winter 1995–96 from November to April as a function of altitude. The first time PSCs possibly exist at the beginning of December 1995, are in agreement with no chlorine activation being detected from HALOE observations in November 1995 and significant chlorine activation being detected in January 1996.

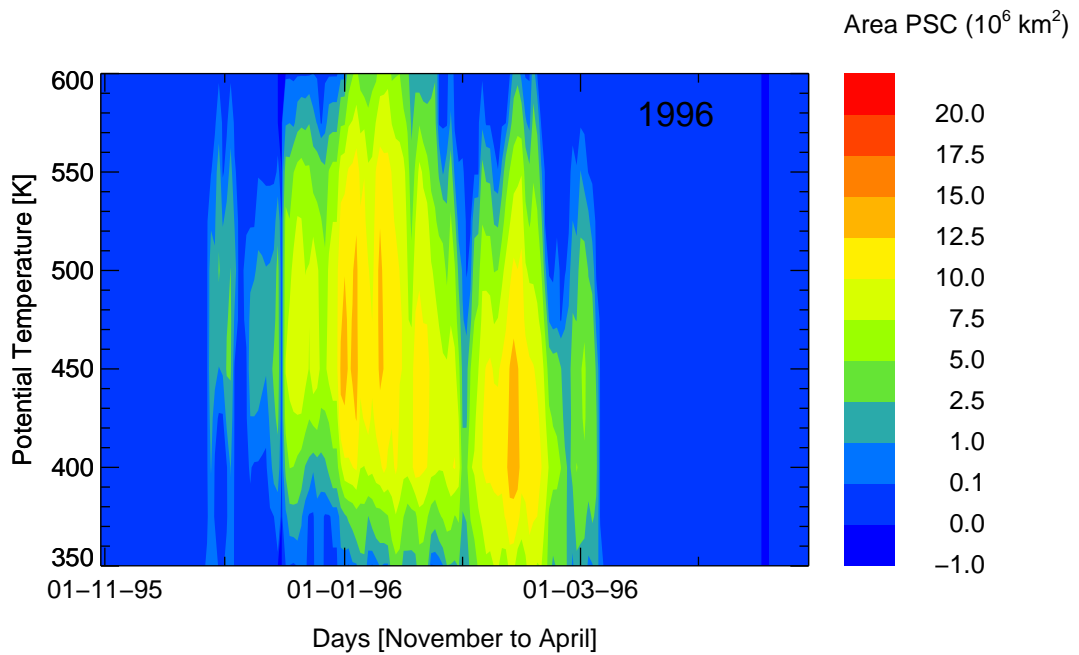


Figure 4.7: Area of possible PSC existence over the entire polar vortex as a function of altitude, shown for the winter 1995–96 from November 1995 to April 1996, determined from the meteorological analysis from the UKMO and from the PSC threshold temperature calculated for HNO_3 mixing ratio: 10 ppbv and H_2O mixing ratio: 5 ppmv.

The early winter reference function is fitted by a third or fourth order polynomial. As an example, Figure 4.6, top panel, shows the fitted early winter reference function as a black line. Here, values on the x axis are given in ppbv and values on the y axis are given in ppmv. The functional representation of this relation is:

$$y = 1.92 \cdot x^3 - 6.08 \cdot x^2 + 7.93 \cdot x - 0.17 \quad , \quad (4.14)$$

where y gives the ozone mixing ratio μ_{O_3} in ppmv and x the HF mixing ratio μ_{HF} in ppbv. This relation holds for a range of $0.1 \text{ ppbv} < \mu_{\text{HF}} < 1.0 \text{ ppbv}$. The

uncertainty of the ozone mixing ratio of this reference function is $\sigma = 0.12$ ppmv. σ is the standard deviation of the observation points from the fitted reference function.

For the winters considered, improved early winter reference functions were derived, using HALOE measurements (if available) inside an isolated vortex, in the same way as described above. Also, additional data sources such as ILAS satellite data, balloon measurements, and ozone sonde data were used to derive the reference functions. In this way, in nine out of eleven years reliable early winter O₃-tracer reference functions could be derived (see Section 7.2 and Figure 7.8).

No early winter reference function could be derived directly for the winters 1997–98 and 2000–01, due to the lack of measurements inside the early vortex for these two years (see Section 7.2). In the present work, the TRAC technique is extended so that it is possible to estimate single reference functions valid for each of these two years. For this purpose, all the HALOE measurements available inside the early vortex over a period of six years were averaged. Additionally, the HF and CH₄ growth rate per year was included, as described in detail in Section 7.2. Therefore, chemical ozone loss can be calculated for all the eleven years between 1991–92 and 2001–02.

4.4.3 Specific Improvements to the HALOE Analysis

Besides the improvements with respect to meteorological analysis and the calculation of the early winter reference function, further improvements were made to the HALOE analysis in this work. The HALOE instrument measures two long-lived tracers, namely CH₄ and HF. Each of the tracers can be used to calculate chemical ozone loss with the TRAC technique. Additionally, the use of these two long-lived tracers enable a further improved selection of the HALOE profiles, as described in the following section.

The relationship between CH₄ and HF does not change significantly over the whole lifetime of the vortex in each year, as described in Section 7.1. Therefore, profiles deviating by more than 0.2 ppmv from the constant CH₄/HF relation are neglected in order to eliminate profile observations that are uncertain or influenced by air from outside the vortex.

The improved selection of profiles during the winter and improved determination of the early winter reference function clearly reduces the uncertainty of the calculated ozone loss. An error analysis is consistently performed for all the years in the present work. The major uncertainty in the results arises from the determination of the early winter reference function, due to variability in the ozone-tracer relations inside the early vortex. The scatter of the ozone-tracer relations arises, on the one hand, due to variability of the mixing ratios of tracers inside the vortex, and, on the other hand, they may possibly be due to the random error of the satellite measurements. These uncertainties are estimated with the calculation of the standard deviation of the profiles contributing to the early winter reference function. Further, any systematic error of the satellite measurements is not taken into account, because assuming that all available measurements of one satellite

are affected in the same way it would therefore have no impact on the ozone loss calculation.

To derive results with minimum uncertainty, it is also necessary to calculate ozone loss in the appropriate altitude range. Ozone loss is therefore calculated for a maximum altitude range of 380–550 K from HALOE observations, because within this range the empirical ozone-tracer reference relations are valid. Earlier studies calculated the column ozone for an altitude range of 350–550 K (see Table 4.1). These results are more uncertain, since the early winter reference function is not necessarily valid below 380 K. For example in winter 1999–2000, the ozone-tracer profiles (see Figure 4.1, top panel) scatter above the derived early winter reference function at altitudes below the 0.15 ppbv HF level. Although the altitude range between 350 and 380 K level is small, these values significantly influence the calculated column of ozone loss, because the molecule density at lower altitudes is much larger compared to higher altitudes. Further, the uncertainty of calculated ozone loss increases at lower altitudes due to the decreasing precision of the satellite measurements (see Table B.1). A comparison of calculated ozone loss between the altitude ranges of 350–550 K and 380–550 K is shown in Table 9.1. The tracer values from ILAS observations (here N₂O) greatly scatter at altitudes lower than 450 K, thus the ILAS ozone loss is calculated for an altitude range of 450–550 K.

A further major improvement, with respect to new scientific insights, is the application of the TRAC technique over an eleven-year period. The consistent evaluation of all eleven winters, between 1991–92 and 2001–02, allows the chemical ozone loss and meteorological features of each winter to be compared. This allows conclusions to be made on the coupling between climate change and ozone loss.

Chapter 5

Verification of the (TRAC) Technique Using ILAS Data in 1996–97

The ozone-tracer correlation technique, as described in the previous chapter, is now verified with the use of the ILAS satellite data set. The improvements to the TRAC technique (see Section 4.4) are implemented in the procedure of the analysis and are further discussed in this section.

The ILAS observations are made over high northern latitudes and are available for the entire lifetime of the polar vortex in 1996–97. First, the meteorological situation of the winter 1996–97 is described (see Section 5.1). In Section 5.2, the evolution of ozone-tracer relations is considered for the early vortex from November 1996 to January 1997 and for the isolated vortex from January to April 1997 and, moreover, in vortex remnants in May 1997 (see Section 5.3). Further, the influence of horizontal mixing across the transport barrier at the vortex edge is discussed in Section 5.4. The main parts of Sections 5.2 and 5.3 are adapted from *Tilmes et al.* [2003].

The tracers CH_4 and N_2O measured by ILAS are in principle suitable for the ozone-tracer correlation method, but the data quality is only adequate for N_2O . CH_4 was not used because the ILAS Version 5.2 CH_4 data still differ from the validation data with the magnitude of the discrepancy depending on season [*Kanzawa et al.*, 2002].

5.1 Meteorology of the Polar Vortex 1996–97

A short overview of the meteorology of the polar vortex 1996–97 is given in this section to provide a basis for the discussion of the evolution of the observed O_3 -tracer relation in the following sections.

In winter 1996–97, the polar vortex formed relatively late. Before it was fully established at the end of December, horizontal mixing between air from inside and outside the vortex occurred and the minimum temperature remained above

195 K. After the late formation, the vortex was very cold and strong. At the 475 K potential temperature level, the lowest temperatures in an 18-year data set were reached in this year in March and April (temperatures were below the PSC threshold of about 195 K (see Section 2.2.1) until the beginning of April) inside the vortex core [Coy *et al.*, 1997]. In March, the vortex core was small and strong whereas the boundary region was wide.

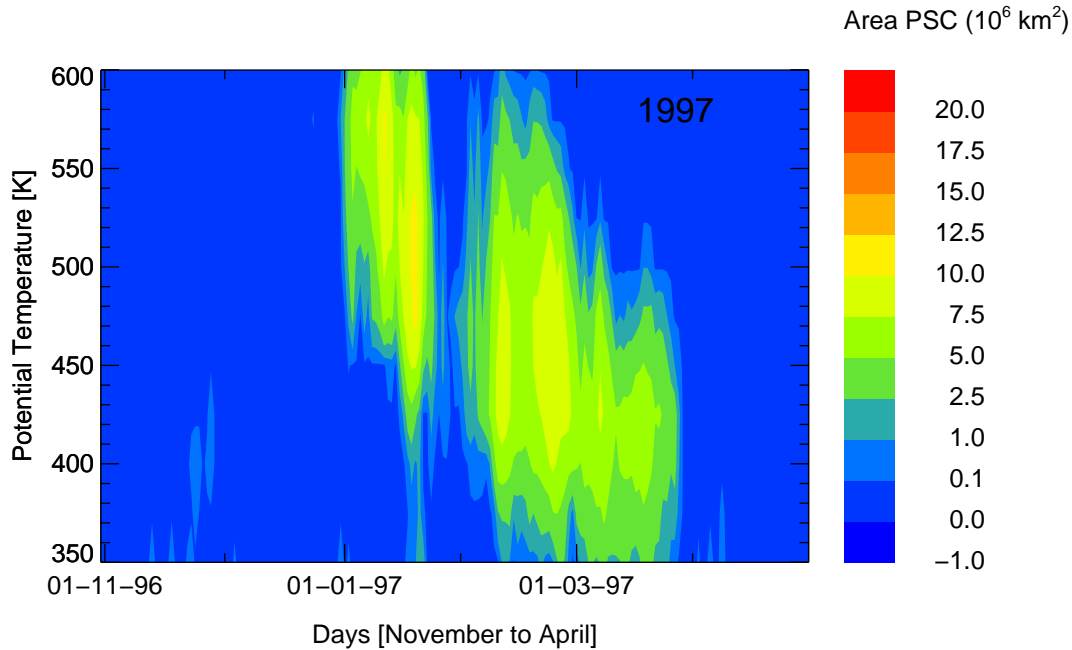


Figure 5.1: Area of possible PSC existence over the entire polar vortex, as a function of altitude, is shown for the winter 1996–97 from November 1996 to April 1997, determined from the analysis from the UKMO and from the PSC threshold temperature calculated for HNO_3 mixing ratio: 10 ppbv and H_2O mixing ratio: 5 ppmv.

In Figure 5.1, the area of possible PSC existence during the winter 1996–97 (see Section 4.4.2) from November to April is shown. PSC occurrence was not possible before January 1997 (see Figure 5.1), therefore no chlorine activation and thus no ozone loss can be expected in November and December 1996. Until the end of March the temperatures were low enough for possible PSCs, the potential for chemical ozone loss. During mid-February, this potential was enhanced by significant denitrification [Kondo *et al.*, 2000].

5.2 Evolution of Ozone-Tracer Relations in the Early Vortex

For the application of the ozone-tracer technique it is necessary to derive an early winter reference function. This reference function represents an ozone-tracer rela-

tion for chemically unperturbed conditions inside the isolated vortex, as described in Section 4.4.2. It is necessary to ensure that the vortex is fully established when the early winter reference function is derived, because horizontal isentropic mixing across the vortex boundary may change the ozone-tracer relation, as described in Section 4.3. In this section, it is shown that changes in the ozone-tracer relation are possible if the polar vortex is not yet well isolated as is the case in November and December 1996.

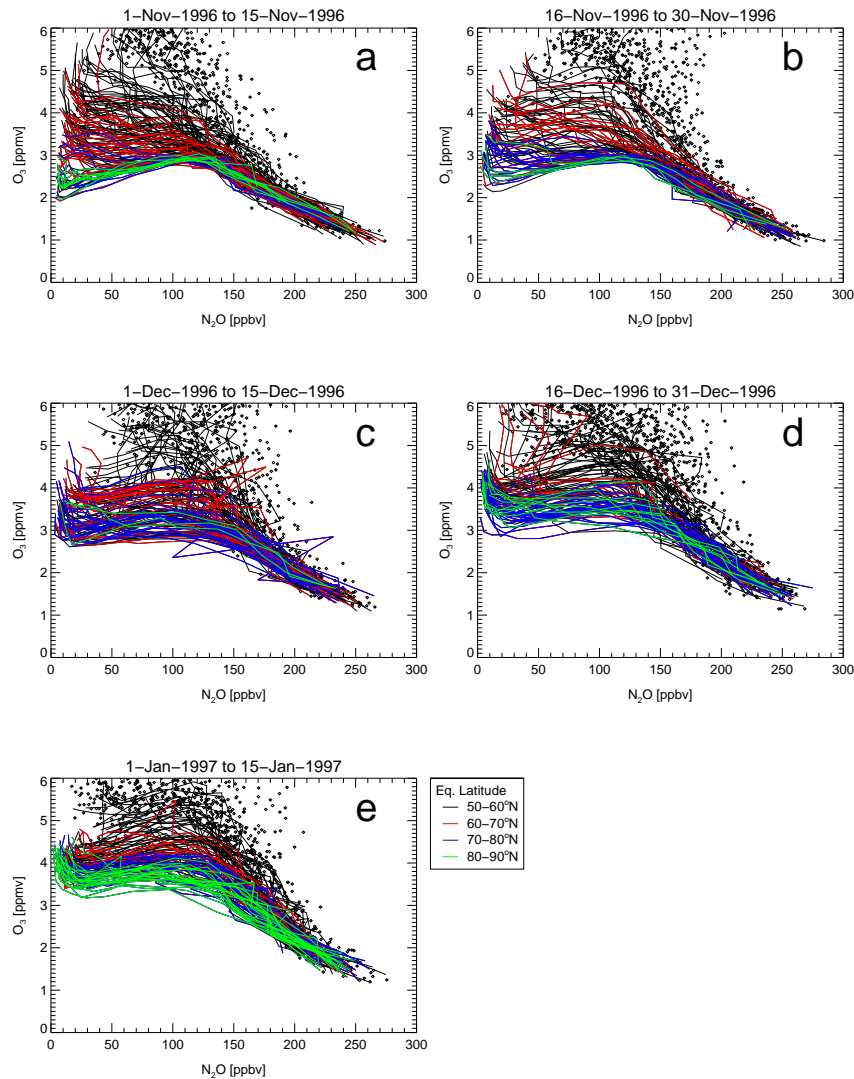


Figure 5.2: O_3/N_2O [ppmv/ppbv] relation of ILAS observations is shown for different time periods (at the top of every panel). Different line colours indicate different parts of the vortex, sorted by different equivalent latitudes, 50–60°N black, 60–70°N red, 70–80°N blue and 80–90°N green. Black diamonds indicate all other profiles outside the vortex, with an equivalent latitude < 50°N. Only every third of the observed profiles is shown in red for better readability (copyright by AGU).

Utilising the large number of profiles measured by ILAS in November and December 1996 in high latitudes, it is possible to describe the evolution of the ozone-tracer relation inside and at the edge of the early vortex with N_2O as the long-lived tracer (see Figure 5.2). The different colours of the profiles of the ILAS observations denote different parts of the vortex sorted by the equivalent latitude at three isentropic levels: 475, 550 and 675 K [e.g., Lary *et al.*, 1995]. Profiles with an equivalent latitude between 50 and 60°N are measured outside the vortex (black lines). Red lines indicate profiles located at the edge (equivalent latitude $60 < 70^\circ\text{N}$), blue profiles are measured inside the vortex towards the edge (equivalent latitude $70 < 80^\circ\text{N}$), and green profiles are measured inside the vortex towards the core (equivalent latitude $> 80^\circ\text{N}$). All other profiles outside the vortex with an equivalent latitude lower than 50°N are indicated as black diamonds.

From November to January there is a separation of profiles inside (coloured profiles) and outside the vortex (black profiles) (see Figure 5.2, all panels). The relation of profiles inside and at the edge of the early vortex changed over the course of this period. At the beginning of November when the vortex began to form, there was a large scatter of the ozone mixing ratios from 2 to 4.5 ppmv at higher altitudes ($\text{N}_2\text{O} < 130$ ppbv, above ≈ 400 K) (see Figure 5.2, panels a and b). Mixing across the vortex edge was strong enough to change the relation in the vortex core in November and December and led to an increase of ozone in the vortex, so that the very low ozone mixing ratios of 2 ppmv had vanished by January. During the first half of December the vortex was strongly disturbed by air from outside due to mixing processes. Profiles between 70° – 80° equivalent latitude (blue profiles in Figure 5.2 panels c and d) inside the vortex show a stronger scatter in December than in November. Towards the end of December, the vortex became stronger and more isolated. From then on, the $\text{O}_3/\text{N}_2\text{O}$ relation did not change significantly until mid-January.

In January, there was still some mixing of air from outside the vortex to the edge of the vortex (see Figure 5.2 panel d, red lines). However, inside the vortex towards the core (see Figure 5.2 panel d, green lines) the ozone-tracer relation became more uniform and was no longer influenced by mixing processes (see Section 5.4). A similar result was likewise obtained for winter 1999–2000 by Ray *et al.* [2002]. Thus, the early winter reference function can be deduced from observations obtained at the beginning of January.

5.3 Evolution of Ozone Loss over the Entire Lifetime of the Vortex

The temporal evolution of the destruction of ozone inside the polar vortex can be followed chronologically by analysing the ILAS $\text{O}_3/\text{N}_2\text{O}$ relation (see Figure 5.3).

An early winter reference function for winter 1996–1997 was fitted to the ILAS profiles inside the early polar vortex for the period January 1–8 (see Section 5.2). Using N_2O as a long-lived tracer (mixing ratios in ppbv) and O_3 (mixing ratios in ppmv) the early winter reference function of $\text{O}_3/\text{N}_2\text{O}$ is characterised by the

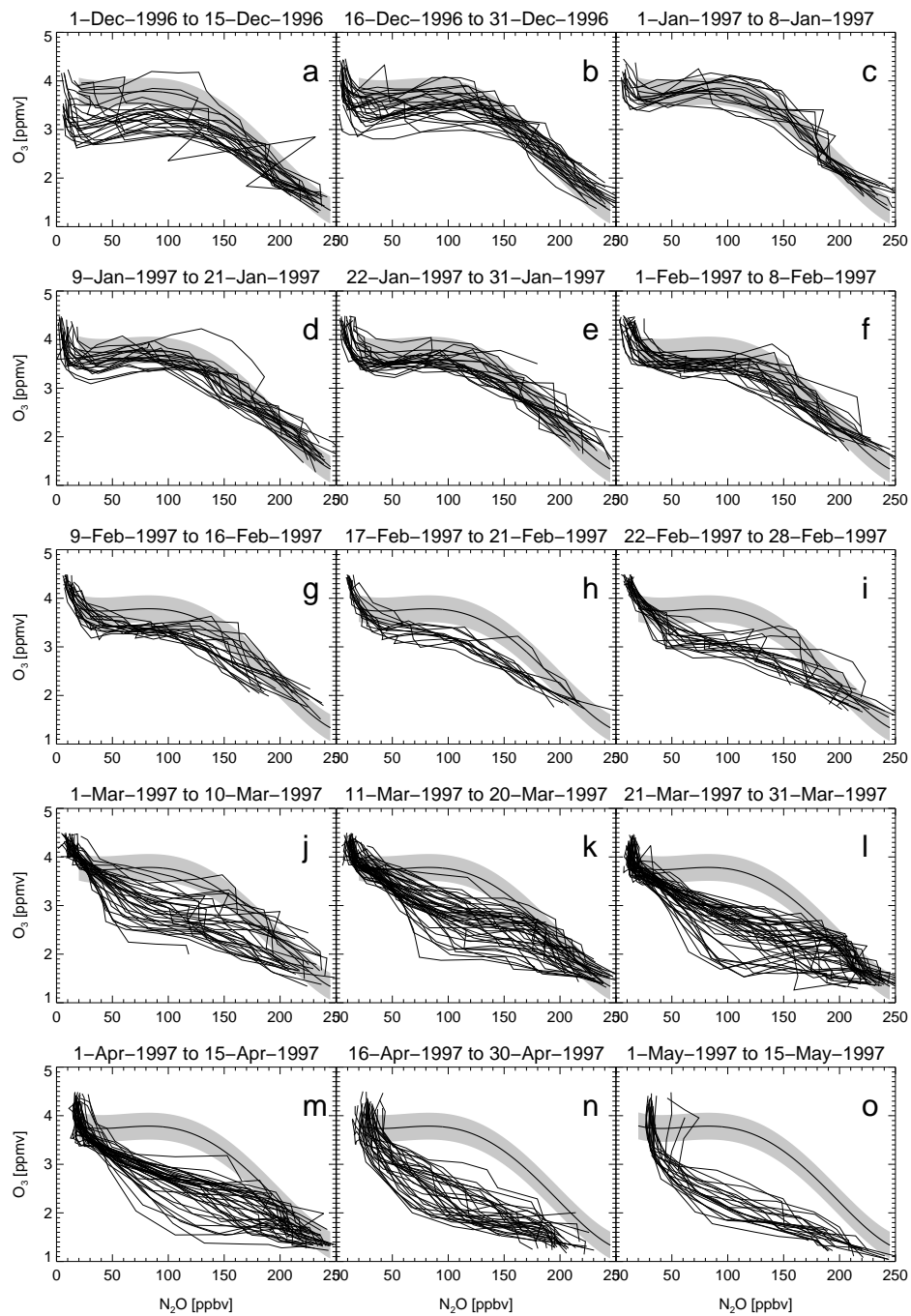


Figure 5.3: O₃/N₂O [ppmv/ppbv] relation of ILAS observations inside the polar vortex for different periods from December 1996 to May 1997. Thin black lines indicate the different profiles with an accuracy larger 40 ppbv for N₂O and larger 0.5 ppmv for O₃. The thick black line in every single panel indicates the calculated early winter reference function (Equation 5.1), fitted to data for the period January 1–8, with the uncertainty indicated by the area shaded in grey (see text) (copyright by AGU).

polynomial:

$$y = 4.84 \cdot 10^{-9} \cdot x^4 - 2.50 \cdot 10^{-6} \cdot x^3 + 3.47 \cdot 10^{-4} \cdot x^2 - 1.71 \cdot 10^{-2} \cdot x + 4.01 \quad , \quad (5.1)$$

where the y axis describes the ozone mixing ratio μ_{O_3} in ppmv and the x axis describes the N_2O mixing ratio $\mu_{\text{N}_2\text{O}}$ in ppbv. The reference function is valid for range $20 \text{ ppbv} < \mu_{\text{N}_2\text{O}} < 250 \text{ ppbv}$ and has an uncertainty $\sigma = 0.28 \text{ ppmv}$ (see Figure 5.3). σ is shown in all panels of Figure 5.3 with the corresponding uncertainty indicated by the area shaded in grey.

The changes in the ozone-tracer relation that are due to isentropic mixing processes caused by an incomplete isolation of the early vortex (panels a and b) have been discussed (see Section 5.2). In January, the $\text{O}_3/\text{N}_2\text{O}$ relation inside the vortex is inside the range of uncertainty of the early winter reference function (see Equation 5.1, Figure 5.3, panels c, d and e). Deviations from the reference function due to the chemical destruction of ozone by active halogen compounds are expected to increase with increasing sunlight duration. This is observed in the ILAS data. At the beginning of February, profiles scatter somewhat below the reference function for N_2O smaller $\approx 120 \text{ ppbv}$ in the $\text{O}_3/\text{N}_2\text{O}$ relation. This deviation from the reference function above 450 K potential temperature indicates the beginning of chemical ozone loss (see Figure 5.3, panel e). After mid-February, deviations of the early winter reference function are clearly noticeable and become more and more pronounced in the course of spring (see Figure 5.3, panels f to m). Between mid-March to early April (see Figure 5.3, panels k to m) deviations of ozone-tracer profiles from the early winter reference function are separated into two groups, one group shows moderate deviations of the reference function, the other group shows strong deviations. From the middle of April to May, the deviation from the reference function becomes more and more uniform (see Figure 5.3, panels n and o). In May, low ozone mixing ratios are consistently measured inside the vortex core.

Table 5.1 summarises the average of the derived column ozone loss between 450–550 K for different time intervals and for different parts of the vortex. The column ozone loss is calculated from the end of February to the middle of May. The TRAC technique is not well suited to quantify the very small amounts of ozone loss at the beginning of February, because the range of uncertainty is larger than the calculated ozone loss. The standard deviation of the column ozone loss (σ in brackets in Table 5.1) is shown for each part of the vortex. The error was estimated from the uncertainty of the reference function (see Section 4.4.3). The most rapid change in the $\text{O}_3/\text{N}_2\text{O}$ relation occurred between February 22 and March 20, when the temperatures inside the vortex were still very low (see Figure 5.3, panels i to k). Sufficiently large mixing ratios of active chlorine were present and ozone loss was enhanced by the denitrification of the vortex in the middle of February (see Section 5.1). *Mann et al.* [2002] found that more than 30 % of the HNO_3 was denitrified inside the cold vortex core. At the end of March, HCl begins to recover from the extremely low activated levels [*Müller*

Table 5.1: Ozone loss in Dobson units in 450–550 K calculated from ILAS data for the entire vortex, the vortex core and the outer vortex, respectively. Additionally shown is the maximum ozone loss of the entire vortex. Values are shown with the range of uncertainty and the standard deviation σ in brackets.

Period	Entire Vortex	Vortex Core	Outer Vortex	Maximum
22–28 Feb.	7.3 ± 5.6 (6.9)	9.4 ± 5.3 (4.9)	5.8 ± 5.8 (7.9)	17.4 ± 6.3
1–10 Mar.	7.4 ± 5.7 (11.5)	13.9 ± 5.5 (8.6)	0.7 ± 6.0 (10.3)	26.8 ± 6.1
11–20 Mar.	7.6 ± 5.9 (12.5)	15.5 ± 5.6 (8.9)	0.7 ± 6.1 (11.0)	35.4 ± 6.0
21–31 Mar.	11.9 ± 5.9 (11.4)	19.9 ± 5.5 (8.3)	4.6 ± 6.2 (8.5)	35.3 ± 4.6
1–15 Apr.	13.3 ± 6.0 (9.7)	18.9 ± 5.8 (8.8)	8.8 ± 6.2 (8.0)	39.1 ± 6.2
16–30 Apr.	24.4 ± 6.5 (12.3)	32.4 ± 6.4 (5.8)	16.7 ± 6.6 (12.0)	41.4 ± 6.4
1–15 May.	32.6 ± 6.6 (7.0)	33.8 ± 6.5 (6.7)	29.9 ± 6.9 (7.4)	45.2 ± 5.4

et al., 1997b]. Therefore, any further chemical ozone loss observed later in the season is likely due to NO_x chemistry later in the season [Grooß *et al.*, 1998; Hansen and Chipperfield, 1999]. From February 22 to March 20, the maximum ozone loss increased by about 18 DU (from 17 ± 6 DU up to 35 ± 6 DU) for 450–550 K (see Table 5.1, fifth column). Both the column ozone loss over the entire vortex and within the vortex core increased over this period. However, the derived column ozone loss inside the outer vortex is almost zero from March 1 to 20 (see Table 5.1). Significant differences in the derived ozone loss between the outer vortex and the vortex core during this time period arose due to temperature differences inside different vortex regions. Later on these inhomogeneities were distributed throughout the entire vortex.

During March and the beginning of April, the standard deviation of average ozone loss inside the vortex core (above 8 DU) is larger than for February and for the end of April and May. In this time period, deviations of ozone-tracer profiles from the reference function are very inhomogeneous, especially between March 21 and April 15, 1997, (Figure 5.3, panels l and m). A separation between some profiles with relatively low ozone mixing ratios and many more profiles with moderate ozone mixing ratios becomes obvious. Such an inhomogeneous ozone loss pattern is consistent with the notion of inhomogeneous denitrification and, thus, inhomogeneous chlorine activation inside the vortex in 1997 [McKenna *et al.*, 2002, see also Section 6.2.3].

The column ozone loss inside the vortex core increases further to 32 ± 6 DU in April and 34 ± 7 DU in May with a maximum ozone loss of 45 ± 5 DU (see Table 5.1, third column and fifth column). In 1997, the polar vortex was still very strong until the end of April. Also, the $\text{O}_3/\text{N}_2\text{O}$ relation inside the vortex became more and more compact towards April as presumably mixing within the vortex air masses leads to uniform ozone mixing ratio profiles throughout the vortex.

5.4 Influence of Mixing on the Ozone-Tracer Relationship

As argued in Section 4.3, the effect of anomalous mixing through the isolated vortex edge would only lead to increased ozone mixing ratios relative to a constant tracer mixing ratio, and therefore, to an underestimation of ozone loss. In this section, the argumentation is corroborated by investigating ILAS observations and further discussion is presented concerning the impact of mixing on different parts of the vortex.

Due to diabatic descent of ozone rich air towards lower Θ levels within the polar vortex, the ozone mixing ratios on potential temperature surfaces outside the vortex are in general significantly lower than inside. Thus, possible mixing of air masses from outside the vortex to inside the vortex is expected to lead to a decrease of ozone mixing ratios inside the vortex. The situation is different, however, if the ozone-tracer relationship is considered, because isentropic mixing between air from outside the vortex with air from inside the vortex affects the ozone-tracer relationship differently than the ozone-potential temperature relationship (as discussed in Section 4.3).

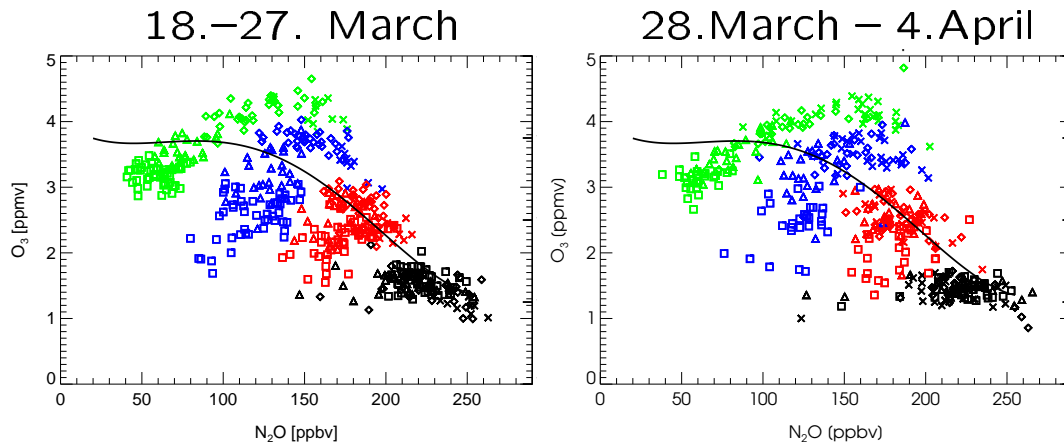


Figure 5.4: O_3/N_2O [ppmv/ppbv] relation of ILAS observations, for two different time intervals in March/April 1997. The different colours denote different isentropic levels: 400 K: black; 450 K: red, 500 K: blue and 550 K: green. The different symbols denote different parts of the vortex: squares: inside the vortex core; triangles: outer vortex, diamonds: outside the vortex edge, inside the outer boundary region of the vortex; crosses: all other profiles outside the vortex. Black line is the early vortex reference function, Equation (5.1).

Following isentropic levels from inside to outside the vortex (see Figure 5.4, different colours) mixing occurs between air masses containing low ozone and low tracer mixing ratios and air masses containing high ozone and high tracer mixing

ratios. These ILAS measurements on different isentropic lines, taken at the end of March and April 1997, also indicate that the strongest ozone loss occurred inside the vortex core (see Figure 5.4, coloured squares) and moderate ozone loss occurred mainly inside the outer vortex (see Figure 5.4, coloured triangles). These profiles, measured inside the outer part of the vortex, scatter above the early winter reference function and are, therefore, significantly influenced by mixing processes.

When for example ozone-tracer relations for the early winter 1997 are considered (see Figure 5.2), the ozone mixing ratios below the ozone maximum from profiles obtained at high equivalent latitudes are lower than those from profiles obtained at lower equivalent latitudes over the whole tracer range. Therefore, the influence of horizontal mixing at the vortex boundary can only result in an underestimation of the calculated ozone loss [see also, *Müller et al.*, 2001, and the discussion in Section 4.3].

In addition, mixing processes leading to a straight line in a correlation diagram, as shown in Figure 4.3, panel a, dotted line, may not cause the shape of the O₃-tracer relation derived from observations measured since March 1997 (see Figure 5.3, panel j to o).

The low ozone mixing ratios in the air of the vortex remnants in May are first of all due to the very low ozone mixing ratios already present in the vortex in March. Further, an additional ozone loss will occur in the vortex remnants due to NO_x chemistry, as described above. The fact that such low values of ozone are observed in the vortex remnants indicates that they must have remained largely intact and that no substantial mixing of outside air has occurred. Further, air masses inside the vortex remnants are relatively homogeneous, because the ozone-tracer relations in May (see Figure 6.9) are quite compact.

This argumentation shows that the ozone-tracer relation inside the isolated vortex, as is the case in 1996–97, is not significantly influenced by mixing processes.

Chapter 6

Re-analysis of HALOE and ILAS Observations in Winter 1996–97

The winter 1996–97 is a special case insofar as both HALOE and ILAS satellite observations are available. The improved TRAC technique, as described in Section 4.4, is applied to the two data sets to calculate chemical ozone loss for this winter. The main parts of this chapter are adapted from *Tilmes et al.* [2003].

6.1 Comparison of ILAS and HALOE Ozone Observations

A comparison of the ozone mixing ratio measured by ILAS (Version 5.2), HALOE (Version 19) and ozone sondes is performed since both data sets will be used together to calculate ozone loss. The comparison is also performed to derive an early winter reference function for the calculation of ozone loss based on HALOE observations, as outlined below (see Section 6.2.1). HALOE measurements inside the outer vortex and in the vortex core are available from March 4 to April 4 so that ILAS and HALOE are directly comparable in this time interval. Comparing ILAS and HALOE mean ozone profiles over this time period (see Figure 6.1) the ozone mixing ratios measured by ILAS are systematically larger than those measured by HALOE.

The mean deviation between HALOE and ILAS ozone profiles in 380–550 K is 0.25 ± 0.06 ppmv for profiles inside the outer vortex and 0.16 ± 0.09 ppmv for profiles inside the vortex core. This result is in agreement with the validation analysis of *Sugita et al.* [2002] and *Lee et al.* [1999], who found that ILAS ozone mixing ratios are on average about 8 % larger than correlative measurements obtained by HALOE for the relevant altitude range from March 24 to April 2. The bias between HALOE and ILAS ozone mixing ratios is rather robust and there is no identification of strong deviations from this bias with time (T. Sugita pers. comm., 2003). Therefore it is assumed that the mean deviation between HALOE and ILAS does not change significantly inside the outer vortex and the vortex core over the course of the winter and spring.

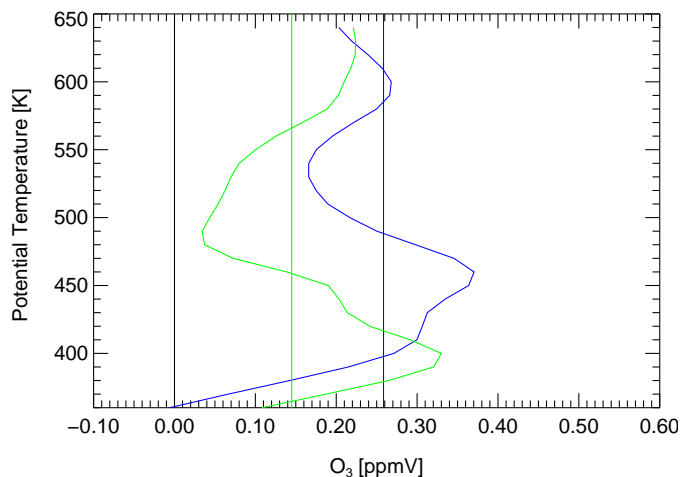


Figure 6.1: The difference of mean ozone profiles from ILAS and HALOE (ILAS-HALOE) in an altitude range from 360–650 K is shown as a green profile for values inside the vortex core and as a blue profile for values inside the outer vortex. The mean ozone profiles from ILAS and HALOE were calculated from all profiles inside the vortex core/ outer vortex in the time period March 4 to April 4, 1997. Also shown are green and blue straight lines indicating the mean deviation of each difference profile between 360-650 K (copyright by AGU).

For the period March 25 to 31, the ILAS and HALOE measurements are obtained at adjacent positions and times inside the polar vortex (see Figures 4.5 and B.1). Thus, the corresponding ILAS and HALOE profiles probably represent the conditions in the same air masses for this time period.

For example, on March 26 and 28 (see Figure 6.2) some HALOE profiles (solid lines) were measured at nearly the same geographic longitude and latitude as some of the profiles observed by ILAS (dashed lines). Ozone profiles with two different characteristics in an altitude range of 450–550 K were observed from both HALOE and ILAS. On the one hand, there were profiles showing relatively low ozone mixing ratios (minimum mixing ratios, HALOE: 0.9–1.1 ppmv, ILAS: 1.6–1.8 ppmv), on the other hand, there were profiles with moderate ozone mixing ratios (above 2 ppmv at ≈ 475 K). The ozone profiles with relatively low ozone mixing ratios were located inside a region characterised by high PV values, i.e. inside the vortex core (see Figure 4.5). Profiles located outside that region show much larger ozone mixing ratios, as is observed both by ILAS and HALOE.

At the end of March, HALOE measurements show much lower minimum ozone mixing ratios than found by ILAS. Considering the minimum of the low ozone mixing ratios, the difference between HALOE and ILAS measurements (about 0.6 ppmv) is much larger than the systematic deviation between HALOE and ILAS ozone profiles in general.

A comparison between the satellite data and ozone sonde measurements was

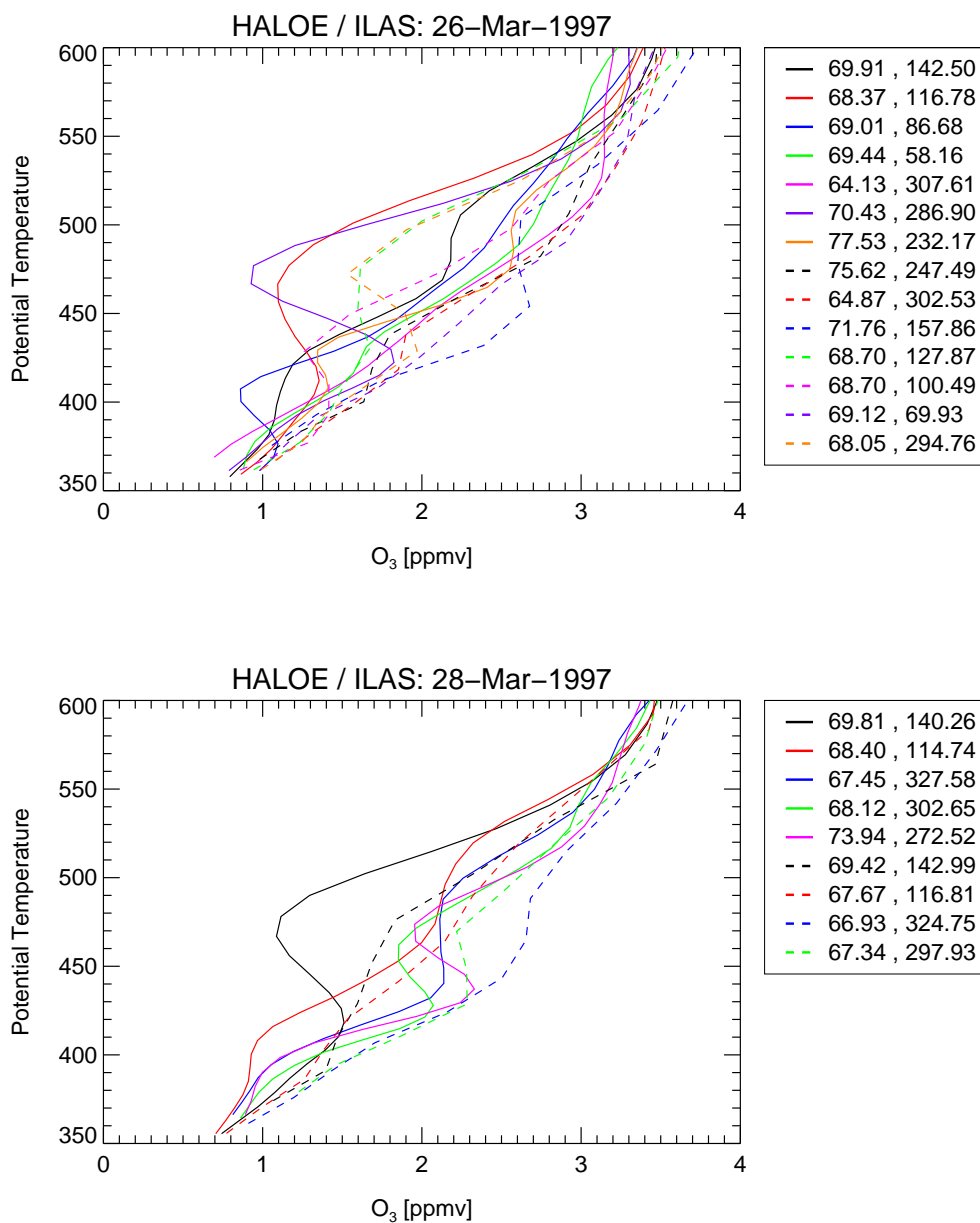


Figure 6.2: Ozone profiles in an altitude range from 350–600 K derived from ILAS (dashed lines), HALOE (solid lines). All satellite profiles were repositioned to 12 UTC through trajectory calculations. The geographic position (latitude/longitude) of profiles at 12 UTC on the 475 K potential temperature level is listed on the right. Top panel: March 26, 1997; bottom panel: March 28, 1997 (copyright by AGU).

performed to assess the observed differences between the satellite data sets. The moderate ozone mixing ratios measured by HALOE and ILAS instruments from 26 March to 2 April are in the same range. As shown above, ILAS ozone mixing ratios are slightly larger (see Figure 6.3). A large amount of information is available from ozone sonde measurements inside the polar vortex in March and April, displaying similar ozone mixing ratios.

Those ozone profiles obtained by ILAS and HALOE displaying very low minimum ozone mixing ratios between 450–500 K are specifically investigated. At the end of March and the beginning of April about six ozone sonde measurements showed minimum ozone mixing ratios below 1.5 ppmv. Three of these profiles (see Figure 6.3) show an extremely low minimum (about 1 ppmv) comparable to the HALOE minimum values.

The balloon observations above NyÅlesund were made $\approx 10^\circ$ north of the position of HALOE and ILAS observations and are, therefore, not directly comparable. Nonetheless, these measurements were made at the same equivalent latitude (corresponding to 50–55 PVU at 475 K) as the HALOE and ILAS observations at 69°N and $110\text{--}140^\circ\text{E}$ (see Figures 6.2 and 6.3 in Appendix B). However, the low ozone mixing ratios were measured by the ozone sondes over a rather narrow layer. Such an ozone profile will be smoothed in the observations of a satellite instrument even with the characteristics of HALOE or ILAS that process comparably good vertical resolutions (see Appendix B). The resulting profile depends on the specific instrument characteristics and further on the smoothing algorithm employed. When the regions of substantially depleted and strongly layered ozone in March are observed by HALOE, the HALOE ozone is biased low below the ozone minimum compared to the ozone sonde measurements, while the minimum of the ozone profile is in agreement. On the other hand, ILAS tends to be biased high around the minimum of the ozone sonde profiles.

In summary, the moderate ozone mixing ratios measured by ILAS are slightly larger than measured by the HALOE instrument at the end of March. This systematic difference between ILAS and HALOE does not affect the results, because ozone loss is calculated with respect to the relative deviation of the O_3 -tracer from the derived early winter reference function. This is different considering these measurements at the end of March that show very low ozone mixing ratios. Differences between measurements taken from HALOE and ILAS are much larger than the systematic bias.

6.2 Ozone Loss in the Winter 1996–97, ILAS and HALOE in Comparison

6.2.1 Ozone Loss Derived From HALOE Measurements

Ozone loss is derived from HALOE observation with the TRAC technique, where both CH_4 and HF were used as the long-lived tracer. For this purpose, two early winter reference functions were developed, one using CH_4 as the long-lived tracer

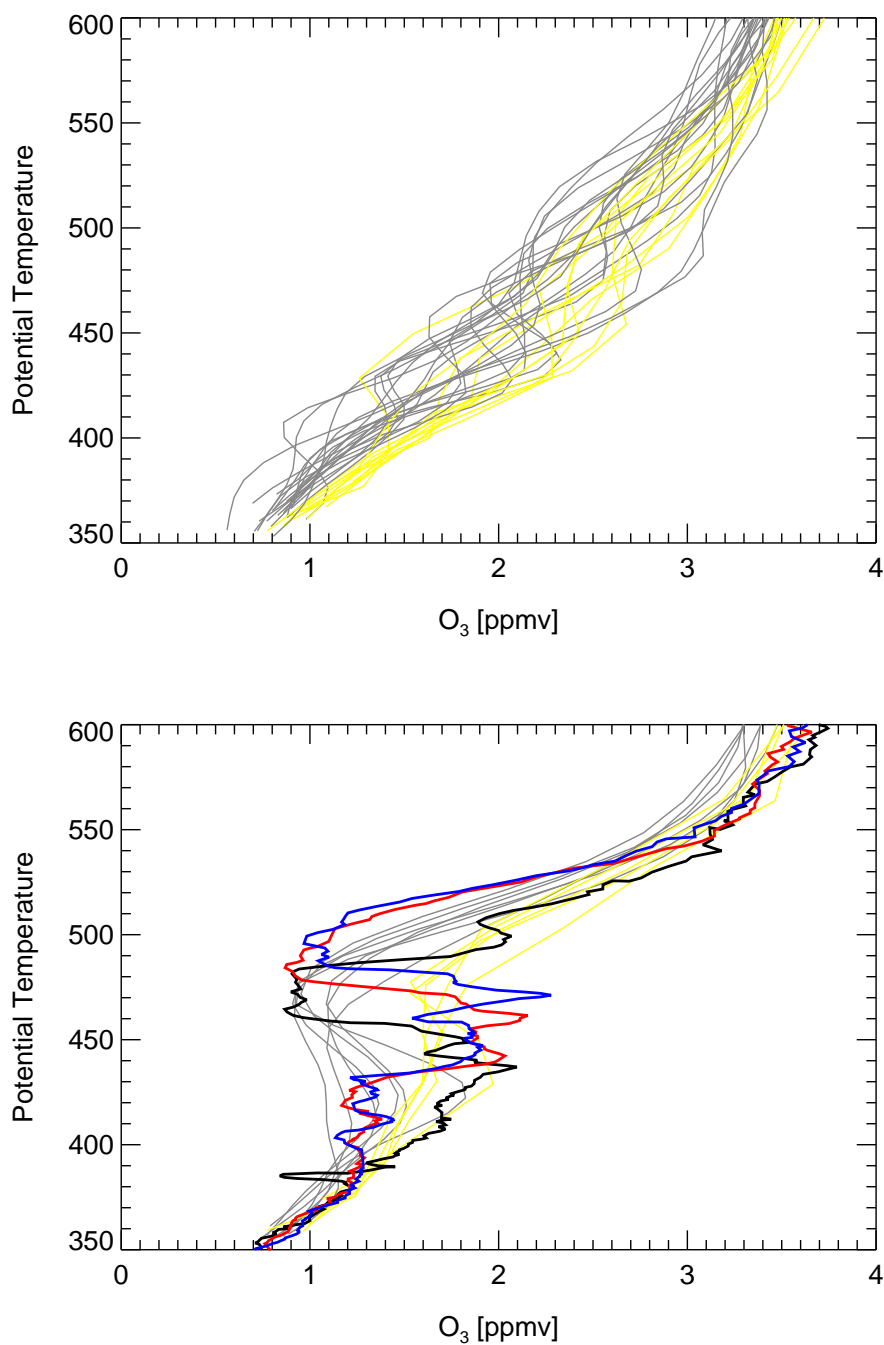


Figure 6.3: Ozone profiles measured from ILAS (yellow lines), HALOE (grey lines) in the time period March 26 to April 2, 1997 are shown in an altitude range from 350–600 K. Top panel: only moderate ozone profiles selected. Bottom panel: only profiles with relatively low ozone in 450–500 K are shown. Additionally, ozone sonde measurements from NyÅlesund (at 78.9°N/11.9°E) in this time period are shown: black profile: March 28, 1997; red profile: March 30, 1997; blue profile: April 5, 1997 (copyright by AGU).

and the second using HF.

HALOE took measurements in northern latitudes up to a maximum of 49°N in November and 48°N in December 1996. *Müller et al.* [1997b] derived an ozone-tracer reference relation from HALOE data for November 1996 using HF as the long-lived tracer. However, since the vortex was not fully established in November 1996 (see Figure 6.4, black asterisks), this relation is not well suited as a reference relation. A better choice would be to employ the HALOE observations in high northern latitudes in December, but these measurements are located very much towards the edge of the polar vortex. A reference relation deduced from those observations would thus be influenced by air from outside the vortex (see Figure 6.4, red asterisks).

Thus, an early winter reference function for the long-lived tracer CH₄ and HF from the ILAS reference function is derived here. The O₃/N₂O reference function (Equation 5.1) is converted to the O₃/CH₄ and O₃/HF reference by using a N₂O/CH₄ and a CH₄/HF relation. *Engel et al.* [1996] reported a linear relation for N₂O/CH₄ from whole-air sampler measurements at different seasons and mid and high northern latitudes between 1988 and 1992:

$$\mu_{\text{N}_2\text{O}} = 261.8 \cdot \mu_{\text{CH}_4} - 136.1 \quad , \quad (6.1)$$

where $\mu_{\text{N}_2\text{O}}$ is the ozone mixing ratio of N₂O in ppbv and μ_{CH_4} the mixing ratio of CH₄, valid for the range $0.65 \text{ ppmv} < \mu_{\text{CH}_4} < 1.6 \text{ ppmv}$.

As described in Section 6.1, ozone mixing ratios obtained by ILAS are systematically larger than HALOE mixing ratios ($0.16 \pm 0.09 \text{ ppmv}$ inside the vortex core and $0.25 \pm 0.06 \text{ ppmv}$ inside the outer vortex). Therefore, a shift of $-0.21 \pm 0.05 \text{ ppmv}$, which is the average of the systematic error between the vortex core and the outer vortex in O₃, was applied to the early winter reference function derived for the HALOE calculations.

The O₃/CH₄ relation derived from Equation 5.1 in this way (shown in Figure 6.4, bottom panel, black line) is characterised by the polynomial:

$$y = 22.73 \cdot x^4 + 2.411 \cdot x^3 - 9.288 \cdot x^2 - 3.328 \cdot x + 3.264 \quad , \quad (6.2)$$

where the y axis describes the ozone mixing ratio μ_{O_3} in ppmv and the x axis describes the CH₄ mixing ratio μ_{CH_4} in ppbv.

The indicated range of uncertainty, $\sigma = 0.28 \text{ ppmv}$ (shaded in grey), corresponds with the uncertainty of the reference function, $\sigma = 0.276 \text{ ppmv}$, as calculated from ILAS early vortex profiles and the uncertainty of the mean difference between HALOE and ILAS ozone mixing ratios, $\sigma = 0.05 \text{ ppmv}$.

To obtain a reference function for HF as the long-lived tracer, the O₃/CH₄ relation, Equation (6.2), is converted to an O₃/HF relation (see Figure 6.4, top panel, black line). For this purpose the following CH₄/HF relation was derived from HALOE observations inside the vortex core in March 1997, mathematically described by the polynomial:

$$y = 0.5867 \cdot x^4 - 2.003 \cdot x^3 + 2.248 \cdot x^2 - 1.885 \cdot x + 1.758 \quad , \quad (6.3)$$

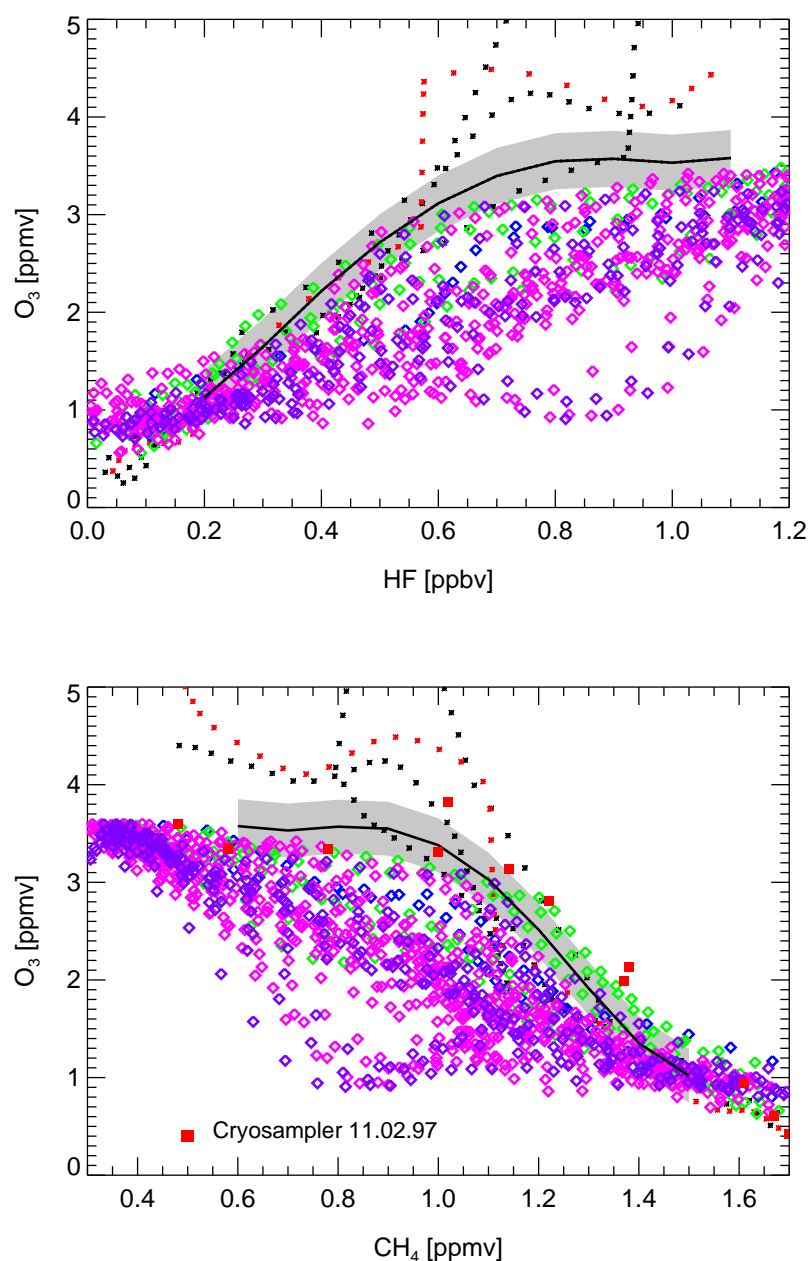


Figure 6.4: Top panel: O_3 /HF [ppmv/ppbv] relation, bottom panel: O_3 /CH₄ [ppmv/ppmv] relation of HALOE observations; black asterisks: November 4–15, 1996, red asterisks: December 12–19, 1996, blue diamonds: March 4–9, 1997, green diamonds: March 10–16 1997, magenta diamonds: March 18–27, 1997, violet diamonds: March 28 to April 4, 1997, all inside the vortex core; the black line indicates the calculated correlation function, Equation (6.2) with the uncertainty indicated as a shaded area in grey (see text). Additionally, the O_3 /CH₄ relation of balloon-borne cryogenic whole-air samplers and concurrent ozone sondes in February 11, 1997 is shown (bottom panel) (copyright by AGU).

where y describes the CH_4 mixing ratio μ_{CH_4} in ppmv and x the HF mixing ratio μ_{HF} in ppbv. This relation is valid for the $0.1 \text{ ppbv} < \mu_{\text{HF}} < 1.5 \text{ ppbv}$ range with an uncertainty of $\sigma = 0.079 \text{ ppmv}$. The uncertainty $\sigma = 0.079 \text{ ppmv}$ and the uncertainty of the O_3/CH_4 relation ($\sigma = 0.28 \text{ ppmv}$) was taken into account to calculate the uncertainty of the O_3/HF relation. HALOE profiles

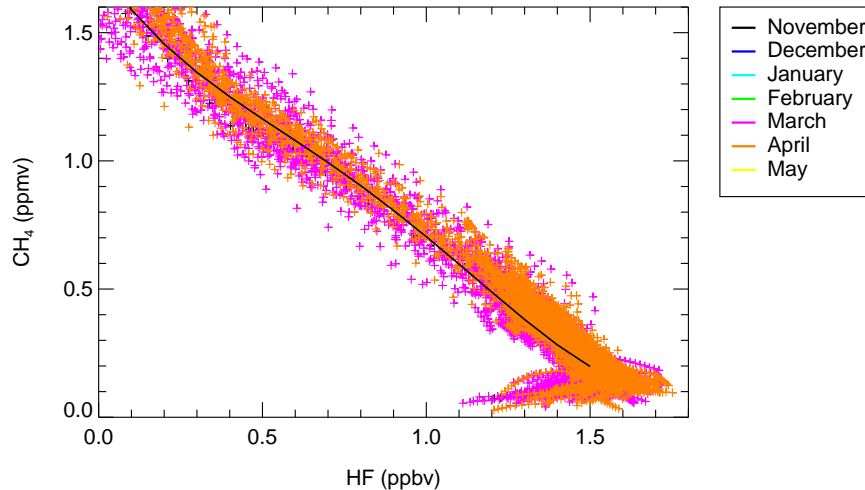


Figure 6.5: CH_4/HF [ppmv/ppbv] relation of HALOE observations inside the vortex core in March and April, 1997, and inside the outer part of the vortex boundary region in November, December and May, 1997. The black line is the relation, Equation (6.3), derived from profiles inside the vortex core.

inside the vortex in May and measurements outside the vortex close to the edge in November and December (when no vortex profiles were observed by HALOE) confirm this relation (see Figure 6.5). A deviation of more than 0.2 ppmv in the CH_4 mixing ratios from the relation occurs in the period from March 4 to 16, 1997 (see Figure 6.5, for example, green dots). These profiles are characterised by large beta angles¹ (see Section 7.1) and were not used in the further analysis.

Deviations from the derived relations O_3/HF and O_3/CH_4 are noticeable for early March (see Figure 6.4, blue and green diamonds) and are stronger at the end of March (see Figure 6.4, magenta and violet diamonds). The strongest reduction of ozone appears at the end of March (18–31), when ozone mixing ratios as low as 0.9 ppmv (at 0.8–0.9 ppbv HF) were observed.

Vertical profiles of long-lived tracers and ozone (employing balloon-borne cryogenic whole-air samplers and concurrent ozone sondes from the University of Frankfurt [*Schmidt et al.*, 1987]) were measured (on February 11, 1997 [*Kondo et al.*, 1999]) above Kiruna, Sweden, inside the outer vortex. No substantial ozone loss occurred up to that time inside this outer vortex region (see Figure 6.4, bottom panel). This finding was confirmed by the ILAS observations, as discussed in Section 5.3, Figure 5.3.

¹The beta angle is the angle between the plane of the spacecraft’s orbit, and the line con-

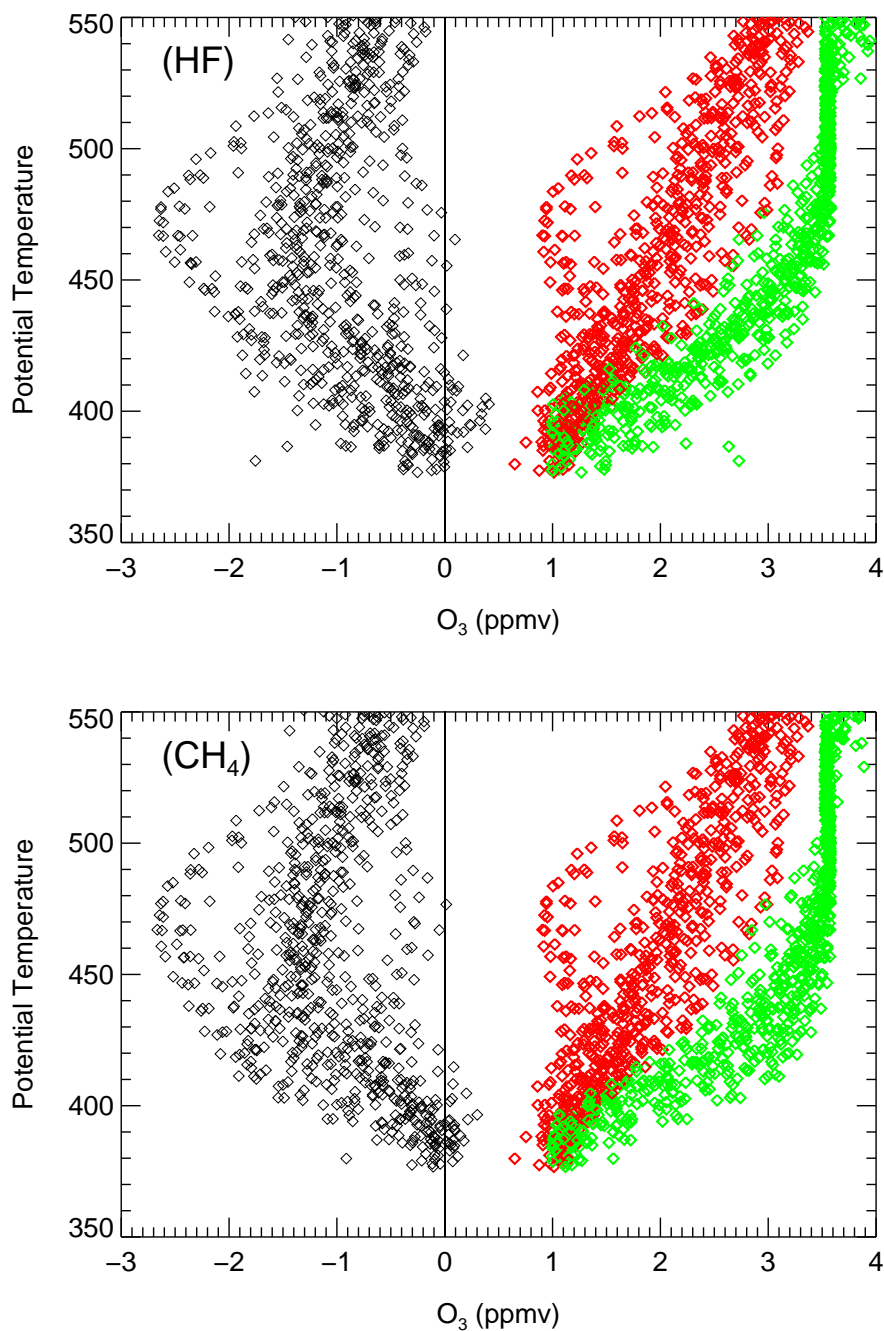


Figure 6.6: Vertical profiles (potential temperature as vertical coordinate) of O₃ mixing ratios (red diamonds) measured by HALOE. The ozone mixing ratios expected in the absence of chemical change, \hat{O}_3 (green diamonds), and the difference in mixing ratio between expected and observed O₃ (black diamonds) are shown for March in winter 1996–97. \hat{O}_3 was derived using HF (top panel) and CH₄ (bottom panel) as the long-lived tracers and the early winter reference functions (see Table C.4) from profiles inside the vortex core (copyright by AGU).

Figure 6.6 shows the measured ozone profiles, O_3 , the proxy for the chemically unperturbed ozone, \hat{O}_3 , and the difference between measured and proxy profiles, ΔO_3 , for the period March 18–31, 1997 over the altitude range of 380–550 K. Individual ozone loss profiles, ΔO_3 , vary from very small up to strong ozone loss values in an altitude range between the 430–500 K level with a maximum ozone loss of 2.6 ppmv at ≈ 475 K. The derived ozone loss from January to the end of March 1997 at the 475 K level can be grouped into three types, those with weak ozone loss (about 0.3 ppmv), those with moderate loss (0.9–1.4 ppmv) and those with strong ozone loss (2.4–2.6 ppmv). At lower altitudes, below 420 K (see Figure 6.6) the scatter of the profiles is stronger, especially when HF is used as the long-lived tracer.

Table 6.1: Column ozone loss (DU) in 380–550 K derived for profiles inside the outer vortex, the entire vortex and the vortex core for two time intervals in March, 1997 from HALOE observations. HF is used as the long-lived tracer in Column 2 and CH_4 in Column 3. The error was derived from the uncertainty of the early winter reference function and the standard deviation σ of the result is shown in brackets.

	HALOE (HF) (σ)	HALOE (CH_4) (σ)
<i>March 4–16, 1997</i>		
Mean Vortex	29.5 \pm 21.3 (15.1)	23.0 \pm 20.5 (23.5)
Mean Core	29.6 \pm 20.8 (18.2)	26.1 \pm 20.0 (25.0)
Mean Outer Vortex	29.3 \pm 21.6 (13.2)	20.5 \pm 20.8 (23.3)
Maximum	52.7 \pm 23.3	58.6 \pm 19.7
<i>March 18 to April 4, 1997</i>		
Mean Vortex	43.7 \pm 20.7 (28.1)	44.5 \pm 19.9 (33.4)
Mean Core	59.0 \pm 20.2 (19.8)	62.6 \pm 19.4 (22.0)
Mean Outer Vortex	25.7 \pm 21.4 (25.8)	23.4 \pm 20.6 (32.2)
Maximum	101.9 \pm 17.9	112.2 \pm 17.8

The mean ozone loss inside the entire vortex for the period March 18 to April 4, 1997, is determined as 44 ± 21 DU using HF and 45 ± 20 DU using CH_4 as the tracer in an altitude range 380–550 K (see Table 6.1). The reported uncertainty (see Tables 6.2 and 6.1) is derived from the uncertainty of the early vortex reference relation. The calculated ozone loss should be independent of the tracer utilised, and indeed the values determined for CH_4 and HF as tracers agree very well inside the uncertainty introduced by the uncertainty of the reference function. The ozone loss reported here was calculated as the average of the results from CH_4 and HF: entire vortex mean = 44 ± 21 DU and vortex core mean = 61 ± 20 DU. The reported uncertainty includes the variability introduced by employing two different tracers. For the altitude range of 450–550 K, the ozone

necting the center of the Earth with the Sun.

Table 6.2: Column ozone loss (DU) in 450–500 K derived for profiles inside the outer vortex, the entire vortex and the vortex core for two time intervals in March, 1997 from HALOE observations. HF is used as the long-lived tracer in Column 2 and CH₄ in Column 3. The error was derived from the uncertainty of the early winter reference function and the standard deviation σ of the result is shown in brackets.

	HALOE (HF) (σ)	HALOE (CH ₄) (σ)
<i>March 4–16, 1997</i>		
Mean Vortex	14.4 \pm 7.3 (6.7)	12.6 \pm 7.0 (8.4)
Mean Core	15.9 \pm 7.0 (7.1)	14.4 \pm 6.7 (8.3)
Mean Outer Vortex	13.1 \pm 7.6 (6.2)	11.2 \pm 7.3 (8.7)
Maximum	25.9 \pm 7.3	26.3 \pm 6.2
<i>March 18 to April 4, 1997</i>		
Mean Vortex	18.7 \pm 7.2 (15.2)	18.8 \pm 6.9 (15.9)
Mean Core	27.8 \pm 6.9 (10.0)	28.1 \pm 6.6 (9.6)
Mean Outer Vortex	8.2 \pm 7.5 (13.3)	7.8 \pm 7.3 (14.7)
Maximum	46.1 \pm 6.7	48.3 \pm 6.3

loss calculated using the two long-lived tracers is nearly identical (see Table 6.2). Indeed, in this altitude range the vortex is more stable and thus less permeable than above and below so that the variability introduced by mixing of air from outside the vortex is expected to be small. In this altitude range the mean of the ozone loss inside the vortex core for both tracers is about 34 ± 8 %, corresponding to 28 ± 7 DU, and the maximum loss is 58 ± 4 % (47 ± 7 DU).

In Figure 6.7, 6.8 the probability distribution of calculated ozone loss in the vortex core is shown as a solid line, and the probability distribution of calculated ozone loss inside the outer vortex is indicated as a dashed line. There are two groups of losses in these probability distributions of the calculated ozone loss of HALOE observations (see Figure 6.7 and 6.8), a large ozone loss of 90–110 DU was determined mainly in the vortex core for 380–550 K and 40–45 DU for 450–550 K. Smaller losses of between 20 and 80 DU for 380–550 K and 15–30 DU for 450–550 K were calculated for the entire vortex.

In May 1997 three profiles were found in vortex remnants with very low ozone mixing ratios (see Figure 6.9). The ozone loss in the vortex remnants was calculated as 69 ± 23 DU in the period May 12–13, 1997, with a maximum of 98 ± 22 DU in 380–550 K (the average of the results from CH₄ and HF). The maximum column ozone loss is not as large as calculated in March, but the ozone-tracer relations are much more compact and the mean ozone loss is about 8 DU larger compared to March. In the altitude range of 450–550 K, the mean ozone loss was calculated as 38 ± 8 DU, which is an increase of 10 DU compared to March.

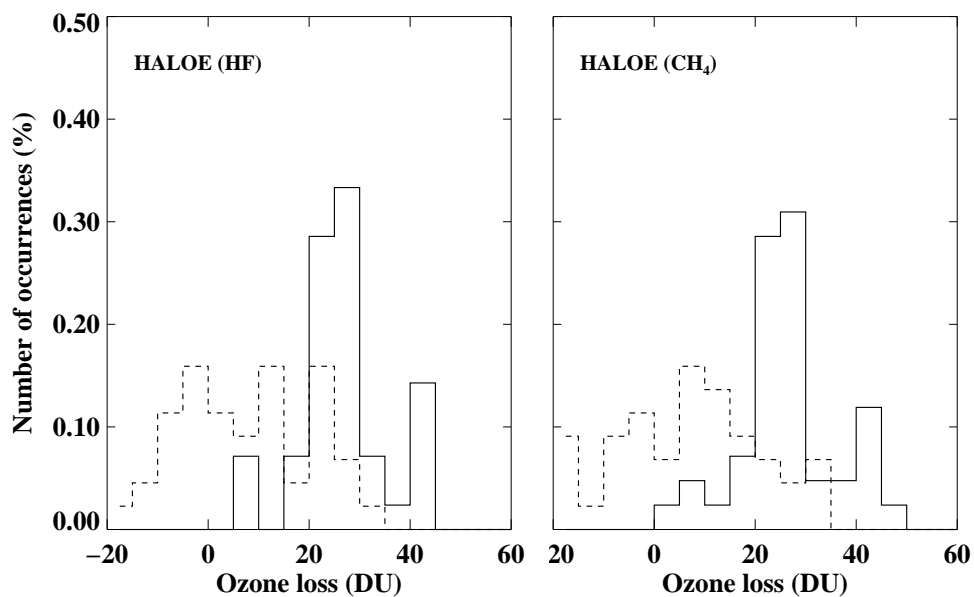


Figure 6.7: Probability distribution of ozone loss in an altitude range of 450–550 K for profiles inside the polar vortex shown as dashed lines and inside the vortex core shown as solid lines from March 18 to April 4, 1997; HALOE results, left panel: long-lived tracer is HF, right panel: long-lived tracer is CH₄.

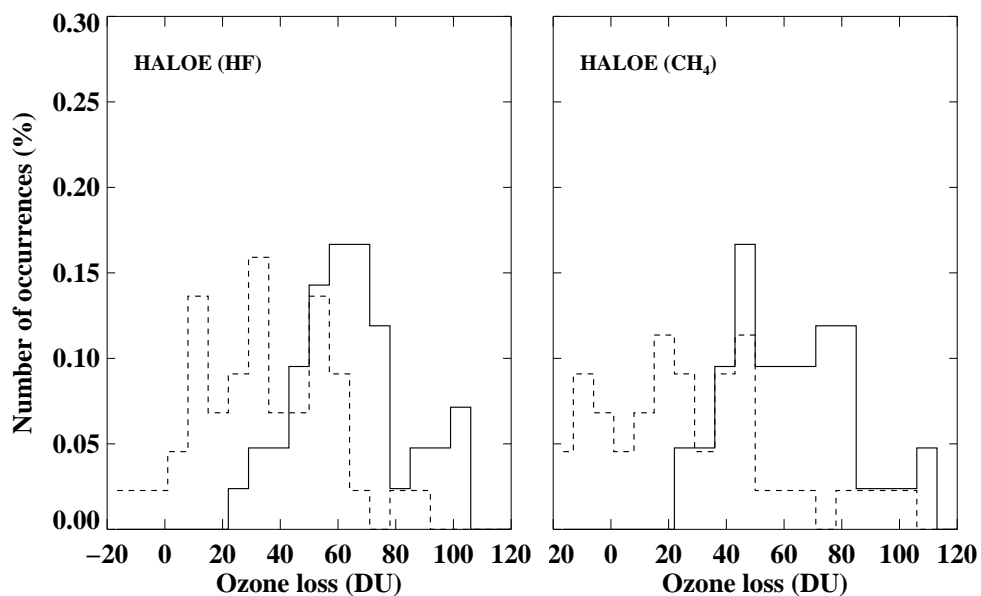


Figure 6.8: As Figure 6.7, but in an altitude range of 380–550 K.

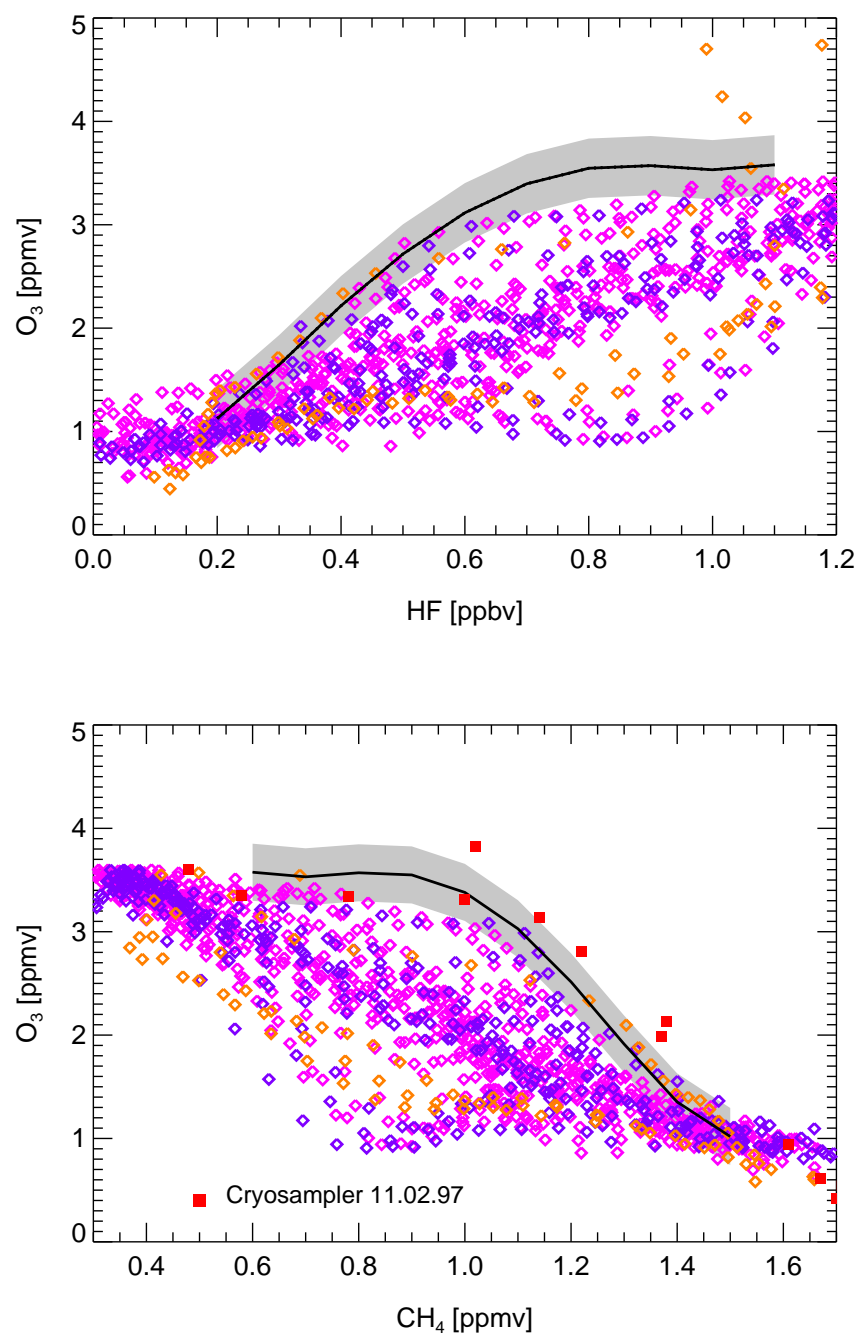


Figure 6.9: As Fig. 6.4, but for different time periods. Magenta diamonds: March 18–27, 1997, violet diamonds: March 28 to April 4, orange diamonds: May 12–13, 1997, all inside the vortex (copyright by AGU).

6.2.2 Ozone Loss Derived From ILAS Measurements

In this section, ozone loss from ILAS measurements was derived for the same time intervals, for which HALOE measurements are available.

The majority of accumulated ozone loss profiles (see Figure 6.10, black lines) for the end of March and the beginning of April 1997, show moderate losses (0.5–1.0 ppmv). Only two profiles at the end of March and one at the beginning of April show strong ozone loss up to 2.0 ppmv in 470–490 K. Strong scatter of the profiles occurs at altitudes below 500 K (see Figure 6.10).

Table 6.3: Column ozone loss (DU) in 450–500 K derived for profiles inside the outer vortex, the entire vortex and the vortex core for two time intervals in March, 1997 from ILAS observations. N₂O is used as the long-lived tracer. The error was derived from the uncertainty of the early winter reference function and the standard deviation σ of the result is shown in brackets.

	ILAS (N ₂ O) (σ)
<i>March 4–16, 1997</i>	
Mean Vortex	8.3 ± 5.7 (12.2)
Mean Core	15.1 ± 5.5 (10.3)
Mean Outer Vortex	1.2 ± 5.9 (9.8)
Maximum	35.4 ± 6.0
<i>March 18 to April 4, 1997</i>	
Mean Vortex	11.3 ± 6.0 (11.3)
Mean Core	18.8 ± 5.6 (8.3)
Mean Outer Vortex	5.3 ± 6.2 (9.0)
Maximum	39.1 ± 6.2

For the period from March 18 to April 4, 1997, the mean ozone loss in the vortex core is calculated as 19 ± 6 DU with a maximum of 39 ± 6 DU for the altitude range of 450–550 K (see Table 6.3). The corresponding percentage values are $26 \% \pm 6 \%$ with a maximum of $47 \% \pm 4 \%$. (The percentage of ozone loss is calculated as: difference profile $\Delta O_3 / \text{ozone proxy } \hat{O}_3 * 100$).

In this time period, a separation of profiles inside the vortex core with large ozone loss (30–40 DU) from profiles with moderate ozone loss (5–25 DU) becomes apparent (see Figure 6.11, panel a, solid line). In the outer vortex, only profiles with moderate or with very little ozone loss were observed.

6.2.3 Comparison of HALOE and ILAS Results

HALOE and ILAS measurements are comparable in March 1997 (see Sections 6.2.1 and 6.2.2), especially at the end of March, where the instruments made measurements at positions very close to each other. Calculated ozone loss from both ILAS and HALOE measurements is based on the same ozone-tracer

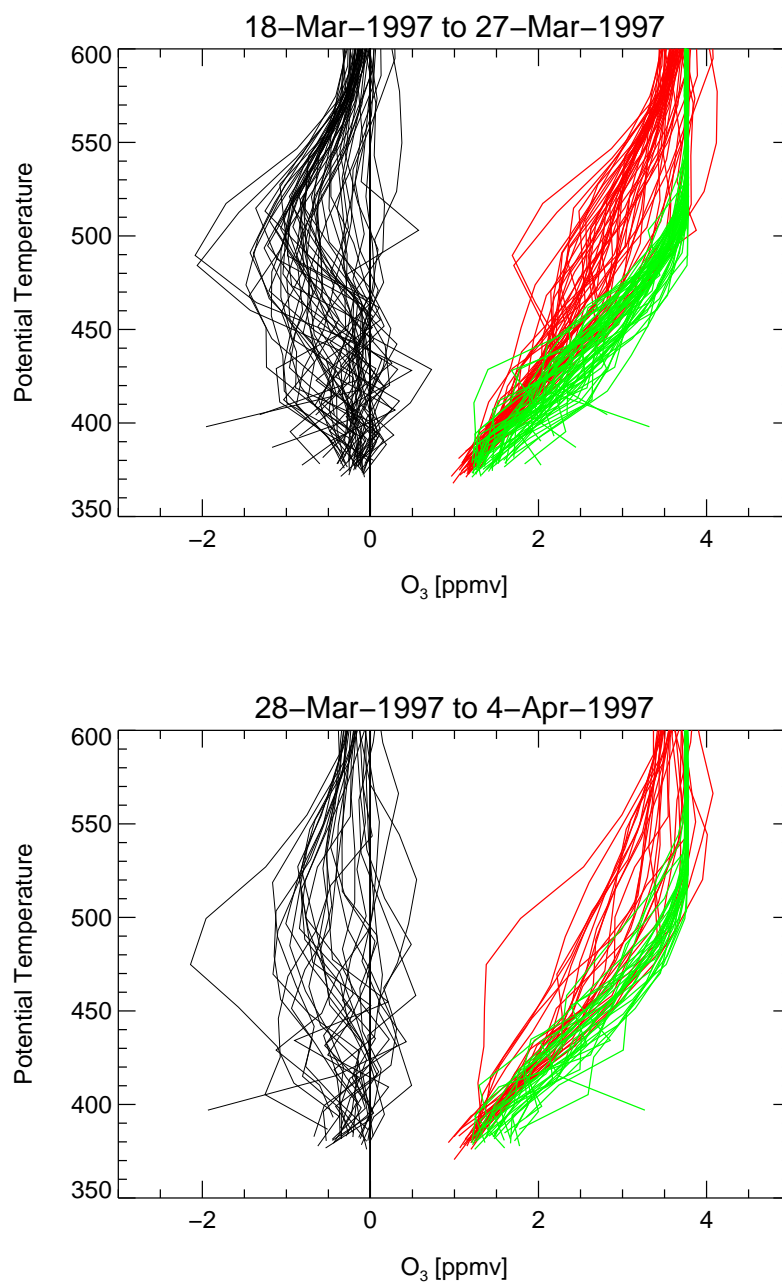


Figure 6.10: Vertical profiles (potential temperature as vertical coordinate) of measured O_3 mixing ratios (red lines) by ILAS. The ozone mixing ratios expected in the absence of chemical change, \hat{O}_3 (green lines), and the difference in mixing ratio between expected and observed O_3 (black lines) are shown for 18 – 27 March (top panel) and 18 March – 4 April (bottom panel) in winter 1996–97. \hat{O}_3 was determined using N_2O as the long-lived tracer and the early winter reference functions (see Table C.4) from profiles inside the vortex core.

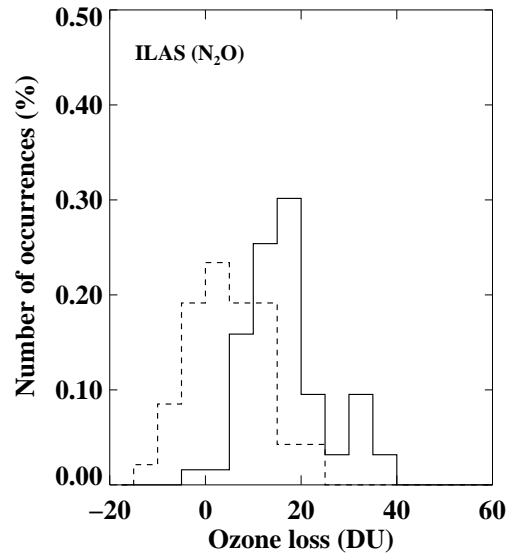


Figure 6.11: Probability distribution of ozone loss in an altitude range of 450–550 K for profiles inside the polar vortex shown as dashed lines and inside the vortex core shown as solid lines from March 18 to April 4, 1997; ILAS results, N_2O is used as the long-lived tracer.

correlation function derived from ILAS data for January 1997 (see Equation 5.1). The systematic difference between HALOE and ILAS mean ozone mixing ratios was considered. Here, a comparison is made for the column ozone loss calculated over an altitude range of 450–550 K (see Tables 6.2 and 6.3). Over the period March 4 – 16, 1997, the ozone loss of HALOE and ILAS inside the vortex core is in agreement inside a range of 2 DU. The average of the results obtained with both instruments is 15 ± 7 Dobson units (DU). In this time period, the maximum ozone loss calculated from ILAS is 9 DU larger than from HALOE. At the end of March, significantly larger loss values were obtained from HALOE than from ILAS data considering the vortex core. The difference between the HALOE and ILAS mean ozone loss is estimated to be about 8 DU.

In summary, HALOE and ILAS ozone mixing ratios are in agreement, except for the large difference in the calculated ozone loss resulting from the differences of lowest ozone mixing ratios measured at the end of March. In the first half of March, moderate ozone mixing ratios were measured consistently by HALOE and ILAS and the results are in good agreement.

The calculated ozone losses of both sets of satellite data consistently show an inhomogeneity of ozone loss inside the entire vortex. The mean ozone loss in the vortex core differs significantly from the mean ozone loss in the outer vortex, especially in ILAS results (see Table 6.2). Moreover, in the probability distribution of ozone loss a separation inside the vortex core into two distinct parts was found. Large values of ozone loss occur mainly inside the vortex core, while smaller losses were found in the vortex core and in the outer vortex. Model

calculations of ozone depletion patterns inside the vortex using the Chemical Lagrangian Model of Stratosphere (CLaMS) show a good agreement with this pattern of ozone loss derived from HALOE and ILAS observations [McKenna *et al.*, 2002]. For the end of March, the model simulated a filament of vortex air out of the core going through the outer vortex [McKenna *et al.*, 2002]. This air mass is characterised by lower ozone mixing ratios than air masses observed in the outer vortex but not as low as those in the cold parts of the vortex core. Thus the outer vortex is also divided into a part with stronger ozone loss and a part with moderate ozone loss (see Figure 6.8). Larger ozone loss is caused by lower temperatures and stronger denitrification occurring earlier in the season inside this region [McKenna *et al.*, 2002]. Ozone loss in March 1996–97 is spatially much more inhomogeneous than that observed in previous winters [Müller *et al.*, 1996, 1997a; Schulz *et al.*, 2000]. The range of moderate loss values for 450–550 K inside the vortex core is 15–30 DU for HALOE and 5–25 DU for ILAS and for the strong ozone loss about 40–45 DU for HALOE and 30–35 DU for ILAS.

The vortex-averaged ozone loss derived from ILAS observations reached its maximum for the period May 1 – 15, 1997 (see Table 5.1) for the remnants of vortex air. A large ozone loss of 33 ± 7 DU and a maximum of 45 ± 5 DU was calculated. The HALOE ozone loss in May was derived only from four profiles with a maximum of 54 ± 7 DU. Deviations from the reference function are not as large as in March (HALOE) (see Figure 6.9) and April (ILAS) (see Figure 5.3), although the mean ozone loss increases by up to 10 DU (HALOE) and 8 DU (ILAS) compared to March.

In a previous study of the same winter 1996–97, HALOE observations were available only in November inside the vortex to derive an early winter reference function [Müller *et al.*, 1997b]. This ozone-tracer relationship from HALOE observations continued to change to larger ozone mixing ratios until January, as described above. Therefore, the ozone loss determined by Müller *et al.* [1997b] was an underestimate. The maximum column ozone loss inside the vortex was underestimated by up to ≈ 20 % for the altitude range of 380–550 K and the local loss at 475 K was underestimated by ≈ 15 % (0.4 ppbv). Further comparison of the results derived from ILAS and HALOE and other methods is described in detail in Section 9.2.

The ozone loss calculated from ILAS observations did not reach such large ozone losses as that calculated from HALOE data. However, HALOE and ILAS results still agree inside the range of uncertainty for the altitude range of 450–550 K. Also, the results of both data sets consistently show a separation of the ozone loss into moderate ozone losses and large ozone losses inside the vortex core at the end of March.

The peculiarity of the polar vortex in this winter is the strong inhomogeneity of the distribution of the ozone loss inside the entire vortex until March. Further, the vortex existed for a very long time up to the end of April. Very low ozone mixing ratios were still observed inside the remaining vortex air during May 1997.

Chapter 7

Development of the Tracer-Tracer Relation from 1991 to 2002

Measurements made by the HALOE instrument are available from October 1991. In this chapter, a comprehensive analysis of the development of the relationship between different tracers is performed for the eleven winters between 1991–92 and 2001–02 based on Version 19 data (see Appendix B.2). The relationship between the long-lived tracers CH_4 and HF is described in Section 7.1. Further, the stratospheric HF growth rate per year is calculated from the CH_4/HF evolution in the eleven-year period.

In the previous chapter, the validated TRAC technique was used to calculate chemical ozone loss for winter 1996–97 using both ILAS and HALOE data sets. Here, it is done for all eleven winters. In Section 7.2, the early winter reference functions are derived. The interactions between chlorine activation, ozone loss and meteorological conditions are described in Section 7.3. For this, the relationships between ozone and the long-lived tracer HF and, additionally, the relationships between HCl and HF are discussed for each winter.

7.1 The CH_4/HF Relation for all Winters

The HALOE instrument measures two long-lived tracers, namely HF and CH_4 . The relationship between CH_4 and HF differs for different dynamical isolated regions (polar vortex, mid-latitudes, and the tropics) [Luo *et al.*, 1995]. In the present work, the region of the Arctic polar vortex is investigated. A correlation function for the CH_4/HF relation for each year has been derived, which is valid for all HALOE profiles inside the vortex core over the whole lifetime of the vortex (see Table C.1, Appendix C). In Section 6.2.1, this has already been done for winter 1996–97 (see Figure 6.5). CH_4/HF relations for individual profiles are very close to the derived correlation function (see Figure 7.1, black line). For all years the standard deviation (σ) was less than 0.1 ppmv (see Table C.1, column 7).

Single profiles show a deviation from the correlation function greater than 0.2 ppmv, which cannot occur for such long-lived species [Plumb and Ko, 1992].

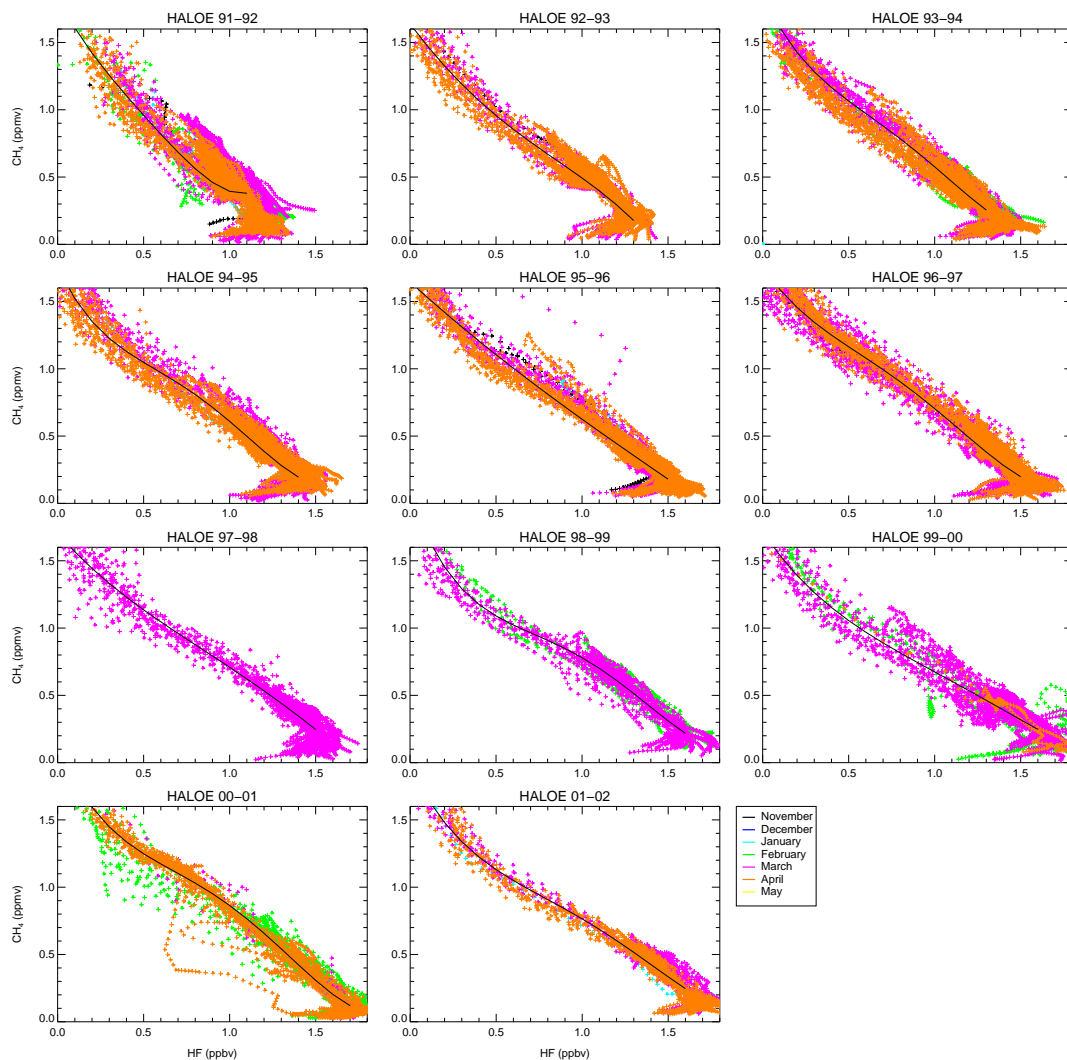


Figure 7.1: CH_4/HF relationship is shown for the eleven winters between 1991-92 and 2001-02 as measured by HALOE inside the vortex core. Different colours indicate the different months when profiles were measured (see Figure 6.5). Black lines indicate the reference function derived for each year (see Table C.1).

These profiles are considered to be uncertain and are thus rejected for the calculation of the ozone loss, e.g. the strong deviation in April 2001. Uncertainties in data could have arisen due to large beta angles of the measurement line of the satellite (J. Russell pers. comm., 2002) which is the case at the beginning of March 1997 (see Section 6.2.1). Further, the HALOE HF channel is the most sensitive to sunspot occurrence, which may contaminate the HF data. Additionally, although the the Nash criteria (used to decide whether profiles are located inside or outside the vortex) are applied some profiles may be still influenced by air masses from outside the vortex. Thus, the elimination of these kinds of uncertainties permits an improved selection of HALOE profiles.

An evolution of the derived CH₄/HF correlation functions over the period from 1991–92 to 2001–02 is shown in Figure 7.2. These changes of the CH₄/HF correlation arise owing to the increase of CH₄ and HF mixing ratios in the stratosphere.

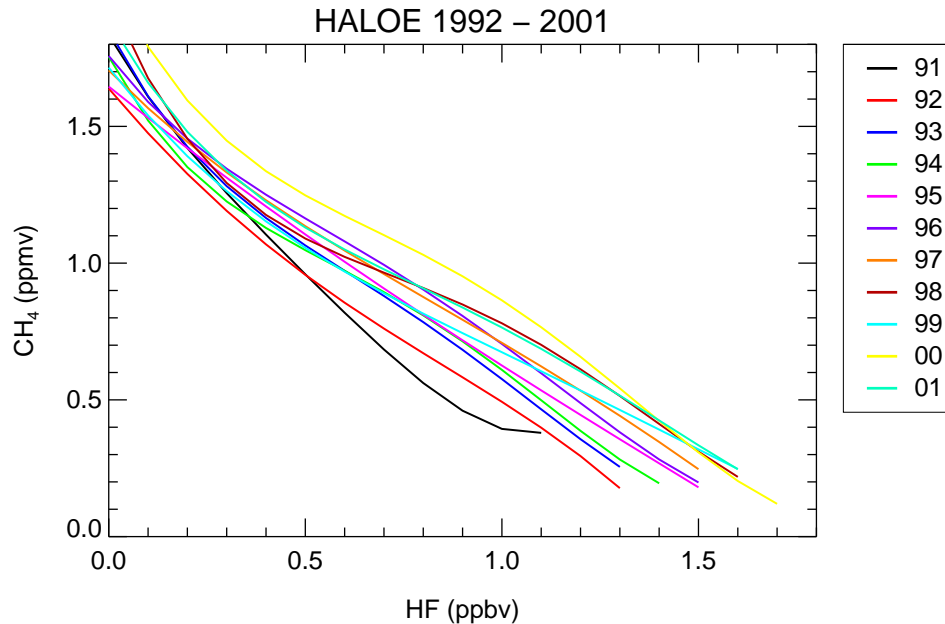


Figure 7.2: CH₄/HF reference functions for the eleven years between 1991–92 and 2001–02, as derived from measurements made by HALOE (listed in Table C.1). The different colours of the lines indicate the different years.

The tropospheric growth rate (ppbv/year) of CH₄ was derived from global tropospheric measurements over 23 years [Simpson *et al.*, 2002]. The mixing ratio of tropospheric CH₄ increased by about 60 ppbv between 1991–92 and 1999–2000. For the first time since 1985 the growth rate for the year 2000 was negative (–2.1 ppbv).

The changes of CH₄ in the troposphere spread out into the stratosphere with a time lag. Nevertheless, the CH₄ growth rate in the troposphere can be assumed to be valid in the stratosphere. The growth rate of 60 ppbv in eleven years is

only a very small fraction of the observed stratospheric CH_4 mixing ratios (1.5–0.5 ppmv). Thus, the evolution of the CH_4/HF relation over the eleven-year period is mainly due to the increase of the HF mixing ratio in the stratosphere.

The temporal development of the mixing ratio of HF for different CH_4 levels (including the tropospheric growth rate for CH_4 each year) is shown in Figure 7.3, top panel. It was calculated from profiles measured by HALOE inside the vortex core from 1991–92 to 2001–02.

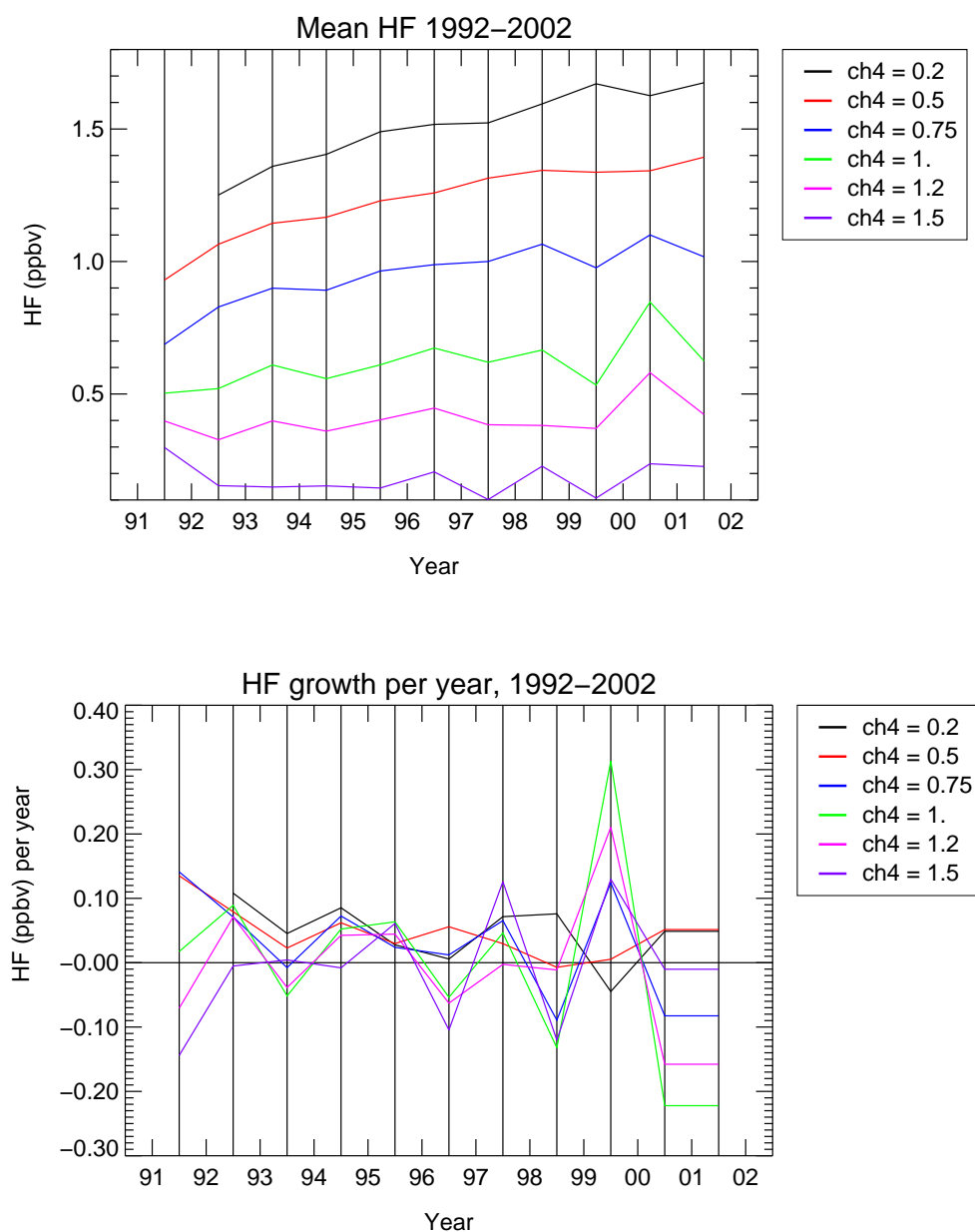


Figure 7.3: Top panel: Temporal development of the mixing ratio of HF in ppbv for different CH_4 levels of profiles measured by HALOE inside the vortex core from 1991–92 to 2001–02. Bottom panel: HF growth rate in ppbv/year.

HF mixing ratios become constant towards higher altitudes, for low CH_4 levels (below 0.2 ppmv, which corresponds to altitudes in the mesosphere) (see Figure 7.1). The mean HF mixing ratio at this altitude is nearly the total amount of inorganic fluorine. An annual increase of the constant HF value, from 1.2 ppbv in 1992 up to 1.7 ppbv in 2001–02 (see Figure 7.3, top panel, black line), arises due to the increasing atmospheric concentration of HF with time (noted by *Luo et al.* [1995]). This increase is caused by the increasing CFC concentration (see Section 1.1). At the CH_4 mixing ratio level of 0.5 ppmv the strongest increase of HF is measured from 1991–92 to 1992–93. Figure 7.3, bottom panel, indicates a positive growth rate of HF for the 0.2 ppmv and 0.5 ppmv CH_4 level (black and red line), except for 2000 and 2001. At lower altitudes at the 0.75 ppmv CH_4 level the HF growth rate per year is slightly smaller. A significantly negative growth rate occurs in 1999–2000 at CH_4 levels > 0.5 ppmv. This is one year earlier than the time when the growth rate at $\text{CH}_4 = 0.2$ ppmv becomes negative in 2000–01, possibly due to the delay of changes in mixing ratios of the tracers at higher altitudes. In the tropopause region ($\text{CH}_4 = 1.2$ – 1.5 ppmv) the mean HF value rises more slowly than in the stratosphere (see Figure 7.3, purple and magenta line). The HF growth rate derived from HALOE measurements seems to be more variable at high CH_4 levels than that at low CH_4 levels (at higher altitudes).

All in all, a trend towards a smaller annual HF growth rate is becoming apparent, but at present there is no evidence of a downward trend in the stratosphere. Further, the derived growth rate is used to calculate the early winter reference function for those years where no observations are available inside the early vortex (see Section 7.2).

7.2 The Early Winter Ozone-Tracer Reference Relation

To calculate chemical ozone loss with the TRAC technique, it is very important to determine a reliable early winter reference function. A reference relation has to be derived from profiles inside a mainly isolated early vortex, as described in Section 4.4.2. Observations made by HALOE inside the early polar vortex are primarily available for some time between November and January, varying from year to year due to the variable latitudinal coverage of HALOE measurements. The development of the early winter reference functions from these measurements made by HALOE is described first. In some years, no HALOE measurements are available or only outside the edge of the early vortex and the early winter reference function has to be derived in another way, as outlined below.

HALOE measurements inside the early vortex are available for the periods 1992–93 to 1995–96 and in 1998–99 and 2001–01: In 1992–93, the early winter reference function is derived from the available profiles inside the vortex at the beginning of November and at the beginning of December. The vortex already starts developing in November and was fully developed at the beginning of De-

ember.

In 1993–94, HALOE observations are available at the end of November and at the beginning of January. Profiles from both periods inside the vortex show a very similar ozone-tracer relation, from which the early winter reference function was derived. Thus, no ozone loss was identified from HALOE measurements between November and early January.

In 1994–95, the early winter reference function was derived from measurements available for the middle of January. The vortex developed in December, as can be seen in meteorological analysis (e.g. UKMO data). Also, a large area of possible PSC existence was detected in December and at the beginning of January for this winter (see Figure 7.11). Therefore, the occurrence of a small amount of ozone loss at this time cannot be excluded. *Rex et al.* [2003] reported large ozone loss rates for January 1995.

In 1995–96, measurements are available for the middle of November and for the end of January. As for 1993–94, the O₃-tracer relation for these two months does not indicate significant differences and, thus, no ozone loss was determined until the end of January, as described in detail in Section 4.4.2. In this winter, the early winter reference function was derived from both November and January profiles.

In 1998–99, the early winter reference function was derived from measurements available well inside the vortex at the beginning of December 1998.

In 2001–02, one profile was available well inside the early vortex at the beginning of January 2002 to derive the early winter reference function.

In summary, these early winter reference functions (O₃/CH₄ and O₃/HF), derived from HALOE profiles only, are listed in Tables C.2 and C.3 (see Appendix C).

In 1991–92 and 1999–2000, early winter reference functions were derived from balloon observations. For winter 1991–92, the early winter reference function was derived from measurements of ozone and N₂O made by Cryosampler [*Schmidt et al.*, 1987] (see Figure 7.4) on 5 and 12 December 1991, respectively [*Müller et al.*, 2001]:

$$y = -6.40 \cdot 10^{-5} \cdot x^2 - 4.84 \cdot 10^{-3} \cdot x + 3.94 \quad , \quad (7.1)$$

where y describes the ozone mixing ratio μ_{O_3} in ppmv and the x the N₂O mixing ratio $\mu_{\text{N}_2\text{O}}$ in ppbv. The reference function is valid for the range $10 \text{ ppbv} < \mu_{\text{N}_2\text{O}} < 260 \text{ ppbv}$. The O₃/N₂O profiles were transformed to O₃/CH₄ with the relationship from *Engel et al.* [1996] (see Section 6.2.1, Equation 6.1).

To derive the O₃/HF reference function the O₃/CH₄ relation was converted using the CH₄/HF relation derived for 1991–92 (see Table C.1, Appendix C). The vortex started forming in November 1991. One HALOE profile was found inside the early vortex at the beginning of November, with low ozone mixing ratios compared to profiles inside the vortex measured in January (see Figure 7.4, black asterisks). At that time the vortex was not well developed and mixing in of air masses from outside the early vortex was still possible. Therefore, the low ozone mixing ratios observed in November increased until the vortex became fully

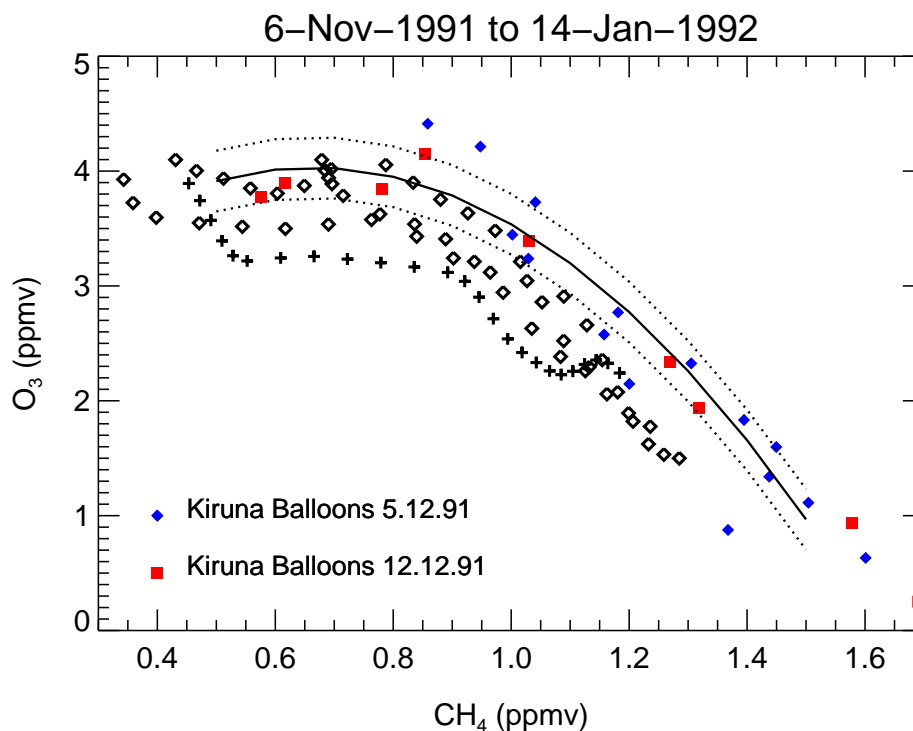


Figure 7.4: The early winter reference function 1991–92 shown as a black line was derived from balloon measurements from December 1991 (coloured symbols). Dotted lines indicate the range of uncertainty in the reference function. Observations made by HALOE within the vortex in November 1991 (black asterisks) and in January (black squares) are also shown.

isolated. The effect of mixing at the beginning of another winter is described in detail for the early winter 1996–97 in Section 5.2. The HALOE profiles in January 1992 tend to scatter below the derived reference relation (see Figure 7.4). This indicates that ozone loss may have already occurred during January 1992, which was also described by *Rex et al.* [2003], corresponding to a small detected area of possible PSC existence at the beginning of January (see Figure 7.11).

In 1999–2000 no HALOE observations were available inside the early vortex to derive the early winter reference function. Fortunately, during the SOLVETHESEO 2000 campaign two balloon flights were conducted inside the early vortex, the OMS (Observations of the Middle Stratosphere) in-situ flight on 19 November 1999 and OMS remote flight on 3 December 1999. HF measurements were only available from the MkVI instrument on the OMS-remote flight. Thus, these data were used to derive the O₃/HF reference function for this winter [*Müller et al.*, 2002]. Two early winter reference functions were derived using CH₄ as the long-lived tracer, one was derived using the OMS-in-situ measurements and the second using the OMS-remote flight measurements [*Müller et al.*, 2002] (see Appendix C, Table C.4).

These two reference functions differ substantially (see Figure 7.5) and they

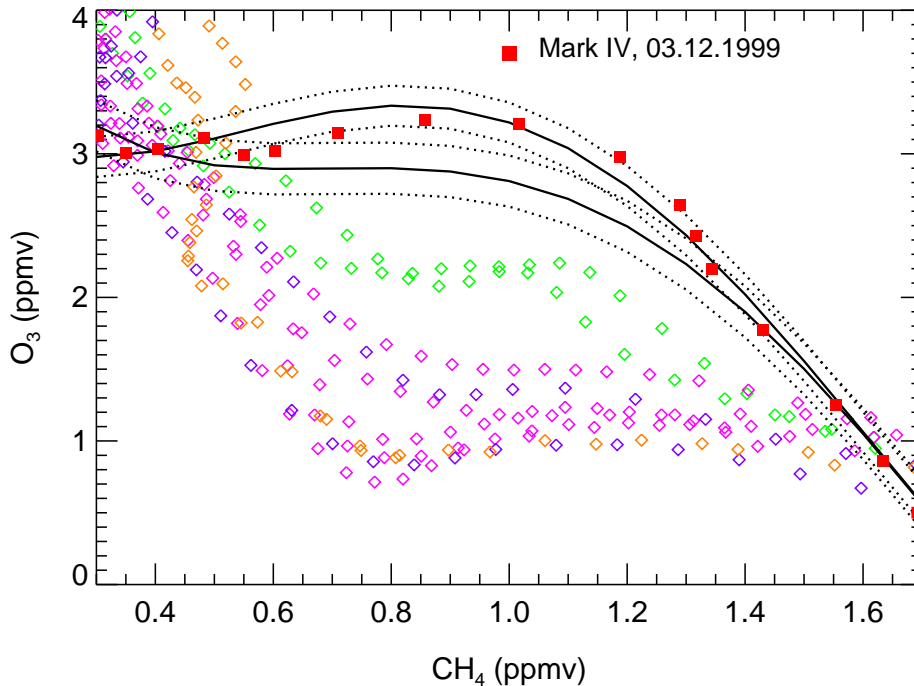


Figure 7.5: O_3/CH_4 relations from profiles inside the vortex of the year 1999–2000 from HALOE measurements are shown. Two different early winter reference functions for the O_3/CH_4 relation 1999–2000 were derived from balloon observations (see text) are indicated as a black solid line and the uncertainty of the reference function is represented by black dotted lines. Also shown are the observations of the MkIV instruments on 3 December 1999 in the early vortex (red squares). Different colours of HALOE profiles indicate the different time intervals when profiles were observed: February (green), first part of March (magenta), second part of March (purple), first part of April (orange).

do not overlap within their ranges of uncertainty. The derived reference function using the December measurements indicates greater mixing ratios of O_3 at a constant CH_4 so that greater ozone loss is derived than using the November reference. In this work, the average of the calculated ozone loss is derived from the results calculated with the use of the November reference function and the December reference function (see also *Salawitch et al.* [2002] and *Müller et al.* [2002]). The derived ozone-tracer early winter reference functions for nine out of eleven years are shown in Figure 7.6.

In 1997–98 and 2000–01 again no HALOE observations were obtained inside the early vortex and, unfortunately, no alternative measurements are available. Therefore, two reference functions for these two years were derived from the measurement of O_3 and the long-lived tracer inside early vortex from all those years for which HALOE measurements are available (i.e. 1992–93, 1993–94, 1994–95, 1995–96, 1998–99 and 2001–02).

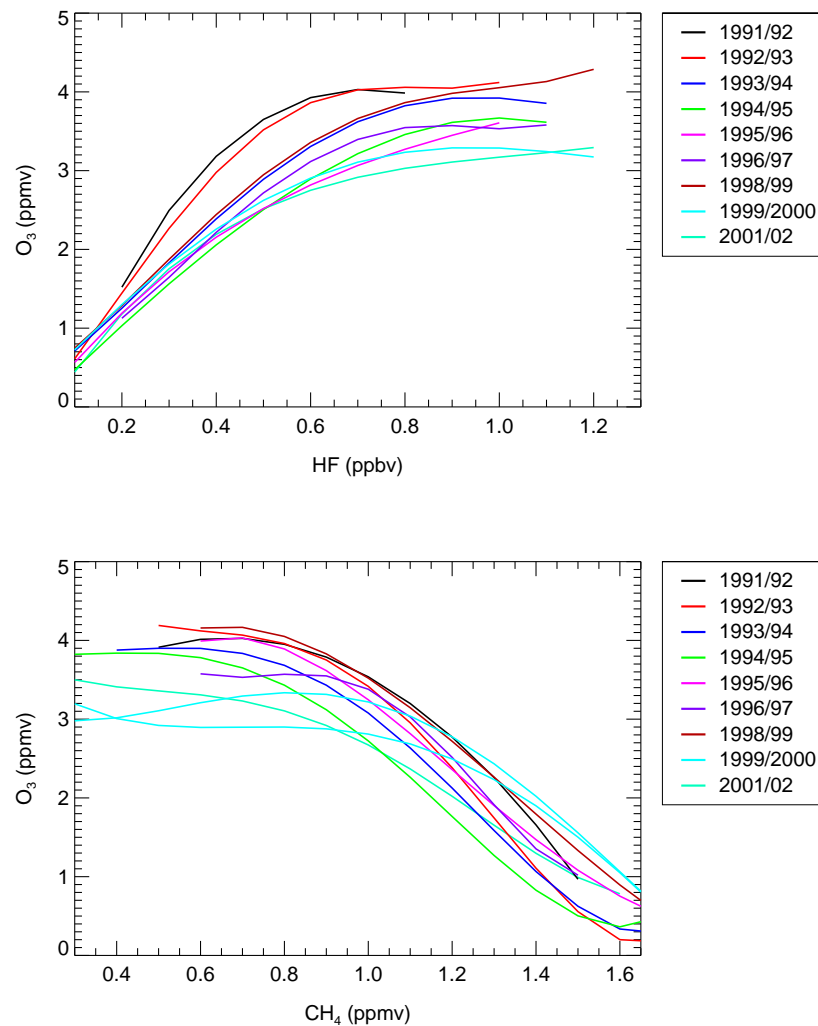


Figure 7.6: Early winter reference relations for the nine years between 1991–92 to 2001–2002 are indicated as coloured lines. O_3/HF is shown in the top panel and O_3/CH_4 is shown in the bottom panel.

The ozone and tracer relation in the early winter has its own characteristics each year, mainly due to inter-annual differences in polar vortex development and not due to chemical loss [Manney *et al.*, 1996b]. Thus, it is not possible to use one single reference function for all years. Year to year variations are also possible due to the changes of mixing ratios of the long-lived tracer used. Especially the increase of HF from 1991 to 2000 has an influence on the O_3/HF reference function.

Therefore, two early winter reference functions, one for winter 1997–98 and another for 2000–01, were constructed from a climatology of all HALOE profiles that were measured inside the early vortex over the eleven year period 1991–2002. Actually, measurements inside the early vortex are available for six winters

(1992–93, 1993–94, 1994–95, 1995–96, 1998–99 and 2001–02).

To obtain the O₃-tracer early winter reference function for the winters 1997–98 and 2000–01 from measurements of different winters, CH₄ and HF mixing ratios have to be corrected for the annual growth rate of these two tracers. For this purpose, the CH₄ growth from each single year to the year 1997–98 (2000–01) was taken from the tropospheric growth rate derived by *Simpson et al.* [2002]. HF mixing ratios are corrected for each CH₄ level, using the difference, Δ HF, between the HF mixing ratio (at each CH₄ level) of the year 1997–98 (2000–01) and the corresponding HF mixing ratio of each of the other years (see Figure 7.7, different coloured lines). These Δ HF values are interpolated between the different CH₄ levels to cover the range from 0.2 to 1.5 ppmv CH₄.

The corrected CH₄ and HF mixing ratios are used to transform the early winter O₃-tracer profiles of different years to the year 1998–99 (2000–01) for each altitude. The HALOE instrument measures different trace species (CH₄, HF, O₃ amongst others) at the same measurement points. Therefore, the CH₄ value corresponding to each O₃ value can be considered.

The O₃/CH₄ and O₃/HF profiles inside the early vortex of the six years transformed in this way are used to construct reference functions for 1997–98 and 2000–2001 determined from all available HALOE measurements inside the early vortex. Thus, for the winter 1997–98 and 2000–01 in each case two early winter reference relations were derived, one using HF as the long-lived tracer and one using CH₄ (see Figure 7.8, Tables C.2 and C.3).

7.3 Meteorological Conditions and the HCl-Tracer and O₃-Tracer Relation in Arctic Winters 1991–2002

Active chlorine inside the polar vortex causes chemical ozone loss, as described in Chapter 4. Using measurements made by HALOE, the evolution of the chlorine chemistry can be inferred from the development of the HCl-tracer relation during each year. Similar to the chlorine chemistry, ozone loss depends mainly on the meteorological conditions, in particular, vortex strength and temperature. If temperatures are sufficiently low (see Section 2.2) PSCs can occur in the polar stratosphere. The extent of the derived area of possible PSC existence during the entire lifetime of the vortex, as described in Section 4.4.2, based on meteorological analysis from the UKMO, is used to analyse the interaction between meteorology and tracer development for each winter (see Figures 7.9, 7.10 and 7.11). Further, a division into cold, moderately cold and warm winters is carried out.

- 1991–92:

The cold vortex in winter 1991–92 was disturbed by several warming pulses between November and February [*Naujokat et al.*, 1992]. The threshold temperature for PSCs was only reached during January. As described above (see Section 7.2, Figure 7.4), ozone loss already occurred in January 1992.

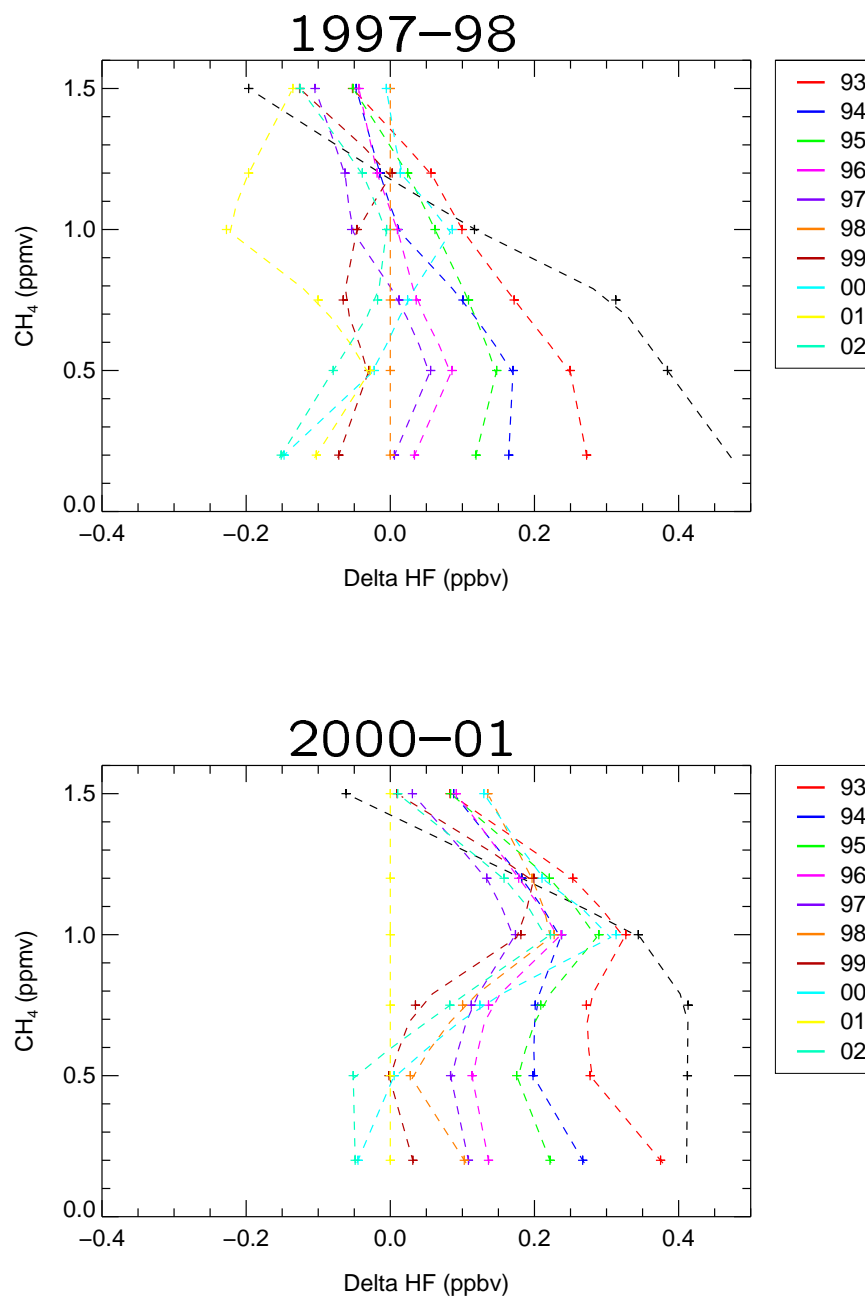
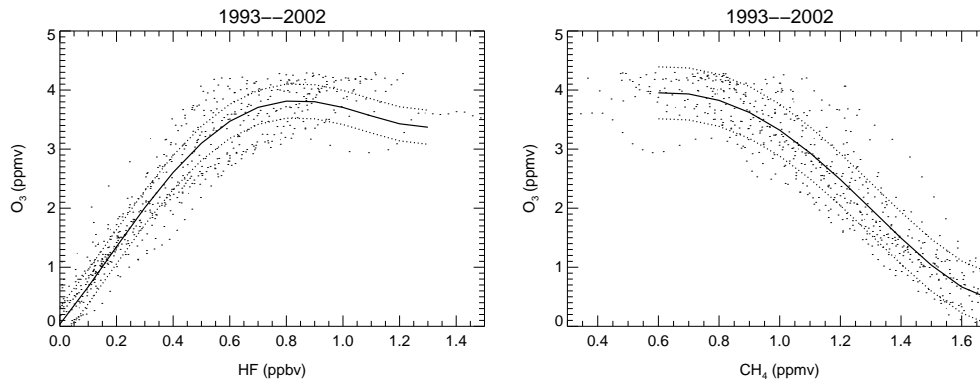


Figure 7.7: CH₄ in ppmv vs. Δ HF, the difference between HF mixing ratio of the year 1997–98 (top panel) and 2000–01 (bottom panel) and the corresponding HF mixing ratio of each of the other years at different CH₄ levels, shown in coloured lines.

1997–98



2000–01

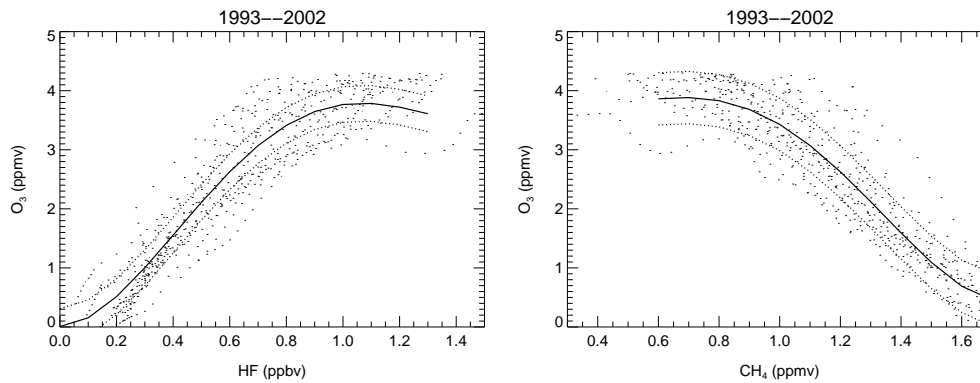


Figure 7.8: Ozone-tracer profiles inside the early vortex of the years 1992–93 to 1995–96, 1998–99 and 2001–02 (see text), black dots. The reference functions are indicated as black solid lines with an uncertainty represented by black dotted lines, valid for 1997–98 (top panels) and for 2000–01 (bottom panels). O_3 /HF is shown in the left-hand panels and O_3 / CH_4 is shown in the right-hand panels.

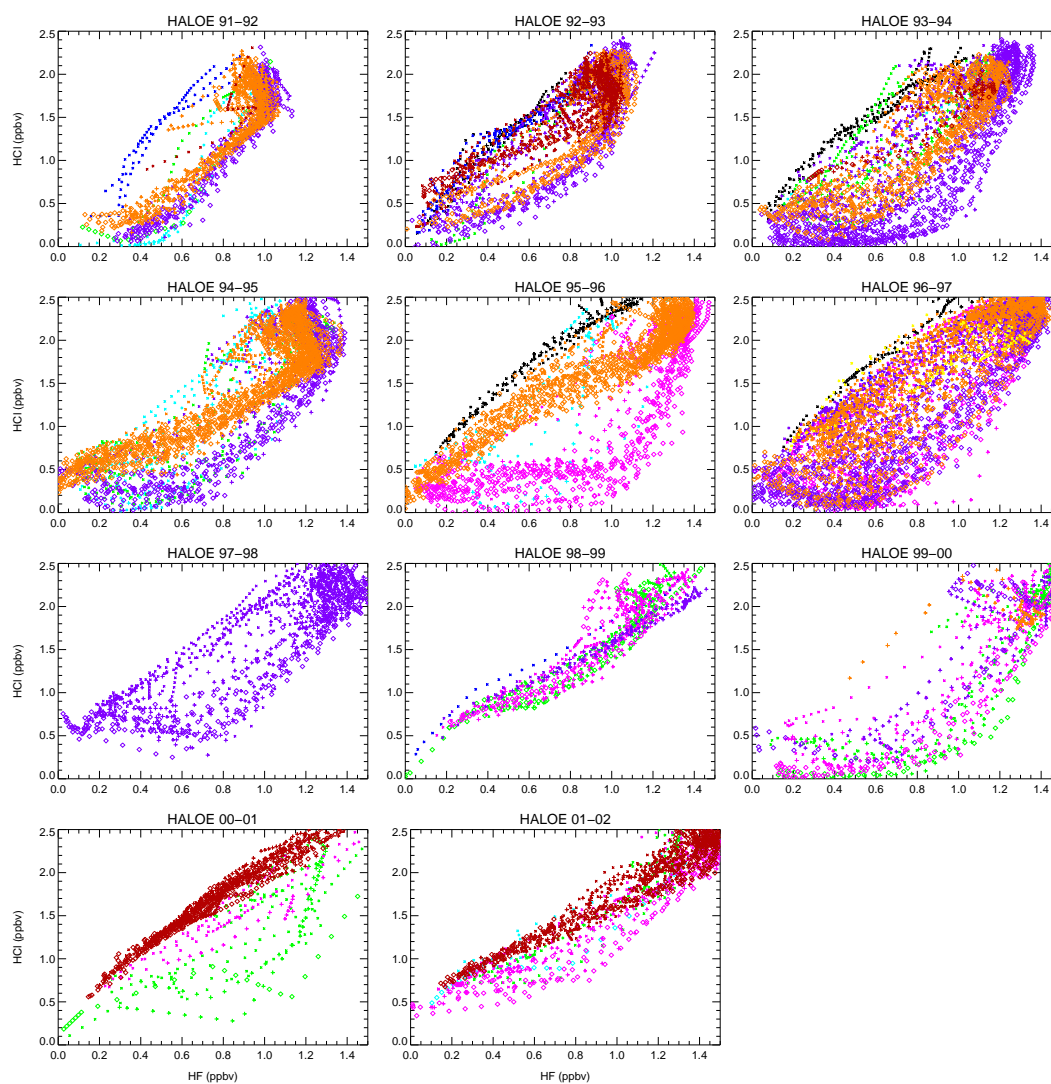


Figure 7.9: HCl/HF relations for the eleven winters between 1991-92 and 2001-02 as measured from profiles inside the vortex core (diamonds), inside the outer vortex (large plus signs), inside an outer part of the outer vortex (small crosses) by HALOE are shown. Different colours of profiles indicate the different time intervals when profiles were observed: November (black), December (blue), January (cyan), February (green), first part of March (magenta), second part of March (purple), first part of April (orange), second part of April (dark red).

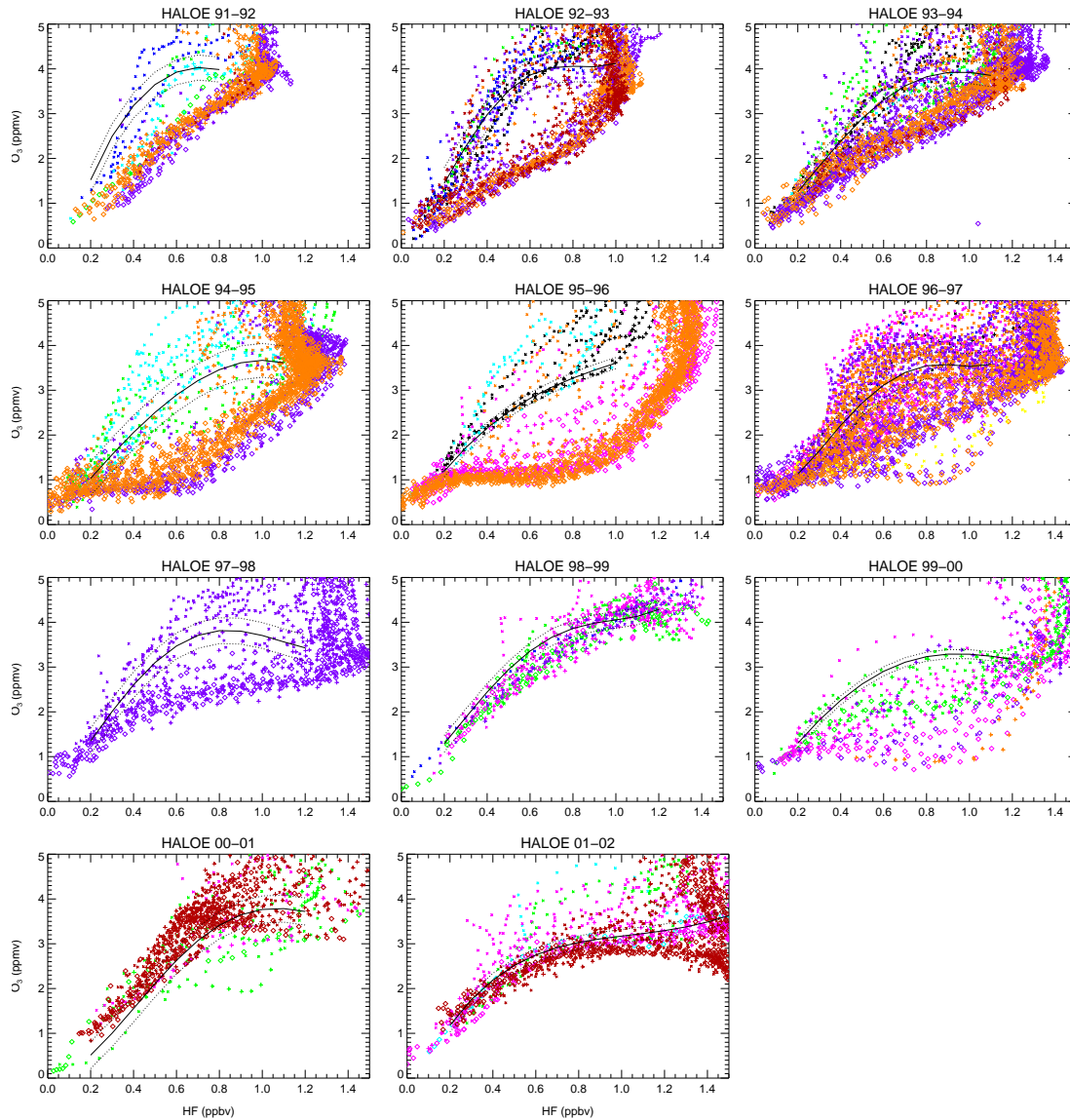


Figure 7.10: O_3 /HF relations for the eleven winters between 1991-92 and 2001-02 as measured from profiles inside the vortex core (diamonds), inside the outer vortex (large plus signs), inside an outer part of the outer vortex (small crosses) by HALOE are shown. Different colours of profiles indicate the different time intervals when profiles were observed: November (black), December (blue), January (cyan), February (green), first part of March (magenta), second part of March (purple), first part of April (orange), second part of April (dark red). Black lines indicate the reference functions derived for each year with the area of uncertainty (dotted lines).

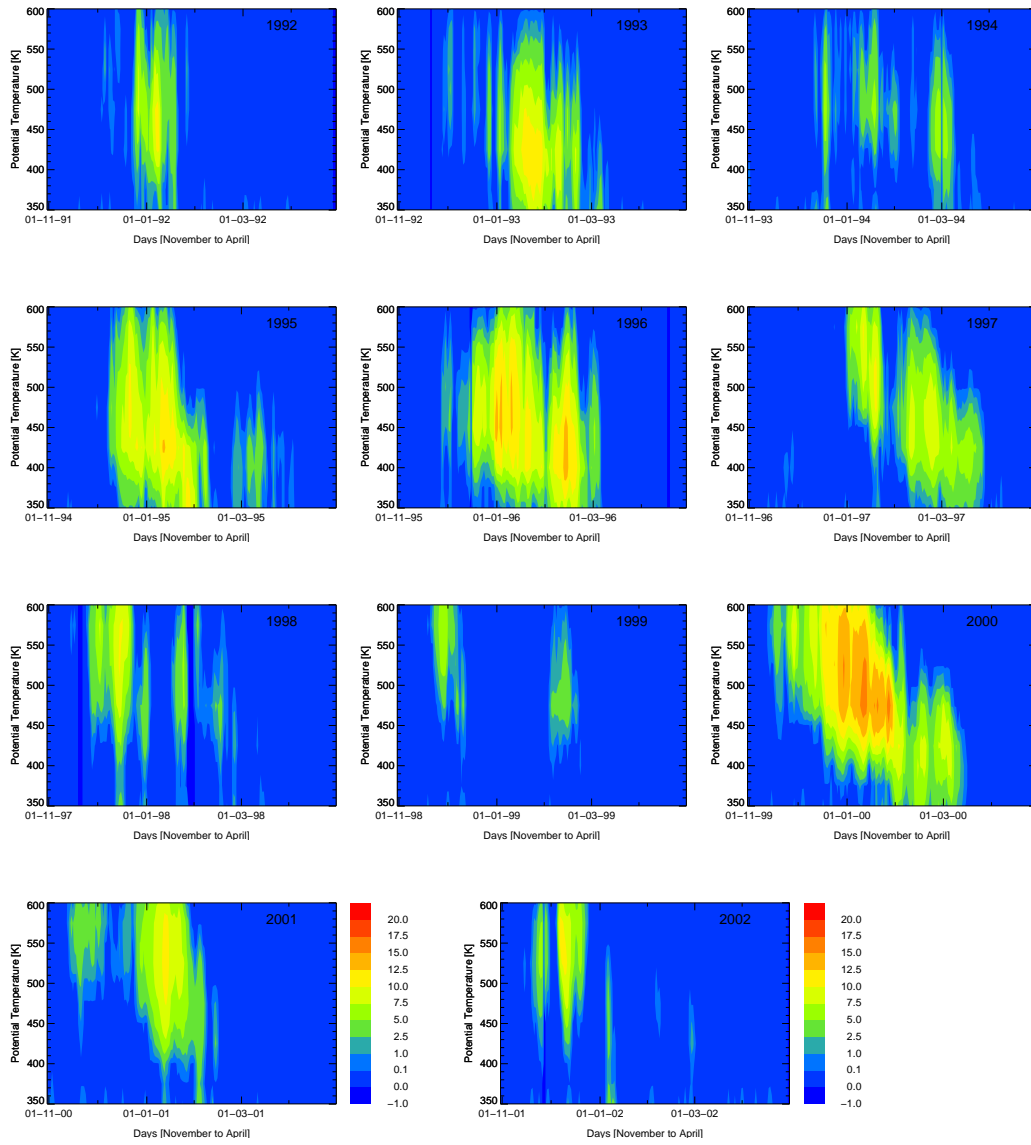


Figure 7.11: The area of possible PSC existence in 10^6 km^2 over the entire polar vortex, as a function of altitude, is shown for the time period from November to April for the eleven winters between 1991–92 and 2001–02. The PSC threshold temperature was calculated with the analysed UKMO temperatures and pressures together with typical stratospheric mixing ratios of HNO₃ (10 ppbv) and H₂O (5 ppmv) [Hanson and Mauersberger, 1988].

During March the temperatures at the north pole steadily increased and the vortex finally broke down at the end of April [Naujokat *et al.*, 1992]. In February and at the beginning of March a strong decrease in HCl and possibly strong chlorine activation (see Figure 7.9) occurred in the lower stratosphere (below ≈ 420 K). This effect is possibly caused by enhanced abundance of liquid aerosol sulphate in the lower stratosphere owing to the volcanic eruption of Mount Pinatubo (see Section 2.2.1). By April, the chlorine chemistry had recovered. The vortex became steadily weaker during April. From February up to the beginning of April a homogeneous moderate deviation from O₃/HF reference functions occurred.

- 1992–93:

The vortex in winter 1992–93 was cold and nearly undisturbed until the end of January. A strong minor warming in February shifted the cold air (with low ozone values) towards Europe. This, together with a blocking anticyclone in the troposphere, led to low total ozone values over Europe in February [Naujokat and Labitzke, 1993]. Conditions for chemical ozone loss were reached, because of the low stratospheric temperatures (see Figure 7.11). Unfortunately, no measurements were taken inside the vortex in February, but HCl measurements inside the outer part of the vortex boundary region indicate a strong chlorine activation in February at lower altitudes (see Figure 7.9, small green crosses). Temperatures started rising in March and the final break-up of the vortex occurred around April 10. At that time the recovery of the chlorine chemistry had taken place. Strong (homogeneous) deviation from the O₃-tracer reference function occurred in March and April. Until the end of April, the deviation from the O₃/HF reference function does not further change inside the remaining parts of the vortex.

- 1993–94:

The early vortex in winter 1993–94 was slightly disturbed in November, December and January [Naujokat *et al.*, 1995a]. Owing to the warming over Europe in February, the vortex was split most of the time. At the end of February and the beginning of March, the vortex air masses cooled down again and temperatures were below the threshold for the existence of PSCs for a few days. A small decrease of HCl from the HCl/HF relation chlorine activation is noticeable in February, afterwards it strongly decreased during March (HCl mixing ratios were below 0.1 ppbv for HF mixing ratios below 0.7 ppbv). During April the chlorine chemistry quickly recovered while the vortex became weaker. In March and April moderate deviations from the O₃/HF reference function became noticeable, also the chlorine activation seemed to be quiet pronounced.

- 1994–95:

The vortex in 1994–95 formed early and was very cold and strong especially between mid-December and mid-January. A large area of PSCs was possible

during the whole of January 1995. After a warming event in February, record low temperatures were reached in the lower stratosphere in March [Naujokat *et al.*, 1995b]. In April the vortex split and one part rapidly weakened and disintegrated over eastern Asia. The main vortex centre vanished more slowly. As in winter 1992–93, a strong decrease of HCl mixing ratio in the outer part of the vortex boundary region was observed by HALOE in February. Although the chlorine activation in March was not as strong as in the previous winter 1993–94, much stronger deviations from the O₃-tracer reference relation in March were observed, because of the possibly strong chlorine activation inside the vortex in February. During April the chlorine chemistry recovered quickly.

- 1995–96:

The winter 1995–96 was the coldest recorded by the US National Meteorology Center (NMC) in 18 years [Manney *et al.*, 1996b]. Since December 1995, the stratospheric temperatures in the Arctic were below the PSC threshold until March. The final warming began in early March. Measurements taken by HALOE in the vortex are available for the first part of March and the first part of April. The strongest chlorine activation in March for this eleven-year overview was observed. The chlorine chemistry had almost completely recovered in April. The deviation from the early winter reference function O₃/HF is the same for March and April. Thus, in April no further ozone loss was identified.

- 1996–97:

The meteorology of this winter was described in detail in Section 5.1. Deviations from the O₃-tracer early winter reference function (see Section 5.3) are separated into two parts. The chlorine activation is also rather inhomogeneous with the strongest decrease of HCl inside the vortex core. The strongest April decrease of HCl mixing ratio was observed in this year, because the vortex remained intact for an extremely long period.

- 1997–98:

The vortex in 1997–98 was slightly disturbed throughout the whole winter. The final warming began in the middle of March [Pawson and Naujokat, 1999]. Minimum temperatures were low enough to activate HCl during December and during January (see Figure 7.11). Moderate chlorine activation was observed by HALOE in March and small deviations from the reference function for O₃-tracer occurred. In that winter HALOE data are only available for March inside the polar vortex.

- 1998–99:

The winter 1998–98 was unusually warm due to a major stratospheric warming in mid-December [Manney *et al.*, 1999]. The vortex in 1998–99 was very weak and disturbed. Almost no changes in the HCl/HF relation occurred, owing to a small possible area of PSCs and thus, very little chlorine acti-

vation at the end of February. However, small deviations from the early winter reference function were found.

- 1999–2000:

In 1999–2000 the Arctic stratosphere was very cold from the middle of November to late March [Manney and Sabutis, 2000]. The lowest values of the February HCl mixing ratios for any of the observed years were reached, owing to the largest possible area of PSCs during January in the observed period. HCl mixing ratios are comparable to the low mixing ratios in March 1996. In March 2000, a slight recovery of chlorine chemistry became noticeable, with a total recovery at the end of April. The small deviation from the early winter reference function HF/O₃ in February strongly increased in March up to April.

- 2000–01:

The vortex in 2000–01 developed during October and November 2000. A strong Canadian warming at the end of November greatly disturbed the vortex. An undisturbed cold period followed from late December until mid-January. Afterwards, a major warming broke down the vortex in mid-February. During this warming, the vortex drifted over central Europe for a few days and PSC conditions were reached due to a short-term cooling of the vortex in the stratosphere. The vortex was re-established in March and lasted until April. Figure 7.9 displays strong chlorine activation in February 2001. From March to April activated chlorine disappeared. In the ozone-tracer relation in February 2001 one profile inside the outer vortex indicates a significant deviation from the early winter reference function. In March and April the early winter reference function is possibly not valid any more, owing to the temporary break-up of the vortex in February. Therefore, the TRAC technique cannot be applied to ozone-tracer profiles inside the late vortex April that scatter above the early winter reference function.

- 2001–02:

The winter 2001–02 was very warm winter. Although the temperatures at the end of November reached a record minimum in 1979–2001, a strong warming in the second half of December occurred so that the vortex significantly weakened. After the vortex was re-established in January, it was weak and warm until it broke down in May. Very little chlorine activation is noticeable at the end of March 2002 (see Figure 7.9) and very little deviation from the early winter reference relation is apparent at the end of April.

To summarise the temperature conditions for winters between 1991–92 and 2001–02, five winters are characterised as being cold (1992–93, 1994–95, 1995–96, 1996–97 and 1999–2000). These winters show a strong decrease of the HCl mixing ratio in the HCl/HF relation in spring and strong deviations of O₃-tracer profiles from the early winter reference function. Moderate deviations from the

O₃/HF reference were found in 1991–92, 1993–94 and 1997–98. These winters indicating a more frequently disturbed vortex are characterised as moderately cold. The winters 1998–99, 2000–01 and 2001–02 are warm with very little chlorine activation and very little deviation from the early winter ozone-tracer reference function. The determination of the amount of ozone loss based on the O₃-tracer relation is discussed in the next chapter.

Chapter 8

Column Ozone Loss and Ozone Loss Profiles

The development of the ozone-tracer relation over winter and spring was described in Chapter 7. Here, the ozone loss in the total column for the eleven years between 1991–92 and 2001–02 is calculated by the vertical integration of ozone loss profiles. First, the ozone loss profiles are considered (see Section 8.1). For each year, the ozone loss profiles differ with respect to the altitude range where ozone loss occurs, the maximum local ozone loss, the altitude where this maximum loss occurs and the extent of homogeneity of the distribution. In Section 8.2, the column ozone loss over the eleven-year period is summarised. Differences between the results using different long-lived tracers are described as well as the differences between results calculated from profiles inside the vortex core and inside the outer vortex. At the end of this chapter, a comprehensive discussion of the TRAC technique is presented. In particular, an error analysis of the chemical ozone loss derived using the TRAC technique is performed (see Section 8.3).

8.1 Vertical Ozone Loss Profiles in Arctic Winters 1991–2002

Vertical ozone loss profiles (see Figure 8.1, 8.2 and 8.3, green symbols) are calculated as the difference between the actually measured ozone concentration O_3 (red symbols) and the corresponding ozone proxy \hat{O}_3 (black symbols), as described in detail in Section 4.1.

In all winters considered, significant ozone loss arose mainly in an altitude range between 380 and 550 K. At altitudes below 380 K the uncertainty of profiles increased in most winters, because of the influence of tropospheric variability, that is the influence of mixing processes.

The shape of the vertical ozone loss profiles and, therefore, the amount of ozone destroyed at different altitudes depends on the different meteorological conditions inside the polar vortex for each winter. The maximum of the vertical ozone loss profile (in mixing ratio) and the corresponding altitude range (in

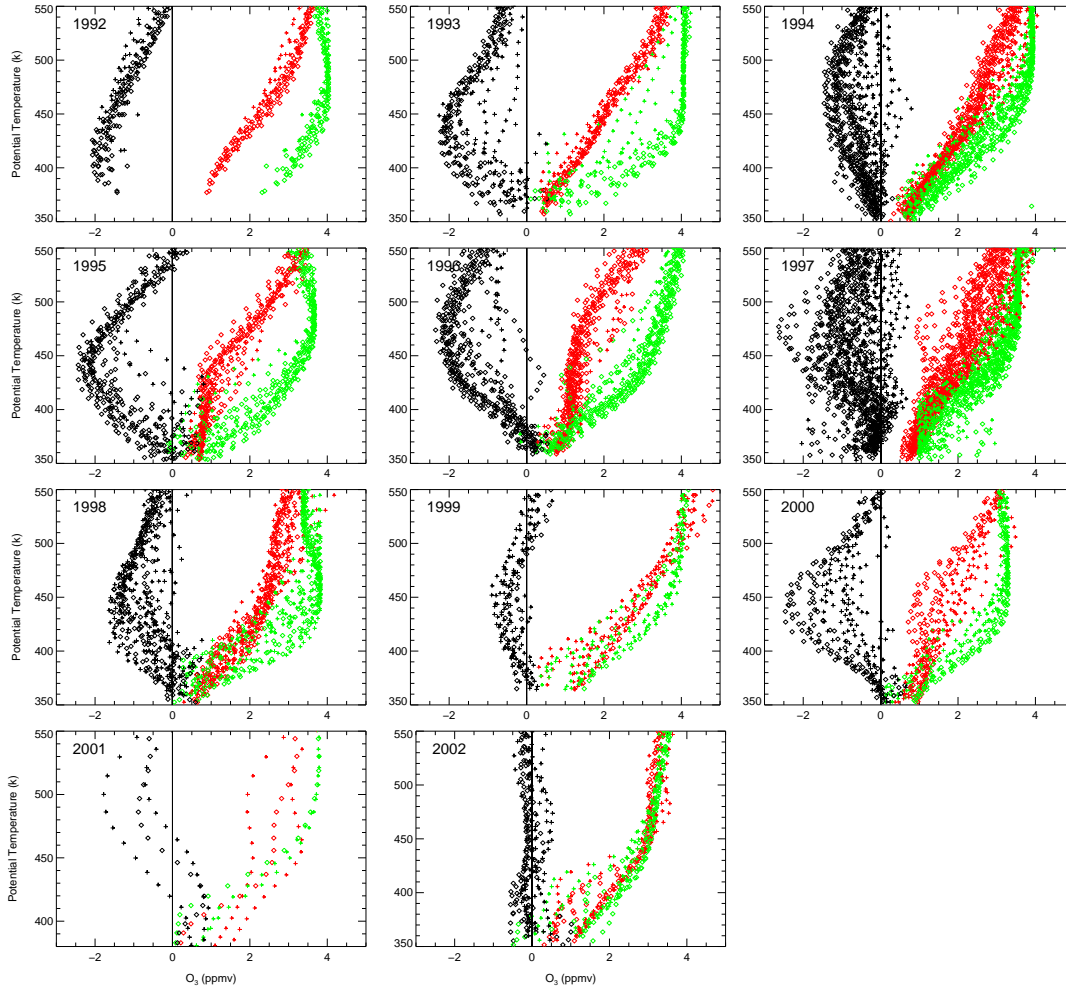


Figure 8.1: Vertical profiles (plotted against potential temperature) of measured O_3 mixing ratios (red diamonds) by HALOE, the ozone mixing ratios expected in the absence of chemical change (\hat{O}_3 , green diamonds), and the difference between expected and observed O_3 (ΔO_3 , black diamonds) are shown for the winters between 1991–92 and 2001–02 in March (2000–01 in February). \hat{O}_3 was inferred using HF as the long-lived tracer and the early winter reference functions (see Table C.4), from profiles inside the vortex core (squares) and inside the outer vortex (plus signs).

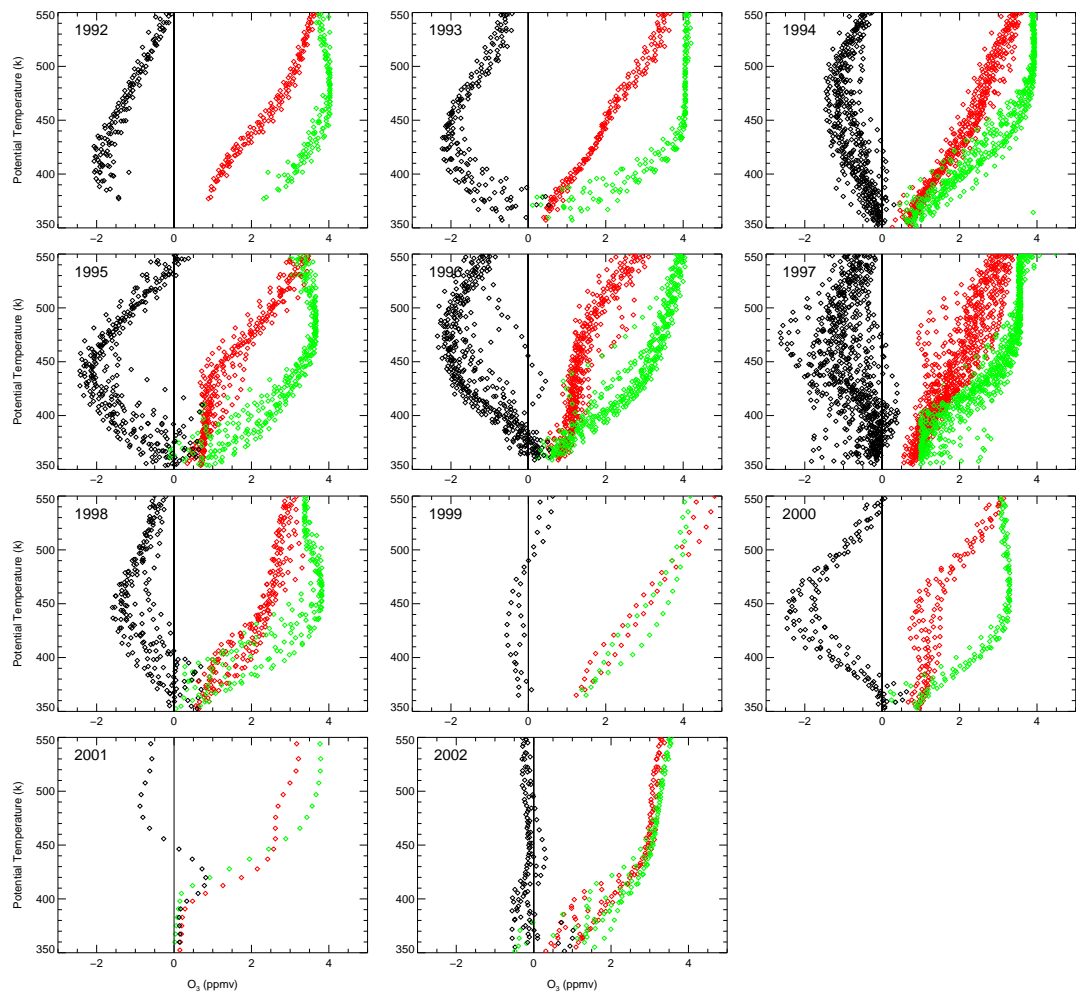


Figure 8.2: As in Figure 8.1, but only profiles inside the vortex core are shown.

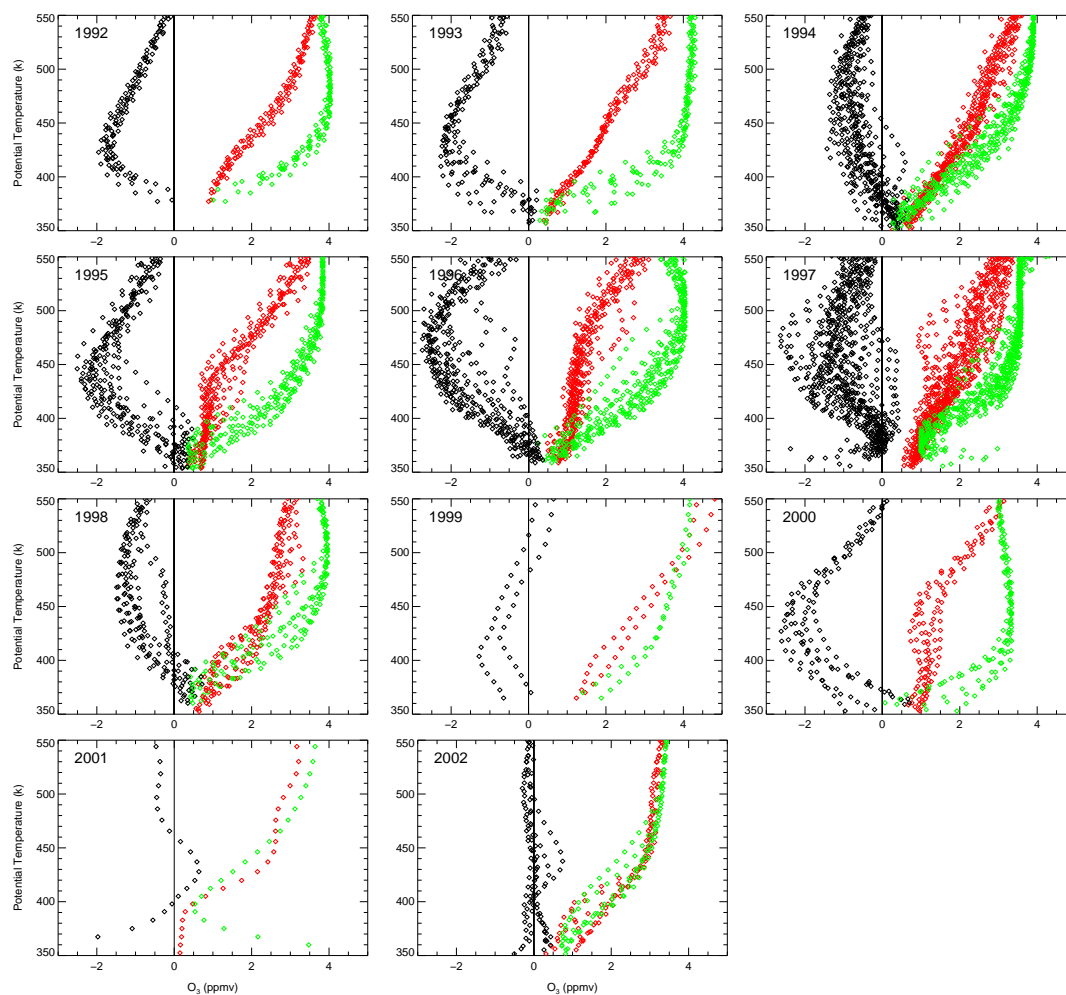


Figure 8.3: As in Figure 8.2, but with CH₄ used as the long-lived tracer and only profiles inside the vortex core are shown.

potential temperature) is shown in Table 8.1 for March (or February in the year 2001) of each year. The uncertainty was determined from the uncertainty of the

Table 8.1: Maximum of the local accumulated ozone loss in ppmv in March (February in 2001) for the winters between 1991–92 and 2001–02 in the altitude range (in potential temperature), where the loss profile reaches a maximum ± 0.1 ppmv, is determined employing both the reference relation using HF and CH₄ as the long-lived tracer, respectively, for the HALOE measurements inside the entire vortex, with an uncertainty derived from the uncertainty of early winter reference function. Additionally, the averages between the maximum derived using HF and CH₄ as the long-lived tracer are shown.

date	tracer	altitude	tracer	altitude	tracer
	HF	range (K)	CH ₄	range (K)	HF and CH ₄
March 1992	2.0 \pm 0.3	390–445	1.9 \pm 0.3	410–450	2.0 \pm 0.4
March 1993	2.2 \pm 0.3	405–460	2.2 \pm 0.2	390–460	2.2 \pm 0.2
March 1994	1.4 \pm 0.2	420–460	1.4 \pm 0.3	400–475	1.4 \pm 0.3
March 1995	2.3 \pm 0.4	420–470	2.5 \pm 0.4	410–460	2.4 \pm 0.5
March 1996	2.2 \pm 0.1	455–515	2.6 \pm 0.3	450–500	2.4 \pm 0.5
March 1997	2.5 \pm 0.2	460–485	2.5 \pm 0.2	460–485	2.5 \pm 0.2
March 1998	1.5 \pm 0.3	410–455	1.4 \pm 0.4	430–510	1.5 \pm 0.5
March 1999	0.8 \pm 0.2	400–480	1.2 \pm 0.1	395–415	1.0 \pm 0.2
March 2000	2.4 \pm 0.1	430–455	2.5 \pm 0.1	410–455	2.5 \pm 0.2
February 2001	1.7 \pm 0.3	475–535	1.7 \pm 0.4	490–515	1.7 \pm 0.4
March 2002	0.5 \pm 0.2	380–540	0.3 \pm 0.2	380–540	0.4 \pm 0.3

early winter reference function (see Table C.4, Appendix C). The results of the two different tracers are inside the uncertainty for each year, except for the year 2000–01. To perform a comparison between the different years, the average of the maximum ozone loss of the two different long-lived tracers is calculated (see Table 8.1, column 6). The strongest local ozone loss of all the years considered, about 2.4 ppmv in 1995–96 and 2.5 ppmv 1996–97, was found in the altitude range from about 450–490 K. In the winters of 1994–95 and of 1999–2000 the maximum of local ozone loss profiles was similarly strong in the altitude range from about 410–460 K. In March 1992 and 1993 local ozone loss is also rather strong, 2.0 ppmv in 1992 and 2.2 ppmv in 1993 at very low altitudes in 390–460 K. Winters termed moderately cold, in the section above, 1991–92, 1993–94 and 1997–98, show local ozone loss from about 1.5 ppmv, except for the winter 1991–92. In warm winters, 1998–99 and 2001–02, the local ozone loss is 1.0 ppmv and 0.4 ppmv respectively. In 2000–01 local ozone loss reached 1.7 ppmv from profiles inside the outer vortex in February only (see Figure 8.1), whereas the local ozone loss profiles inside the vortex core do not exceed 1.0 ppmv in February 2000–01.

To discuss the homogeneity of ozone loss profiles (see Figure 8.1) the distribution of single loss profiles inside the vortex core and, further, the differences

between vortex core and outer vortex are presented.

In some years 1991–92, 1992–93, 1999–2000, the ozone loss profiles taken inside the vortex core are very homogeneous for March (see Figure 8.3). This is the result of an isolated vortex core with homogeneous ozone loss.

For 1993–94, 1994–95, 1995–96 and 1997–98, a few profiles of ozone loss indicate somewhat smaller deviation from the reference function inside the vortex core but the majority of profiles inside the vortex core are homogeneously distributed. In 1993–94 and 1994–95 a warming in February disturbed the isolated vortex. In 1995–96, the vortex shifted off the pole and the cold region was near the edge of the vortex. At this time rapid ozone destruction occurred at the vortex edge [Manney *et al.*, 2003a]. The vortex in 1995–96 and 1997–98 was already weakening at the end of February and broke down in March. The ozone loss profiles ΔO_3 in 1996–97 are separated in two distinct parts inside the entire vortex and the vortex core, as described in Section 6.2.3.

The homogeneity of ozone loss profiles in a particular month in the different winters corresponds to the extent of isolation of the vortex during winter. The described meteorological developments during various winters may be responsible for inhomogeneous temperature distributions inside the vortex and, therefore, are responsible for the inhomogeneities in ozone destruction inside the vortex core.

Considering the conditions inside the outer vortex (see Figure 8.1) ozone loss profiles indicate less ozone loss for all years. The temperatures are generally not as low inside the vortex core in March and, therefore, less ozone loss occurred. In 1998–99 and 2000–01 small deviations occurred for profiles inside the vortex core, but slightly stronger deviations are found for the outer vortex. It is possible that the intensity of solar radiation is stronger inside the outer vortex, which is generally located more towards lower latitudes. In winter 2001–02 no significant ozone loss is determined in March. Further discussion of the differences between ozone loss inside the vortex core and the outer vortex is given in the next section.

8.2 Column Ozone Loss in Arctic Winters 1991–2002

A measure of ozone loss is derived by integrating the ozone loss profile ΔO_3 , as described in Section 4.1. It can be interpreted as the total amount of destroyed ozone in a period between the time of the early winter reference function and the time of the investigated profile. This value constitutes a good approximation of the total amount of ozone loss over the entire column of ozone if the vertical integration is extended over a sufficiently large vertical range (≈ 380 – 550 K). The column ozone loss was calculated for different altitude ranges between 350 and 550 K in this work. Further, monthly averages are considered and differences of the results deduced from two long-lived tracers are discussed.

The column ozone loss averaged over different months, i.e. February, March, April and May (May only in winter 1996–97), was calculated for each year if measurements were available (see Figure 8.4 and Tables 8.2 and 8.3). The un-

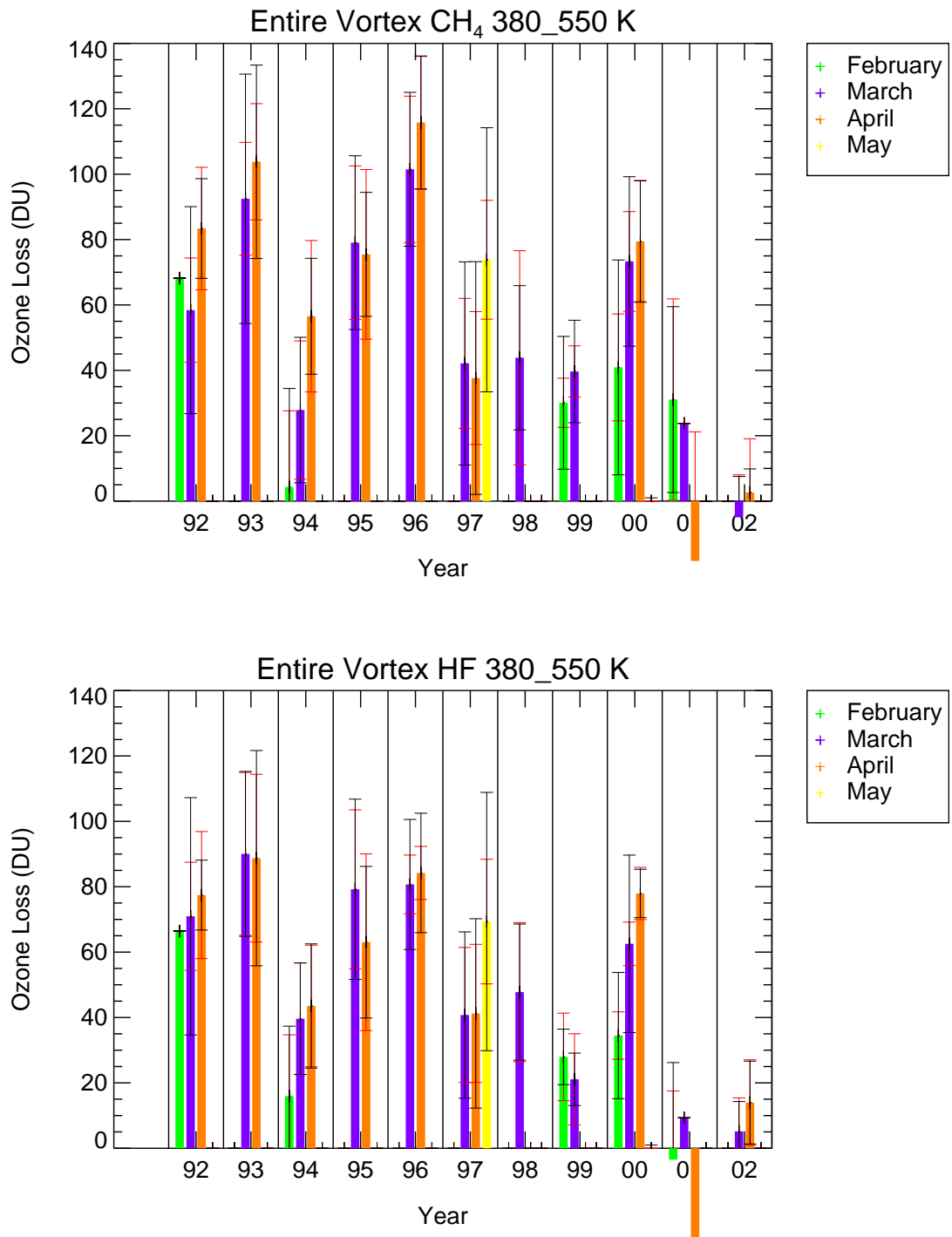


Figure 8.4: Mean column ozone loss for February (green), March (purple), April (orange) and May (yellow) in winters between 1991–92 and 2001–02 is shown. The red error bar indicates the uncertainty of the early winter reference function, the black error bar the standard deviation. Top panel: CH₄ was used as the long-lived tracer, bottom panel: HF was used as the long-lived tracer. Ozone loss was derived from profiles inside the entire vortex.

certainty of the mean column ozone loss is described by two parameters. On the one hand, the uncertainty which only arose due to the uncertainty of the early winter reference function, the red error bar, in Figure 8.4. On the other hand, the standard deviation of the column ozone loss deduced from the individual profiles, which is a measure of the homogeneity of the ozone loss during the considered period, the black error bar. Inhomogeneities may be caused by both, the inhomogeneity of the ozone loss inside the vortex, and, the random error of the satellite measurements.

The uncertainty of the early winter reference function is about 15–25 DU in the altitude range of 380–550 K (see Table 8.2) depending on the scatter of profiles inside the early vortex from which the reference function was derived (see Figure 8.4, top and middle panel). If there is very little scatter the error in the results is smaller than 10 DU as is the case in the year 1995–96 using HF as the long-lived tracer and in 1998–99 using CH₄ as the long-lived tracer. In 1999–2000 the early winter reference was deduced from balloon observations with a rather small uncertainty.

The standard deviation of the column ozone loss depends on the homogeneity of single loss profiles, as described in Section 8.1. For March 1997 the standard deviation of averaged column ozone is larger compared to the other winters and is much larger than the early winter reference error (see Figure 8.4, top and middle panel). As described in a previous Section 6.2.3, in March 1996–97 the vortex is divided into two parts, a part with stronger ozone loss and a part with moderate ozone loss [Tilmes *et al.*, 2003]. The ozone loss in March 1996–97 is spatially much more inhomogeneous than the ozone loss observed in all the other winters investigated here (see Figure 8.1).

The mean calculated column ozone loss differs depending on whether HF or CH₄ is used as the long-lived tracer and whether the vortex core or the entire vortex was considered. At first, the difference between the results derived with the two long-lived tracers are discussed (see Figure 8.5).

The differences between the results are ≈ 10 –20 DU for most of the observed years and are similar for the entire vortex and the vortex core (not shown). In March 1996 and February 2001, the results differ by more than 30 DU for the entire vortex. In 1996–97 and 1997–98 differences are insignificant (below 5 DU). The uncertainty of the early winter reference functions using the two different long-lived tracers are mostly responsible for the different results. In most observed years the results obtained using CH₄ as the long-lived tracer agree with those using HF inside the uncertainty introduced by the uncertainty of the reference function.

In some years, ozone loss calculated employing CH₄ as the long-lived tracer has a tendency towards larger ozone loss for April compared to HF (see Figure 8.4). The CH₄ mixing ratios inside the Arctic vortex at altitudes below about 450 K may be problematic in these years, due to signal saturation problems (J. Russell pers. comm., 2001). Such problems are also discussed for the winter 1999–2000 in [Müller *et al.*, 2002]. The significant uncertainties in March 1996 and February 2001 may be explained by this effect.

Table 8.2: Column ozone loss (DU) in 380–550 K derived for profiles inside the entire vortex and the vortex core for different months and years (Column 1), using HF (Column 2 and 3) and CH₄ as the long-lived tracer (Column 4 and 5). The error was derived from the uncertainty of the early winter reference function and the standard deviation σ of the result is shown in brackets. No standard deviation is shown if the column ozone loss was calculated from only one profile.

date	HF: entire (σ)	HF: core (σ)	CH ₄ : entire (σ)	CH ₄ : core (σ)
1992				
February	66 ± 18	66 ± 18	68 ± 17	68 ± 17
March	71 ± 17 (36)	85 ± 17 (30)	58 ± 16 (32)	71 ± 16 (24)
April	77 ± 19 (11)	73 ± 19 (12)	83 ± 19 (15)	83 ± 18 (15)
1993				
March	90 ± 25 (25)	104 ± 24 (11)	93 ± 17 (38)	109 ± 17 (27)
April	89 ± 26 (33)	100 ± 25 (21)	104 ± 18 (30)	117 ± 17 (23)
1994				
February	16 ± 19 (21)		4 ± 23 (30)	
March	40 ± 17 (17)	48 ± 16 (11)	28 ± 21 (22)	37 ± 20 (16)
April	44 ± 19 (19)	41 ± 19 (20)	57 ± 23 (18)	56 ± 23 (16)
1995				
March	79 ± 24 (28)	84 ± 24 (21)	79 ± 24 (27)	83 ± 23 (22)
April	63 ± 27 (23)	62 ± 27 (23)	76 ± 26 (19)	75 ± 26 (19)
1996				
March	81 ± 9 (20)	82 ± 9 (19)	102 ± 22 (24)	102 ± 22 (24)
April	84 ± 8 (18)	87 ± 8 (13)	116 ± 20 (20)	119 ± 20 (14)
1997				
March	41 ± 21 (25)	52 ± 20 (21)	42 ± 20 (31)	56 ± 20 (26)
April	42 ± 21 (29)	61 ± 20 (24)	38 ± 20 (36)	59 ± 19 (28)
May	69 ± 19 (40)		74 ± 18 (40)	
1998				
March	48 ± 21 (21)	50 ± 21 (17)	43 ± 33 (21)	47 ± 32 (20)
1999				
February	28 ± 13 (9)	26 ± 13 (8)	30 ± 8 (20)	28 ± 8 (23)
March	21 ± 14 (8)	15 ± 13 (4)	40 ± 8 (16)	38 ± 7 (28)
2000				
February	35 ± 7 (19)	42 ± 7 (7)	41 ± 16 (33)	52 ± 16 (8)
March	63 ± 7 (27)	83 ± 6 (13)	73 ± 15 (26)	89 ± 15 (17)
April	78 ± 8 (7)		79 ± 19 (19)	
2001				
February	-4 ± 21 (30)	-5 ± 21	31 ± 31 (28)	7 ± 39
March	9 ± 27		4 ± 29	
April	-36 ± 28 (11)	-32 ± 27 (10)	-18 ± 40 (17)	-6 ± 39 (9)
2002				
March	12 ± 10 (4)	5 ± 10 (9)	-5 ± 13 (13)	0 ± 13 (9)
April	16 ± 13 (9)	14 ± 13 (13)	3 ± 16 (7)	2 ± 17 (8)

Table 8.3: Column ozone loss (DU) in the altitude range of 400–500 K derived for profiles inside the entire vortex and the vortex core for different month and years (Column 1), using HF (Column 2 and 3) and CH₄ as the long-lived tracer (Column 4 and 5). The error was derived from the uncertainty of the early winter reference function and the standard deviation σ of the result is shown in brackets. No standard deviation is shown if the column ozone loss was calculated from only one profile.

date	HF: entire (σ)	HF: core (σ)	CH ₄ : entire (σ)	CH ₄ : core (σ)
1992				
February	50 ± 11	50 ± 11	53 ± 11	53 ± 11
March	54 ± 11 (21)	60 ± 11 (20)	48 ± 10 (21)	55 ± 10 (19)
April	53 ± 12 (7)	53 ± 12 (6)	59 ± 11 (6)	60 ± 11 (5)
1993				
March	68 ± 15 (18)	77 ± 15 (5)	67 ± 10 (21)	78 ± 10 (10)
April	67 ± 16 (22)	73 ± 16 (13)	74 ± 11 (18)	82 ± 10 (11)
1994				
February	11 ± 11 (17)		6 ± 14 (25)	
March	27 ± 10 (14)	34 ± 10 (8)	21 ± 13 (17)	27 ± 13 (12)
April	31 ± 12 (13)	30 ± 12 (12)	42 ± 14 (12)	41 ± 14 (10)
1995				
March	61 ± 14 (20)	65 ± 15 (14)	61 ± 14 (18)	64 ± 14 (13)
April	33 ± 16 (14)	52 ± 16 (13)	62 ± 15 (14)	62 ± 15 (14)
1996				
March	62 ± 6 (19)	62 ± 6 (19)	78 ± 14 (20)	78 ± 14 (20)
April	64 ± 5 (14)	66 ± 5 (10)	88 ± 13 (16)	91 ± 12 (11)
1997				
March	31 ± 13 (21)	40 ± 13 (18)	35 ± 13 (26)	46 ± 12 (22)
April	30 ± 13 (24)	47 ± 13 (20)	30 ± 13 (29)	47 ± 12 (22)
May	46 ± 12 (32)		50 ± 11 (34)	
1998				
March	39 ± 13 (15)	42 ± 13 (14)	36 ± 20 (18)	37 ± 20 (16)
1999				
February	21 ± 8 (6)	20 ± 8 (7)	24 ± 5 (19)	22 ± 5 (17)
March	19 ± 9 (8)	13 ± 8 (8)	31 ± 5 (8)	28 ± 5 (14)
2000				
February	27 ± 5 (18)	42 ± 7 (7)	30 ± 10 (22)	35 ± 10 (3)
March	50 ± 4 (22)	67 ± 4 (10)	55 ± 9 (22)	67 ± 9 (12)
April	77 ± 5 (5)		80 ± 11 (2)	
2001				
February	-2 ± 13 (24)	-7 ± 12	18 ± 19 (23)	-1 ± 17
March	13 ± 17		26 ± 24	
April	-19 ± 17 (9)	-17 ± 17 (11)	-6 ± 25 (12)	3 ± 25 (5)
2002				
March	1 ± 7 (7)	5 ± 6 (5)	-6 ± 8 (10)	-2 ± 8 (8)
April	10 ± 8 (5)	10 ± 8 (4)	4 ± 10 (5)	4 ± 10 (5)

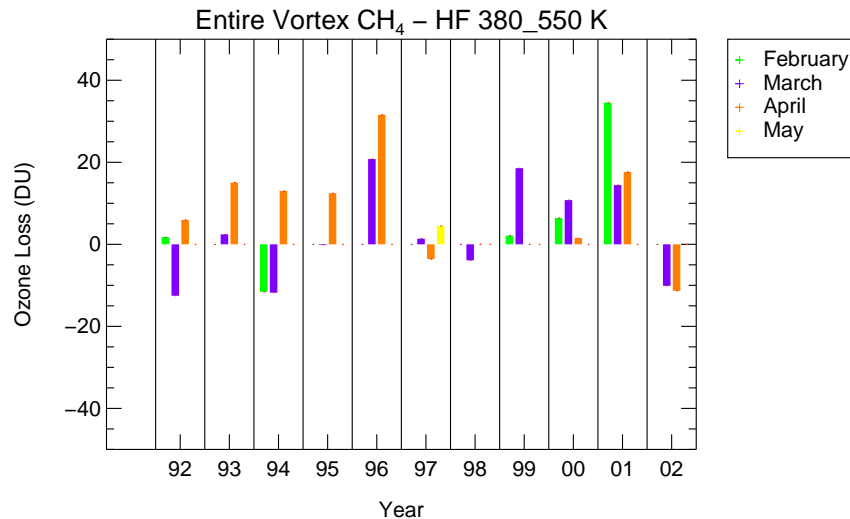


Figure 8.5: Difference between mean column ozone loss using HF and CH₄ as the long-lived tracer (see Figure 8.4 top and bottom panel) for February (green), March (purple), April (orange) and May (yellow) in winters between 1991–92 and 2001–02 is shown. Ozone loss was derived from profiles inside the entire vortex.

The mean column ozone loss, the average between the results calculated using CH₄ and HF as the long-lived tracer is calculated for each month/year, in an altitude range from 380–550 K and 400–500 K (see Figure 8.6). Furthermore, the mean column ozone loss between the 400–550 K level was calculated to compare the results with other studies (see Chapter 9). The calculated column ozone loss between the 400–500 K level for profiles inside the vortex core is showing the smallest error (see Figure 8.6, bottom right). Here, uncertainties at lower altitudes between the 380–400 K level are excluded, such as the horizontal mixing of air from outside the vortex into the edge of the vortex. The error which arises owing to the early winter reference function is significantly smaller in an altitude range of 400–500 K than in 380–550 K.

The calculated ozone loss for the cold winters 1992–93, 1994–95, 1995–96 and 1999–2000 is 60–80 DU between the 400–500 K level. The maximum of the mean column ozone loss in this eleven-year study was obtained for the winters 1992–93 and 1995–96. In 1996–97 the strongest mean ozone loss in May was reached (48 DU in the 400–500 K level). Although the winter 1996–97 was cold, the mean column ozone loss for this winter (47 ± 17 DU inside the vortex core in the 400–550 K level in April) is comparable with the results of the moderate winters, because of the inhomogeneity of the ozone loss in the vortex. Anyway, the maximum ozone loss of this winter is comparable with results of the cold winters (see Figure 6.7). The moderately cold winters 1991–92, 1994–95 and 1997–98 reach a mean column ozone loss between 31 DU (in winter 1994–95) and 57 DU (in winter 1991–92) inside the vortex core in March. The warm winter

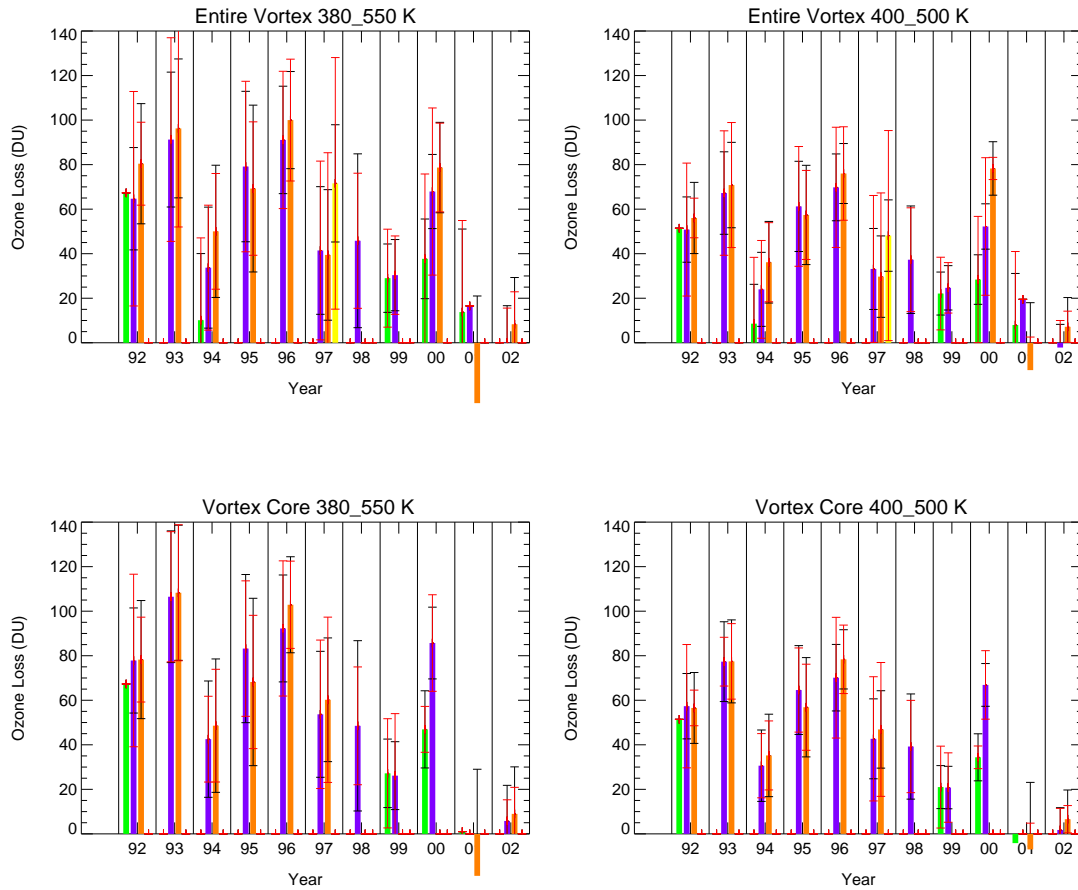


Figure 8.6: Mean column ozone loss for February (green), March (purple), April (orange) and May (yellow) in winters between 1991–92 and 2001–02 is shown. The values are the means between the results using HF and CH₄ as the long-lived tracers (see Figure 8.4 top and middle panel). The red error bar indicates the uncertainty of the early winter reference function, the black error bar the standard deviation. Top panels: ozone loss was derived from profiles inside the entire vortex, bottom panels: ozone loss was derived from profiles inside the vortex core. Results were derived in an altitude range of 380–550 K (left panels) and 400–500 K (right panels)

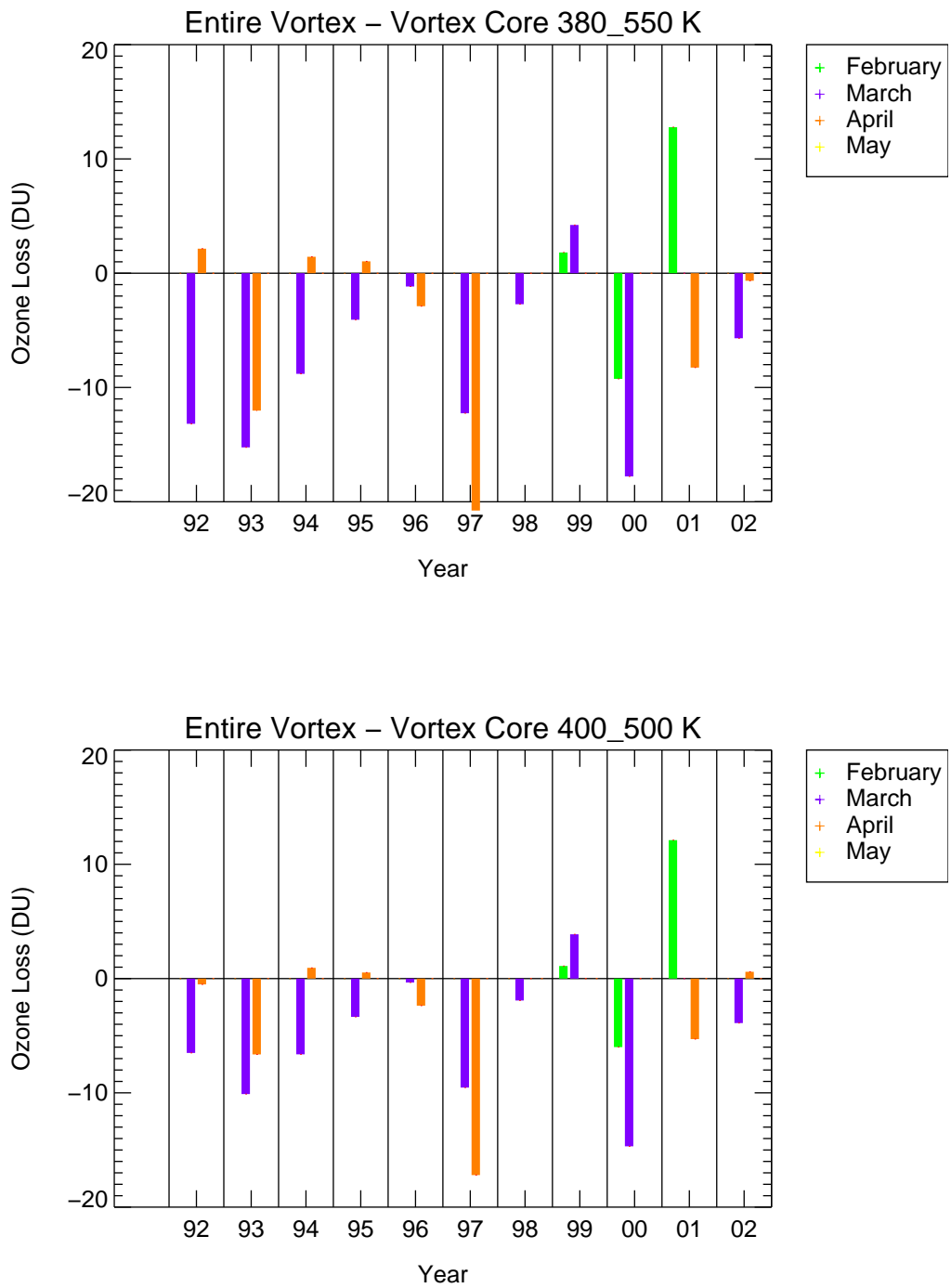


Figure 8.7: Difference of mean column ozone loss using CH_4 and HF as the long-lived tracers between the entire vortex and the vortex core for all winters between 1991–92 and 2000–01. Results were derived in an altitude range of 380–550 K (top panel) and 400–500 K (bottom panel).

1998–99 ozone loss still reaches 22 ± 10 DU derived for an altitude range of 400–500 K from profiles inside the entire vortex and 21 ± 10 DU for profiles inside the vortex core. In 2000–01 ozone loss from only one profile was calculated inside the outer vortex as 19 DU. Inside the vortex core in 2000–01 and inside the entire vortex in 2001–02 no ozone loss is diagnosed with the TRAC technique.

For April 2000–01 a negative ozone loss is calculated. The mixing ratio of ozone inside the vortex is greater compared to the ozone mixing ratios apparent in the early vortex (see Figure 7.10). Due to a major warming in February the vortex broke down and then reformed again with probably a different chemical composition than for the early winter conditions. Thus, under these conditions the early winter reference function is unlikely to be a reliable reference function to calculate ozone loss, as described above.

Inside the outer vortex, the mean column ozone loss is in most cases less than inside the vortex core (see Figure 8.7). The vortex core usually is colder than the outer vortex and, thus, the extent of ozone loss is expected to be stronger. In some years the standard deviation for profiles in the outer vortex is significantly larger than inside the vortex core (1992–93, 1994–95, 1995–96 and 1999–2000). That is because the ozone loss inside the outer vortex was much more inhomogeneous than in the vortex core in these winters. These inhomogeneities may be caused by inhomogeneous temperature distributions inside the outer vortex, as described in Section 8.1. The vortex during the winter of 1998–99 was very weak and disturbed. In this year the vortex core seems to have been less homogeneous than the outer vortex.

In warm winters the difference of the results in the vortex core and the outer vortex is rather small. In some years the ozone loss is insignificantly greater inside the outer vortex than inside the vortex core (in April 1992, 1994 and 1995, February and March 1999 and February 2001). Only for February 2000 does the difference reach about 20 DU, which is still inside the range of uncertainty.

8.3 Discussion of the TRAC Technique

The ozone-tracer correlation technique was applied to measurements in the Arctic polar region made by the ILAS instrument for the winter 1996–97 and to measurements made by HALOE from 1991–92 to 2001–02. The local maximum of ozone loss at a certain height was derived and the total amount of ozone loss for different months and years using HALOE observations.

First, the TRAC technique was validated (see Chapter 5). A comprehensive analysis of ozone loss was performed for the winter 1996–97. ILAS results show that since the vortex was isolated from the beginning of January 1997 onwards the O_3 -tracer relation inside the vortex core did not change due to mixing processes. Thus, deviations of O_3 -tracer profiles from the early winter reference function that occur later in the season should be interpreted as being due to chemical ozone loss.

The results derived from HALOE and ILAS observations for the winter 1996–

97 demonstrate that the early winter reference function has to be derived carefully. A major proportion of the uncertainties in the final results result from the uncertainty of this reference function. The relationship has to be derived for a time during the development of the polar vortex. The earliest time that is chosen may be the turning point from summer to winter circulation. But the time has also to be late enough so that a strong vortex has formed (that is largely isolated from the surrounding air masses), and also early enough so that no ozone loss will have already occurred. Nevertheless, the time that is chosen to derive the early winter reference function strongly depends on the availability of observations inside the early vortex. These are, in most years, limited, due to the incomplete temporal coverage of measurement inside high northern latitudes.

Early winter reference functions for all winters between 1991-92 and 2001-02 were derived with the TRAC technique and deviations from this reference function are discussed with respect to the different meteorological conditions in each winter. Additionally, the connection between the amount of ozone loss that has occurred and the strength of HCl activation can be discussed with the use of the TRAC technique.

If the temperatures inside the vortex are low enough strong chlorine activation is identified through the very small HCl mixing ratios in the HCl-tracer relation. Available measurements made by the HALOE instrument indicate a strong ozone loss occurring in the following weeks. On the other hand, strong chlorine activation during February and March does not necessarily cause strong ozone destruction. If the vortex is weakening and getting warmer (for example in 1993-94 and 2000-01) a pronounced chlorine activation in February and March did not result in further ozone destruction and the observed ozone loss is rather small.

With the recovery of chlorine chemistry, as observed for example in April 1991-92 to 1995-96, ozone loss comes to a halt. If the vortex or remnants of the vortex are still isolated in April, deviation from the reference function remains unaltered from the conditions observed earlier in the year inside the vortex (as in 1992-93, 1995-96) or additional ozone loss may occur, due to NO_x chemistry (as in May 1996-97, see Section 5.4). Mixing in of air from outside the vortex, due to the break-up of the vortex results in a decrease of the deviation from the reference function as observed in 1994-95.

The TRAC technique also permits the homogeneity of ozone loss inside the vortex to be described for the eleven year period. For example, in winter 1996-97 the calculated ozone losses of both sets of satellite data consistently show a strong inhomogeneity of ozone loss inside the entire vortex. The mean ozone loss in the vortex core differs significantly from the mean ozone loss in the outer vortex. Moreover, in the probability distribution of ozone loss (see Figures 6.7, 6.8 and 6.11) a separation inside the vortex core into two distinct parts was found. Large values of ozone loss occur mainly inside the vortex core, while smaller losses were found in the vortex core and in the outer vortex. Model calculations in high spatial resolution confirm this result [McKenna *et al.*, 2002].

Very homogeneous distributions of ozone loss inside the vortex core, for exam-

ple in 1992–93 and 1999–2000, indicate that the vortex core was well isolated up to the time when the observations were made and the meteorological conditions inside the vortex were rather homogeneous. A more inhomogeneous distribution of the temperature inside the entire vortex results in a larger value of standard deviation of the calculated ozone loss. Thus, inhomogeneous ozone loss profiles indicate an inhomogeneous temperature distribution inside the entire vortex. The TRAC technique allows a differentiation to be made between ozone loss inside the vortex core and inside the outer vortex.

As described above, the uncertainty of the reference function derived for early winter conditions is mainly responsible for the uncertainty of the results and is rather large in some winters. The smallest error of the determined ozone loss caused by the uncertainty of the reference function is $\approx 10\%$ in the cold winter 1995–96 and $\approx 15\%$ in the cold winter 1999–2000. In the other cold and moderately cold winters, the error is 20–40%. The error for the warm winters that show only little ozone loss is about 50%. For example in 1998–99 the mean column ozone loss is about 30 DU, and the error reaches about 15 DU. In winters 2000–01 and 2001–02 the error is much greater than the result of less than 10 DU ozone loss so that the results derived here are compatible with zero ozone loss.

Thus, the very small ozone losses occurring in warm winters cannot be determined with sufficient accuracy by using the TRAC technique. The more reliably the early winter reference function can be derived, owing to the availability of measurements inside the early vortex, and the more ozone is destroyed in the course of the winter, the more certain the calculated ozone loss is.

In summary, the application of the TRAC technique permits chemical ozone loss to be calculated as a function of the variability of different meteorological conditions inside the range of uncertainty denoted.

Chapter 9

Comparison of Results With Earlier Studies

The improved and extended ozone-tracer correlation technique to calculate chemical ozone loss in the Arctic polar stratosphere has been described in detail in the present work. Two satellite data sets, namely HALOE and ILAS were analysed using this technique. The measurements made by ILAS, were available for the winter 1996–97. The HALOE observations are available for the eleven winters between 1991–92 and 2001–02. The comparison of the calculated ozone loss based, on the one hand, on HALOE measurements, and, on the other hand, on ILAS measurements for the winter 1996–97 was discussed above (see Section 6.2.3).

In this chapter, the HALOE results of the years investigated are compared to HALOE results available from earlier studies, calculated with the previous implementation of the ozone-tracer correlation technique and using older data versions of HALOE (see Section 9.1). Moreover, the results of the present work are compared with published results obtained by different methods for the determination of chemical ozone loss (see Section 9.2). Finally, an analysis of the relationship between the possible area of PSC existence and the accumulated ozone loss is performed using HALOE results (see Section 9.3).

9.1 HALOE Results in Comparison With Earlier Studies Based on HALOE

Ozone loss was calculated with the use of the ozone-tracer relationship applied to HALOE measurements in several earlier studies [*Müller et al.*, 1996, 1997a,b, 2001, 2002]. The column ozone loss in the Arctic over six winters from 1991–92 to 1996–97 was calculated from HALOE measurements Version 18 in *Müller et al.* [1996, 1997a, 1999, 2001].

In these earlier studies, the decision whether profiles were considered inside or outside the early vortex was not based on the maximum gradient in PV, that is on the *Nash et al.* [1996] criteria. PV charts were analysed ‘by hand’ to find measurements inside the polar vortex. In the analysis of HALOE observations

1996–97 [Müller *et al.*, 1997b] consistent PV criteria were employed on certain isentropic layers. Moreover, measurement locations were not transformed to 12 UTC to compare them with the PV fields. The uncertainty whether profiles belong inside the vortex or not is larger, if the vortex edge is not exactly defined. Thus, in previous studies the early winter reference function was derived from profiles that did not all clearly belong to the vortex. Early winter profiles, which are located too far towards the edge of the vortex or outside the vortex, have larger ozone mixing ratios in the ozone-tracer space than inside the vortex (see e.g. Section 4.3). An early winter reference function influenced by profiles that are located equatorwards of the vortex edge would be shifted towards larger ozone mixing ratios. This was the case in winters 1993–94 to 1995–96 and most pronounced in 1993–94 (see Figure 9.1).

The ozone loss calculated here for the years between 1992–93 and 1995–96 is compared in Table 9.1 with results (based on HALOE Version 18) published previously [Müller *et al.*, 1997a, 1999] for the altitude range of 350–550 K. Only CH₄ was used as the long-lived tracer. The calculation of ozone loss in the altitude range 350–550 K by Müller *et al.* [1997a] and Müller *et al.* [1999] causes larger uncertainties due to the extension of the vertical integration below 380 K. On the one hand, the early winter reference function will be less reliable and, on the other hand, vortex air below 380 K is influenced more strongly by mixing processes. Column ozone loss obtained with the TRAC technique in this altitude range using the two different long-lived tracers show substantial differences. Therefore, ozone losses calculated in 380–550 K is also shown in Table 9.1.

The previously published ozone losses are significantly larger for the winters 1992–93 to 1995–96 than those calculated in the present work. Ozone mixing ratios of the early winter reference functions in the previous studies are larger, though still inside the range of uncertainty derived in the present work. An exception is the winter 1993–94, for which a significant difference between the reference functions arose. The reference function derived for the winter 1993–94 in earlier studies shows much larger ozone mixing ratios, at CH₄ mixing ratios of less than 1.0 ppmv (i.e. at altitudes above \approx 420 K) (see Figure 9.1). The individual profiles that were originally employed to derive the reference function for this winter [Müller *et al.*, 1999] were influenced significantly by air masses outside the vortex, as discussed above. However, the other “old” reference functions are inside the range of uncertainty of those derived here and, thus, the results also agree inside the range of uncertainty.

The early winter reference function for winter 1991–92 in the present work was taken from Müller *et al.* [2001]. Here, an O₃/N₂O relation was derived from balloon observations in December 1991 made during the EASOE campaign. In the study by Müller *et al.* [2001], HALOE data of Version 18 were used to calculate the column ozone loss. There, for the end of March 1992 74 DU were calculated in 400–550 K with HF and CH₄ as the long-lived tracers. These results agree with the ozone loss (62 ± 15 DU) derived with the TRAC technique in March 1992 inside the vortex core for the same altitude range (see Table 9.3, Section 9.2).

The results obtained for winter 1996–97 were already compared in detail with

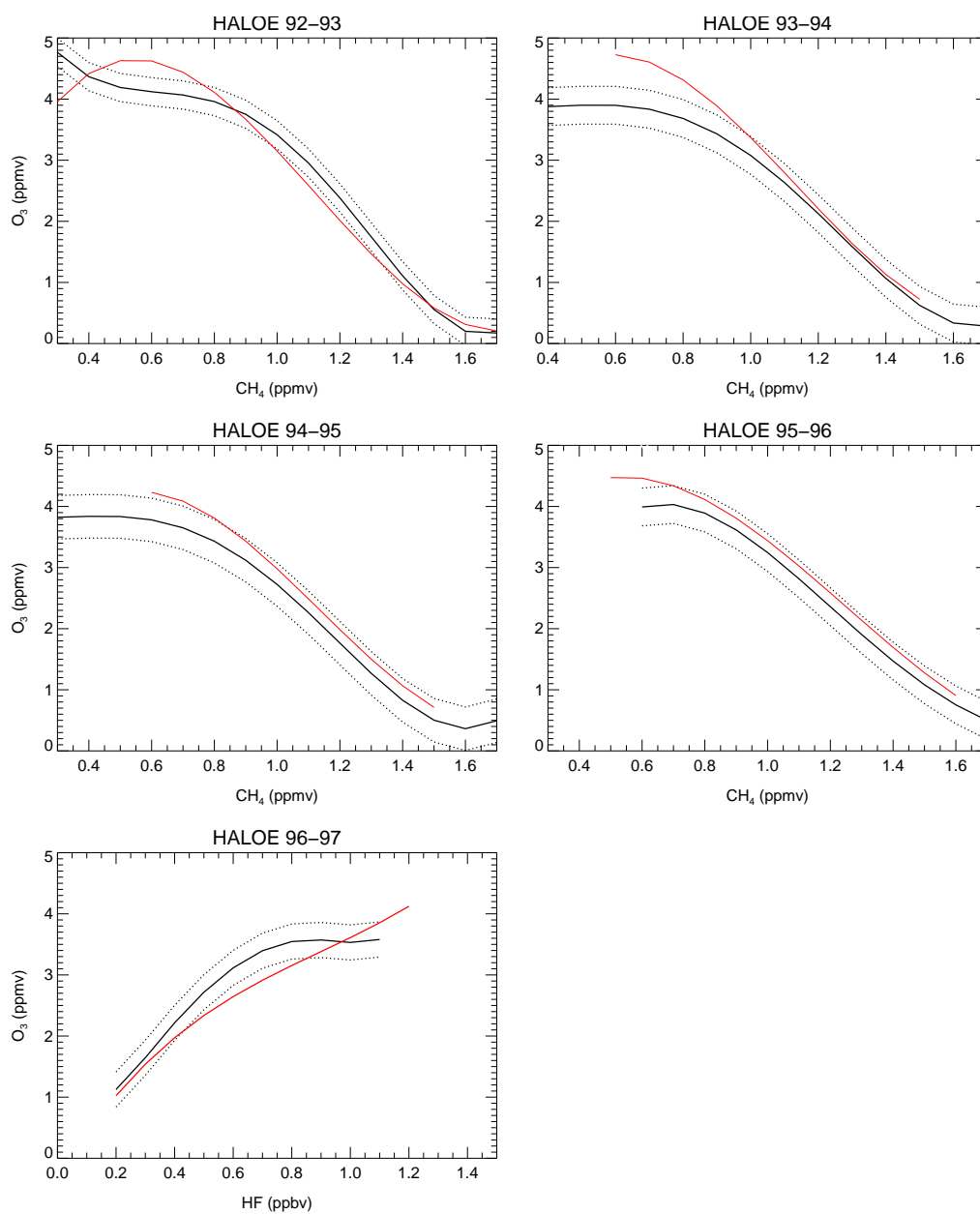


Figure 9.1: Comparison of early winter O₃-tracer relations derived here by HALOE Version 19 (shown as a black line) with those employed in previous studies from HALOE Version 18 [Müller *et al.*, 1999] (shown as a red line).

Table 9.1: Calculated chemical loss in column ozone loss in the Arctic over 5 winters, new and earlier studies [Müller *et al.*, 1999] are compared

date	tracer	earlier study ozone loss (DU) in 350–550 K	new results (core) ozone loss (DU) in 380–550 K	new results (core) ozone loss (DU) in 350–550 K
March 1993	CH ₄	133 ± 14	109 ± 17	119 ± 25
March 1994	CH ₄	102 ± 10	37 ± 20	32 ± 31
March 1995	CH ₄	116 ± 20	83 ± 23	94 ± 35
April 1995	CH ₄	81 ± 26	75 ± 26	97 ± 39
March 1996	CH ₄	140 ± 19	102 ± 22	101 ± 33
April 1996	CH ₄	131 ± 9	119 ± 14	121 ± 30
March 1997	HF	53 ± 23	58 ± 18	67 ± 31

earlier studies (see Section 6.2.3). In summary, in Müller *et al.* [1997b] the maximum column ozone loss inside the vortex was underestimated by up to $\approx 20\%$ for the altitude range of 380–550 K and the local loss at 475 K was underestimated by 15 % (0.4 ppbv) compared to the results of the present study.

The improved TRAC method was already applied by [Müller *et al.*, 2002] to calculate the column ozone loss for the winter 1999–2000. For the years 1997–98, 1998–99, 2000–01 and 2001–02 ozone loss in the Arctic vortex was calculated here using the ozone tracer correlation technique for the first time.

9.2 Comparison of Ozone Loss Derived Using Different Methods

Chemical ozone loss in the Arctic vortex in the past decade was estimated by a variety of techniques for different winters [Harris *et al.*, 2002; Newman *et al.*, 2002]. However, a comparison between the different ozone loss estimates is only meaningful, if the figures compared are determined for exactly the same conditions [Harris *et al.*, 2002]. In Section 4.2 different techniques were presented and some results were compared with HALOE results derived in earlier studies (see Table 4.1). In this section, results obtained in the present work are compared with results derived using other methods.

The column ozone loss in DU, shown in Table 9.2, was derived from the SAOZ/REPROBUS and POAM/REPROBUS technique, the Match technique [Rex *et al.*, 1998; Schulz *et al.*, 2000] and the improved and extended TRAC technique. A comparison with MLS [Manney *et al.*, 2003a] is made in Table 9.3.

The column ozone loss averaged over the entire vortex in the three winters 1994–95, 1995–96 and 1996–97 determined by SAOZ is much larger than that derived from HALOE measurements with the correlation technique — the differ-

Table 9.2: Calculated chemical loss in column ozone loss in the Arctic in winters 1994–95 to 1996–97. Comparison between HALOE results and results from other methods.

date	SAOZ/ REPROBUS ^a in 380–600 K	Match ^a in 370–700 K	HALOE entire vortex in 380–550 K	HALOE vortex core in 380–550 K
March 1995	140	127 ± 14	79 ± 34	83 ± 23
March 1996	125		91 ± 24	92 ± 24
March 1997	110		41 ± 29	54 ± 28

^a taken from *Harris et al.* [2002], Table 4.

ence is about 60 DU in 1994–95 and 1996–97 and 30 DU in 1995–96. For 1996–97 the result from SAOZ agrees with the largest ozone loss calculated by HALOE inside the vortex core (90–110 DU), but averages still do not agree. The ozone loss derived with the Match technique for 1994–95 is more than 40 DU larger than that from HALOE for the same winter. Thus, major discrepancies are apparent between the results of the SAOZ, Match and TRAC technique.

Table 9.3: Calculated chemical loss in column ozone loss (DU) in the Arctic over seven winters, HALOE results and MLS results [*Manney et al.*, 2003a], are compared.

date	MLS ^a above 100 hPa	HALOE entire vortex in 400–550 K	HALOE vortex core in 400–550 K
March 1992	29	56 ± 15	62 ± 15
March 1993	54	78 ± 19	89 ± 19
March 1994	35	29 ± 18	37 ± 16
March 1995	36	67 ± 18	71 ± 19
March 1996	63	83 ± 20	84 ± 20
March 1997	35	38 ± 16	50 ± 17
February 1998	22	45 ± 25	47 ± 25

^a taken from *Manney et al.* [2003a], Table 3

The column ozone loss from UARS microwave limb sounder (MLS) measurements [*Manney et al.*, 2003a] for the winters 1991–92 to 1997–98 was calculated for above 100 hPa. Therefore, the results should be comparable with HALOE results in 400–550 K. The results of the two methods are in principle similar, although the ozone losses determined by MLS are about 20–30 DU smaller than those derived with HALOE for profiles inside the entire vortex for the winters

1991–92, 1992–93, 1994–95, 1995–96 and 1997–98. The strongest ozone loss was found for the winters 1995–96 and 1992–93 with both techniques. In 1993–94 values calculated from HALOE observations are insignificantly smaller (6 DU) than calculated from MLS observations inside the entire vortex. For 1996–97 the average value of the entire vortex is in accordance with the MLS observations.

In winter 1999–2000 the column ozone loss inside the Arctic was derived from various measurements and different techniques, because an extensive measurement campaign was conducted: SOLVE-THESEO 2000 [Newman *et al.*, 2002]. The calculated ozone loss between early January and mid-March by the Match technique is 71 ± 12 DU [Rex *et al.*, 2002]. Results from the OMS balloon measurements [Salawitch *et al.*, 2002] were calculated up to 5 March 2000 as 61 ± 14 DU. An extrapolation of the result for 5 March to mid-March (based on Match-derived ozone loss rates Müller *et al.* [2002]) yielded 84 ± 13 DU. Ozone loss from POAM/REPROBUS was determined as 80 DU in 380–700 K, as reported by Harris *et al.* [2002]. These results agree well with the column ozone loss found in the present work (81 ± 14 DU in 380–550 K inside the vortex core).

Accumulated losses in the vortex in ppmv were estimated at certain altitudes for various time periods and for given subsiding layers of air with the Match technique [Rex *et al.*, 1998; Schulz *et al.*, 2000], from the MLS observations [Manney *et al.*, 2003a] and Knudsen *et al.* [1998] using the vortex average approach. The results should be comparable with the accumulated local ozone loss derived with the TRAC technique, if the time interval considered is comparable.

The accumulated chemical ozone loss was calculated from MLS observations for the winters 1991–92 to 1997–98 from December/January to the end of February/March at the 465 K and 520 K level [Manney *et al.*, 2003a] (see Table 9.4). Local ozone loss at the 465 K level derived from HALOE data is consistently ≈ 1 ppmv larger than that derived from MLS observations. For the 520 K level, the deviations are less strong; the difference is ≈ 0.3 ppmv. The strongest accumulated ozone loss was found in 1995–96 from both techniques. Accordingly, like the estimated column ozone loss, the accumulated ozone loss is in principle similar when derived by both methods.

For the years 1992, 1995, 1996 and 2000, largely unexplained stratospheric ozone loss rates during January were found, using a combination of data from Match, POAM II, POAM III and MLS [Becker *et al.*, 1998, 2000; Rex *et al.*, 2003; Kilbane-Dawe *et al.*, 2001]. In the present work, ozone loss in January is apparent in 1991–92 (see Figure 7.4) based on HALOE observations. During January 1997, very small deviations of the ozone-tracer relation from the reference function occurred based on ILAS observations. This is in accordance with the small amount of ozone loss that was calculated by Match [Schulz *et al.*, 2000]. However, very small ozone losses occurring, for example, in mid-winter and during warm winters cannot be determined with the sufficient accuracy with the TRAC technique, as described in Section 8.3.

In winter 1996–97, accumulated ozone loss was estimated in the time period between the end of January and the end of March by the Match technique (1.1 ppmv) and by Knudsen (0.9 ± 0.2 ppmv) at the 455 K potential temperature

Table 9.4: Accumulated ozone loss estimated by MLS over the calculation period in 465 K and 520 K taken from *Manney et al.* [2003a], Table 1 and 2. HALOE results at 465 K and 520 K inside the vortex core were estimated from Figures 8.2 and 8.3; in February 1997 no HALOE observations are available and, therefore, no ozone loss could be derived for February.

date	ozone loss 465 K (MLS)	ozone loss 465 (HALOE)	ozone loss 520 K (MLS)	ozone loss 520 K (HALOE)
March 1992	0.5	1.4	0.3	0.6
March 1993	1.0	2.0	0.7	0.9
March 1994	0.5	1.4	0.7	1.0
March 1995	0.8	2.0	0.2	0.8
March 1996	1.3	2.2	1.4	1.6
February 1997	0.5		0.9	
February 1998	0.4	1.3	0.02	0.6

level [*Harris et al.*, 2002]. Such values are approximately in agreement with the moderate ozone loss deduced here from ILAS 0.5–1.0 ppmv (± 0.2 ppmv) and HALOE 0.9–1.4 ppmv (± 0.2 ppmv) at the 475 K level (see Figures 6.6 and 6.10). Further calculations of ozone loss were performed with the Match technique based on ILAS observations for the winter 1996–97 [*Terao et al.*, 2002]. There, the integrated ozone loss during February and March reached 2.0 ± 0.1 ppmv at 475–529 K levels. This result is in good agreement with the maximum of the ozone loss profile of 2.0 ± 0.3 ppmv derived from ILAS with the TRAC technique in a similar altitude range (see Figure 6.10).

However, in winter 1996–97 vortex average losses obtained by different methods are very difficult to compare, because ozone loss inside the vortex was spatially very inhomogeneous [*McKenna et al.*, 2002; *Schulz et al.*, 2000]. Thus, the averages derived will greatly depend on what fraction of the data entering the average originates from the vortex region showing the stronger ozone loss.

In 1999–2000 HALOE local ozone loss in 430–450 K (2.3 ± 0.2 ppmv) is in good agreement with the accumulated ozone loss in the vortex in mid-March derived by the Match technique (2.0 ± 0.3 ppmv) [*Rex et al.*, 2002]. The ozone and the tracer measurements between early January and mid-March 2000 from the ER-2 were used to deduce chemical ozone loss (1.8 ± 0.3 ppmv) [*Richard et al.*, 2001]. Ozone loss deduced from POAM III satellite measurements only reached 1.5 ± 0.3 ppmv for mid-March [*Hoppel et al.*, 2002].

The accumulated ozone loss derived using the vortex average approach (see Section 4.2) is most similar to the results derived using the TRAC technique, although there are some significant deviations as described in detail in the next section.

9.3 The Relationship Between Ozone Loss and the Area of PSCs

Ozone loss is related to the particular dynamic conditions of the polar vortex in each year. The eleven-year time series of ozone loss obtained in a consistent manner in this thesis allows this question to be addressed in detail. Recently, *Rex et al.* [2002] reported a similar analysis. They investigated the relationship between the accumulated ozone loss in mixing ratios between day 15 and day 85 of a particular year – averaged between 400–500 K – and the total area of possible PSC existence (see Section 4.4.2) in the Arctic polar vortex during this time period based on meteorological analysis from ECMWF (see Figure 9.2, top panel, coloured open circles). The ozone loss was calculated with the vortex average approach (see Section 4.2) inferred from measurements of the Arctic ozone sonde network.

Here, the ozone loss profile deduced from the TRAC technique for measurements inside the vortex core, which describes the accumulated ozone loss between January and March, is averaged between the 400–500 K level for each year, except for the winter 2000–01. Thus, these values are comparable with the values deduced from the average approach. For the winter 2000–01 local ozone loss averaged between 400–500 K is zero for profiles inside the vortex core, because ozone loss arose in higher altitudes. Nevertheless, an estimate is possible for the altitude range of 450–500 K in February 2001 (see Figures 8.2 and 8.3).

In the present thesis, the area of possible PSC existence was determined from the analysis from UKMO in the same altitude range as was done by *Rex et al.* [2002]. For this, the PSC threshold temperature was calculated [*Hanson and Mauersberger*, 1988] for HNO_3 mixing ratio: 10 ppbv and H_2O mixing ratio: 5 ppmv (see also Section 4.4.2).

Rex et al. [2002] reported that the possible area of PSCs during the lifetime of the vortex correlates well with the derived accumulated ozone loss with the use of the average approach in the years between 1991–92 and 1999–2000 (see Figure 9.2, open circles, top panel).

Results derived with the TRAC technique show that ozone loss and A_{PSC} are positively correlated and thus support the results obtained using the vortex average approach. However, the ozone losses deduced with the TRAC technique indicate more complicated relations. Local ozone loss derived by the TRAC technique is in good agreement with the results of the vortex average approach (see Figure 9.2, top panel) especially for the cold winters 1995–96, 1996–97 and 1999–2000. Differences exceeding the uncertainty are found for the winters, 1991–92, 1992–93, 1994–95 and 1997–98. The analysis for these winters shows significantly larger ozone loss derived with the TRAC technique.

The calculated loss in ozone (in DU) over the altitude range 400–500 K likewise also correlates with the A_{PSC} , especially for the cold winters, but there are the some outliers (the winter 1991–92, 1992–93, 1997–98) as already observed for the ozone loss mixing ratios (see Figure 9.2, squares and diamonds, bottom panel).

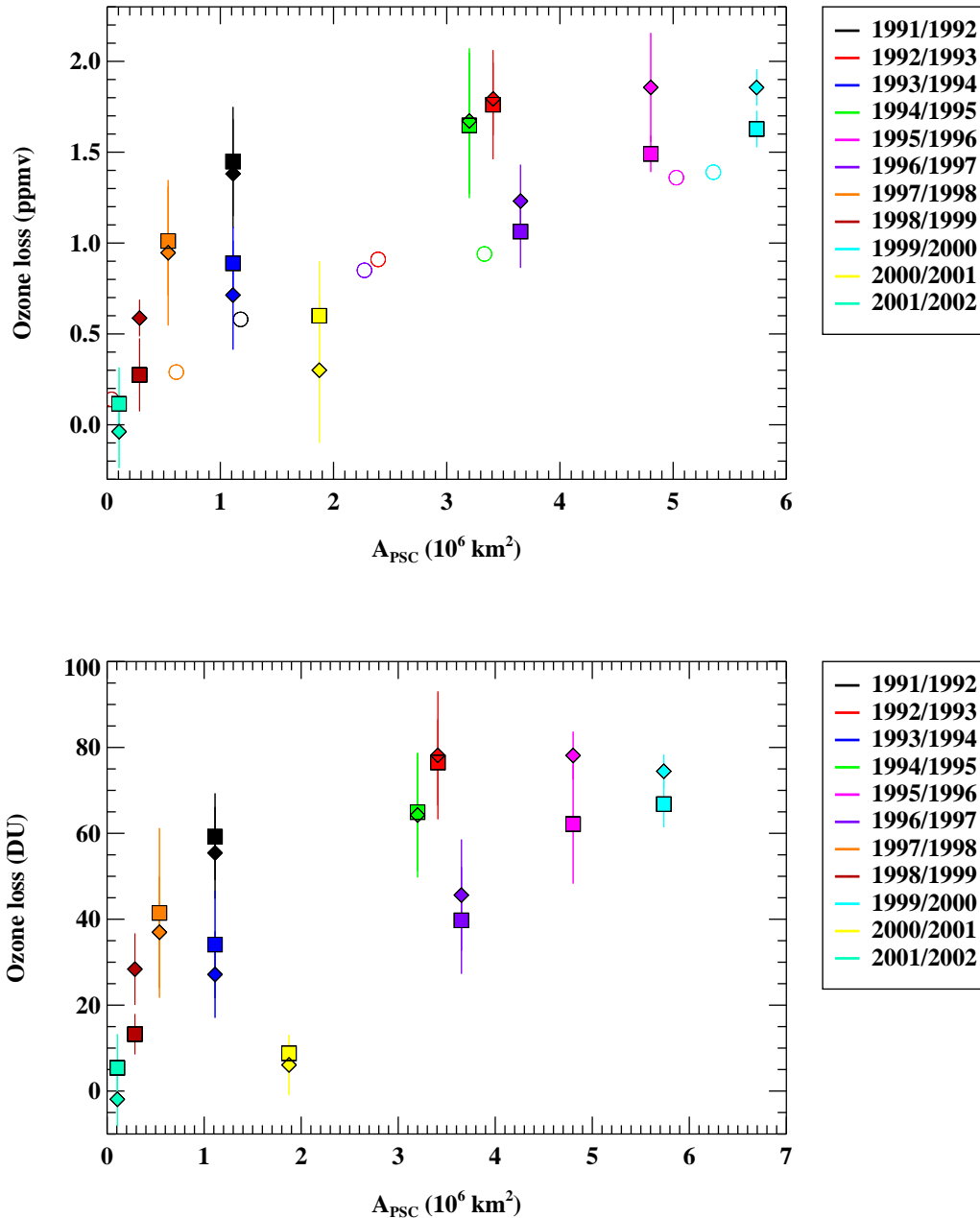


Figure 9.2: Top panel: relation between the accumulated ozone loss in mixing ratio and the total area of possible existing PSC (A_{PSC}) in the Arctic polar vortex is shown for the years 1991–92 to 2001–02 in different colours. A_{PSC} and ozone loss were calculated from January to March of each year and was averaged between 400–500 K. Ozone loss derived with the average approach [Rex *et al.*, 2002] is shown in coloured open circles, ozone loss deduced from the TRAC technique (from HALOE measurements inside the vortex core) is shown in coloured solid squares (HF is used as the long-lived tracer) and solid diamonds (CH_4 is used as the long-lived tracer) Bottom panel: as top panel, but the column ozone loss (DU) for the altitude range 400–500 K derived only from HALOE observations is apparent.

In 1992–93 and 1994–95, strong chlorine activation was observed in the outer part of the vortex boundary region and, therefore, stronger ozone loss can be expected in the outer vortex than in other winters. Such an effect means that the ozone destruction is not necessarily related to the area of PSC occurrence only, but also, for example, to the location of the area of PSCs. That is, continuing PSC activity in vortex regions that are already strongly activated does not enhance the ozone loss, whereas PSC activity in parts of the vortex that are not yet activated (e.g. towards the vortex edge) does.

Further, a small A_{PSC} in lower latitudes with stronger solar illumination may cause the same amount of ozone loss as a larger A_{PSC} in higher latitudes. This effect may be responsible for the strong ozone loss in the winters 1991–92 and 1997–98. In these winters, the area of possible PSC existence inside the vortex A_{PSC} was on average located in lower latitudes compared to other winters.

Additionally, in 1991–92, deviations from the linear correlation between A_{PSC} and ozone loss may be caused by the strong increase in background liquid sulphate aerosols, after the major volcanic eruption of Mount Pinatubo on 15 June 1991. Heterogeneous chemical reactions are possible on the surface of these particles, which increases the chlorine activation and, therefore, the amount of ozone loss (see Section 2.2.1).

In summary, a comparison of the results derived with the TRAC technique and the results derived with the techniques using meteorological models to simulate the transport processes in the stratospheric Arctic vortex was performed. The calculated column ozone loss and local accumulated ozone loss determined in the present work are in agreement with the results of previous studies for the cold and undisturbed vortex in winter 1999–2000. In the other winters results estimated with the TRAC technique are in principle similar to the results derived from MLS measurements in the altitude range of 400–550 K, although HALOE results are consistently larger. The column ozone loss derived from SAOZ/REPROBUS seems to be problematic insofar as the strongest ozone loss in all the years of SAOZ observations was detected for March 1995, a result that is in contrast to the results derived using other methods.

Furthermore, the results of the TRAC technique and of the vortex average approach agree best for the winters 1995–96, 1996–97, 1998–99, 1999–2000 and 2000–01. Nevertheless, larger differences occur in winters where other influences than the possible area of PSC occurrence may affect the amount of ozone loss, as described above. Thus, possibly model simulations cannot properly reproduce all the complicated transport processes within a strongly disturbed polar vortex. If this were the case, the TRAC technique would produce more reliable results than techniques relying on transport calculations, in spite of the fact that the reported error estimates, especially for the warm winters, are rather large.

Chapter 10

Summary and Outlook

The main objective of this thesis was the deduction of chemical ozone loss with the use of the ozone-tracer correlation (TRAC) technique.

Relationships between ozone and a long-lived tracer were first considered by *Proffitt et al.* [1989, 1990] to deduce chemical ozone loss in the Arctic and the Antarctic. Later, the method was extended to satellite [e.g., *Müller et al.*, 1996, 1997b,a] and balloon [*Müller et al.*, 2001; *Salawitch et al.*, 2002] measurements and studies were performed for several Arctic winter periods in the nineties. Although these early studies at that time provided important insights into ozone loss the methodology was somewhat empirical in some aspects. Moreover, the available data did not allow several important issues to be addressed. Indeed, studies were published that questioned the reliability of the technique as a tool for diagnosing chemical ozone loss.

In the present work the TRAC methodology was improved in a variety of ways and questions raised about the earlier studies were revisited. These studies were made possible through the availability of new data sources, in particular, the ILAS satellite observations that are available over the entire winter 1996-97 in the Arctic. Further, data from field campaigns (e.g. THESEO2000/SOLVE and EASOE) were employed. Moreover, the existence of comprehensive satellite observations for the eleven winters between 1991-92 and 2001-02 by the HALOE instrument permitted a consistent data set to be produced on Arctic chemical ozone loss over this period and thus relate ozone loss to the very different meteorological conditions of these eleven winters.

In this way, the TRAC technique was developed into a reliable tool for calculating chemical ozone loss in column ozone and the local accumulated ozone loss over an altitude range between 380 and 550 K. Further, the quantification of the uncertainties has been improved. The connection between ozone loss and chlorine activation was investigated in this work and moreover, the growth rate of HF at different altitudes in the eleven-year period was derived.

A division between the results for different parts of the vortex is possible with the use of the improved method and the extent of the homogeneity of ozone loss inside different parts of the vortex may be determined.

The relationship between the total area of possible PSC existence in a partic-

ular year and the calculated ozone loss does not turn out to be a simple, linear relation. In comparing the results with results obtained by other methods, one advantage of the TRAC technique becomes apparent. The TRAC technique does not need to simulate the complicated dynamic situation inside the vortex as other methods have to.

However, the results and insights obtained in this work still suffer to some extent from the uncertainty due to the incomplete temporal coverage of measurements within high northern latitudes by HALOE. Especially the scarcity of observations inside the early vortex causes uncertainties that significantly influence the accuracy of the results.

In the near future, a wealth of new satellite data will become available that are well suited for the application of the improved TRAC method derived in this work. The first data from ENVISAT (launched in March 2002) are now becoming available; the availability of several independent tracer and ozone measurements with a good coverage of the polar regions make this data set very attractive for a TRAC analysis. ILAS-II aboard the ADEOS-II (launched on 14 December 2002) will provide very similar data to those from ILAS which were successfully employed in the present work. For ILAS-II, the availability of occultation profiles with a good vertical resolution and a good coverage of the polar regions are the most attractive features¹ Further interesting measurements will be provided by the HIRDLS (High Resolution Dynamics Limb Sounder) instrument on the Aura mission, part of the NASA's earth observing System (EOS) scheduled for launch in January 2004. HIRDLS will measure the concentration of e.g., O₃, CH₄, N₂O, and ClONO₂ in the upper troposphere, stratosphere and mesosphere in unprecedented spatial resolution for a long term satellite mission. Finally, it should not be forgotten that HALOE continues to collect data and so that the time series of HALOE analyses presented here can be continued in a consistent manner into the future. The future development of the polar ozone loss will be of great interest, both to detect the recovery of ozone loss (as is expected owing to the slowly decreasing atmospheric halogen concentration) and to investigate the interaction of ozone loss processes with climate change. In summary, in future years there will be several high-quality satellite data sources available that permit both further improvements of the technique and the analysis of chemical ozone loss in a changing stratosphere in future winters.

¹After this work was completed, unfortunately, NASDA announced that ADEOS-II began to miss data-transmission appointments on 25 October, 2003, and ILAS-II ceased collection data.

Appendix A

Zusammenfassung

Im Rahmen dieser Arbeit wurde der chemische Ozonverlust in der arktischen Stratosphäre über elf Jahre hinweg untersucht. Dabei lag der Schwerpunkt auf der Bestimmung von Ozonverlust im Winter und Frühjahr innerhalb des Polarwirbels. Die chemische Ozonzerstörung zwischen Winter und Frühjahr wurde quantifiziert zum einen durch die Berechnung des lokalen Ozonverlustes in Mischungsverhältnissen und zum anderen durch die Berechnung des Ozonverlustes in einer Säule in Dobson Units (DU)¹ über einen bestimmten Höhenbereich. Die dazu verwendete Methode, die „Ozon-Tracer Korrelationstechnik“ („ozone-tracer correlation (TRAC) technique“), konnte in dieser Arbeit deutlich verbessert werden.

Die hier verwendeten Datensätze zur Berechnung des Ozonverlustes stammen vom HALOE (Halogen Occultation Experiment) Instrument auf dem UARS (Upper Atmosphere Research Satellite) der NASA und vom ILAS (Improved Limb Atmospheric Spectrometer) Instrument auf dem japanischen Satelliten ADEOS (Advanced Earth Observing Satellite). HALOE und ILAS sind Okkultations-Instrumente und liefern vertikal aufgelöste Messungen von Ozon und verschiedenen anderen Spezies, die für die Stratosphärenchemie relevant sind. Das HALOE Instrument liefert seit Oktober 1991 kontinuierlich Messungen. Durch die Umlaufbahn des Satelliten misst HALOE 15 mal pro Tag bei Sonnenaufgang und Sonnenuntergang. Der Satellit bewegt sich dabei innerhalb von ungefähr 45 Tagen auf einer Bahn zwischen 80°N und 80°S. Daher gibt es, variabel für die verschiedenen Jahre, alle zwei bis drei Monate Messdaten in höheren Breiten. Für die meisten Jahre stehen Daten im winterlichen Frühwirbel und dann erst wieder im Spätwinter oder Frühling zur Verfügung, so dass man jeweils ein „vorher-nachher“ Bild der Ozonzerstörung erhält. Das ILAS Instrument lieferte nur im Jahre 1996–97 Messungen. Trotzdem waren die Messungen dieses Instrumentes äußerst nützlich für die vorliegende Arbeit, da sie kontinuierlich von November 1996 bis Ende Mai 1997 für hohe nördliche (und südliche) polare Breiten zur Verfügung stehen. Damit konnte die zeitliche Entwicklung der Ozonzerstörung

¹Unter Ozon in einer Säule versteht man die gesamte Menge Ozon-Moleküle pro Fläche integriert über einen bestimmten Höhenbereich. Die Ozonsäule wird im allgemeinen in Dobson Units angegeben; eine Dobson Unit ist $2.69 \cdot 10^{16}$ molecules/cm².

in diesem Winter nachvollzogen werden und die hier verwendete Methode zur Bestimmung des chemischen Ozonverlustes validiert werden.

Das Ozonmischungsverhältnis wird einerseits von Transportprozessen und andererseits von chemischen Reaktionen beeinflusst. Daher wurden Methoden entwickelt, um aus den Messdaten den reinen chemischen Ozonverlust abzuleiten. Im Gegensatz zu Methoden, bei denen zu diesem Zweck Transportprozesse durch Modellrechnungen nachvollzogen werden, wurde hier eine Technik verwendet (die TRAC Technik), bei der die Beschreibung der Dynamik im abgeschlossenen Polarwirbel unnötig ist. Diese TRAC Methode macht sich zu eigen, dass zwei im Polarwirbel gemessene Spezies, wie Ozon und ein langlebiger Spurenstoff ("Tracer") ins Verhältnis gesetzt werden können. So konnten Transportprozesse implizit eliminiert werden: es wird bei dieser Methode ausgenutzt, dass Transportprozesse (wie das Absinken des Wirbels) auf alle Konstituenten im gleichen Maße wirken. Die Beziehung zwischen Ozon und einem anderen langlebigen Spurengas (wie CH_4 , HF und N_2O) wird sich somit in einem hinreichend abgeschlossenen Wirbel nicht ändern, solange keine chemischen Veränderungen stattfinden. Eine Referenzfunktion kann aus dieser Relation für chemisch ungestörte Bedingungen berechnet werden. Nur eine Verringerung des Ozonmischungsverhältnisses durch chemischen Ozonverlust kann demnach eine Abweichung von der Referenzfunktion, d.h. eine Veränderung des Ozon-Tracer Verhältnisses bewirken. Ebenso wie Ozon, kann auch HCl mit einer langlebigen Substanz ins Verhältnis gesetzt werden. Verändert sich im Laufe des Winters diese HCl/Tracer Relation zu niedrigeren HCl Mischungsverhältnissen, kann man auf eine chemisch bedingte Verringerung der HCl Mischungsverhältnisse schließen und damit auf die Aktivierung von Chlor.

Nach diesem Prinzip wurde in der Vergangenheit u.a. der Ozonverlust für einige Winter seit dem Winter 1991–92 aus den HALOE Daten berechnet. Jedoch war die Methodik für die Auswertung bei diesen frühen Studien noch nicht genug ausgefeilt. Außerdem waren die verwendeten Daten noch nicht hinreichend präzise, es gab später mehrere Änderungen der Datenversionen. Die frühen Ergebnisse waren daher mit verschiedenen signifikanten Fehlerquellen behaftet.

Vergleiche von chemischen Ozonverlusten, die mit unterschiedlichen Methoden abgeleitet wurden, zeigten teilweise starke Abweichungen voneinander. Dies führte dazu, dass das Prinzip der TRAC Technik in den letzten Jahren von mehreren Seiten kritisiert wurde. Dabei wurde besonders auf den möglichen Einfluss von horizontalen Mischungsvorgängen am Wirbelrand eingegangen. Es wurde erörtert, ob starke Mischungsprozesse einen Ozonverlust vortäuschen könnten. Da die TRAC Methode auf der Annahme der Abgeschlossenheit des Wirbels basiert, würde sich diese Technik als nur bedingt brauchbar erweisen. In der vorliegenden Arbeit wurden die Einflüsse von horizontaler Mischung untersucht und es konnte gezeigt werden, dass eine geringfügige Unterschätzung des Ozonverlustes durch diesen Effekt möglich ist, nicht aber eine Überschätzung, wie es von Kritikern beschrieben wurde.

Darüber hinaus wurden im Rahmen in dieser Arbeit wesentliche Verbesserungen der Methodik durchgeführt. Zunächst wurde eine meteorologischen Analyse

zur Bestimmung bestimmter Wirbelregionen eingeführt, die es ermöglicht, die Grenzen des Polarwirbels eindeutig festzulegen. Die richtige Zuordnung der Position von Messdaten bezüglich dieser Wirbelregionen ist sehr wichtig, um zuverlässige und konsistente Ergebnisse zu erhalten, da innerhalb und außerhalb des Wirbels deutlich andere Verhältnisse vorherrschen. Da das HALOE Instrument zwei langlebige Tracer misst (CH_4 und HF), war eine weitere Qualitätskontrolle der gemessenen Profile möglich: Das CH_4/HF Verhältnis zeigt sich, wie sich in dieser Arbeit herausstellte, während des gesamten Jahres im Wirbel konstant. Profilmessungen im Wirbel, bei denen eine starke Abweichung von diesem Verhältnis zu beobachten war, wurden bei der Ozonverlustberechnung vernachlässigt, da solche Profile nicht die Charakteristik aufwiesen, die Wirbelluft auszeichnet.

Eine möglichst genaue Bestimmung der Referenzfunktion für chemisch ungestörte Verhältnisse im Wirbel ist maßgeblich für eine exakte Berechnung des Ozonverlustes. Daher wurden zur Bestimmung der Referenzfunktion die vorhandenen HALOE und ILAS Daten sowie Daten von Ozonsonden und Ballonmessungen verwendet. Weiterhin sollte die Referenzfunktion eines Jahres möglichst für einen Zeitpunkt ermittelt werden, an dem noch keine chemischen Prozesse zu erwartet sind, was im Frühwirbel der Fall ist. Im weiteren wird daher auch von der „Frühwinter-Referenzfunktion“ gesprochen. Den frühest möglichen Zeitpunkt für die Ermittlung so einer Referenzfunktion stellt der Wendepunkt zwischen Sommer und Winterzirkulation in der arktischen Stratosphäre dar, welcher mit dem Minimum der gesamten Ozonsäule übereinstimmt. Andererseits sollte der Zeitpunkt der Bestimmung der Referenzfunktion so gewählt werden, dass der Frühwirbel hinreichend abgeschlossen ist. Aus den ILAS Daten ergibt sich, dass sich das Verhältnis zwischen Ozon und einem langlebigen Tracer, hier N_2O , im November und Dezember deutlich zu höheren Ozonmischungsverhältnissen verschiebt. Das lässt auf horizontale Mischungsprozesse und damit auf einen nicht genügend isolierten Wirbel schließen. Die Frühwinter-Referenzfunktion in dem Winter 1996–97 wurde daher aus Messdaten ermittelt werden, die Anfang Januar gemessen wurden. Tatsächlich hängt der Zeitpunkt der Bestimmung der Frühwinterreferenz maßgeblich von den vorhandenen Messdaten im Frühwirbel ab, welche in den meisten untersuchten Wintern sehr begrenzt sind.

Die Anwendung der TRAC Technik auf den ILAS Datensatz ergab weiterhin, dass horizontale Mischungsvorgänge nach Isolation des Wirbels im Januar, vernachlässigt werden können. Die zeitliche Entwicklung der Ozonerstörung im Winter 1996–97 wurde ausführlich mit Hilfe der ILAS und den vorhandenen HALOE Daten (von März bis Mai) untersucht. Der chemische Ozonverlust beginnt Mitte Februar mit ansteigendem Ozonverlust bis Mitte Mai, gemittelt über den gesamten Wirbel. Ende März wird ein stark inhomogener Ozonverlust, mit den stärksten Verlustraten im Wirbelkern, festgestellt. Der Wirbel ist unterteilt in einem Bereich mit hohem Ozonverlust (HALOE 40–45 DU, ILAS 30–35 DU) und einem Bereich mit mittlerem Ozonverlust (HALOE 15–30 DU, ILAS 5–25 DU) in 450–550 K. Die Zweiteilung des Wirbels wird für HALOE und ILAS Daten konsistent gefunden, obwohl der berechnete Ozonverlust aus den HALOE Messungen besonders Ende März deutlich größer ist, als der aus ILAS Daten berechnete.

Ein möglicher Grund für die Differenzen ist die Tatsache, dass die Ozonprofile Ende März 1997 von HALOE ein deutlich geringeres Minimum (0.6 ppmv) in 475 K aufweisen, als die ILAS Profile. Außerdem liegen im März/April die HALOE Ozondaten im Wirbel durchschnittlich ca. 0.2 ppmv niedriger als die gemessenen ILAS Ozondaten. Ab April werden die Ozonprofile innerhalb des Wirbels im Vergleich zu Ende März wieder einheitlicher. Die Verringerung von Ozon in den immer noch vorhandenen Wirbelteilen im April und Mai wird durch NO_x Chemie hervorgerufen.

Die verbesserte Methode wurde darüber hinaus konsistent für elf Winter (1991–92 bis 2001–02) auf Daten der aktuellsten HALOE Version 19 angewendet. Zunächst wurde für alle Winter jeweils eine CH_4/HF Funktion ermittelt, die, wie sich herausstellte für die gesamte Lebenszeit des Wirbels gilt. Damit konnte die oben beschriebene CH_4/HF Korrektur durchgeführt werden. Weiterhin konnte aus der jährliche Entwicklung der einzelnen CH_4/HF Funktionen, in Richtung höherer Mischungsverhältnisse der beiden Tracer, das jährliche Wachstum von HF in Abhängigkeit von der Höhe in der Stratosphäre bestimmt werden.

Zur Berechnung des Ozonverlustes konnten Frühwinterkorrelationen in sechs Wintern direkt aus HALOE Daten ermittelt werden, für drei weitere Winter aus Daten von Ozonsonden, Ballonmessungen und aus der ILAS Frühwinterreferenz. Für zwei Winter, für die weder HALOE noch andere Messungen im Frühwirbel vorliegen, wurde jeweils eine Referenzkorrelation bestimmt. Dazu wurden HALOE Messdaten aller der Winter verwendet, welche im Frühwinter vorliegen. Außerdem wurde der jährliche Anstieg von CH_4 und HF in der Stratosphäre in die Berechnung mit einbezogen.

Aufgrund der Analyse über elf Jahre hinweg, konnte der Zusammenhang zwischen meteorologischen Verhältnissen im Polarwirbel und dem berechneten Ozonverlust aufgezeigt werden. Sind die Temperaturverhältnisse eines Winters kalt, so zeigt sich eine starke Abweichung der O_3 -Tracer Verhältnisse im März/April von der Frühwirbel Referenzfunktion. Das ist der Fall in den Wintern 1992–93, 1994–95, 1995–96, 1996–97 und 1999–2000. In den nicht ganz so kalten Wintern, 1991–92, 1993–94, 1997–98, ist entsprechend die Abweichung von der Referenzfunktion geringer. Die warmen Winter zeigen sehr geringe Abweichungen und damit einen geringen Ozonverlust. Besonderheiten konnten herausgestellt werden, wie zum Beispiel für den warmen Winter 2000–01. Dieser Winter zeichnet sich durch eine sehr kurze Periode von mittlerem Ozonverlust ausschließlich im Februar aus. Eine kurzzeitige Verschiebung des Wirbels nach Mitteleuropa sorgte für eine Abkühlung des Wirbels und damit für die starke Chloraktivierung, was die Ursache für den auftretenden Ozonverlust sein kann.

Die Betrachtung der HCl-Tracer Relation deutet auch darauf hin, dass im allgemeinen eine starke Chloraktivierung zeitlich verzögert hohen Ozonverlust mit sich bringt, wenn es die meteorologischen Bedingungen nach der Chloraktivierung zulassen. Jedoch gibt es nicht allzu viele HALOE Daten, die dies bestätigen können. 1992–93 und 1994–95 gab es nur in einem äußerem Bereich der Wirbelgrenzregion Messungen im Februar, die eine starke Chloraktivierung zeigten. Andererseits bedeutet eine starke Verringerung von HCl, wie im März 1994 beob-

achtet, nicht notwendig das Auftreten von hohem Ozonverlust. Die Verringerung der HCl Werte erreichte in diesem Winter vergleichbare Werte, wie sie in den sehr kalten Wintern gemessen wurden. Bedingt durch eine Erwärmung des Wirbels im April, wurden nur mäßige Ozonverlustwerte erreicht.

Der zwischen Winter und Frühling in einer Höhe zwischen 380–550 K ermittelte Ozonverlust zeigt ein Maximum, dessen Wert und Höhenposition mit den Jahren variiert. Dieses Maximum im Ozonverlust im entsprechenden Höhenbereich wurde für jedes Jahr ermittelt. Besonders starke Verlustraten wurden für die kalten Jahre berechnet. So liegt der maximale Ozonverlust im März (bzw. im Jahr 2001 im Februar 2001) über 2 ppmv in den kalten Jahren und für die mittelmäßig kalten Winter wurden 1.3–1.6 ppmv maximaler Ozonverlust ermittelt. Für die warmen Winter waren die Abweichungen von der Frühwinterreferenz noch geringer. Diese Werte können zuverlässig innerhalb der Fehlergrenzen (maximal ± 0.4 ppmv) angegeben werden, da abgesehen von der Unsicherheit der Frühwinterreferenz keine weiteren Unsicherheiten auftreten. Mit Hilfe der Ozon-Verlustprofile kann auch auf die Homogenität des Ozonverlustes z.B. in einem bestimmten Monat geschlossen werden. Der Winter 1996–97 zeigt sich als ein Winter mit besonders inhomogener Ozonverlustverteilung.

Bei der Berechnung des Ozonverlustes in der Säule über ein bestimmtes Höhenintervall, im Mittel über einen Monat, können die Ergebnisse von weiteren Fehlern beeinflusst sein. Zum Beispiel können Mischungsvorgänge in niedrigen Höhen unterhalb von 400 K neben der Unsicherheit der Frühwinterreferenz zu weiteren Unsicherheiten führen. Mit einer ausführlichen Fehleranalyse zeigt sich, dass die Integration des Ozon-Verlustprofils zur Berechnung des Ozonverlustes in DU für ein Intervall von 400–500 K und für Profile im Wirbelkern, die geringsten Unsicherheiten besitzt. In dieser Arbeit wurden ebenso Ergebnisse für 350–550 K, 380–550 K und 400–550 K ermittelt, um Vergleichsmöglichkeiten mit anderen Studien zu schaffen.

Für die kalten Winter wurden im Höhenbereich zwischen 380–550 K im April 1993 und 1996 über 100 DU Ozonverlust, im April 2000 78 DU, vorwiegend im Wirbelkern ermittelt. Der Ozonverlust in den mittelmäßig kalten Wintern erreichte 40–60 DU im gleichen Höhenintervall. Der Winter 1991–92 zeigt deutlich höhere Verlustwerte, bis zu 80 DU. Dies lässt sich durch eine deutlich erhöhte Anzahl flüssiger Sulfataerosole in der Atmosphäre erklären, die als Folge des Mount Pinatubo Ausbruchs 1991 in die Stratosphäre gelangt sind.

Die Größe des Unterschiedes zwischen dem berechneten Ozonverlustes für den Wirbelkern und den äußeren Wirbel lässt auf die Kompaktheit des Wirbels schließen. Die Homogenität des Ozonverlustes im Wirbel wird auch an einer geringen berechneten Standardabweichung des Ozonverlustes über eine Säule im Mittel über einen Monat deutlich. Der kalte Winter 1996–97 zeigte sich als sehr inhomogen, die Standardabweichung des Ozonverlustes in DU ist deutlich größer als in den anderen untersuchten Wintern. Durch seine Inhomogenität wurde in diesem Winter der Ozonverlust, im Mittel über den Wirbelkern mit 60 DU als deutlich geringer berechnet, als für die anderen kalten Winter. Der Unterschied zwischen dem Ozonverlust im Wirbelkern und dem im äußeren Wirbel zeigt, dass

im März 1997 im Kern mehr Ozon abgebaut wird, da dort niedrigere Temperaturen auftreten. Ein möglicher Einfluss von Einmischung ozonreicher Luft aus niedrigeren Breiten auf den Ozonverlust im Wirbelkern ist zu vernachlässigen.

Aus den Ergebnissen der Datenanalyse von ILAS und HALOE lässt sich schließen, dass die größte Unsicherheit der Methode aus der Unsicherheit der Referenzfunktion resultiert. In sehr warmen Wintern liegt der berechnete Ozonverlust zum Teil im Bereich der Unsicherheit der Referenzfunktion. Trotzdem liegen diese Ergebnisse in zu erwartenden Wertebereichen.

Der mit der vorgestellten TRAC Technik für elf Winter konsistent berechnete Ozonverlust kann den meteorologischen Verhältnissen des jeweiligen Winters gegenübergestellt werden. Es zeigt sich, dass es einen Zusammenhang zwischen den über die gesamte Lebensdauer des Wirbels auftretenden möglichen PSC-Flächen² und mit den akkumulierten Ozonverlusten gibt. Anders als in jüngsten Studien beschrieben, ist dieser Zusammenhang aber nicht linear. Die Ergebnisse dieser Arbeit deuten darauf hin, dass der Ozonverlust von deutlich mehr Einflüssen als nur der Fläche von PSCs bestimmt ist, sondern zum Beispiel auch von der Stärke der Sonneneinstrahlung. Zum Beispiel wird für die Winter, in denen der Wirbelkern in niedrigere Breiten verschoben war, ein stärkerer Ozonabbau gefunden. Außerdem lassen sich Auswirkungen von Vulkanausbrüchen, wie zum Beispiel 1991 des Mount Pinatubo, identifizieren.

Vergleiche mit anderen veröffentlichten Studien zeigen darüber hinaus, dass für sehr kalte Winter mit einem homogenen Wirbel, wie z.B. 1999–2000, einheitliche Ergebnisse durch verschiedene Techniken ermittelt werden. In mäßig kalten und in warmen Wintern mit komplizierten Transportprozessen im Wirbel gibt es dagegen größere Unterschiede. Die Ursachen für diese Diskrepanzen sind zum jetzigen Zeitpunkt ungeklärt. Ein wichtiger Vorteil der hier eingesetzten TRAC Technik ist die Unabhängigkeit von Modellrechnungen zur Berechnung der Transportprozesse, was bei allen anderen Methoden zur Bestimmung des chemischen Ozonverlustes notwendig ist.

Weiteren Aufschluss gäben Satelliteninstrumente, die wie ILAS kontinuierlich während eines Winters in hohen Breiten messen würden. Solche Messdaten sind in naher Zukunft von ILAS II und den atmosphärischen Instrumenten des ENVISAT zu erwarten.

²Die möglichen PSC (Polar Stratospheric Cloud)-Flächen sind die – mit Hilfe meteorologischer Analysen – ermittelten Flächen im Wirbel, welche die wahrscheinliche Bildungstemperatur von PSC (≈ 195 K) nicht überschreiten.

Appendix B

Satellite Measurements

The basis for the enhanced TRAC technique applied in the present work are observations obtained by two solar occultation satellite instruments: ILAS (Improved Limb Atmospheric Spectrometer) aboard the ADEOS satellite (Advanced Earth Observing Satellite) and HALOE (Halogen Occultation Experiment) aboard the UARS, the Upper Atmosphere Research satellite [Russell *et al.*, 1993; Suzuki *et al.*, 1995; Sasano *et al.*, 1999].

The principle of a solar occultation instrument measuring concentrations of chemical trace species in the stratosphere and above is to integrate the absorption in the infrared along a tangential path through the atmosphere between the sun and the instrument over the tangential ray path. A vertical scan is obtained by stepwise tracking the position of the sun during each occultation, that is during each sunrise and sunset. This yields high vertical resolution data profiles of chemical compounds in the stratosphere.

B.1 ILAS

The ILAS instrument is designed to take measurements in high latitudes of both hemispheres. Unfortunately, the instrument was only able to deliver measurements in one year, 1996–97. However, an 8-month record of data for trace species from November 1996 to June 1997 was obtained [Suzuki *et al.*, 1995; Sasano *et al.*, 1999]. The instrument took measurements about fourteen times per day in the high latitude region of both hemispheres. Vertical profiles of O₃, NO₂, N₂O, HNO₃, CH₄, CFC11, CFC12, H₂O, N₂O₅ were measured in the range from ≈ 10 km or cloud-top up to 60 km. In the present work, the focus is on O₃, N₂O and CH₄. The spatial and temporal coverage of ILAS data in the northern hemisphere is shown in Figure B.1 (green symbols).

In the present work measurements of the Version 5.20 ILAS retrieval algorithm [Yokota *et al.*, 2002] were used. For this data version the estimated root-sum-square of the total uncertainties in ozone values are 14 % at 15 km, 9 % at 20 km and 7 % at 23 km on average in the northern hemisphere during the entire measurement period [Yokota *et al.*, 2002; Terao *et al.*, 2002]. Numerical

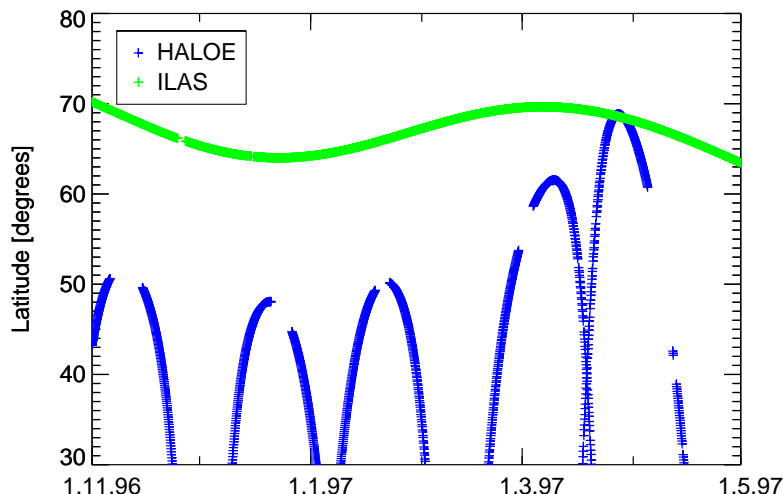


Figure B.1: Temporal and spatial coverage of ILAS and HALOE observations in northern latitudes from November 1, 1996 to May 1, 1997 (copyright by AGU).

simulations show that the ozone values may have a large positive bias of 1.11 ppmv at 20 km when observing ice PSCs. During the entire winter, ILAS ozone mixing ratios are on average $\approx 8\%$ greater than HALOE for the altitude range between 380–550 K *Sugita et al.* [2002]. In the present work, substantial discrepancies in the very low ozone minimum measured at the 475 K potential temperature level were found at the end of March comparing HALOE and ILAS observations (see Section 6.1).

B.2 HALOE

Measurements by the HALOE instrument [*Russell et al.*, 1993] began on October 11, 1991. HALOE provides measurements of vertical profiles of ozone, methane, hydrogen chloride, hydrogen fluoride, water vapour, NO_2 and NO. The altitude range of measurements extends from the lower stratosphere (upper troposphere in some cases) to the mesosphere and is thus similar to ILAS observations. The HALOE instrument makes measurements fifteen times per day at sunrise and sunset along two latitude lines that move between 80°N and 80°S in about 45 days (see Figure B.2). Therefore, measurements in high northern latitudes are available every two or three months, depending on the year. Thus, HALOE data are available usually inside the early vortex and afterwards later in spring. For example, for 1996–97 HALOE observations are available inside the vortex in spring (March, April and May 1997) only (see Figure B.1, blue symbols).

The analysis presented here is based on Version 19 HALOE data processing algorithm with accuracies shown in Table B.1. Owing to the algorithm improvements between Version 18, and even more more so Version 17 and Version 19

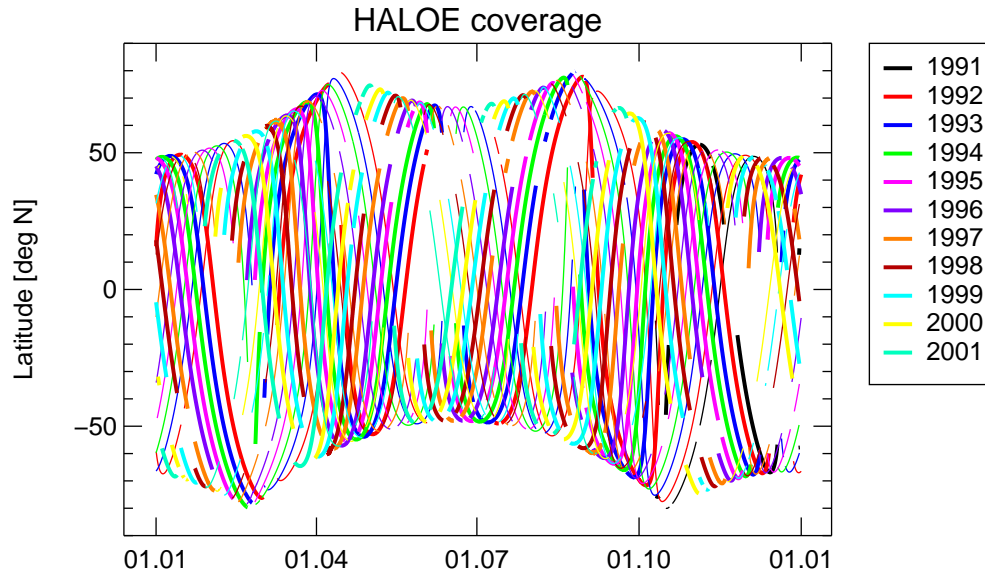


Figure B.2: Temporal and spatial coverage of HALOE observations from 1991 to 2001.

HALOE data, results based on the Version 19 are more reliable compared to earlier studies (see Section 9.1). Major modifications were made between Version 17 and 18, which clearly influenced the ozone loss [Harris *et al.*, 2002] determined. In the present work, the Version 19 data employed have a better accuracy for the retrieved species at altitudes below 70 hPa and show substantial improvements in sunrise and sunset differences, as described in more detail on the HALOE website. Ozone shows minor differences from Version 18 values throughout the entire profile.

Table B.1: Accuracy of HALOE V19 Data, J. M. Russell, pers. comm., 2003.

Pressure, hPa	1	5	10	50	100			
O ₃ , %	8	9	12	18	30	NO	cloud to 25 km	102 %
CH ₄ , %	6	9	11	15	19		25 km to 40 km	14 %
HCl, %	15	12	14	21	24		> 40 km	101 %
HF, %	15	14	15	21	27	NO ₂	cloud to 25 km	100 %
H ₂ O, %	14	14	17	24	27		25 km to 40 km	10 %
							> 40 km	100 %

Some remaining uncertainties in HALOE Version 19 data can not be excluded (J. M. Russell III pers. comm., 2002), there may be problematic data at large beta angles (beta angle is the angle between the plane of the spacecraft's orbit, and the line connecting the center of the Earth with the Sun). This is the case at the beginning of March 1997 (see Section 6.2.1). Further, the quality of a few HALOE HF measurements may be reduced owing to sunspot occurrence. In some

years (for example 1999–2000, the CH₄ mixing ratios inside the Arctic vortex at altitudes below about 450 K may be problematic, due to signal saturation problems (J.M. Russell III, pers. comm., 2001).

Appendix C

Tracer-Tracer Reference Relations

In this chapter a summary of the mathematically formulated relations of different tracers is given. Polynomial functions of the form: $[y] = \sum_{i=0}^n a_i \cdot [x]^i$ with $n \leq 4$ are reported and the standard deviation of the observation points from the fitted reference function σ . In Table D.1 CH₄/HF relations were derived from measurements made by HALOE inside the vortex core. Reference relations O₃ to tracer were derived from measurements made by HALOE for the early vortex (Table D.2 and D.3). Table D.4 summarises all tracer-tracer reference relations used in this work derived from measurements made by HALOE, ILAS or balloon observations (M-IV). These reference relations derived from the HALOE profiles available in the early vortex of all investigated years are indicated as “HALOE all”.

The empirical relations are valid for mixing ratios of CH₄ in ppmv, HF in ppbv, O₃ in ppmv and N₂O in ppbv, respectively.

Table C.1: CH₄/HF reference relations from HALOE observations inside the vortex core: 1991–92 to 2001–02.

valid [x]	a_0	a_1	a_2	a_3	a_4	σ	
1991–92							
0.1–1.1	1.83	–2.49	2.72	–3.31	1.63	$9.03 \cdot 10^{-2}$	R1
1992–93							
0.1–1.3	1.64	–1.71	$7.33 \cdot 10^{-1}$	$-1.91 \cdot 10^{-2}$	$-1.55 \cdot 10^{-1}$	$9.95 \cdot 10^{-2}$	R2
1993–94							
0.1–1.35	1.85	–2.75	3.70	–3.15	$9.31 \cdot 10^{-1}$	$1.04 \cdot 10^{-1}$	R3
1994–95							
0.1–1.4	1.76	–2.71	4.18	–3.71	1.10	$8.98 \cdot 10^{-2}$	R4
1995–96							
0.1–1.5	1.65	–1.16	$1.77 \cdot 10^{-1}$	$-3.63 \cdot 10^{-2}$		$8.11 \cdot 10^{-2}$	R5
1996–97							
0.1–1.5	1.76	–1.88	2.25	–2.00	$5.87 \cdot 10^{-1}$	$7.92 \cdot 10^{-2}$	R6
1997–98							
0.1–1.55	1.71	–1.47	$8.75 \cdot 10^{-1}$	$-4.91 \cdot 10^{-1}$	$8.44 \cdot 10^{-2}$	$8.14 \cdot 10^{-2}$	R7
1998–99							
0.2–1.6	1.98	–3.44	4.84	–3.40	$8.07 \cdot 10^{-1}$	$8.46 \cdot 10^{-2}$	R8
1999–2000							
0.1–1.65	1.72	–1.89	1.53	$-8.55 \cdot 10^{-1}$	$1.73 \cdot 10^{-1}$	$8.67 \cdot 10^{-2}$	R9
2000–01							
0.1–1.7	2.05	–2.99	4.10	–3.05	$7.54 \cdot 10^{-1}$	$7.27 \cdot 10^{-2}$	R10
2001–02							
0.1–1.6	1.89	–2.54	2.90	–1.93	$4.40 \cdot 10^{-1}$	$7.39 \cdot 10^{-2}$	R11

Table C.2: O₃/HF reference relations from HALOE observations: 1991–92 to 2001–02.

valid [x]	a_0	a_1	a_2	a_3	a_4	σ	
1992–93							
0.01–1.	$-9.82 \cdot 10^{-2}$	5.93	$1.47 \cdot 10^1$	$-3.19 \cdot 10^1$	$1.55 \cdot 10^1$	$3.46 \cdot 10^{-1}$	R12
1993–94							
0.01–1.1	$2.60 \cdot 10^{-1}$	3.81	8.16	$-1.27 \cdot 10^1$	4.42	$2.49 \cdot 10^{-1}$	R13
1994–95							
0.01–1.1	$-1.03 \cdot 10^{-1}$	5.80	$-3.04 \cdot 10^{-1}$	-1.73	$4.79 \cdot 10^{-3}$	$3.77 \cdot 10^{-1}$	R14
1995–96							
0.01–1.0	$-1.70 \cdot 10^{-1}$	7.93	-6.08	1.92		$1.24 \cdot 10^{-1}$	R15
1997–98							
0.–1.3	$3.66 \cdot 10^{-2}$	5.87	5.91	$-1.35 \cdot 10^1$	5.37	$2.89 \cdot 10^{-1}$	R16
1998–99							
0.01–1.2	$3.30 \cdot 10^{-1}$	3.23	$1.10 \cdot 10^1$	$-1.74 \cdot 10^1$	6.91	$1.86 \cdot 10^{-1}$	R17
2000–01							
0.–1.3	$7.27 \cdot 10^{-3}$	$1.36 \cdot 10^{-1}$	$1.50 \cdot 10^1$	$-1.60 \cdot 10^1$	4.66	$3.02 \cdot 10^{-1}$	R18
2001–02							
0.1–1.5	$-4.83 \cdot 10^{-1}$	$1.03 \cdot 10^1$	$-1.09 \cdot 10^1$	4.98	$-7.06 \cdot 10^{-1}$	$1.48 \cdot 10^{-1}$	R19

Table C.3: O₃/CH₄ reference relations from HALOE observations: 1991–92 to 2001–02.

valid [x]	a_0	a_1	a_2	a_3	a_4	σ	
1992–93							
0.45–1.65	8.77	$-2.39 \cdot 10^1$	$4.51 \cdot 10^1$	$-3.59 \cdot 10^1$	9.34	$2.31 \cdot 10^{-1}$	R20
1993–94							
0.4–1.7	4.72	-6.55	$1.73 \cdot 10^1$	$-1.75 \cdot 10^1$	5.12	$3.09 \cdot 10^{-1}$	R21
1994–95							
0.45–1.6	4.19	-3.51	$1.14 \cdot 10^1$	$-1.38 \cdot 10^1$	4.44	$3.56 \cdot 10^{-1}$	R22
1995–96							
0.6–1.7	-2.98	$2.55 \cdot 10^1$	$-3.00 \cdot 10^1$	$1.24 \cdot 10^1$	-1.68	$3.09 \cdot 10^{-1}$	R23
1997–98							
0.6–1.7	3.70	-2.09	$1.00 \cdot 10^1$	$-1.19 \cdot 10^1$	3.55	$4.40 \cdot 10^{-1}$	R24
1998–99							
0.6–1.7	$4.55 \cdot 10^{-1}$	$1.27 \cdot 10^1$	$-1.27 \cdot 10^1$	3.11		$1.04524 \cdot 10^{-1}$	R25
2000–01							
0.6–1.7	5.00	-8.95	$2.14 \cdot 10^1$	$-1.92 \cdot 10^1$	5.16	$4.43 \cdot 10^{-1}$	R26
2001–02							
0.6–1.7	4.49	-6.35	$1.36 \cdot 10^1$	$-1.26 \cdot 10^1$	3.55	$1.85 \cdot 10^{-1}$	R27

Table C.4: Overview of all tracer-tracer reference relations: 1991–92 to 2001–02.

Ref.	valid [x]		a_0	a_1	a_2	a_3	a_4	σ	
1991–92									
Balloon	O ₃	N ₂ O	10–260	3.94	$-4.84 \cdot 10^{-3}$	$-6.40 \cdot 10^{-5}$		$2.64 \cdot 10^{-1}$	
1992–93									
HALOE	CH ₄	HF	0.1–1.3	1.64	-1.71	$7.33 \cdot 10^{-1}$	$-1.91 \cdot 10^{-2}$	$-1.55 \cdot 10^{-1}$	$9.95 \cdot 10^{-2}$
HALOE	O ₃	CH ₄	0.45–1.65	8.77	$-2.39 \cdot 10^1$	$4.51 \cdot 10^1$	$-3.59 \cdot 10^1$	9.34	$2.31 \cdot 10^{-1}$
HALOE	O ₃	HF	0.01–1.	$-9.82 \cdot 10^{-2}$	5.93	$1.47 \cdot 10^1$	$-3.19 \cdot 10^1$	$1.55 \cdot 10^1$	$3.46 \cdot 10^{-1}$
1993–94									
HALOE	CH ₄	HF	0.1–1.35	1.85	-2.75	3.70	-3.15	$9.31 \cdot 10^{-1}$	$1.04 \cdot 10^{-1}$
HALOE	O ₃	CH ₄	0.4–1.7	4.72	-6.55	$1.73 \cdot 10^1$	$-1.75 \cdot 10^1$	5.12	$3.09 \cdot 10^{-1}$
HALOE	O ₃	HF	0.01–1.1	$2.60 \cdot 10^{-1}$	3.81	8.16	$-1.27 \cdot 10^1$	4.42	$2.49 \cdot 10^{-1}$
1994–95									
HALOE	CH ₄	HF	0.1–1.4	1.76	-2.71	4.18	-3.71	1.10	$8.98 \cdot 10^{-2}$
HALOE	O ₃	CH ₄	0.45–1.6	4.19	-3.51	$1.14 \cdot 10^1$	$-1.38 \cdot 10^1$	4.44	$3.56 \cdot 10^{-1}$
HALOE	O ₃	HF	0.01–1.1	$-1.03 \cdot 10^{-1}$	5.80	$-3.04 \cdot 10^{-1}$	-1.73	$4.79 \cdot 10^{-3}$	$3.77 \cdot 10^{-1}$
1995–96									
HALOE	CH ₄	HF	0.1–1.5	1.65	-1.16	$1.77 \cdot 10^{-1}$	$-3.63 \cdot 10^{-2}$		$8.11 \cdot 10^{-2}$
HALOE	O ₃	CH ₄	0.6–1.7	-2.98	$2.55 \cdot 10^1$	$-3.00 \cdot 10^1$	$1.24 \cdot 10^1$	-1.68	$3.09 \cdot 10^{-1}$
HALOE	O ₃	HF	0.01–1.0	$-1.70 \cdot 10^{-1}$	7.93	-6.08	1.92		$1.24 \cdot 10^{-1}$
1996–97									
HALOE	CH ₄	HF	0.1–1.5	1.76	-1.88	2.25	-2.00	$5.87 \cdot 10^{-1}$	$7.92 \cdot 10^{-2}$
HALOE	O ₃	CH ₄	0.6–1.5	3.26	-3.33	-9.30	2.41	$2.27 \cdot 10^1$	$2.8 \cdot 10^{-1}$
ILAS	O ₃	N ₂ O	20–250	3.83	$-1.71 \cdot 10^{-2}$	$3.47 \cdot 10^{-4}$	$-2.50 \cdot 10^{-6}$	$-4.84 \cdot 10^{-9}$	$2.76 \cdot 10^{-1}$
1997–98									
HALOE	CH ₄	HF	0.1–1.55	1.71	-1.47	$8.75 \cdot 10^{-1}$	$-4.91 \cdot 10^{-1}$	$8.44 \cdot 10^{-2}$	$8.14 \cdot 10^{-2}$
HALOE all	O ₃	CH ₄	0.6–1.7	3.70	-2.09	$1.00 \cdot 10^1$	$-1.19 \cdot 10^1$	3.55	$4.40 \cdot 10^{-1}$
HALOE all	O ₃	HF	0.–1.3	$3.66 \cdot 10^{-2}$	5.87	5.91	$-1.35 \cdot 10^1$	5.37	$2.89 \cdot 10^{-1}$
1998–99									
HALOE	CH ₄	HF	0.2–1.6	1.98	-3.44	4.84	-3.40	$8.07 \cdot 10^{-1}$	$8.46 \cdot 10^{-2}$
HALOE	O ₃	CH ₄	0.6–1.7	$4.55 \cdot 10^{-1}$	$1.27 \cdot 10^1$	$-1.27 \cdot 10^1$	3.11		$1.04524 \cdot 10^{-1}$
HALOE	O ₃	HF	0.01–1.2	$3.30 \cdot 10^{-1}$	3.23	$1.10 \cdot 10^1$	$-1.74 \cdot 10^1$	6.91	$1.86 \cdot 10^{-1}$
1999–2000									
HALOE	CH ₄	HF	0.1–1.65	1.72	-1.89	1.53	$-8.55 \cdot 10^{-1}$	$1.73 \cdot 10^{-1}$	$8.67 \cdot 10^{-2}$
M-IV Dec	O ₃	CH ₄	0.1–1.7	3.63	-5.15	$1.29 \cdot 10^1$	$-1.07 \cdot 10^1$	2.49	$1.39 \cdot 10^{-1}$
M-IV Nov	O ₃	CH ₄	0.4–1.85	4.82	-9.13	$1.52 \cdot 10^1$	$-1.02 \cdot 10^1$	2.06	$1.78 \cdot 10^{-1}$
M-IV	O ₃	HF	0.01–1.3	$1.03 \cdot 10^{-1}$	6.39	-1.43	-3.31	1.53	$1.01 \cdot 10^{-1}$
2000–01									
HALOE	CH ₄	HF	0.1–1.7	2.05	-2.99	4.10	-3.05	$7.54 \cdot 10^{-1}$	$7.27 \cdot 10^{-2}$
HALOE all	O ₃	CH ₄	0.6–1.7	5.00	-8.95	$2.14 \cdot 10^1$	$-1.92 \cdot 10^1$	5.16	$4.43 \cdot 10^{-1}$
HALOE all	O ₃	HF	0.–1.3	$7.27 \cdot 10^{-3}$	$1.36 \cdot 10^{-1}$	$1.50 \cdot 10^1$	$-1.60 \cdot 10^1$	4.66	$3.02 \cdot 10^{-1}$
2001–02									
HALOE	CH ₄	HF	0.1–1.6	1.89	-2.54	2.90	-1.93	$4.40 \cdot 10^{-1}$	$7.39 \cdot 10^{-2}$
HALOE	O ₃	CH ₄	0.6–1.7	4.49	-6.35	$1.36 \cdot 10^1$	$-1.26 \cdot 10^1$	3.55	$1.85 \cdot 10^{-1}$
HALOE	O ₃	HF	0.1–1.5	$-4.83 \cdot 10^{-1}$	$1.03 \cdot 10^1$	$-1.09 \cdot 10^1$	4.98	$-7.06 \cdot 10^{-1}$	$1.48 \cdot 10^{-1}$
all winter									
Engel1996	N ₂ O	CH ₄	0.5–1.7	$-1.36 \cdot 10^2$	$2.62 \cdot 10^2$				

List of Figures

1.1	The vertical distribution of stratospheric ozone decline for northern and mid-latitudes from 1980 to 1996	2
1.2	Zonally averaged distribution of ozone mixing ratios in ppmv in September	3
3.1	Schematic view of the meridional circulation in the stratosphere and interactions between troposphere and stratosphere	19
3.2	Schematic view of the Arctic polar vortex	21
3.3	Schematic view of the polar vortex regions	23
3.4	The annual ozone column density in DU for twelve years between 1979 and 1999	25
3.5	The time (in days of the year) of the minimum of TOMS ozone column density in one year averaged over northern Europe, shown for 16 years	26
4.1	Tracer-tracer profiles inside the vortex of the year 1999–2000 from HALOE measurements with HF as the passive tracer	31
4.2	Vertical ozone profiles and ozone loss profiles for March in winter 1999–2000	33
4.3	Schematic view of the impact of mixing and chemical ozone loss on the ozone-tracer relationship inside the vortex	37
4.4	Threshold PV value for different vortex regions	40
4.5	Potential vorticity derived from UKMO data on the 475 K potential temperature level and for the same Θ level, ozone mixing ratios in ppmv as derived from satellite profiles	40
4.6	Tracer-tracer profiles inside the outer early vortex of the year 1995–96 from HALOE measurements with HF as the passive tracer	42
4.7	Area of possible PSC existence determined from UKMO data over the entire polar vortex as a function of altitude from November 1995 to April 1996	43
5.1	Area of possible PSC existence from UKMO data over the entire polar vortex as a function of altitude from November 1996 to April 1997	48
5.2	O_3/N_2O relation of ILAS observations from November to January 1997	49

5.3	O ₃ /N ₂ O relation of ILAS observations inside the polar vortex for different periods from December 1996 to May 1997	51
5.4	O ₃ /N ₂ O relation of ILAS observations on different isentropic levels	54
6.1	The difference between mean ozone profiles from ILAS and HALOE	58
6.2	Ozone profiles from ILAS and HALOE at the end of March 1997 .	59
6.3	Ozone profiles measured from ILAS and HALOE, top panel: only moderate ozone profiles selected, bottom panel: only profiles with relatively low ozone in 450-500 K are shown	61
6.4	The O ₃ /HF relation and the O ₃ /CH ₄ relation for HALOE observations in winter 1996–97	63
6.5	CH ₄ /HF relation of HALOE observations 1996–97	64
6.6	Vertical profiles of measured O ₃ mixing ratios, proxy O ₃ mixing ratios, \hat{O}_3 , and ozone loss profiles, March 1997 by HALOE	65
6.7	Probability distribution of ozone loss in an altitude range of 450–550 K, HALOE results	68
6.8	Probability distribution of ozone loss in an altitude range of 380–550 K, HALOE results	68
6.9	As Figure 6.4, but for March, April and May	69
6.10	Vertical profiles O ₃ mixing ratios, ILAS, 18 March to 4 April, 1997	71
6.11	Probability distribution of ozone loss in an altitude range of 450–550 K, ILAS results	72
7.1	The CH ₄ /HF relationship for the eleven winters between 1991–92 and 2001–02 as measured by HALOE inside the vortex core	76
7.2	CH ₄ /HF reference functions for the eleven years between 1991–92 and 2001-02	77
7.3	Temporal development of the mixing ratio of HF for different CH ₄ levels of profiles measured by HALOE inside the vortex core from 1991–92 to 2001–02	78
7.4	The early winter reference function 1991–92 shown as a black line was derived from balloon measurements from December 1991 (coloured symbols)	81
7.5	O ₃ /CH ₄ relations from profiles inside the vortex of the year 1999–2000 from HALOE measurements are shown	82
7.6	Early winter reference relations for the nine years between 1991–92 to 2001-2002 are indicated as coloured lines	83
7.7	CH ₄ vs. Δ HF for the winters 1997–98 and 2000–01	85
7.8	Ozone-tracer profiles inside the early vortex of the years 1992–93 to 1995-96, 1998–99 and 2001–02 and the “reference functions for 1997-98 and 2000-2001	86
7.9	HCl/HF relations for the eleven winters between 1991-92 and 2001-02	87
7.10	O ₃ /HF relations for the eleven winters between 1991-92 and 2001-02	88
7.11	The area of possible PSC existence averaged over the entire polar vortex	89

8.1	Vertical profiles of measured O ₃ mixing ratios, proxy O ₃ mixing ratios, \hat{O}_3 , and ozone loss profiles, by HALOE for the winters between 1991–92 and 2001–02	96
8.2	As in Figure 8.1, but only profiles inside the vortex core are shown.	97
8.3	As in Figure 8.2, but with CH ₄ used as the long-lived tracer and only profiles inside the vortex core are shown.	98
8.4	Mean column ozone loss in winters between 1991–92 and 2001–02, using HF and CH ₄ as the long-lived tracers	101
8.5	Difference between mean column ozone loss using HF and CH ₄ as the long-lived tracer	105
8.6	Mean column ozone loss from profiles inside the entire vortex and from profiles inside the vortex core	106
8.7	Difference of mean column ozone loss using CH ₄ and HF as the long-lived tracers between the entire vortex and the vortex core for all winters between 1991–92 and 2000–01	107
9.1	Comparison of early winter O ₃ -tracer relations derived here by HALOE Version 19 with those by previous studies	113
9.2	Relation between ozone loss and total area of possible existing PSC (A _{PSC}) in the Arctic polar vortex for the years 1991–92 to 2001–02	119
B.1	Temporal and spatial coverage of ILAS and HALOE observations in northern latitudes from November 1, 1996 to May 1, 1997 (copyright by AGU).	130
B.2	Temporal and spatial coverage of HALOE observations from 1991 to 2001.	131

List of Tables

4.1	Calculated chemical loss in column ozone loss in the Arctic in winters 1992–93 to 1996–97. Comparison between HALOE results [Müller <i>et al.</i> , 1996, 1997a, 1999] and results from other methods described above.	36
5.1	Ozone loss in Dobson units in 450–550 K calculated from ILAS data	53
6.1	Column ozone loss in DU in 380–550 K, HALOE results	66
6.2	Column ozone loss in DU in 450–550 K, HALOE results	67
6.3	Column ozone loss in DU in 450–550 K, ILAS results	70
8.1	Maximum of the local accumulated ozone loss in ppmv in March (February in 2001) for the winters between 1991–92 and 2001–02	99
8.2	Column ozone loss in DU in 380–550 K, HALOE results	103
8.3	Column ozone loss in DU in 400–500 K, HALOE results	104
9.1	Calculated chemical loss in column ozone loss in the Arctic over 5 winters, new and earlier studies [Müller <i>et al.</i> , 1999] are compared	114
9.2	Calculated chemical loss in column ozone loss in the Arctic in winters 1994–95 to 1996–97. Comparison between HALOE results and results from other methods.	115
9.3	Calculated chemical loss in column ozone loss (DU) in the Arctic over seven winters, HALOE results and MLS results [Manney <i>et al.</i> , 2003a], are compared.	115
9.4	Accumulated ozone loss estimated by MLS and HALOE in comparison	117
B.1	Accuracy of HALOE V19 Data, J. M. Russell, pers. comm., 2003.	131
C.1	CH ₄ /HF reference relations from HALOE observations inside the vortex core: 1991–92 to 2001–02.	134
C.2	O ₃ /HF reference relations from HALOE observations: 1991–92 to 2001–02.	135
C.3	O ₃ /CH ₄ reference relations from HALOE observations: 1991–92 to 2001–02.	136
C.4	Overview of all tracer-tracer reference relations: 1991–92 to 2001–02.	137

Abbreviations and Symbols

Organisations

ECMWF	European Centre for Medium Range Weather Forecasts
EU	European Union
FZJ	Forschungszentrum Jülich (Research Centre Jülich)
NASA	National Aeronautics and Space Administration
NASDA	National Space Development Agency of Japan
UKMO	United Kingdom Meteorological Office
US NMC	US National Meteorological Center
WMO	World Meteorological Organisation

Measurement Campaigns

EASOE	European Arctic Stratospheric Ozone Experiment
EOS	Earth Observing System
SOLVE	SAGE III Ozone Loss and Validation Experiment
THESEO 2000	Third European Stratospheric Experiment on Ozone 2000

Measurements

ADEOS	Advanced Earth Observing Satellite
EP-TOMS	Earth Probe Total Ozone Mapping Spectrometer
HALOE	Halogen Occultation Experiment
HIRDLS	High Resolution Dynamics Limb Sounder
ILAS	Improved Limb Atmospheric Spectrometer
MkIV	Mark IV
MLS	Microwave Limb Sounder
OMS	Observations of the Middle Stratosphere
POAM	Polar Ozone and Aerosol Measurement
REPROBUS	Reactive Processes Ruling the Ozone Budget in the Stratosphere
SAGE II/III	Stratospheric Aerosol Gas Experiment II/III
SAOZ	Système d'Analyse par Observation Zénithale
TOMS	Total Ozone Mapping Spectrometer
UARS	Upper Atmospheric Research Satellite

Chemical and Physical Compounds

2-d	two-dimensional (latitude, height)
BrO	Bromine Oxide
CCl ₄	Carbon Tetrachloride
CFCs	Chlorofluorocarbons
CFC-11	CFCl ₃
CFC-12	CF ₂ Cl ₂
CH ₄	Methane
ClO	Chlorine Monoxide
ClONO ₂	Chlorine Nitrate
c_p	Specific heat for dry air [JK ⁻¹ mol ⁻¹]
DU	Dobson Units [1 DU = 2.69 * 10 ¹⁶ molecules/cm ²]
f	Coriolis Parameter
g	Acceleration of Gravity [9.81 ms ⁻¹]
HCl	Hydrogen Chloride
HNO ₃	Nitric Acid
$h\nu$	Photon (energy) with frequency ν
H ₂ O	Water Vapour
HO	Hydroxyl Radical
HO ₂	Hydroperoxyl Radical
HOCl	Hydroxyl Acid
HF	Hydrogen Fluoride
LT	Lagrangian Transport
m_L	Molecular Mass of dry Air [29 g/Mol]
N ₂	Molecular Nitrogen
N_A	Avogadro Number [6.02205 * 10 ²³ molec/mol]
NAT	Nitric Acid Trihydrate
NAD	Nitric Acid Dihydrate
NO	Nitric Oxide
NO _x	NO + NO ₂ + NO ₃
NO ₂	Nitrogen Dioxide
NO ₃	Nitrogen Trioxide
O	Atomic Oxygen
O _x	Odd Oxygen
O ₂	Molecular Oxygen
O ₃	Ozone
PSCs	Polar Stratospheric Clouds
STS	Super Cooled Ternary Solutions
T	Temperature
p	pressure
p_0	standard pressure [1013 hPa]
ppb	parts per billion
ppm	parts per million
PV	Potential Vorticity [1 PVU = 10 ⁻⁶ K m ² /(kg s)]

R	Universal Gas Constant [8.314 JK ⁻¹ mol ⁻¹]
SAD	Surface Area Density
TTL	Tropical Transition Layer
UTC	Universal Time (also known as Greenwich Mean Time (GMT))
UV-B	Ultraviolet-B Radiation (290 nm ≤ λ ≤ 320 nm)
ζ_a	Absolute Vorticity
ζ_θ	Relative Vorticity perpendicular to an Isentropic Surface
ζ_p	Relative Vorticity perpendicular to an Isobaric Surface
Θ	Potential Temperature
κ	Adiabatic Exponent [R/ c_p]
λ	Wavelength
σ	Standard Deviation
σ_v	Specific Volume
γ	Geographic Latitude [degrees]
Ω	Angular velocity of the Earth [7.292 · 10 ⁻⁵ s ⁻¹]

Bibliography

- Allen, D., and N. Nakamura, Tracer equivalent latitude: a diagnostic tool for isentropic transport studies, *J. Atmos. Sci.*, *60*, 287–304, 2003.
- Becker, G., R. Müller, D. S. McKenna, M. Rex, and K. S. Carslaw, Ozone loss rates in the Arctic stratosphere in the winter 1991/92: Model calculations compared with Match results, *Geophys. Res. Lett.*, *25*, 4325–4328, 1998.
- Becker, G., R. Müller, D. S. McKenna, M. Rex, K. S. Carslaw, and H. Oelhaf, Ozone loss rates in the Arctic stratosphere in the winter 1994/1995: Model simulations underestimate results of the Match analysis, *J. Geophys. Res.*, *105*, 15175–15184, 2000.
- Borrmann, S., J. Dye, D. Baumgardner, J. Wilson, H. Johnson, C. Brock, M. Loewenstein, J. Podolske, G. Ferry, and K. Barr, In situ measurements of changes in stratospheric aerosol and in the N₂O-aerosol relationship inside and outside of the polar vortex, *Geophys. Res. Lett.*, *20*, 2559–2562, 1993.
- Brewer, A. W., Evidence for a world circulation provided by the measurements of helium and water vapor distribution in the stratosphere, *Q. J. R. Meteorol. Soc.*, *75*, 351–363, 1949.
- Browell, E. V., C. F. Butler, M. A. Fenn, W. B. Grant, S. Ismail, M. Schoeberl, O. B. Toon, M. Loewenstein, and J. R. Podolske, Ozone and aerosol changes during the 1991-1992 Airborne Arctic Stratospheric Expedition, *Science*, *261*, 1155–1158, 1993.
- Butchart, N., and E. E. Remsberg, The area of the stratospheric polar vortex as a diagnostic for tracer transport on an isentropic surface, *J. Atmos. Sci.*, *43*(13), 1319–1339, 1986.
- Butler, J. H., M. Battle, S. A. Bender, S. A. Montzka, A. D. Clarke, E. S. Saltzman, C. Sucher, J. Severinghaus, and J. W. Elkins, A twentieth century record of atmospheric halocarbons in polar firn air, *Nature*, *399*, 749–755, 1999.
- Carslaw, K. S., J. A. Kettleborough, M. J. Northway, S. Davies, R. Gao, D. W. Fahey, D. G. Baumgardner, M. P. Chipperfield, and A. Kleinböhl, A vortex-scale simulation of the growth and sedimentation of large nitric acid hydrate particles, *J. Geophys. Res.*, *107*(D20), 10.1029/2001JD000467, 2002.

- Chapman, S., A theory of upper atmospheric ozone, *Mem. Roy. Soc.*, *3*, 103–109, 1930.
- Chipperfield, M. P., E. R. Lutman, J. A. Kettleborough, and J. A. Pyle, Model studies of chlorine deactivation and formation of ClONO₂ collar in the Arctic polar vortex, *J. Geophys. Res.*, *102*, 1467–1478, 1997.
- Clough, S. A., N. S. Grahame, and A. O'Neill, Potential vorticity in the stratosphere derived using data from satellites, *Q. J. R. Meteorol. Soc.*, *111*, 335–358, 1985.
- Coy, L., E. Nash, and P. Newman, Meteorology of the polar vortex: Spring 1997, *Geophys. Res. Lett.*, *24*, 2693–2696, 1997.
- Crutzen, P. J., The influence of nitrogen oxides on the atmospheric ozone content, *Q. J. R. Meteorol. Soc.*, *96*, 320–325, 1970.
- Crutzen, P. J., Estimates of possible future ozone reductions from continued use of fluoro-chloro-methanes (CF₂Cl₂, CFC₁₃), *Geophys. Res. Lett.*, *1*, 205–208, 1974.
- Crutzen, P. J., and U. Schmailzl, Chemical budgets of the stratosphere, *Planet. Space Sci.*, *31*, 1009–1032, 1983.
- Crutzen, P. J., J.-U. Grooß, C. Brühl, R. Müller, and J. M. Russell III, A reevaluation of the ozone budget with HALOE UARS data: No evidence for the ozone deficit, *Science*, *268*, 705–708, 1995.
- Deniel, C., R. M. Bevilacqua, J. P. Pommereau, and F. Lefèvre, Arctic chemical ozone depletion during the 1994-95 winter deduced from POAM II satellite observations and the REPROBUS three-dimensional model, *J. Geophys. Res.*, *103*, 19231–19244, 1998.
- Deshler, T., B. J. Bryan, D. J. Hofmann, and B. Nardi, Correlation between ozone loss and volcanic aerosol at altitudes below 14 km over mcMurdo station, antarctica, *Geophys. Res. Lett.*, *21*, 2931–2934, 1996.
- Dessler, A. E., The chemistry and physics of stratospheric ozone, in *International Geophysics Series*, edited by R. Dmowska, J. R. Holton, and H. T. Rossby, vol. 74, p. 214, Academic Press, London, San Diego, 2000.
- Dobson, G. M. B., Annual variations of ozone in Antarctica, *Q. J. R. Meteorol. Soc.*, *92*, 549–552, 1966.
- Dobson, G. M. B., D. Harrison, and J. Lawrence, Measurements of the amount of ozone in the Earth's atmosphere and its relation to other geophysical conditions, *Proc. R. Soc. London, Ser. A*, *122*, 456–486, 1929.

- Douglass, A. R., M. R. Schoeberl, R. S. Stolarski, J. W. Waters, J. M. Russell III, A. E. Roche, and S. T. Massie, Interhemispheric differences in springtime production of HCl and ClONO₂ in the polar vortices, *J. Geophys. Res.*, *100*, 13967–13978, 1995.
- Drdla, K., M. R. Schoeberl, and E. V. Browell, Microphysical modeling of the 1999-2000 Arctic winter 1. Polar stratospheric clouds, denitrification, and dehydration, *J. Geophys. Res.*, *108*(5), 55–1,21, 2002, doi:10.1029/2001JD000782.
- Engel, A., C. Schiller, U. Schmidt, R. Borchers, H. Ovarlez, and J. Ovarlez, The total hydrogen budget in the Arctic winter stratosphere during the European Arctic Stratospheric Ozone Experiment, *J. Geophys. Res.*, *101*, 14495–14503, 1996.
- Engel, A., M. Strunk, M. Müller, H. Haase, C. Poss, I. Levin, and U. Schmidt, Temporal development of total chlorine in the high-latitude stratosphere based on reference distributions of mean age derived from CO₂ and SF₆, *J. Geophys. Res.*, *107*(D12), 10.1029/2001JD000584, 2002.
- Ertel, H., Ein neuer hydrodynamischer Wirbelsatz, *Meteorol. Z.*, *59*, 277–281, 1942a.
- Ertel, H., Ein neuer hydrodynamischer Erhaltungssatz, *Naturwissenschaften*, *30*, 543–544, 1942b.
- Esler, J. G., and D. W. Waugh, A method for estimating the extent of denitrification of arctic polar vortex air from tracer-tracer scatter plots, *J. Geophys. Res.*, *107*, 6 1–14, 2002.
- Fahey, D., and A. Ravishankara, Summer in the stratosphere, *Science*, *285*, 208–210, 1999.
- Fahey, D. W., K. K. Kelly, S. R. Kawa, A. F. Tuck, M. Loewenstein, K. R. Chan, and L. E. Heid, Observations of denitrification and dehydration in the winter polar stratosphere, *Nature*, *344*, 321–324, 1990.
- Fahey, D. W., S. Solomon, S. R. Kawa, M. Loewenstein, J. R. Podolske, S. E. Strahan, and K. R. Chan, A diagnostic for denitrification in the winter polar stratospheres, *Nature*, *345*, 698–702, 1990.
- Fahey, D. W., et al., The detection of large HNO₃-containing particles in the winter Arctic stratosphere, *Science*, *291*, 1026–1031, 2001.
- Farman, J. C., B. G. Gardiner, and J. D. Shanklin, Large losses of total ozone in Antarctica reveal seasonal ClO_x/NO_x interaction, *Nature*, *315*, 207–210, 1985.
- Folkins, I., and C. Appenzeller, Ozone and potential vorticity at the subtropical tropopause break, *J. Geophys. Res.*, *101*, 18787–18792, 1996.

- Fueglistaler, S., B. P. Luo, C. Voigt, K. S. Carslaw, and T. Peter, NAT-rock formation by mother clouds: a microphysical model study, *Atmos. Chem. Phys. Discuss.*, *2*, 29–42, 2002.
- Girolamo, P. D., M. Cacciani, A. di Sarra, G. Fiocco, and D. Fua, Lidar observations of the pinatubo aerosol layer at thule, greenland, *grl*, *13*, 1295–1298, 1994.
- Goutail, F., et al., Total ozone depletion in the Arctic during the winters of 1993-94 and 1994-95, *J. Atmos. Chem.*, *32*, 35–59, 1999.
- Greenblatt, J., et al., Defining the polar vortex edge from an N₂O:potential temperature correlation, *J. Geophys. Res.*, *107*, 8268, doi:10.1029/2001JD000575, 2002.
- Grooß, J.-U., R. Müller, D. S. McKenna, and J. M. Russell III, HALOE observations of vortex air masses in late boreal spring 1997, in *Polar stratospheric ozone 1997, Proceedings of the fourth European symposium*, edited by N. R. P. Harris, I. Kilbane-Dawe, and G. T. Amanatidis, Air pollution research report 66, pp. 331–334, European Commission, 1998.
- Grooß, J.-U., R. Müller, G. Becker, D. S. McKenna, and P. J. Crutzen, An update of the upper stratospheric ozone budget calculations based on HALOE data, *J. Atmos. Chem.*, *34*, 171–183, 1999.
- Grooß, J.-U., et al., Simulation of ozone depletion in spring 2000 with the Chemical Lagrangian Model of the Stratosphere (CLaMS), *J. Geophys. Res.*, *107*, 8295, doi:10.1029/2001JD000456, 2002.
- Hansen, G., and M. P. Chipperfield, Ozone depletion at the edge of the Arctic polar vortex 1996/1997, *J. Geophys. Res.*, *104*, 1837–1845, 1999.
- Hanson, D. R., and K. Mauersberger, Laboratory studies of the nitric acid trihydrate: Implications for the south polar stratosphere, *Geophys. Res. Lett.*, *15*, 855–858, 1988.
- Harris, N., M. Rex, F. Goutail, B. Knudsen, G. Manney, R. Müller, and P. von der Gathen, Comparison of empirically derived ozone loss rates in the Arctic vortex, *J. Geophys. Res.*, *107*(D20), doi: 10.1029/2001JD000482, 2002.
- Hartmann, D., On potential vorticity and transport in the stratosphere, *J. Atmos. Sci.*, *34*, 968–977, 1977.
- Hofmann, D. J., and T. L. Deshler, Evidence from balloon measurements for chemical depletion of stratospheric ozone in the Arctic winter of 1989-90, *Nature*, *349*, 300–305, 1991.

- Hofmann, D. J., T. L. Deshler, P. Amedieu, W. A. Matthews, P. V. Johnston, Y. Kondo, W. R. S. G. J. Byrne, and J. R. Benbrook, Stratospheric clouds and ozone depletion in the Arctic during January 1989, *Nature*, *340*, 117–121, 1989.
- Holton, J. R., *An Introduction to Dynamic Meteorology*, Academic Press, London, 1992.
- Holton, J. R., P. Haynes, M. E. McIntyre, A. R. Douglass, R. B. Rood, and L. Pfister, Stratosphere-troposphere exchange, *Rev. of Geophys.*, *33*, 403–439, 1995.
- Hoppel, K., R. Bevilacqua, G. Nedoluha, C. Deniel, F. Lefèvre, J. Lumpe, M. Fromm, C. Randall, J. Rosenfield, and M. Rex, POAM III observations of Arctic ozone for the 1999/2000 winter, *J. Geophys. Res.*, *107*, 8262, 2002.
- Hoppel, K., R. Bevilacqua, D. Allen, G. Nedoluha, and C. Randall, POAM III Observations of the anomalous 2002 Antarctic ozone hole, *Geophys. Res. Lett.*, *30*, 1394, doi:10.1029/2002GL016899, 2003.
- Hoskins, B. J., Towards a PV- θ view of the general circulation, *Tellus*, pp. 27–35, 1991.
- Jackman, C. H., E. L. Fleming, S. Chandra, D. B. Considine, and J. E. Rosenfield, Past, present, and future modeled ozone trends with comparisons to observed trends, *J. Geophys. Res.*, *101*, 28753 – 27767, 1996.
- Jones, A. E., and J. D. Shanklin, Continued decline of total ozone over Halley, Antarctica since 1985, *Nature*, *376*, 409–411, 1995.
- Kanzawa, H., et al., Validation and data characteristics of water vapor profiles observed by the the Improved Limb Atmospheric Spectrometer (ILAS) and processed with the Version 5.20 algorithm, *J. Geophys. Res.*, *107*, 8217, doi:10.1029/2001JD000881, 2002.
- Keene, W. C., et al., Composite global emissions of reactive chlorine from anthropogenic and natural sources: Reactive chlorine emissions inventory, *J. Geophys. Res.*, *104*, 8429–8440, 1999.
- Kilbane-Dawe, I., N. Harris, J. Pyle, M. Rex, A. Lee, and M. Chipperfield, A comparison of Match and 3D model ozone loss rates in the Arctic polar vortex during the winters of 1994/95 and 1995/96, *J. Atmos. Chem.*, *39*, 123–138, 2001.
- Knudsen, B. M., et al., Ozone depletion in and below the Arctic vortex for 1997, *Geophys. Res. Lett.*, *25*, 627–630, 1998.
- Koike, M., Y. Kondo, H. Hayashi, Y. Iwasaka, P. A. Newman, M. Helten, and P. Amedieu, Depletion of Arctic ozone in the winter 1990, *Geophys. Res. Lett.*, *18*, 791–794, 1991.

- Kondo, Y., M. Koike, A. Engel, U. Schmidt, M. Mueller, T. Sugita, H. Kanzawa, T. Nakazawa, S. Aoki, H. Irie, N. Toriyama, S. T, and Y. Sasano, NO_y - N_2O correlation observed inside the Arctic vortex in February 1997: dynamical and chemical effects, *J. Geophys. Res.*, *104*, 8215–8224, 1999.
- Kondo, Y., H. Irie, M. Koike, and G. Bodecker, Denitrification and nitrification in the Arctic stratosphere during the winter of 1996-1997, *Geophys. Res. Lett.*, *27*, 337–340, 2000.
- Kyro et al., Analysis of the ozone soundings made during the first quarter of 1989 in the Arctic, *J. Geophys. Res.*, *97*, 8083–8091, 1992.
- Larsen, N., B. M. Knudsen, T. S. Jorgensen, A. D. Sarra, D. Fua, P. D. Girolamo, g. Fiocco, M. Cacciani, J. M. Rosen, and N. T. Kjome, Backscatter measurements of stratospheric aerosols at Thule during January-February 1992, *Geophys. Res. Lett.*, *13*, 1303–1306, 1994.
- Lary, D. J., M. P. Chipperfield, J. A. Pyle, W. A. Norton, and L. P. Riishøjgaard, Three-dimensional tracer initialization and general diagnostics using equivalent PV latitude-potential-temperature coordinates, *Q. J. R. Meteorol. Soc.*, *121*, 187–210, 1995.
- Lee, K. M., J. M. McInerney, Y. Sasano, J. H. Park, W. Choi, and J. M. Russell III, Intercomparison of ILAS and HALOE ozone at high latitudes, *Geophys. Res. Lett.*, *26*, 835–838, 1999.
- Lefèvre, F., F. Figarol, K. S. Carslaw, and T. Peter, The 1997 Arctic ozone depletion quantified from three-dimensional model simulations, *Geophys. Res. Lett.*, *25*, 2425–2428, 1998.
- Luo, B., K. S. Carslaw, T. Peter, and S. L. Clegg, Vapour pressures of $\text{H}_2\text{SO}_4/\text{HNO}_3/\text{HCl}/\text{HBr}/\text{H}_2\text{O}$ solutions to low stratospheric temperatures, *Geophys. Res. Lett.*, *22*, 247–250, 1995.
- Mann, G. W., S. Davies, K. S. Carslaw, and M. P. Chipperfield, Factors controlling arctic denitrification in cold winters of the 1990s, *Atmos. Chem. Phys. Discuss.*, *2*, 2557–2586, 2002.
- Manney, G., L. Froidevaux, M. Santee, N. Livesey, J. Sabutis, and J. Waters, Variability of ozone loss during Arctic winter (1991 to 2000) estimated from UARS Microwave Limb Sounder measurements, *J. Geophys. Res.*, *108*, doi: 10.1029/2002JD002634, 2003a.
- Manney, G., W. Lahoz, J. Sabutis, A. O'Neill, and L. Steenman-Clark, Simulations of fall and early winter in the stratosphere, *Quart. J. Roy. Meteor. Soc.*, p. in press, 2003b.
- Manney, G. L., and J. L. Sabutis, Development of the polar vortex in the 1999-2000 Arctic winter stratosphere, *Geophys. Res. Lett.*, *27*, 2589–2592, 2000.

- Manney, G. L., R. W. Zurek, A. O'Neill, R. Swinbank, J. B. Kumer, J. L. Mergenthaler, and A. E. Roche, Stratospheric warmings during February and March 1993, *Geophys. Res. Lett.*, *21*, 813–816, 1994.
- Manney, G. L., L. Froidevaux, J. W. Waters, M. L. Santee, W. G. Read, D. A. Flower, R. F. Jarnot, and R. W. Zurek, Arctic ozone depletion observed by UARS MLS during the 1994-95 winter, *Geophys. Res. Lett.*, *23*, 85–88, 1996a.
- Manney, G. L., M. L. Santee, L. Froidevaux, J. W. Waters, and R. W. Zurek, Polar vortex conditions during the 1995-96 Arctic winter: Meteorology and MLS ozone, *Geophys. Res. Lett.*, *23*, 3203–3206, 1996b.
- Manney, G. L., L. Froidevaux, M. L. Santee, R. W. Zurek, and J. W. Waters, MLS observations of Arctic ozone loss in 1996-97, *Geophys. Res. Lett.*, *24*, 2697–2700, 1997.
- Manney, G. L., W. A. Lahoz, R. Swinbank, A. O'Neill, P. M. Connew, and R. W. Zurek, Simulation of the December 1998 stratospheric major warming, *Geophys. Res. Lett.*, *26*, 2733–2736, 1999.
- McElroy, M. B., R. J. Salawitch, S. C. Wofsy, and J. A. Logan, Antarctic ozone: Reductions due to synergistic interactions of chlorine and bromine, *Nature*, *321*, 759–762, 1986.
- McIntyre, M. E., Atmospheric dynamics: Some fundamentals, with observational implications, in *Proc. Int. School Phys. "Enrico Fermi" CXV Course*, edited by J. C. Gille and G. Visconti, pp. 313–386, North-Holland, Amsterdam, 1992.
- McIntyre, M. E., and T. N. Palmer, Breaking planetary waves in the stratosphere, *Nature*, *305*, 593–600, 1983.
- McKenna, D. S., J.-U. Grooß, G. Günther, P. Konopka, R. Müller, G. Carver, and Y. Sasano, A new Chemical Lagrangian Model of the Stratosphere (CLaMS): Part II Formulation of chemistry-scheme and initialisation, *J. Geophys. Res.*, *107*(D15), 10.1029/2000JD000113, 2002.
- Michelsen, H. A., G. L. Manney, M. R. Gunson, and R. Zander, Correlations of stratospheric abundances of NO_y , O_3 , N_2O , and CH_4 derived from ATMOS measurements, *J. Geophys. Res.*, *103*, 28347–28359, 1998.
- Molina, L. T., and M. J. Molina, Production of Cl_2O_2 from the selfreaction of the ClO radical, *J. Phys. Chem.*, *91*, 433–436, 1987.
- Molina, M. J., and F. S. Rowland, Stratospheric sink for chlorofluoromethanes: Chlorine atom catalysed destruction of ozone, *Nature*, *249*, 810–812, 1974.
- Morris, G. A., M. R. Schoeberl, L. C. Sparling, P. A. Newman, L. R. Lait, L. Elson, J. Waters, R. A. Suttie, A. Roche, J. Kumer, and J. M. Russell III, Trajectory mapping and applications to data from the Upper Atmosphere Research Satellite, *J. Geophys. Res.*, *100*, 16491–16505, 1995.

- Müller, R., and G. Günther, A generalized form of Lait's modified potential vorticity, *J. Atmos. Sci.*, *60*, 2229–2237, 2003.
- Müller, R., P. J. Crutzen, H. Oelhaf, G. P. Adrian, T. v. Clarmann, A. Wegner, U. Schmidt, and D. Lary, Chlorine chemistry and the potential for ozone depletion in the Arctic stratosphere in the winter of 1991/92, *Geophys. Res. Lett.*, *21*, 1427–1430, 1994.
- Müller, R., P. J. Crutzen, J.-U. Grooß, C. Brühl, J. M. Russel III, and A. F. Tuck, Chlorine activation and ozone depletion in the Arctic vortex: Observations by the Halogen Occultation Experiment on the Upper Atmosphere Research Satellite, *J. Geophys. Res.*, *101*, 12531–12554, 1996.
- Müller, R., P. J. Crutzen, J.-U. Grooß, C. Brühl, J. M. Russell III, H. Gernandt, D. S. McKenna, and A. F. Tuck, Severe chemical ozone loss in the Arctic during the winter of 1995-96, *Nature*, *389*, 709–712, 1997a.
- Müller, R., J.-U. Grooß, D. McKenna, P. J. Crutzen, C. Brühl, J. M. Russell, and A. F. Tuck, HALOE observations of the vertical structure of chemical ozone depletion in the Arctic vortex during winter and early spring 1996-1997, *Geophys. Res. Lett.*, *24*, 2717–2720, 1997b.
- Müller, R., J.-U. Grooß, D. S. McKenna, P. J. Crutzen, C. Brühl, J. M. Russell, L. Gordley, J. Burrows, and A. F. Tuck, Chemical ozone loss in the Arctic vortex in the winter 1995-1996: HALOE measurements in conjunction with other observations, *Ann. Geophysicae*, *17*, 101–114, 1999.
- Müller, R., U. Schmidt, A. Engel, D. McKenna, and M. Proffitt, The O₃/N₂O relationship from balloon-borne observations as a measure of Arctic ozone loss in 1991-1992, *Q. J. R. Meteorol. Soc.*, *127*, 1389–1412, 2001.
- Müller, R., S. Tilmes, J.-U. Grooß, D. S. McKenna, M. Müller, U. Schmidt, G. C. Toon, R. A. Stachnik, J. J. Margitan, J. W. Elkins, J. Arvelius, and J. M. Russell III, Chlorine activation and chemical ozone loss deduced from HALOE and balloon measurements in the Arctic during the winter of 1999-2000, *J. Geophys. Res.*, *107*, 8302, doi:10.1029/2001JD001423, 2002.
- Nakamura, N., Two-dimensional mixing, edge formation, and permeability diagnosed in area coordinates, *J. Atmos. Sci.*, *53*, 1524–1537, 1996.
- Nash, E. R., P. A. Newman, J. E. Rosenfield, and M. R. Schoeberl, An objective determination of the polar vortex using Ertel's potential vorticity, *J. Geophys. Res.*, *101*, 9471–9478, 1996.
- Naujokat, B., and K. Labitzke, eds., *Collection of reports on the stratospheric circulation during the winters 1974/75-1991/92*, STEP, 1993.

- Naujokat, B., K. Labitzke, R. Lenschow, B. Rajewski, M. Wiesner, and R. Wohlfart, The stratospheric winter 1991/92, the winter of the European Arctic Stratospheric Ozone Experiment, *Beilage zur Berliner Wetterkarte*, Freie Universität Berlin, 1992.
- Naujokat, B., K. Labitzke, R. Lenschow, B. Rajewski, M. Wiesner, and R. Wohlfart, The stratospheric winter 1993/94: A cold winter with some minor warmings and a final warming, *Beilage zur Berliner Wetterkarte*, Freie Universität Berlin, 1995a.
- Naujokat, B., K. Labitzke, R. Lenschow, B. Rajewski, M. Wiesner, and R. Wohlfart, The stratospheric winter 1994/95: A cold winter with a strong minor warming, *Beilage zur Berliner Wetterkarte*, Freie Universität Berlin, 1995b.
- Newman, P., F. Gleason, R. McPeters, and R. Stolarski, Anomalously low ozone over the Arctic, *Geophys. Res. Lett.*, *24*, 2689–2692, 1997.
- Newman, P., et al., An overview of the SOLVE-THESEO 2000 campaign, *J. Geophys. Res.*, *107*, 8259, 2002.
- Pawson, S., and B. Naujokat, The cold winters of the middle 1990s in the northern lower stratosphere, *J. Geophys. Res.*, *104*, 14,209–14,222, 1999.
- Peter, T., Microphysics and heterogeneous chemistry of polar stratospheric clouds, *Annu. Rev. Phys. Chem.*, *48*, 785–822, 1997.
- Plumb, R. A., and M. K. W. Ko, Interrelationships between mixing ratios of long-lived stratospheric constituents, *J. Geophys. Res.*, *97*, 10145–10156, 1992.
- Plumb, R. A., D. W. Waugh, and M. P. Chipperfield, The effect of mixing on tracer relationships in the polar vortices, *J. Geophys. Res.*, *105*, 10047–10062, 2000.
- Proffitt, M. H., D. Fahey, K. Kelly, and A. Tuck, High latitude ozone loss outside the Antarctic ozone hole, *Nature*, *342*, 233–237, 1989.
- Proffitt, M. H., J. J. Margitan, K. K. Kelly, M. Loewenstein, J. R. Podolske, and K. R. Chan, Ozone loss in the Arctic polar vortex inferred from high altitude aircraft measurements, *Nature*, *347*, 31–36, 1990.
- Proffitt, M. H., S. Solomon, and M. Loewenstein, Comparison of 2-D model simulations of ozone and nitrous oxide at high latitudes with stratospheric measurements, *J. Geophys. Res.*, *97*, 939–944, 1992.
- Proffitt, M. H., K. Aikin, J. J. Margitan, M. Loewenstein, J. R. Podolske, A. Weaver, K. R. Chan, H. Fast, and J. W. Elkins, Ozone loss inside the northern polar vortex during the 1991-1992 winter, *Science*, *261*, 1150–1154, 1993.

- Proffitt, M. H., K. Aikin, A. Tuck, J. Margitan, C. Webster, G. Toon, and J. Elkins, Seasonally averaged ozone and nitrous oxide in the northern hemisphere lower stratosphere, *J. Geophys. Res.*, *108*, doi:10.1029/2002JD002657, 4110, 2003.
- Ray, E. A., F. L. Moore, J. W. Elkins, D. F. Hurst, P. A. Romashkin, G. S. Dutton, and D. W. Fahey, Descent and mixing in the 1999-2000 northern polar vortex inferred from in situ tracer measurements, *J. Geophys. Res.*, *107*, 8285, 2002.
- Rex, M., R. J. Salawitch, M. L. Santee, J. W. Waters, and N. R. P. Harris M. Chipperfield, and B. Naujokat, Empirical quantification of the dynamical and chemical processes that regulate Arctic ozone during winter, Poster at the workshop on polar ozone loss, Potsdam, March 2002, 2002.
- Rex, M., R. J. Salawitch, M. L. Santee, J. W. Waters, K. Hoppel, and R. Bevilacqua, On the unexplained stratospheric ozone losses during cold Arctic Januaries, *J. Geophys. Res.*, *30*(1), 1010, doi:10.1029/2002GL016008, 2003.
- Rex, M., et al., In situ measurements of stratospheric ozone depletion rates in the Arctic winter 1991/92: A Lagrangian approach, *J. Geophys. Res.*, *103*, 5843–5853, 1998.
- Rex, M., et al., Subsidence, mixing and denitrification of Arctic polar vortex air measured during POLARIS, *J. Geophys. Res.*, *104*, 26611–26623, 1999.
- Rex, M., et al., Chemical depletion of Arctic ozone in winter 1999/2000, *J. Geophys. Res.*, *107*, 8276, 2002.
- Richard, E. C., K. Aikin, A. E. Andrews, B. C. Daube, C. Gerbig, S. C. Wofsy, P. A. Romashkin, D. F. Hurst, E. A. Ray, F. L. Moore, J. W. Elkins, T. Deshler, and G. C. Toon, Severe chemical ozone loss in the Arctic polar vortex during winter 1999-2000 inferred from in-situ airborne measurements, *Geophys. Res. Lett.*, *28*(11), 2197–2000, 2001.
- Rosenfield, J. E., P. A. Newman, and M. R. Schoeberl, Computations of diabatic descent in the stratospheric polar vortex, *J. Geophys. Res.*, *99*(D8), 16677–16689, 1994.
- Russell, J. M., L. L. Gordley, J. H. Park, S. R. Drayson, A. F. Tuck, J. E. Harries, R. J. Cicerone, P. J. Crutzen, and J. E. Frederick, The Halogen Occultation Experiment, *J. Geophys. Res.*, *98*, 10777–10797, 1993.
- Salawitch, R., et al., Chemical loss of ozone during the Arctic winter of 1999-2000: an analysis based on balloon-borne observations, *J. Geophys. Res.*, *107*, 8269, 2002.

- Sasano, Y., M. Suzuki, T. Yokota, and H. Kanzawa, Improved limb atmospheric spectrometer (ILAS) for stratospheric ozone layer measurements by solar occultation technique, *Geophys. Res. Lett.*, *26*, 197–200, 1999.
- Schmidt, U., G. Kulesa, E. Klein, E.-P. Röth, P. Fabian, and R. Borchers, Intercomparison of balloon-borne cryogenic whole air samplers during the MAP/GLOBUS 1983 campaign, *Planet. Space Sci.*, *35*, 647–656, 1987.
- Schoeberl, M. R., and D. L. Hartmann, The dynamics of the stratospheric polar vortex and its relation to springtime ozone depletions, *Science*, *251*, 46–52, 1991.
- Schoeberl, M. R., L. R. Lait, P. A. Newman, and J. E. Rosenfield, The structure of the polar vortex, *J. Geophys. Res.*, *97*, 7859–7882, 1992.
- Schulz, A., et al., Match observations in the Arctic winter 1996/97: High stratospheric ozone loss rates correlate with low temperatures deep inside the polar vortex, *Geophys. Res. Lett.*, *27*, 205–208, 2000.
- Simpson, I. J., D. R. Blake, and F. S. Rowland, Implications of the recent fluctuations in the growth rate of tropospheric methane, *Geophys. Res. Letters*, *29*, No. 10, 2002.
- Sinnhuber et al., Total ozone during the unusual antarctic winter of 2002, *Geophys. Res. Lett.*, *30*, 1580, doi:10.1029/2002GL016798, 2003.
- Solomon, S., Stratospheric ozone depletion: A review of concepts and history, *Rev. of Geophys.*, *37*(3), 275–316, 1999.
- Solomon, S., R. R. Garcia, F. S. Rowland, and D. J. Wuebbles, On the depletion of Antarctic ozone, *Nature*, *321*, 755–758, 1986.
- Solomon, S., R. W. Portmann, R. R. Garcia, W. Randel, F. Wu, R. Nagatani, J. Gleason, L. Thomason, and L. R. P. P. McCormick, Ozone depletion at mid-altitudes: Coupling of volcanic aerosols and temperature variability to anthropogenic chlorine, *Geophys. Res. Lett.*, *25*, 1871–1874, 1998.
- Stein, B., M. D. Guasta, J. Kolenda, M. Morandi, P. Rairoux, L. Stefanutti, J. P. Wolf, and L. Wöste, Stratospheric aerosol size distributions from multispectral lidar measurements at Sodankyla during EASOE, *Geophys. Res. Lett.*, *13*, 1311–1314, 1994.
- Strahan, S., J. Rosenfield, M. Loewenstein, J. Podolske, and A. Weaver, Evolution of the 1991-1992 Arctic vortex and comparison with the Geophysical Fluid Dynamics Laboratory Skyhi general circulation model, *J. Geophys. Res.*, *99*, 20713–20723, 1994.
- Sugita, T., et al., Validation of ozone measurements from Improved Limb Atmospheric Spectrometer (ILAS), *J. Geophys. Res.*, 2002, in press.

- Suzuki, M. A., A. Matsuzaki, T. Ishigaki, N. Kimura, N. Araki, T. Yokota, and Y. Sasano, Ilas, the improved limb atmospheric spectrometer, on the advanced earth observing satellite, *IEICE TRANS. Commun.*, *E78-B,12*, 1560–1570, 1995.
- Terao, Y., Y. Sasano, H. Nakajima, H. Tanaka, and T. Yasunari, Stratospheric ozone loss in the 1996/1997 Arctic winter: Evaluation based on multiple trajectory analysis for double-sounded air parcels by ILAS, *J. Geophys. Res.*, *107(D24)*, 8210, 2002.
- Tilmes, S., R. Müller, J.-U. Grooß, D. McKenna, J. Russell, and Y. Sasano, Calculation of chemical ozone loss in the Arctic winter 1996-1997 using ozone-tracer correlations: comparison of ILAS and HALOE results, *J. Geophys. Res.*, *108*, 4045, doi:10.1029/2002JD002213, 2003.
- Voigt, C., et al., Nitric acid trihydrate (NAT) in polar stratospheric clouds, *Science*, *290*, 1756–1758, 2000.
- Volk, C. M., J. W. Elkins, D. W. Fahey, G. S. Dutton, J. M. Gilligan, M. Loewenstein, J. R. Podolske, and K. R. Chan, On the evaluation of source gas lifetimes from stratospheric observations, *J. Geophys. Res.*, *102*, 25543–25564, 1997.
- von der Gathen, P., et al., Observational evidence for chemical ozone depletion over the Arctic in winter 1991-92, *Nature*, *375*, 131–134, 1995.
- Waibel, A. E., T. Peter, K. S. Carslaw, H. Oelhaf, G. Wetzell, P. J. Crutzen, U. Pöschl, A. Tsias, E. Reimer, and H. Fischer, Arctic ozone loss due to denitrification, *Science*, *283*, 2064–2069, 1999.
- Waugh, D. W., et al., Mixing of polar vortex air into middle latitudes as revealed by tracer-tracer scatterplots, *J. Geophys. Res.*, *102*, 13119–13134, 1997.
- Weber, M., K.-U. Eichmann, K. Bramstedt, L. Hild, A. Richter, J. P. Burrows, and R. Müller, The cold Arctic winter 1995/96 as observed by GOME and HALOE: Tropospheric wave activity and chemical ozone loss, *Q. J. R. Meteorol. Soc.*, *128*, 1293–1319, 2002.
- Wilson, J. C., V. T. Lai, and S. D. Smith, In situ observations of aerosol and chlorine monoxide after the 1991 eruption of Mount Pinatubo: Effect of reactions on sulfate aerosols, *Science*, *261*, 1140, 1993.
- Wirth, M., G. Ethret, P. Mörl, and W. Renger, Two dimensional stratospheric aerosol distributions during easoe, *grl*, *13*, 1287–1290, 1994.
- WMO, *Scientific assessment of ozone depletion: 1989*, Report No. 20, Geneva, 1990.
- WMO, *Scientific assessment of ozone depletion: 1994*, Report No. 37, Geneva, 1995.

- WMO, *Scientific assessment of ozone depletion: 1998*, Report No. 44, Geneva, 1999.
- WMO, *Scientific assessment of Ozone Depletion: 2002*, Report No. 47, Geneva, 2003.
- Woyke, T., R. Müller, F. Stroh, D. S. McKenna, A. Engel, J. J. Margitan, M. Rex, and K. S. Carslaw, A test of our understanding of the ozone chemistry in the Arctic polar vortex based on in-situ measurements of ClO, BrO, and O₃ in the 1994/95 winter, *J. Geophys. Res.*, *104*, 18755–18768, 1999.
- Yokota, T., H. Nakajima, T. Sugita, H. Tsubaki, Y. Itou, M. Kaji, M. Suzuki, H. Kanzawa, J. H. Park, and Y. Sasano, Improved limb atmospheric spectrometer (ilas) data retrieval algorithm for version 5.20 gas profile products, *J. Geophys. Res.*, *107*(D24), 2002.

Acknowledgements

Diese Arbeit wurde am Institut für Meteorologie und Geophysik der Johann Wolfgang-Goethe Universität angenommen unter der Betreuung von Prof. Dr. U. Schmidt. Die Arbeit wurde durchgeführt am Institut für Chemie und Dynamik der Geosphäre, Institut I: Stratosphäre am Forschungszentrum Jülich unter der Leitung von Herrn Prof. Dr. D. McKenna und später von Herrn Prof. Dr. M. Riese.

Herrn Prof. Dr. U. Schmidt danke ich herzlich, dass er diese Arbeit zur Betreuung und Begutachtung angenommen hat und mit vielen guten Vorschlägen bereichert hat. Ebenso gilt mein Dank Herrn Prof. Dr. M. Riese, der die zweite Begutachtung übernommen hat. Er und Prof. Dr. D. McKenna haben mir während meiner Arbeit am Forschungszentrum Jülich ermöglicht an interessanten internationalen Tagungen teilzunehmen.

Ein ganz besonderer Dank gilt meinem Betreuer Herrn Dr. R. Müller. Ihm verdanke ich die interessante Themenstellung der Arbeit, wertvolle Ideen und Diskussionen, die zum Gelingen der Arbeit wesentlich beigetragen haben. Er ermöglichte mir, diese Arbeit unter besonderen Umständen, vorwiegend als Telearbeit von zu Hause aus, durchzuführen. Auch möchte ich mich bei Herrn Dr. J.-U. Grooß herzlich bedanken für die hilfreichen fachlichen Diskussionen und die schnelle Hilfe, wenn es um das Erstellen von Datensätzen und Trajektorienläufen ging, und dafür, dass er mir IDL-Programme und Graphiken zur Verfügung gestellt hat. Herzlich gedankt sei allen Mitarbeitern des ICG-I, die sich immer Zeit nahmen, wenn ich Fragen hatte, und die mich trotz nur sporadischer physikalischer Anwesenheit als Mitarbeiter sehr gut aufgenommen haben. Dabei bedanke ich mich auch besonders bei Herrn R. Bauer für seine Unterstützung bei allen technischen Fragen und IDL Problemen.

Ich möchte mich auch bei allen bedanken, die mir Messdaten zur Verfügung gestellt haben: Zunächst danke ich Herrn Dr. A. Engel für die Daten von mehreren Kryosammler Ballonflügen. Auch danke ich Dr. H. Gernandt und Dr. P. von der Gathen für die Daten aus NyÅlesund Ozonsonden Messungen.

I would like to acknowledge the Halogen Occultation Experiment (HALOE) science team led by J. M. Russell III for providing HALOE (V19) data. Further, I thank the science team of the Improved Limb Atmospheric Spectrometer (ILAS) led by Dr. Y. Sasano and Dr. H. Nakajima for processing ILAS (V5.20) data. ILAS was developed by the Environment Agency of Japan (EA) and was on board the ADEOS satellite launched by the National Space Development Agency

of Japan (NASDA). ILAS data were processed at the ILAS Data Handling Facility, National Institute for Environmental Studies (NIES). The United Kingdom Meteorological Office provided stratospheric wind and temperature data. I thank Dr. L. Gordely and Dr. T. Sugita for helpful comments on the HALOE and ILAS instruments, respectively. A part of the present work was funded by the European Community within the SAMMOA project.

Weiterhin bedanke ich mich bei Frau Carter-Sigglow für grammatikalische and stilistische Korrekturen dieser Arbeit, die ihr den endgültigen Schliff gegeben haben.

Schließlich möchte ich mich bei meinen Verwandten und Freunden bedanken für die Hilfe und die Betreuung meiner Kinder, die mir das Erstellen der Arbeit oft erleichtert haben. Meinem Ehemann, Stefan, möchte ich ganz besonders für seine Unterstützung sowie für fachliche Diskussionen und gründliches Korrekturlesen danken. Ihm und unseren Kindern sei herzlich für ihre Geduld in den arbeitsreichen Wochen und Monaten während der Fertigstellung dieser Arbeit gedankt.

Lebenslauf

Zur Person

Name: Simone Tilmes
Anschrift: Hintergasse 35
65817 Eppstein
Geboren: 5. Juni 1973 in Borken, Westfalen
Familienstand: verheiratet
Ehemann: Dr. Stefan Tilmes
Kinder: zwei Kinder, geb. 6.12.1997 und 14.12.2000

Schulausbildung

1979 – 1983 Engelrading-Grundschule, Borken
1983 – 1992 Gymnasium-Remigianum in Borken
1992 Abitur

Studium

1992 – 1994 Studium der Fächer Physik, Diplom, und Geophysik, an der Westfälischen Wilhelmsuniversität in Münster
1994 Vordiplom in Physik und Geophysik
1994 – 1998 Studium des Faches Geophysik, Diplom, an der Universität zu Köln; Thema der Diplomarbeit: „Die Bestimmung der trockenen Deposition in einem mesoskaligen Chemie-Transport-Modell (EURAD)“

Berufliche Tätigkeiten

10. 1995 – 3. 1998 Studentische Hilfskraft beim Institut für atmosphärische Umweltforschung, EURAD, an der Universität zu Köln
12. 1998 – 3. 1999 Freiberufliche Tätigkeit: HTML-Programmierung
2. – 4. 1999 Werkvertrag beim Deutschen Wetterdienst: IDL-Programmierung
4. – 11. 1999 Wissenschaftliche Arbeiten im Rahmen eines Werkvertrages für den Deutschen Wetterdienst, Offenbach: „Lokale Photochemie an der GAW-Station Hohenpeißenberg“
1. 2000 – 12. 2002 Wissenschaftliche Arbeiten in Form von Werkverträgen für das Forschungszentrum Jülich: „Untersuchung von Transport und chemischem Ozonverlust im arktischen Winter und Frühjahr.“
seit Januar 2003 Wissenschaftliche Mitarbeiterin des Forschungszentrums Jülich

Meine akademischen Lehrer waren:

Prof. Dr. A. Ebel, Köln, Prof. Dr. U. Schmidt, Frankfurt, Prof. Dr. D. McKenna und Prof. Dr. M. Riese, Jülich.